Towards a non-invasive diagnostic aid for abdominal adhesions using dynamic MRI and image processing

David Randall

Medical Physics Group

Mathematical Modelling in Medicine

Infection Immunity and Cardiovascular Disease

Faculty of Medicine, Dentistry and Health

The University of Sheffield

Thesis submitted for the degree of PhD

August 2017

Abstract

This work presents a strategy for detection of abdominal adhesions based on cine-MRI data, image processing and the production of a 'sheargram'. Abdominal adhesions are a common complication of abdominal surgery and can cause serious morbidity. Diagnosis is difficult and often one of exclusion. A conclusive diagnosis typically requires laparoscopic explorative surgery, which itself may cause further adhesions. A non-invasive means of diagnosis is preferred and likely to aid patient management. Cine-MRI can capture the motion of the abdominal structures during respiration and has shown promise for adhesion detection. However, such images are difficult and time consuming to interpret. A previous PhD considered augmenting cine-MRI by quantifying movement for detection of gross adhesive pathology. This thesis presents a refined image processing approach aimed at detection of more subtle adhesions to the abdominal wall.

In the absence of adhesive pathology, the abdominal contents (bowels, kidneys, liver) slide smoothly against the perimeter of the abdominal cavity – a process termed visceral slide. An adhesion is expected to produce a localised resistance that inhibits smooth visceral sliding. In this PhD, development of a 2D technique to quantify sliding around the perimeter of the abdominal cavity (with particular emphasis on the abdominal wall) sought to highlight regions of reduced sliding. Segmentation and image registration were employed to quantify movement and shear, the latter used as an analogue for sliding. The magnitude of shear over all frames in the dynamic MR image sequence was extracted and displayed as a colour plot over the MR image for anatomical context. This final output is termed a 'sheargram'. Suitability of the technique for diagnosis was assessed through a series of experimental tests and correlation with clinical data. The latter involved a retrospective pilot study incorporating data from 52 patients scanned for suspected adhesions. A total of 141 slices were processed and reported.

The validation experiments confirmed the technique had the attributes to accurately and reproducibly report sliding and demonstrated proof of concept for detection of adhered regions. The pilot study confirmed the sheargram matched expert clinical judgement in the vast majority of cases (>84%) and detected >93% of all adhesions. However, the investigation also highlighted limitations, principally structures moving out of the imaging plane creates a fundamental problem and requires a 3D imaging solution. In conclusion, the work has produced encouraging results and merits further development.

Personal Acknowledgements

First and foremost, I would like to express my gratitude for my supervisors: Dr John Fenner and Prof. Karna Dev Bardhan (Chandu). I would not have undertaken this PhD so readily had it not been for a second opportunity to work with John. My supervisors' enthusiasm, encouragement and dedication to both the project and my personal development have provided a remarkable experience: John's dedicated, calm, methodical, scientifically rigorous approach together with Chandu's insight, enthusiasm and unique ability to think outside the box – sometimes very far outside.

I would like to thank the funders, The Bardhan Research and Education Trust of Rotherham (BRET), for the opportunity to work on this project. BRET afforded John, Chandu and me the freedom to explore opportunities peripheral to the core work of the project and in doing so kick-started new areas of research. This freedom has not been taken for granted.

It has been a pleasure to work in the academic Medical Physics team which throughout my time here has shown an enduring cohesion both inside and outside of work. Thanks to Dr Andrew Narracott for always offering a helpful hand when needed. I would like to thank the team at Rotherham, including Bev Mason and Christine Royston, with particular gratitude extended to Richard Gillott for his support with MRI scanning. Also, much of this work would not have been possible without the support of colleagues in Nijmegen and Arnhem. A special thank you to Drs Richard ten Broek, Frank Joosten and Chema Strik for their valued help and input.

Last but not least my parents have been of great help and support, particularly through the torturous process of writing up.

It has been a privilege to work on this project and it is no exaggeration to say the origins of BRET, the work it does and the experience gained through John and Chandu have left me inspired and changed the course of my career.

Publications

The work presented in this thesis is complimented by a series of publications [1, 2, 3, 4] which are listed below. The thesis chapter to which the publication relates is also referenced underneath the citation.

1. D. Randall, C. Strik, H. v. Goor, J. B. Joosten, R. Gillott, P. A. Spencer, J. W. Fenner and K. D. Bardhan, "Mo2016 Intra-Abdominal Adhesions: Identifying the "Sticking Point(s)" Using Novel Cine-Magnetic Resonance Image Analysis. Pilot Results," *Gastroenterology,* vol. 148, no. 4, pp. S-769, 2015.
   CHAPTERS 3 AND 4

2. D. Randall, J. W. Fenner, R. Gillott, P. Spencer, C. Strik, H. Goor, F. Joosten and K. D. Bardhan, "PTH-243 Intra-abdominal adhesions: identifying the "sticking point(s)" using novel cine-magnetic resonance image analysis. pilot results," *Gut,* vol. 64, p. A517, 2015.
   CHAPTERS 3 AND 4

3. D. Randall, J. W. Fenner, R. Gillott, R. t. Broek, C. Strik, P. Spencer and K. D. Bardhan, "A Novel Diagnostic Aid for Detection of Intra-Abdominal Adhesions to the Anterior Abdominal Wall Using Dynamic Magnetic Resonance Imaging," *Gastroenterology Research and Practice,* vol. 2016, p. Article ID 2523768, 2016.
   CHAPTERS 3 AND 4

4. D. Randall, F. Joosten, R. ten Broek, R. Gillott, K. D. Bardhan, C. Strik, W. Prins, H. van Goor and J. W. Fenner, "A novel diagnostic aid for intra-abdominal adhesion detection in cine-MR imaging: Pilot study and initial diagnostic impressions," British Journal of Radiology, 2017.
   CHAPTER 5

The latter stages of the PhD explored aspects of 3D imaging and visualisation. This led to an opportunity to explore the use of virtual reality technology for visualisation of CT colonoscopies and resulted in the publications below:

5. D. Randall, P. Metherall, K. D. Bardhan, P. Spencer, R. Gillott, R. de Noronha and J. W. Fenner, "The Oculus Rift virtual colonoscopy: introducing a new technology and initial impressions," *Journal of Biomedical Graphics and Computing,* vol. 6, no. 1, pp. 34-42, 2016.
   CHAPTER 7

6. D. Randall, P. Metherall, J. Belkhu, K. D. Bardhan, P. Spencer, R. Gillott, R. de Noronha and J. W. Fenner, "The virtual reality virtual colonoscopy: introducing a new technology and a novel application to diagnostic research," in 23rd Congress of the European Society of Biomechanics 2017, Sevilla, 2017.
   CHAPTER 7

Statement of work performed

I would like to confirm that all the work presented in this thesis is my own with the exception of the following:

- Descriptions of work performed in a previous BRET funded PhD outlined in Chapter 1, including AbsCAT.

- In Chapter 6, a MATLAB script was used to convert vector arrows into exportable 3D objects (.dxf) for visualisation in a virtual reality headset. This was written during a vacation scholarship by Madeline Thornbery and Dr John Fenner (although it was adapted and modified by the author).

- Elastography work mentioned in the Conclusion, Chapter 7, was mostly performed by Elizabeth Humble under the author's supervision.

Contents

Table of Figures

List of Tables

Chapter 1

Introduction and clinical background

The origins of this work resulted from inspection of cinematographic magnetic resonance (cine-MR) images acquired in Rotherham District General Hospital (Rotherham) to investigate haemodynamics in the superior mesenteric artery [5]. Smooth movement of the abdominal contents during respiration was observed which led to the proposition of movement analysis aimed at the detection of abdominal adhesions. A Bardhan Research and Education Trust of Rotherham (BRET) funded PhD followed in (2006-2010), the PhD communicated in this thesis (2013-2017) is the continuation of the project.

This PhD aims to develop a non-invasive technique to aid detection of adhesive pathologies in the abdomen. Image processing is applied to cine-MR images, to aid detection of different abdominal movement patterns to separate healthy subjects from pathological subjects. The cine-MR acquisition sequence acquires a set of sequential images separated by ~0.4 seconds while the patient bears down and respires deeply[1]. As the diaphragm moves, the abdominal contents re-position as the abdominal cavity expands and contracts. The primary movement of the intestines is parallel to the abdominal wall as the bowel loops closest to the abdominal wall slide smoothly against it (in healthy patients). This motion is termed visceral slide. The sequence of cine-MR images at different points throughout the respiratory cycle can indicate the extent of visceral slide and in the presence of particular adhesive diseases the visceral slide is expected to be reduced. This project explores how image registration techniques can provide useful information to help detect the presence of such pathology. The focus of the PhD is on the disruption of visceral slide caused by the presence of abdominal adhesions but another, more severe, manifestation of adhesions is also discussed – encapsulating peritoneal sclerosis (EPS) – as this was an important focus of the preceding BRET funded PhD [6].

---

[1] Bearing down and respiring deeply refers to a procedure whereby the subject tenses their abdominal muscles while attempting to respire. A discussion on the practicalities of doing so are considered in Chapter 6, Section 6.4.

Chapter 1 outlines the background to the project. A description of abdominal adhesions (and EPS), their pathogenesis and associated morbidity is offered. A review of diagnostic procedures currently used in clinical practice is provided, followed by a review of diagnostic techniques yet to reach the clinic which remain within the research environment. The chapter concludes with a summary of the work of the previous PhD to place the remainder of this thesis firmly into context.

1.1 Introduction to Abdominal Adhesions

In order to understand what abdominal adhesions are and the problems they can cause, an understanding of the relevant anatomy and physiology is necessary and a brief introduction follows.

1.1.1 The abdomen and adhesions

Figure 1.1 contains a simplified diagram of the abdominal anatomy and indicates the structures and organs which are of concern to this project. The abdominal cavity refers to almost the entirety of Figure 1.1 and is defined as the space within the bounds of the abdominal wall, spine, pelvic floor and diaphragm. It is the contents of the abdominal cavity which are the focus for adhesion detection in this PhD, hereby referred to as 'abdominal contents'. The majority of the organs of the abdominal cavity are covered (to a variable degree) by a membrane called the peritoneum. This supports and lubricates the abdominal structures, hence is an essential consideration in this project when examining the degree of intra-abdominal movement. The small intestines are almost completely wrapped by the peritoneum with just sufficient space to allow access by the arteries, veins and nerves. Other structures are less mobile, for example the kidneys, which are on the posterior abdominal wall, covered by peritoneum stretched over it. The movement of the small intestines is a primary focus of this work as they are prone to developing adhesions and their altered trajectory more readily recognisable than less mobile structures [7, 8]. They are covered by the peritoneum and are tethered to the posterior wall of the abdominal cavity by the mesentery. The mesentery is a loosely hanging structure which allows the small intestine to move with little constraint within the abdominal cavity.

Diaphragm

Liver

Peritoneum

Bowel

Mesentery

Abdominal Wall

Abdominal Cavity

Abdominal Contents
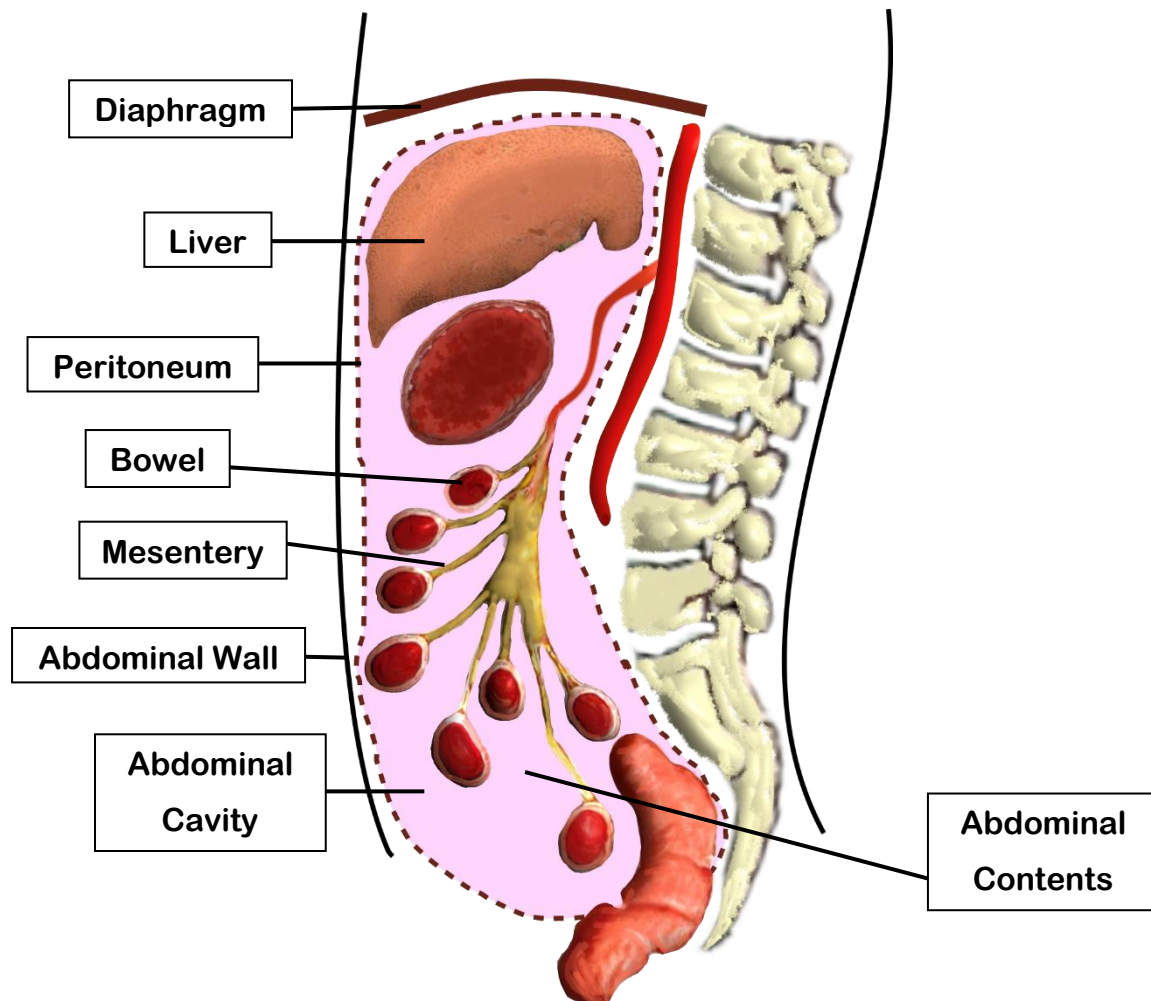
Figure 1.1: Diagram of the abdominal anatomy from a sagittal view

The trajectory of movement within the abdomen during respiration is complex owing to rigidity in certain parts and lack of it in others. Most structures are highly mobile and, with the exception of the liver and kidneys, are deformable; actively changing shape during peristalsis. Structural variations together with large amounts of motion adds complexity to dynamic abdominal images. Moreover, while the general arrangement is common in the population, the organisation, size and structure of the abdominal contents varies considerably between individuals. The highly mobile nature of the abdominal contents favours the hypothesis that when movement is known it can be used to detect a reduction, indicating probable adhesions in the right clinical context. The small intestines are the most mobile, hence adhesions reducing their movement is more discernible. However, this also presents a challenge due to the enormous variability and complexity of motion potentially masking movement restriction that might be taking place.

In health, the peritoneum provides the anti-adhesive lubrication which ensures smooth movement of the abdominal contents. This movement is postulated to be disrupted by the presence of adhesive pathology. Abdominal adhesions, likened to 'internal scars', develop as part of normal wound healing [9, 10]. When complicated by infection, adhesions generally increase [11]. Injury to the peritoneum (e.g. abdominal surgery) causes an inflammatory response and can remove the lubricating barrier that separates the structures. When two surfaces in close proximity are wounded concurrently, the repair process can lead to the opposing surfaces connecting via a permanent structure – an adhesion [12]. The possible causes of injury to the peritoneum and therefore adhesion formation are: congenital, ischaemia, bacterial inflammation, reaction to a foreign body, radiation, endometriosis (uterine cells replicating (usually) in the abdominal cavity) or most commonly, abdominal surgery [13, 10, 14].

1.1.2   Adhesions: severity of the problem

Adhesions can be responsible for serious morbidity, the most common presentations include chronic abdominal pain, intestinal obstruction (60-70% of all obstructions are due to adhesions) and infertility [14]. In a large retrospective study of 18912 abdominal surgery patients 14.3% were found to develop intestinal obstruction within 2 years [15]. Adhesions also have a significant cost implication. In the United States there were 303836 surgical adhesion removal procedures (adhesiolysis) in 1994 costing approximately $1.3bn [16]. While in Sweden adhesions have been estimated to cost up to €59.5 mil/yr, including knock-on effects to the economy (sick leave, benefits etc.) [17].

Numerous papers have reported on the scale of adhesion formation resulting from abdominal surgery [18]. In a post-mortem study examining 752 cadavers, adhesions were found in 67% that had undergone a single laparotomy and in 93% of cadavers that had undergone multiple laparotomies. Adhesions were also found in 28% of patients that had no previous operations [7]. Evidence suggests that the more abdominal surgeries that are performed the greater the risk of developing adhesions; this is also supported in other publications [13]. A similar incidence of adhesion related surgical complications was reported by a meta-analysis study which combined the results from 25 recent publications (1990-2011). In a cohort of 2825 patients, 54% of patients developed adhesions post abdominal surgery, however, large variations between individual studies were observed. The highest incidence of adhesion

formation resulted from gastrointestinal surgery where 66% (of 451 patients) developed adhesions. The study also noted that minimally invasive laparoscopic procedures resulted in a smaller proportion of adhesion development – 38% of 304 patients [8]. It has been estimated that adhesions are responsible for 5.7% of all surgical readmissions [9]. These figures highlight the scale of the problem, especially as adhesion diagnosis is usually made via surgery which in itself is likely to cause more adhesions.

Extreme manifestations of adhesions can be fatal. Encapsulating peritoneal sclerosis (EPS) is a specific example in which the entire abdominal contents become encased in fibrous tissue. This is discussed separately in Section 1.3.

1.2   Diagnosis of abdominal adhesions

Abdominal adhesions can occur anywhere in the abdomen, vary in size and structure and result in a wide range of non-specific clinical symptoms. The combination of these factors makes them challenging to diagnose.

Guidelines relating to adhesion diagnosis and management are minimally documented in the literature [10]. Generally, adhesions are indicated through clinical symptoms and medical history and confirmed via laparoscopy/laparotomy. No non-invasive imaging technique has yet found its way into widespread routine clinical practice. The World Journal of Emergency Surgery has produced guidelines for diagnosis and advised when operation is necessary for adhesive small bowel obstruction [19]. They state a diagnosis of obstruction should be formed based on the presentation of recurrent acute pain, vomiting and abdominal distension and examination of plain film x-rays. CT should only be performed if diagnosis remains inconclusive. The guidelines state that MRI and ultrasound imaging are of little use for adhesive small bowel obstruction and should only be used where diagnosis is uncertain and CT is contraindicated [19].

A wider search of the literature uncovered non-invasive diagnostic techniques which are still in the development stage. Both cine-MRI and ultrasound are the main foci and have shown potential, but neither have demonstrated enough success to be widely adopted [20, 21]. The following two sub-sections discuss these techniques separately.

1.2.1 Ultrasound

The concept of ultrasound for detection of adhesions began with the visceral slide measurement work of Sigel et al. (1991) [21]. This is the first documented attempt to describe the use of visceral slide in a diagnostic imaging procedure. The ultrasound probe is positioned on the abdominal wall and the patient breathes in a supine position. As the patient breathes, the abdominal contents closest to the abdominal wall naturally slide against it and if an adhesion is present the degree of sliding is reduced. Based on preliminary findings, Sigel et al. define abnormal visceral slide to be <1cm movement at any focal point and state that normal visceral slide is between 2 to ≥5 cm [21]. The quantification of visceral slide motion was made using electronic callipers in real time.

Sigel et al.'s initial work has led to several other publications from various research groups who were able to give further credence to this technique [22, 23, 24, 25, 26, 27]. A follow-up paper by Sigel et al. achieved a sensitivity of 90% and specificity of 92%, while another research group, Piccolboni et al. (2009), correctly identified adhesions in 93% of patients [24, 26]. However, these studies used the visceral slide technique for identifying a suitable incision site prior to surgery (to avoid incisions directly into the intestines) rather than as a more widely encompassing diagnostic technique. A group in Bristol applied differing variations of the technique for determining the approximate location of adhesions but achieved far less encouraging results, achieving at best 42% sensitivity and 74% specificity [25]. Where the Bristol study may differ is that it had placed greater emphasis on adhesion location accuracy by assigning adhesions within particular quadrants, whereas Sigel et al.'s statistics were based simply on whether an adhesion was identified or not.

1.2.2 Magnetic Resonance Imaging

Conventional MR imaging (to view anatomical structure) is considered to be relatively insensitive at detecting the clinical features of EPS/adhesions compared to CT [28, 29]. However, in the last decade the use of cine-MRI to diagnose abdominal adhesions based on movement rather than structure has grown as an emerging area of research. Several papers have been published in the wake of a paper by Lienemann et al. (2000) [20]. In Lienemann et al.'s study 27 patients were scanned and the resulting dynamic images were assessed according to the following adhesion detection criteria [20]:

- 'distortion of adjacent organs'

- 'a preserved visceral slide of adjacent structures with a missing separation'
- 'a missing normal excursion along the peritoneal layer within the section orientation'

To document the location of adhesions and compare results to surgical findings, a grid containing 9 segments in the coronal plane was placed over the abdomen. Lienemann (2000) reported a sensitivity of 87.5% and specificity of 92.5% when correlating the location of adhesions to surgical findings in a total of 117 segments. Best results were found for adhesions tethered to the abdominal (parietal) wall. During the study a preliminary investigation involving 3 patients was undertaken to determine certain aspects of the acquisition protocol. It was noted that increasing abdominal pressure (bearing down) provided improved excursion compared to that induced by respiration alone – a conclusion based on visual assessment [20]. As a consequence, this feature was incorporated into a local acquisition protocol at Rotherham District General Hospital prior to commencement of this PhD. (Although the acquisition protocol was developed independently, it closely resembled that described by Lienemann (2000) – the scanning protocol is discussed in Section 1.4).

Two similar papers extended the cine-MRI technique to larger patient cohorts (89 and 90 patients) to evaluate its accuracy followed in 2008 [30, 31]. Both papers used the same cine-MRI acquisition protocol as Lienemann et al. (2000) and correlated cine-MRI and surgical findings. The abdomen was also split into a grid of 9 segments as in Lienemann's study (2000) [20]. Lang et al. (2008) produced impressive results achieving a sensitivity of 93% but a specificity of only 25%. The low specificity was attributed to the fact that they had very few patients without adhesions. Lang (2008) also demonstrated reasonable success by detecting the correct location of adhesions in 66% of cases, while another 21% were located in adjacent segments [31]. Burhmann-Kirchhoff et al. chose only to quote the overall sensitivity of adhesion detection rather than assess the sensitivity of correctly identifying the segment location of an adhesion. Promising results were quoted, achieving a correct correlation between cine-MRI and surgery in 80/90 patients and an overall accuracy of 89% [30].

Zinther et al. (2010) have published a paper comparing ultrasound and cine-MRI using the same technique as Lienemann et al. (2000). Their 60 patient cohort contained equal numbers of patients with and without previous abdominal surgery. All patients were examined with both

cine-MRI and ultrasound. Overall statistical figures for the two imaging modalities are summarised in Table 1.1.

Table 1.1: Results from Zinther et al. (2010) comparing cine-MRI and ultrasound for adhesion detection [32]			
	Sensitivity (%)	Specificity (%)	Accuracy (%)
Cine-MRI	21.5	87.1	72.4
Ultrasound	24.0	97.9	81.3

The statistics are based on whether the correct location of the adhesion was identified. The low sensitivity values do not correlate with previous publications. The reason given for the lack of correlation is that this is the first blinded test, perhaps therefore revealing more applicable figures for clinical examination. High specificities indicate both modalities are reasonably accurate in detecting adhesion free areas. Despite ultrasound boasting the better figures, the statistical difference between them was not significant (in terms of accuracy and negative predictive value) [32].

A paper published by the adhesions research group in Sheffield [33] prompted Stuart (2011) to summarise the use of different imaging modalities' application to EPS diagnosis and offer a critique on the potential of cine-MRI [34]. Stuart (2011) acknowledges that current techniques (CT and ultrasound) aimed at detecting morphological changes that are only present in the latter stages of EPS development are insufficient as screening techniques. Stuart commends the cine-MRI technique for its ingenuity but is sceptical that it could eventually be used to detect early EPS as it relies on the adhesive nature of the disease in its latter stages.

1.2.3   Treatment/Prevention of abdominal adhesions

By far the most effective and most practiced treatment for adhesions is adhesiolysis, which involves surgical removal of adhesions (with varying degrees of invasiveness). The principal problem with this method is the invasive nature of the procedure can itself precipitate further adhesion formation. Consequently, there has been considerable interest in adhesion prevention techniques which include methods such as reducing the introduction of foreign bodies (e.g. powdered gloves) and using warm, humidified gas to inflate the abdomen [10, 35]. One of the more popular preventative measures is Seprafilm (a bioresorbable sheet placed between the incision site and underlying organs) which is reported to significantly reduce adhesion incidence in a study by Beck (1997) [35, 36]. There is also evidence to suggest fewer patients develop adhesions from micro-invasive laparoscopic procedures relative to open surgical

procedures such as laparotomy [36, 13, 8]. This notion intuitively makes sense – minimising the trauma to the peritoneum results in a reduced inflammatory response and a decrease of adhesion formation. However, some literature does not correlate laparoscopy with a decrease in adhesion formation [16, 10]. Adjuvant therapies to reduce adhesion formation, such as pharmaceutical administration, have shown little success [35]. In summary, despite some progress in adhesion prevention it remains problematic.

1.3 Severe adhesions - encapsulating peritoneal sclerosis (EPS)

EPS is an extreme manifestation of adhesions and is characterised by 'peritoneal fibrosis and thickening with encasement of bowel loops' [37]. As the disease progresses a cocoon of stiff fibrous tissue can form around the lining of the intestines fusing bowel loops together to create a 'lump' of intestines, severely compromising their ability to move semi-independently relative to one another. EPS is a known complication of peritoneal dialysis (PD) [38]. PD utilises the peritoneal membrane as a natural filter to remove toxins from the blood. It is used as an effective alternative to haemodialysis for patients in end-stage kidney disease or kidney failure. The number of PD patients worldwide has been estimated at 200000 in 2008 [39]. EPS is a rare but serious condition with incidence ranging between 0.5 – 4.4% of the PD patient population [40, 41, 42, 43, 44] and a reported mortality rate of 56% [45].

Despite being a much rarer condition than abdominal adhesions, guidelines and research into EPS diagnosis are arguably more developed. The International Society of Peritoneal Dialysis (ISPD) has collated all the evidence presented in the literature to produce a set of mature, well-defined guidelines. The ISPD guidelines are best summarised by a group in the Netherlands [46]. They highlight that the route to diagnosis should be made by a combination of clinical symptoms and CT or surgical findings [47]. The EPS related literature is dominated by work based on clinical findings and CT features that are pertinent to diagnosis; examples include development of CT scoring systems [48, 49]. However, CT has proven unsuitable as an EPS screening technique as it is unable to detect progression of the disease until its full onset [50]. Surgical confirmation is considered the gold standard diagnostic technique [20, 32].

EPS diagnosis is considered challenging and an early diagnosis is rarely possible with current methods. Much work has focused on techniques to detect early onset of the disease so drug therapy and cessation of PD may be employed in a timely manner. The majority of research

can be split into four separate areas: biomarkers, animal studies, ultrasound and MRI. Animal studies have so far primarily been aimed at assessing the effectiveness of drugs rather than diagnosis and are therefore less relevant to this work [51, 52]. The use of biomarkers is a major focus for many research groups [53, 54, 55, 56, 57, 58, 59]. Biomarker investigations have resulted in some success but nothing has been sufficiently conclusive to reach the clinic. Ultrasound can also provide useful information and has the obvious advantage of delivering no ionising radiation dose [60, 61]. Hollman et al. (1991) trialled the use of ultrasound for the early detection of EPS with some success [62]. The most common and earliest indicator of EPS was increased peristaltic motion; however, the author acknowledges that it is a challenging parameter to assess. Conventional MR imaging (to view the anatomical structure) is considered to be relatively insensitive at detecting the clinical features of EPS compared to CT [28, 29]. However, with the exception of the Medical Physics group at Sheffield, there is no record of Lienemann et al.'s cine-MR visceral slide technique being applied to evaluate movement in EPS (rather than structure). The imaging process is described in more detail below.

1.4 Capturing abdominal movement using cinematographic MRI

A review of the literature has ascertained there is some potential for the use of cine-MRI to capture abdominal motion for adhesion detection. This PhD has worked closely with two centres who have independently implemented the technique with similar but differing scanning protocols. Dynamic MRI has been used to capture abdominal movement in 2 dimensional planes in both the sagittal and transaxial orientations. During the course of the PhD, images have primarily been received from Rotherham District General Hospital [http://www.therotherhamft.nhs.uk/] and Radboud University Medical Center (UMC) [http://www.ru.nl/english/], Nijmegen, Netherlands (actual MRI scanning undertaken in Rijnstate Hospital, Arnhem). Both centres had local ethical approval to undertake these scans for research purposes. The exact parameters of the scanning protocol vary between scanner model and centres but as collaboration between the two groups developed throughout the PhD, the scanning protocols somewhat converged. Table 1.2 describes the salient features of each of the scanning protocols used at each centre.

Table 1.2: Cine-MRI scanning protocol features for each of the two centres		
Feature	**Rotherham**	**Nijmegen**
Scanner	Siemens Avanto 1.5T	Siemens Avanto 1.5T
Imaging Sequence	True-FISP	True-FISP
Scanning position	Supine	Supine
Patient instructions	Bear down and breathe normally "as though going to the toilet"	Bear down and breathe deeply by distending the abdominal wall
Images acquired	2D sagittal and transaxial	2D sagittal and transaxial
Number of slices/ spacing between slices	1 cm gaps between slices. Number of slices dependent on body habitus (Approx. 20 sagittal and 30 transaxial for an average sized patient).	Typically 5 sagittal slices and 5 transaxial. Space between slices dependent on body habitus. (large patients may have extra slices)
2D imaging slice thickness	7 mm	5 mm
Cine frames per slice	30 frames (15 frames for older data)	30 frames
Framerate	0.4 seconds per frame (0.8 secs per frame for older data)	0.4 seconds per frame
Matrix size	192 x 256 (386 x 512 on older acquisitions)	192 x 256
Flip angle	60°	60°
Echo time	2.26 msec	1.53 msec
Relaxation time	4.51 msec	3.66 msec
Total scan time	30-45 minutes	20 minutes

Many of the features of this imaging protocol were inherited from previous work and most data in this PhD were acquired previously, thus, there was little scope or need to focus on enhancing the scanning protocol. The scanning parameters listed above offer a good compromise in the trade-off between spatial and temporal resolution: fast enough acquisition rate to capture movement throughout the respiratory cycle, yet offering sufficient spatial resolution to comfortably resolve small bowel loops (which is the smallest object of interest). The 1 cm gaps between slices acquired in Rotherham and larger spaces between slices in Nijmegen mean the

whole abdomen is not captured, however, it is a necessary compromise to maintain a comfortable overall scanning time for the patient. The instruction to 'bear down and breathe normally' was introduced from interpretation of Lienemann et al.'s publication which cited increased excursion of abdominal contents in the lower pelvis as advantageous for inducing movement [20].

1.4.1   Reporting of cine-MRI scans

The radiologist typically reviews each slice (in sagittal and transaxial planes) with 15-30 frames concatenated to form a cine video. The radiologist attempts to identify areas where movement appears to be disturbed or hindered and subsequently, upon reviewing several slices, begins to build a 3 dimensional picture of the motion. The movement of the abdominal contents as a result of respiration is predominantly superior-inferior and thus the same objects tend to remain in the sagittal plane while there is considerable and continuous change in the transaxial plane. The transaxial slices can clarify whether an adhesion to the abdominal wall is present as the tethered object may remain in view while all other objects around it traverse through the imaging plane. Examining the motion in all these slices in detail and simultaneously constructing a 3D picture of the abdomen in the mind is a difficult, time-consuming task. The challenges of interpreting such an examination has been voiced by radiologists, providing impetus for an image processing solution to aid the diagnostic process.

1.5   Previous Work – Image processing for gross adhesion diagnosis

This BRET funded PhD is the continuation of a previous PhD and several other contributions from smaller projects that have considered the application of image processing for adhesion diagnosis. Specifically, a 3-year PhD was completed in 2010 by Dr Wright [6], and was complemented by a 1-year Masters project thereafter. The previous PhD used image registration techniques in an attempt to quantify movement of abdominal structures to determine whether anomalous movement was indicative of underlying structural abnormality. The work confirmed that structural abnormalities could be associated with anomalous movement identified by application of image registration to cine-MR images. Details are described in Dr Wright's PhD thesis [6] and in a publication [63]. A brief summary of the path taken is described below:

- Cine-MRI scans were performed and a scanning protocol determined. The scanning parameters are described in Table 1.2.

- Image registration was performed with ShIRT (Sheffield Image Registration Toolkit). This is a locally developed, tried and tested registration tool. A series of idealised tests were designed to confirm ShIRT's performance and suitability. A computer program called ImWarper was developed and used to distort simple images by a known amount and the actual distortion field was compared to the one generated by ShIRT. This task confirmed that ShIRT accurately reported the deformation field imposed on the system (subject to acknowledged limitations of registration approaches).

- Two *in-vitro* models were used to test the overall potential of the technique as a proof of principle exercise. One consisted of a diagrammatic drawing of the abdomen and the other a grid pattern; both were drawn on an elastic material. The elastic sheet was distorted by tugging on a piece of sticky tape attached to one end. 'Adhesions' were simulated by affixing a second small piece of sticky tape to the elastic material to prevent distortion in that area. The results confirmed the potential of image registration to identify structural defects based on a disturbed movement signature [6].

- More sophisticated *in-silico* models were developed. A real sagittal MRI slice and a scanned diagrammatic drawing of the abdomen were stretched with and without computer simulated adhesions. An operator was asked to determine if an adhesion was present or not. The results showed promise that quantifying the motion with image registration helped to detect adhered areas. The same *in-silico* images were used to show promising ROC (Receiver Operating Characteristic) curves, demonstrating clearly that the information generated by the registration technique proved helpful in making a 'diagnosis' [6].

- The technique was applied to real clinical data as a preliminary exercise. Both transaxial and sagittal abdominal cine-MR slices were considered for the registration. Differences between a healthy volunteer and two unhealthy patients with Crohn's disease were not apparent on the movement vector map derived from the registration. As a part of this preliminary study, a processing protocol was inaugurated. It involved registering two cine-MR images at maximal inhalation and exhalation so maximum excursion of the abdominal contents was assessed.

- A small study, involving a handful of EPS patients and healthy volunteers, revealed a potential difference in registration mapping pattern. EPS patients appeared to have a concentration of motion toward the top of the abdominal cavity while healthy patients had a distribution of movement throughout the abdomen. Although encouraging, these

results were qualitative and lacked statistical power due to the small sample size. A clinical study involving a larger cohort of patients was recommended to confirm the findings.

- Movement in and out of the imaging plane was identified as a problem and a move to 3D imaging was suggested.

- The registration technique was aimed specifically at the detection of gross abnormalities such as that produced by EPS.

- Appropriate visualisation techniques to display the results were considered and several approaches were tested (contours of movement vector magnitude, movement vector arrows, movement vector arrows coloured according to magnitude). The opinions of observers varied but overall the use of contours was preferred. Figure 1.2 below displays an example of a contour map from Dr Wright's thesis: a diffuse movement pattern over the abdominal space is observed in a healthy abdomen.
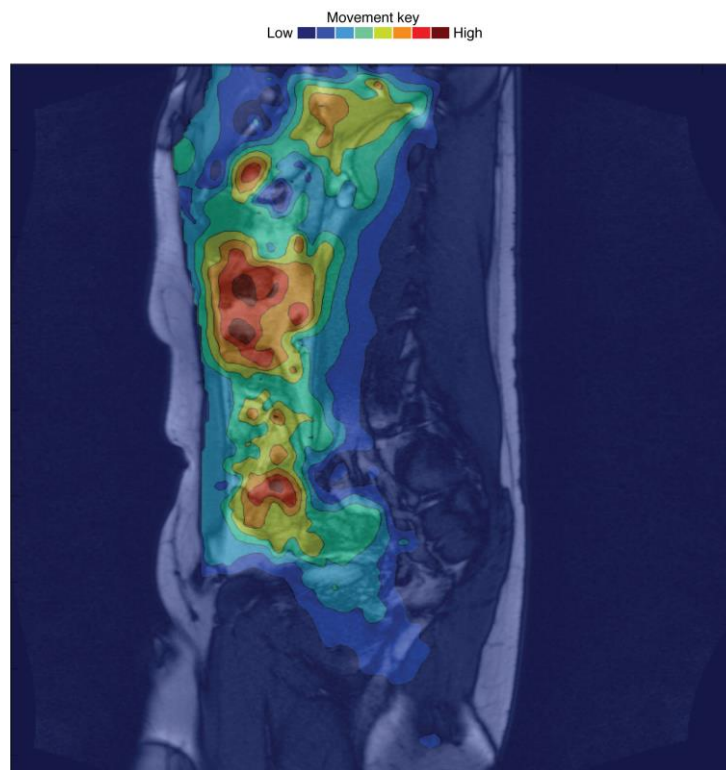
Figure 1.2: Example of a contour map representing the magnitude of movement on a healthy volunteer was the principal output of the registration used for diagnostic purposes. Diagram sourced from [6]

Beyond the PhD, further work was undertaken to design a computer program with an efficient graphical user interface to streamline the processing workflow. A MATLAB [MathWorks, Natick, USA] program named AbsCAT was produced and was inherited by this PhD.

1.5.1 AbsCAT

AbsCAT was the refined end product of the previous work. The AbsCAT program presented a graphical user interface to aid the processing of cine-MRI scans for the detection of gross adhesive abnormalities presented in EPS.

Upon running the program, the user selects the file directory containing the dynamic MR images (accepted formats: DICOM, jpeg, tiff, bmp or png) and two of the frames are displayed in the image selection area as shown in Figure 1.3. The two frames which are displayed can be changed using the slider bars beneath them. Processing relies on selection of frames at opposite ends of the respiratory cycle. Displaying the frames side-by-side allows the user to compare them to qualitatively assess the degree of motion which has taken place. To aid the image selection process, the clock faces in Figure 1.3 were produced to display the overall displacement which had occurred. Each clock face corresponds to a frame in the cine-MRI sequence. The vector arrow within each clock face is produced by registering each frame to an average image of the whole dynamic imaging sequence and subsequently summing all vectors across the image to produce a representation of the overall movement direction.
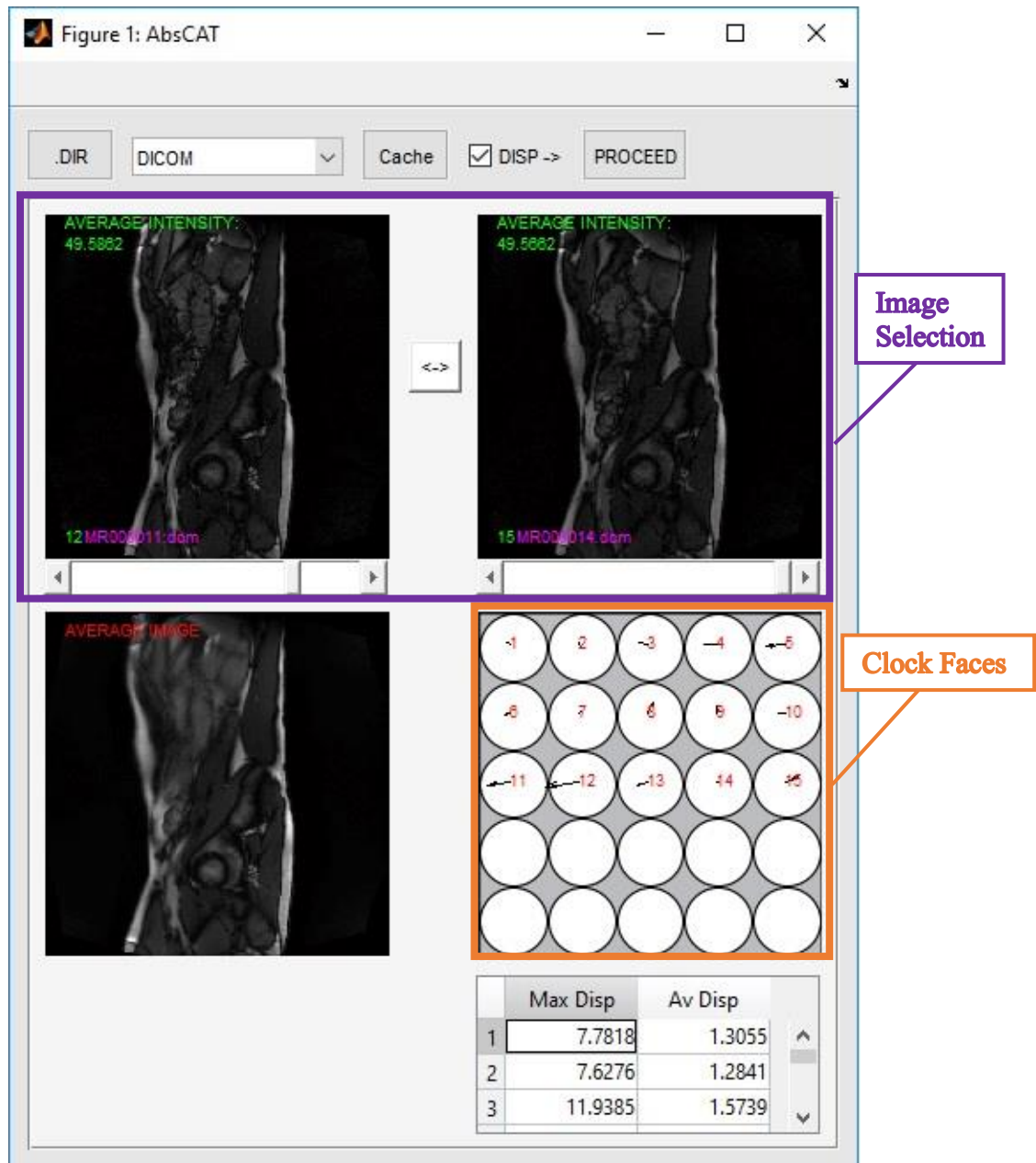
Figure 1.3: AbsCAT interface used to select images at opposing ends of the respiratory cycle for image registration

The two frames exhibiting maximally opposite directions of motion relative to the average image (opposing vectors in the clock faces) are identified and selected to be registered to one another.

Figure 1.4 shows the following user interaction window which allows the user to crop the images using an intensity threshold so that the registration is only performed on the area of the image containing detail.
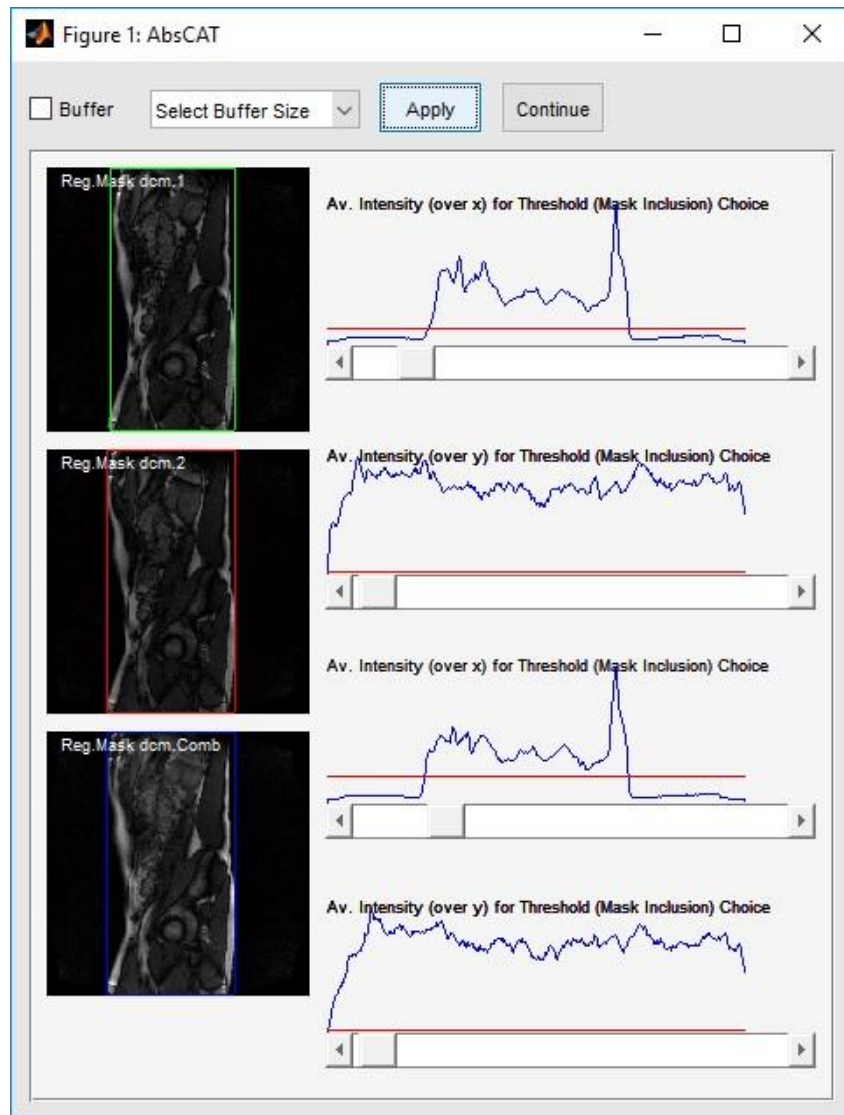
Figure 1.4: AbsCAT interface to crop the images before performing the final registration for movement analysis

The image registration (using ShIRT) is then performed and the result displayed as shown in Figure 1.5. The deformation field is overlaid onto the image which can be displayed either as vectors (Figure 1.5a) or a contour map corresponding to the magnitude of the vectors (Figure 1.5b). The user can change the appearance of the overlay (such as the transparency, size of the arrows etc.) using the interface shown in Figure 1.5.

(a)   *(b)*
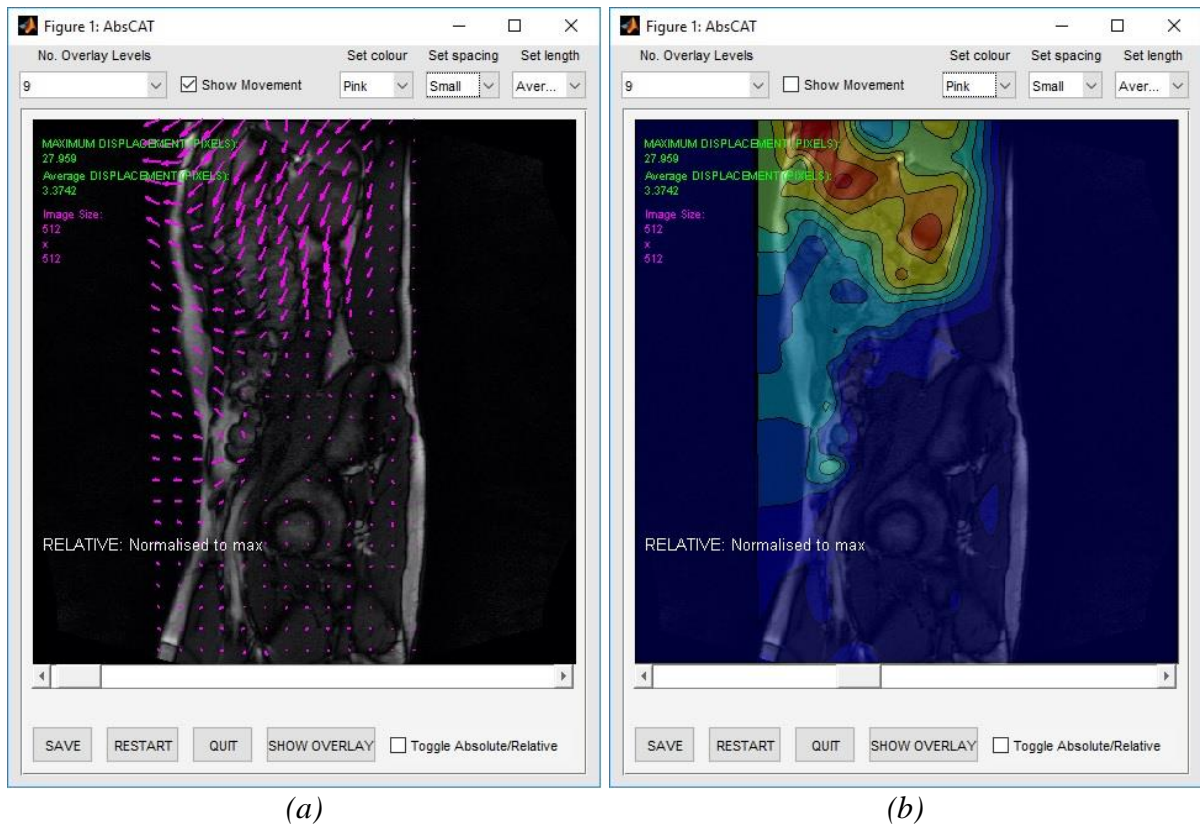
Figure 1.5: The final display in AbsCAT showing the result of the image registration corresponding to movement between the selected frames

Images, such as those shown in Figure 1.5, form the proposed diagnostic output of AbsCAT. Diagnostic interpretation of the result was based on the expectation of more diffuse, localised movement in healthy individuals compared to bulk, less varied movement across the abdomen in the presence of gross adhesive pathology.

1.6 Summary

Diagnosis of adhesions is currently made by clinicians based on medical history and symptoms and is often a diagnosis of exclusion. This is highly subjective with variable results. Invasive procedures are the only reliable method to diagnose adhesions (explorative laparoscopy/laparotomy) and are known to cause further adhesion formation. This is the justification for a more consistent method based on the non-invasive detection/confirmation of abdominal adhesions. This would be of significant clinical benefit. Abdominal adhesions have proven a challenge to detect non-invasively using conventional imaging techniques (CT, static MRI). Both ultrasound and cine-MR have been used to assess visceral sliding motion

anomalies with some success. Ultrasound has advantages (e.g. non-ionising, excellent temporal resolution) but also has drawbacks:

- It has a limited depth of detection and is therefore primarily useful for detection of parietal wall adhesions. This issue becomes exacerbated when scanning obese patients and in the presence of intestinal gas.

- Using conventional 2D ultrasound is suitable for indicating a suitable incision site, as the reviewed papers have shown, but is unlikely to be ideal to diagnose and map adhesions throughout the abdomen. To use the 2D ultrasound visceral slide technique as an adhesion screening procedure may prove too cumbersome and time consuming.

However, despite mixed reports, overall, ultrasound appears to have value in detecting abdominal wall adhesions. In contrast, conventional, static MRI assigned to assess structural changes characteristic of adhesions/EPS has received little attention and is reported to be inadequate [29, 28]. However, cine-MRI to analyse movement and visceral slide has also been identified to have potential. Several groups have reported successful statistics for adhesion detection with cine-MRI, although a study by Zinther et al. (2010) resulted in a lower sensitivity [32, 20, 31].

Despite numerous efforts, a reliable technique for non-invasive detection of adhesions remains elusive. The application of cine-MRI for adhesion detection has shown some success but remains plagued by high inter-operator variability, time-consuming radiologist examination and a large amount of training required to become proficient [63]. The addition of a diagnostic aid for cine-MRI adhesion detection could therefore help improve reliability, particularly with less experienced or trainee radiologists.

Previous work completed at Sheffield has produced a technique for motion analysis of the abdominal contents aimed at the detection of gross abnormalities. A previous PhD has thoroughly tested ShIRT (the primary registration algorithm used throughout this current PhD) for its suitability for abdominal motion analysis in cine-MRI. ShIRT was selected as the registration algorithm and incorporated into AbsCAT – a program created to streamline the processing technique for movement analysis. Work published by the group at Sheffield has demonstrated cine-MRI's potential application for EPS detection when aided by image processing [33].

Early diagnosis of EPS was the main focus of work prior to this PhD and remains an unmet challenge. The AbsCAT technique looked promising but a lack of clinical data limited subsequent application and provoked re-examination of the method for adhesion detection. The outcome was this PhD, which stands on the foundations laid by previous work but pursues the detection of subtler, more common adhesive pathologies rather than its extensive manifestation in conditions such as EPS.

With consideration to the background of the project, the **hypothesis** for this PhD is:

"The appropriate manipulation and analysis of image registration applied to cine-MRI can yield improved diagnostic signatures for detection of abdominal adhesions"

To address the hypothesis, the thesis is arranged into 6 further chapters:

Chapter 2: Discusses the background to image registration and places this theory in the context of adhesion detection in dynamic abdominal imaging.

Chapter 3: Communicates a new approach developed for adhesion detection by quantifying the amount of visceral slide around the perimeter of the abdominal cavity.

Chapter 4: Characterises and tests several features of the technique described in Chapter 3 via a series of experiments.

Chapter 5: Tests the technique on clinical data in a pilot study to determine its efficacy for adhesion detection.

Chapter 6: Provides an overarching discussion of the work presented throughout the thesis.

Chapter 7: Summarises the thesis and confirms the trajectory for future work.

Chapter 2

Image processing in abdominal cine-MRI

The post-processing of medical images can extract or highlight information relevant to a particular diagnostic investigation for enhanced interpretation and diagnostic power [64, 65, 63]. There are two principal image processing techniques which are of relevance to the cine-MRI images in this project: image segmentation and image registration. Image segmentation is the process of separating different regions of an image from one another, usually identifying and isolating coherent anatomical structures [66]. Image registration is a tool used to achieve spatial alignment between corresponding features in two images [67]. Image registration can be used for a wide variety of applications in medical imaging [68, 69, 70, 71, 72]. In this project it is used to track the path of objects in the abdomen through a dynamic imaging sequence. This chapter introduces these image processing techniques to inform project direction and justify choices made. An introduction to image segmentation and registration are offered followed by a review of existing image processing techniques which have been applied to the abdomen. Fundamental components of image registration are presented in 1D, via a specific 1D registration implementation and then generalised for wider application in higher dimensions.

However, it is first important to gain an appreciation of the images which are to be processed. For reference, two typical abdominal sagittal MR frames from different patients are shown in Figure 2.1 to aid subsequent discussions. These images are two frames from a dynamic image set of, typically, 30 frames designed to capture motion.
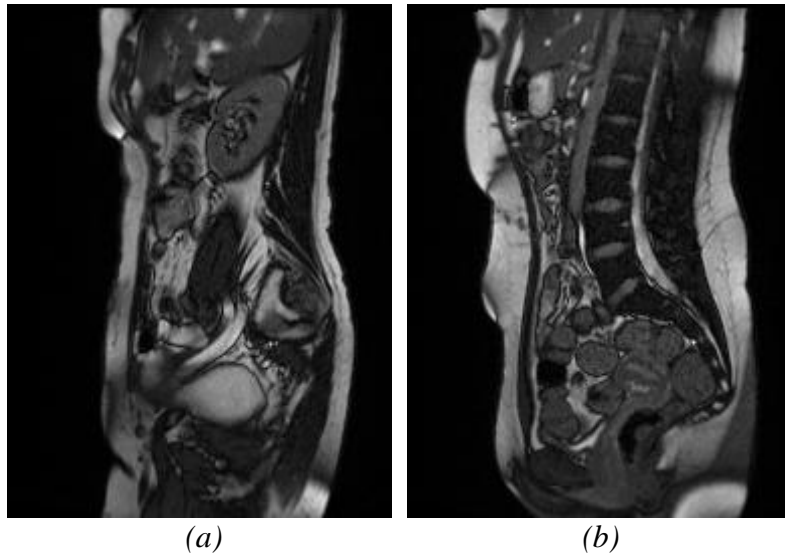
Figure 2.1: Two typical sagittal MR slices from different patients: a) typical right paramedian slice, b) typical midline slice

2.1 Introduction to image segmentation

Image segmentation is the process of compartmentalising an image into different structures or regions of interest (ROIs). A single segmentation technique is unable to address all segmentation problems [66, 73] and consideration of the method should be given for each task. As shown in Figure 2.1 abdominal MR images are complex, containing many different structures with a range of intensity values and a large variation is observed between individuals. These features must be considered for appropriate segmentation technique selection. The amount of user interaction must also be considered; it can vary from fully automated to purely manual demarcation via interpretation of the human eye. A range of established segmentation techniques are subsequently introduced in general terms and then discussed regarding the specific context of the abdominal sagittal cine-MR images exemplified in Figure 2.1.

Manual Segmentation

Manual segmentation usually refers to the process of drawing ROIs based entirely on user input. The most common method of manual segmentation is to place vertices around the edge of the anatomical structure of interest until a contained area/volume is produced. The trained human eye is exceptional at identifying individual structures and their boundaries within a complex image. However, segmentation by eye is a time consuming approach (particularly for 3D data) and ROI placement introduces subjectivity [74]. Manual segmentation of anatomical

structures in the images in Figure 2.1would be achievable but the intricacy of the segmentation is limited by time available.

Intensity thresholding

Intensity thresholding applies a cut-off intensity to define which pixels should be included and excluded from an image. More sophisticated approaches may use multiple upper and lower thresholds rather than a single global threshold. Using intensity thresholds relies on the regions being segmented to be of a distinctively distinguishable intensity and does not consider spatial position. It is most useful for images with a fairly constant background, with the regions of interest exhibiting a different intensity; it is not suitable for complex images with a diverse range of structures and intensities such as the abdominal cine-MRI images shown in Figure 2.1 [75, 76, 77].

Region growing

Region growing usually relies on the user providing a starting point(s) or 'seed location(s)' within the structure of interest from which the region is expanded until a predefined homogeneity criterion, usually based on intensity, is contravened [75]. One example would be to compare new neighbouring pixels to a dynamic mean intensity of the region as it expands, if the new pixels are within an intensity threshold range, they are included in the region. The method's main disadvantage is the dependence of the result on the initial seed location, thus introducing user dependence and potentially lower reproducibility [75]. Its applicability to sagittal MR images depends on the object of interest. For example, segmentation of individual bowel loops would be possible if they were surrounded by high intensity intra-abdominal fat but probably not possible if it were adjacent to another bowel loop/colon, as observed in Figure 2.1b.

Edge detection

Edge detection algorithms focus on the perimeter of objects by examining gradients or second derivatives in intensity. A sharp gradient is frequently associated with the edge of a structure. A number of different methods exist to identify such boundaries and the first or second derivative of the intensity profile in the image could be used. In the simplest terms, if the magnitude of the gradient (and/or second derivative) exceeds a threshold, that point will be highlighted as an edge [77]. Edge detection does not produce a region of interest but a boundary from which a region of interest may be defined. A common problem with edge detection

algorithms (particularly in the presence of noise) is the edge is often an incomplete, unclosed boundary and additional algorithms are required to connect the gaps [78]. As with region growing techniques, edge detection in sagittal cine-MRI is likely to generate some success but is unlikely to be robust enough to be satisfactory for the range of images encountered clinically.

Segmentation using image registration

Image registration is a technique capable of automatically identifying corresponding points in two images to produce a mapping that describes the transformation from one image to the other (discussed in subsequent sections). Image registration alone is not capable of segmentation but when provided with a priori information regarding the structures to be segmented, it can be used to identify those structures in individual images. The source of a priori structural knowledge could be a single patient-specific segmentation which is then applied to that patient's subsequent scans or, most commonly, it is a pre-segmented anatomical atlas; this is discussed in the following sub-section. Using image registration to aid segmentation is a possibility for cine-MRI images but depends on a successful initial segmentation step.

Atlas-based segmentation

Atlas-based segmentation relies on the creation of a pre-segmented image which is representative of an entire specific dataset. The segmented atlas image is registered to an individual target image so that the segmented structures overlay corresponding structures in that image [71]. This is a powerful method as it theoretically allows for identification and segmentation of all structures in the image in one procedure for all individuals. However, for abdominal cine-MRI there is no 'standard' abdomen. Its size and appearance varies greatly with height and weight and the abdominal contents are highly mobile, leading to dramatic variations in their arrangement within the abdominal cavity. These conditions are recognised to be unsuitable for atlas-based segmentation [77] and it is hard to conceive successful production and application of a single abdominal atlas. However, the possibility of a small library of atlases for different height/weight/BMI ranges might be possible, depending on the complexity of the desired segmentation: arguably, identification of the abdominal cavity/wall could be achievable, but segmentation of individual bowel loops is improbable due to the variation of their position between individuals.

Image segmentation summary

Given the large number of frames (~30) within the dynamic image sets and moderate number of sagittal slices per patient, manual segmentation was not considered feasible. However, the complexity of the anatomical structures within the abdominal cavity and frequent lack of contrast between neighbouring structures, made a case for utilising the power of the human eye. Therefore, a semi-automated approach involving human input aided by an automated process was considered a suitable compromise. Of the numerous segmentation strategies available, image registration has been highlighted to contain the attributes suitable for segmentation of the images in our study. The details of the segmentation technique adopted and reasons why are discussed in the discussion of this chapter (Section 2.6) and in Chapter 3.

2.2 Introduction to image registration in 1D

Image registration is the process of determining a coordinate transformation that maps features in one image to matching features on another image. The result of a successful image registration is a deformation field which describes the movement of corresponding features from one image to the other. The image registration challenge is considered ill-posed, lacks a unique solution and the solution determined may also be sensitive to the choice of parameters [79]. To limit the number of possible solutions a process termed regularisation is required which imposes constraints to achieve a sensible transformation [80, 68]. The implementation of different constraints, and methods of judging/measuring similarity in images is what differentiates different registration algorithms.

The variety of registration algorithms is vast, but all contain four fundamental components (other features may be introduced to improve performance) [68]:

- Similarity metric
- Optimisation strategy
- Regularisation
- Deformation model

A metric of similarity is required to define the similarity between the images. The mathematical operation used to determine the similarity is called (or may be a principal component of) the cost function. The optimisation strategy is the method of maximising similarity: For example, the optimisation technique can use differences in the intensity to drive the registration in a direction that minimises intensity differences between the images. The deformation model

consists of a series of rules or constraints which define the permissible paths of the registration. If the images to be registered were of a physically deformed object, the deformation model would ideally incorporate a priori knowledge of the object's physical properties so the constraints on deformation more closely reflect the physical laws governing the real object's deformation. However, detailed a priori knowledge is rarely known resulting in idealised estimations, such as modelling brain deformation as an elastic body [81, 82].

This section introduces each of the principal components (similarity metric etc.) of image registration. The principles can be simply described using a 1D model and much of the understanding gained in 1D is transferable to 2D and 3D. An understanding of the components of image registration in 1D helps to clarify the strategies encountered later in the thesis. The descriptions culminate in the formulation of a functioning 1D registration algorithm.

To facilitate discussion, two arbitrary curves (of infinite extent) are to be registered; they are represented in Figure 2.2. The green curve represents the fixed image, *f(x)*, and the blue curve is the moving image, *m(x)*, which is to be translated to match the green curve. The curves' tangents are shown at x = 5.
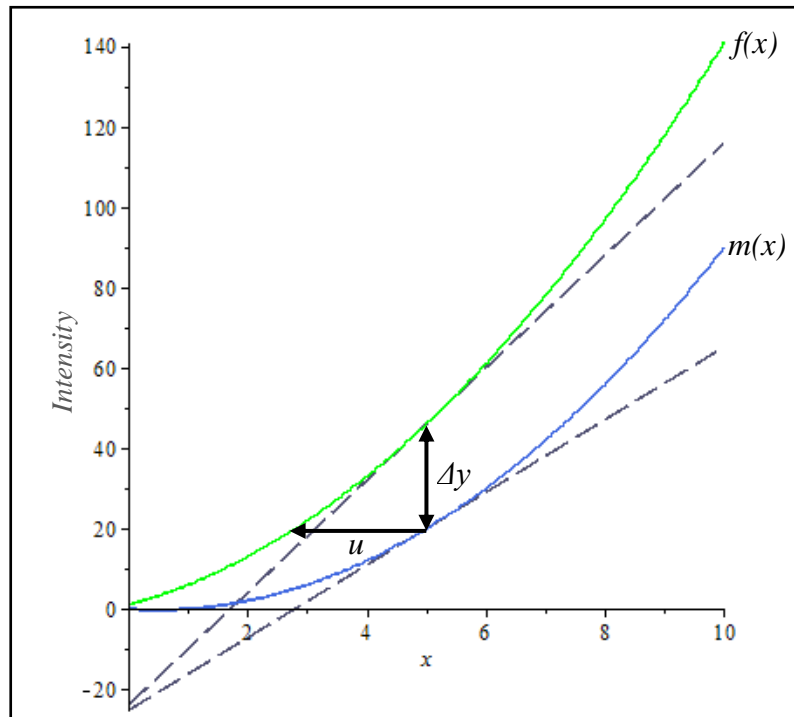
Figure 2.2: Two arbitrary curves (drawn within the range of x=0 to 10) for illustrating some basic concepts of image registration

2.2.1 Similarity metric minimisation

In 1D, the moving curve *m(x)* can only be translated in the x-dimension (as the y-dimension corresponds to intensity). Initially, consider rigid body translation where only a single, constant value, *u*, may be applied to every point on *m(x)*. In this case the registration challenge may be summarised as: 'what displacement u should be applied to *m(x)* to make it as similar to *f(x)* as possible?'. For this, a similarity metric is required to define what is meant by 'similarity' between *m(x)* and *f(x)*. Eq 2.1 introduces an example of a similarity metric that performs this role, identified as a 'cumulative error' term, ε, that is the sum of squared differences between the two curves under a particular translation, *u*. Eq 2.1 and 2.2 define the cumulative error over all curve/image space for both continuous functions and discrete elements (such as pixels) respectively.

$$\varepsilon(u) = \int_{-\infty}^{\infty} (f(x) - m(x - u))^2 \, \mathrm{d}x$$

Eq 2.1

$$\varepsilon(u) = \sum_{i=1}^{n} (f(x_i) - m(x_i - u))^2$$

Eq 2.2

Note that the cumulative error, ε, is a function of *u* because the cumulative error only varies with the position of *m(x-u)*. If the cumulative error is minimised, so is the area between the two curves indicating they are matched as best as possible. The value of *u* that minimises ε is the solution to the 1D rigid body registration. In mathematical terms, this is given when the first derivative of ε is equal to zero (Eq 2.3).

$$\frac{\mathrm{d}}{\mathrm{d}u} \varepsilon(u) = 0$$

Eq 2.3

Where the equations of two curves are known, the two can be rigidly registered by differentiating the error function with respect to *u* and rearranging for *u*. An example of an analytical registration of cos(x) to sin(x) is included in Appendix 1. Similarity metrics based on intensity, such as the example shown in Eq 2.2 in 1D, rely on the features in the images to have similar intensity. In the intra-modal, intra-patient abdominal images in Figure 2.1 this assumption generally holds and intensity similarity metrics are considered suitable [70]. In simple cases *ε(u)* might take the form of a parabolic, u-shaped curve with a single minimum

value, however, for more complex cases the existence of several local minima is likely. For non-analytical problems, an iterative approach is generally adopted where an optimisation strategy determines different values for u in order to update the cost function and drive the direction of the next iteration.

2.2.2 Optimisation strategy

The rigid body example above is a specific example of a more generalised approach in which *u* is not a constant but is a function of position *u(x)*. This non-rigid registration approach is more relevant to the abdominal images in Figure 2.1 recognising that different portions of the image undergo different displacements. Therefore, with the value of *u* changing across the image, a transformation *u(x)* is applied to *m(x)* to match *f(x)*:

$$m(x - u(x)) = f(x)$$

Eq 2.4

The intensity of each curve at every point is known so the difference in intensity can be calculated. Performing a Taylor series expansion on Eq 2.4 and subsequently simplifying the terms produces Eq 2.5 so the intensity difference, *Δy*, at any value of *x* can be related to a translation *u* along the *x* axis.

$$u(x) = \frac{2\,\Delta y}{\dfrac{df(x)}{dx} + \dfrac{dm(x)}{dx}}$$

Eq 2.5

Eq 2.5 provides an opportunity to use gradients to determine a direction to move the images closer to one another. Eq 2.5 makes it possible to determine a *u(x)* for each point on the moving curve. If a complete set of *u(x)* for every point on *m(x)* were obtained to minimise the cost function (*ε*), the mapping to transform *m(x)* onto *f(x)* would be achieved. A spatially varying *u(x)* is akin to a 1D deformable registration whereas using a single constant *u* is representative of a 1D rigid registration.

2.2.3 Regularisation and the use of nodes in discretised systems

The optimisation strategy above permits calculation of the translation *u(x)* for every position over the whole curve. Since digital images are discrete, an elemental approach is required where the registration algorithm operates on a gridded subset of pixels called nodes.

Displacements are imposed on the nodes of the moving image to drive them toward equivalent pixels on the fixed image. The displacements at the nodes use interpolation to derive a displacement on the pixels between them. The power of this approach lies with the opportunity to model the local properties of the image using constraints that reflect the physical structure being registered. This potentially allows the registration result, and/or path, to more closely represent deformations that have taken place in the physical world.

Considering the image as a series of nodes and elements allows for more complex deformations but also increases the complexity of determining a solution. The problem is ill-posed and means the solution needs to be restricted or regularised to achieve a single displacement function [83]. Regularisation is achieved by imposing constraints on the types of deformations and interpolations which are allowed. This concept is illustrated by the example in Figure 2.3, where the displacements of the nodes have already been determined and a single interpolated displacement function is sought between the nodes. Without any constraints, an infinite number of possibilities for the interpolation exist. As an example, interpolation could be constrained by minimisation of curvature. Explicitly, the rules relating to the constraint in this example are:

   i.   The inter-nodal interpolation is modelled by a quadratic equation.

  ii.   There are no discontinuities at the nodes (the gradient is continuous across the nodes).

 iii.   The system is constrained to minimise the cumulative curvature across the whole domain (in this case by mathematically calculating the second derivative of the displacement function).

Figure 2.3 depicts several smooth paths between the nodes (red dashed lines) all in accordance with constraints i and ii, but the solution is collapsed to a single function (blue line) by constraint iii.
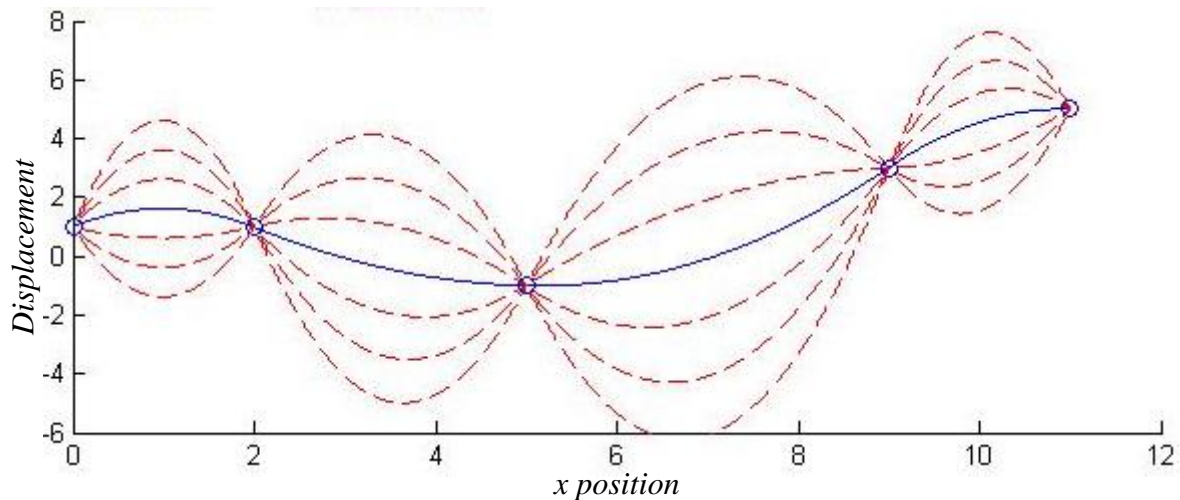
Figure 2.3: Possible inter-nodal interpolation paths (red dashed) and the fully constrained path to minimise curvature marked in blue

This is directly translatable to higher dimensions. In 2D, a regularisation term may collapse the problem to a single solution by minimising the curvature of a deformation field surface rather than a 1D curve as shown in Figure 2.3. Here constraints have only been applied to the interpolated displacement field but it is also necessary to apply constraints pertaining to the determination of the nodal displacements using a deformation model.

2.2.4 Deformation model (an elastic system)

The deformation model controls the progression of displacements. In the case of a physical system, forces can be used to define the motion which occurs. In a registration algorithm the forces operating on the nodes can be calculated and used to derive a set of displacements governed by the laws of the deformation model (e.g. elastic sheet). A set of forces may be calculated by the optimisation strategy and the deformation model might attempt to minimise the potential energy in the system by balancing the forces on every node. Figure 2.4 shows a schematic of a 1D elastic model under consideration.
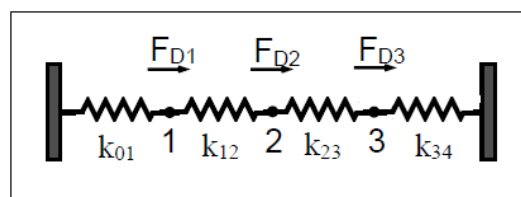
Figure 2.4: Schematic of elastic based model with the zigzags representing springs/elastic rods, circles representing nodes and the vertical lines representing the fixed, immovable edges of the image/curve.

Balancing the forces is achieved from the solution presented in Eq 2.6 (a derivation is included in Appendix 2). It can be used to calculate the displacements of the nodes to reach equilibrium given a set of driving forces, hereby exercising control over the displacement field. The matrix of k-values/stiffness constants is referred to as the stiffness matrix. If desired, different parts of the image could be given different properties by varying the k values of the stiffness matrix with position.

$$\begin{bmatrix} F_{D1} \\ F_{D2} \\ F_{D3} \\ F_{D4} \\ \vdots \end{bmatrix} = \begin{bmatrix} (k_{01} + k_{12}) & -k_{12} & 0 & 0 & \cdots \\ -k_{12} & (k_{12} + k_{23}) & -k_{23} & 0 & \cdots \\ 0 & -k_{23} & (k_{23} + k_{34}) & -k_{34} & \cdots \\ 0 & 0 & -k_{34} & (k_{34} + k_{45}) & \cdots \\ \vdots & \vdots & \vdots & \vdots & \ddots \end{bmatrix} \begin{bmatrix} u_1 \\ u_2 \\ u_3 \\ u_4 \\ \vdots \end{bmatrix} \qquad Eq\ 2.6$$

2.2.5 Implementation of a 1D registration algorithm

By way of example, these principles have been combined to formulate a functional 1D registration algorithm written in MATLAB. The flow diagram in Figure 2.5 displays the registration process employed by the algorithm. It adopts an iterative approach in which gradients at nodal points drive their displacement (Eq 2.5) to minimise a cumulative sum of square differences similarity metric (Eq 2.2). A stiffness matrix (Eq 2.6) was used to control the deformations and the stiffnesses of different elements could be altered prior to launching the algorithm. The displacement of the inter-nodal elements is governed by the minimisation of curvature constraint described in Section 2.2.3. An example of the registration being applied to an idealised 1D abdominal model is shown in Appendix 3.

Inputs

fixed image, moved image, [1xn] matrix of k-values (stiffness of springs between nodes), maximum allowed iterations, spacing between nodes, option for rigid translation

Optional pre-registration rigid translation

Moved curve is translated across a wide range of values. The position which resulted in the lowest image difference is then used as the starting position of the following non-linear registration

Deformation Model & Regularisation

Formation of stiffness matrix

A stiffness matrix is formed from the input k-values (stiffness) between the nodes

Gradient Estimation

To calculate an estimation of the gradients the fixed curve is linearly interpolated between every pixel and the moved curve linearly interpolated between nodes.

Optimisation

'Driving Force' Calculated

Driven by gradients using eq 2.5:

$$F = 2 \frac{\Delta y}{\left(\frac{df}{dx} + \frac{dm}{dx} \right)}$$

Gradients are estimated from the linear interpolation performed in the previous step

Interpolation of inter-nodal displacements

Linear interpolation implemented between the nodes

Deformation model

N

Max no. of iterations reached?

Convergence Criteria

If the difference between the two images (eq 2.2) stops decreasing (i.e. the images begin to diverge) convergence is said to be reached

Minimisation of Similarity Metric

Y

Convergence Not Reached

Convergence

Figure 2.5: Flow chart describing the registration process employed in the 1D algorithm

2.3 Image registration in higher dimensions

When applying image registration, several considerations should be observed to achieve an effective result:

1. The pixel/voxel dimensions of the two images should be the same (although pre-processing can re-sample the images as a simple solution).

2. The same objects should be present in both images being registered. If objects were introduced or removed between the two images, the registration algorithm would attempt to distort or translate non-matching structures. The resulting deformation field would therefore include misinformation about deformations/translations that had occurred.

3. Discontinuous movement between images should be minimised. A discontinuity is not typically permitted by the constraints imposed on the deformation model and would not be accurately reported.

4. For registrations driven by image intensity, the same structures should have similar intensity patterns in each of the images [84].

In all of the above, special adaptations of image registration can be developed to address bespoke cases, but at its most general, there are two main categories of image registration: rigid and deformable. A rigid registration was considered unsuitable because the abdominal cine-MR images contain deformable objects with locally varying movement across the image. A review of image registration techniques applied to abdominal images revealed rigid registration was only used as a pre-processing step before a more complex deformable transformation [72, 85, 86]. Deformable (non-linear) registration permits locally varying changes in the deformation field across the image and is discussed further.

2.3.1 Deformable Registration

Deformable registration techniques encompass a wide variety of algorithms which cannot be comprehensively presented here. How a registration algorithm minimises the difference between two images depends on the constraints and deformation model used. The physical basis of the abdominal motion makes a case for using physically imposed constraints for the registration. Two widely used examples are elastic sheet and fluid based registrations.

Elastic registration

The Navier-Cauchy partial differential equation is often quoted as a generalised basis for modelling an elastic body for incorporation into a registration algorithm [87, 88]:

$$\mu \nabla^2 \underline{u}(x,y,z) + (\lambda + \mu)\nabla\left(\nabla \cdot \underline{u}(x,y,z)\right) + \underline{F}(x,y,z) = 0 \qquad \text{Eq 2.7}$$

Where $\underline{u}$ is the displacement field, $\underline{F}$ is an external force field acting on the elastic body at each point, ∇ is the del operator and ∇^2 the Laplace operator, λ is Lamé's first elasticity coefficient and μ is the second Lamé coefficient or shear modulus [87]. λ and μ together characterise the material's properties and response to external forces. The shear modulus defines the amount of shear strain resulting from a given force i.e. a larger shear modulus increases the material's rigidity and resistance to shear. The first Lamé coefficient, λ, does not have a definable physical interpretation but contributes to the Young's Modulus, E (Eq 2.8), and is closely related to the Poisson's ratio, v (Eq 2.9).

$$E = \frac{stress}{strain} = \frac{\mu(3\lambda + 2\mu)}{\lambda + \mu} \qquad \text{Eq 2.8}$$

$$v = \frac{\lambda}{2(\lambda + \mu)} \qquad \text{Eq 2.9}$$

The Young's Modulus is the ratio of stress to strain. The Poisson's ratio is a ratio of orthogonal strains within an object. It defines the extent a deformed object contracts/expands in the direction perpendicular to an applied stretching/compression, e.g. the thinning and necking of an elastic band as it is stretched.

The Navier-Cauchy equation (Eq 2.7) describes a physical elastic material but it can be usefully aligned with concepts relevant to registration discussed in Section 2.2 (regularisation/constraints, deformation model). As in 1D, the driving forces, $\underline{F}$, and internal stress forces within the elastic sheet resisting the deformation are required to balance and reach equilibrium. In image registration, the driving forces can be derived from the optimisation strategy: an example could be Eq 2.5 in the 1D case.

The other two terms in Eq 2.7 relate to the displacement field $\underline{u}$ and control or regularise the deformation by imposing constraints. The first term multiplies the Laplace operator by the

shear modulus, μ, to moderate the rate of change (or curvature) in the deformation field. In image registration, this biases solutions towards smoothness in the deformation field. A larger shear modulus creates larger internal stress forces for the same changes in displacement, meaning smaller differences in neighbouring displacements will be permitted before balancing with the external force, $\underline{F}$.

The second term uses the sum of both Lamé coefficients to control the rate of change of expansion and contraction at all points across the deformation field. As shown in Eq 2.8 and Eq 2.9, as $(\lambda + \mu)$ increases, the Young's Modulus increases and the Poisson's ratio decreases. This means a greater force is required for the same strain to occur in the object or, in terms of registration, smaller displacements in the deformation field.

Clearly, the two coefficients, λ and μ, strongly influence the resulting deformation field. The selection of appropriate material properties that reflect the physical body captured in the images is an important task for image registration. If the underlying physical structure is accurately modelled, the deformation obtained from image registration should more closely reflect the actual deformation which had occurred in the physical world.

The elastic body model is a well-established technique finding widespread use and is widely regarded as reliable [68]. The constraints associated with the Navier-Cauchy equation (Eq 2.7) mirror physical constraints that encourage the deformation field to remain smooth, suppressing discontinuities. This can be problematic for large deformation gradients: significant locally varying deformations may be inadequately accounted for because of the inherent resistance to stresses [89]. This is a potential problem for the abdominal images processed in this PhD (discussed later), but generally, the elastic sheet model has proven suitable for a wide range of medical problems and different organs: its first and most prevalent application is the brain [82].

Fluid registration

A fluid based image registration is modelled on the principles of fluid dynamics. The general equation describing a fluid is the Navier-Stokes equation and is similarly structured to Eq 2.7 [87]. The principal difference results from an applied force producing a steady state velocity field which has a time component rather than static displacements in an elastic body. Conceptually, forces (derived from the registration) drive the flow of a viscous fluid on which the moving image may be thought to have been 'printed' – honey has been suggested as a

suitable analogue [88]. In fluid based registrations, the penalty associated with the constraints opposing movement/flow is allowed to relax over time thus gradually allowing neighbouring elements to drift further apart [87, 90]. This can allow for larger, more localised deformations to occur in the warping procedure [70] but at the expense of computation time and potentially less robustness [91, 87].

Two specific registration algorithms were considered: ShIRT, which is loosely based on an elastic sheet and ANTs, which has a range of options including a fluid based model.

2.3.2 ShIRT

ShIRT was chosen as the principal registration algorithm for implementation in this PhD. It has a proven track record and is being increasingly recognised for its portfolio of different applications [71, 92, 93, 94, 95], including previous work on this project [63, 6]. ShIRT was developed locally by the Medical Physics Group in Sheffield and therefore its use was supplemented by a wealth of local experience and expertise. It is controlled via a command line interface, most commonly through a bundled library of commands in MATLAB called IRLab. Its accessibility within MATLAB facilitates incorporation of ShIRT commands into larger or existing MATLAB scripts.

The similarity metric used by ShIRT is the sum of square differences in intensity over all (n) pixels in the image, as in Eq 2.10.

$$R = \sum_{i=0}^{n} (f_i - m_i)^2 \qquad\qquad \textit{Eq 2.10}$$

Where *f* and *m* are the fixed and moving images and *R* is termed the residual, which provides a single value indicating the net difference between the two images. Eq 2.10 above is similar to the formulation in 1D in Eq 2.2. As stated previously, this project is concerned with registration of mono-modal, intra-patient images and an intensity-based similarity metric is considered suitable for such problems [70].

A displacement field is required to move the moving image to match the fixed image. In 2D, the displacement field is composed of spatially varying horizontal and vertical vector

components, u and v. The moving image, and therefore also the residual, are functions of u and v. In order to find the optimum registration solution, u and v must be determined so that the residual is minimised. The process of minimisation is similar to the 1D similarity metric minimisation described in Eq 2.3 in Section 2.2 and Appendix 1: the first derivative of the equation describing the residual is set to equal zero. In ShIRT, the residual is a function of the displacement at every node (see Section 2.2.3 for a description of nodes). Summation and multiplying out the squared brackets in Eq 2.10 results in a long quadratic equation consisting of the displacements at each node. Consequently, to find the minimum value of this term, a series of partial derivatives with respect to each of the vector components at each node ($\frac{\partial R}{\partial u_1}$, $\frac{\partial R}{\partial v_1}$, $\frac{\partial R}{\partial u_2}$ ...) are set to equal zero. The result is a series of simultaneous linear equations listed below and represented in matrix form[2]:

$$\frac{\partial R}{\partial u_1} = c_1 u_1 + b_1 v_1 + a_1 = 0$$

$$\frac{\partial R}{\partial v_1} = c_2 v_1 + b_2 u_1 + a_2 = 0$$

$$\frac{\partial R}{\partial u_2} = c_3 u_2 + b_3 v_2 + a_3 = 0$$

$$\vdots$$

$$\begin{bmatrix} c_1 & b_1 & 0 & \cdots \\ b_2 & c_2 & 0 & \cdots \\ 0 & 0 & c_3 & \cdots \\ \vdots & \vdots & \vdots & \ddots \end{bmatrix} \begin{bmatrix} u_1 \\ v_1 \\ u_2 \\ \vdots \end{bmatrix} + \begin{bmatrix} a_1 \\ a_2 \\ a_3 \\ \vdots \end{bmatrix} = 0$$

For convenience, this can be represented as: $[A]\{u\} = -\{a\}$ *Eq 2.11*

The components of *[A]* (*b_i*, *c_i*) and *{a}* are constants originating from the expansion of the bracket in Eq 2.10 (*f_i* values are constant as the fixed image is not a function of u and v). Solving these simultaneous equations for the vector field *{u}* provides the linearly approximated deformation field to minimise the residual. This process is repeated iteratively until a similarity criterion is satisfied. However, in order to rearrange Eq 2.11 to solve for *{u}*, the inverse of *[A]* must be taken. Experience has shown that *[A]* is usually near singular, which means the inverse

---

[2] NOTE: ShIRT actually contains an equation for the residual for every pixel. For simplicity, the equations above show the minimisation only at the nodal points.

cannot be taken and a solution for *u* and *v* is undeterminable. To amend this issue an extra regularisation term is added to the equation to ensure the left-hand-side of Eq 2.11 is non-singular. The Tickhonov regularisation matrix, in ShIRT, takes the form of the Laplace operator, ∇^2. A coefficient is also added to control the weighting given to the Laplace operation, called the smoothness coefficient, τ. Eq 2.11 is therefore modified to become Eq 2.12 below.

$$\tau\nabla^2\{u\} + [A]\{u\} = -\{a\}$$

Eq 2.12[3]

Eq 2.12 shares similarities with the generalised Navier-Cauchy equation (Eq 2.7) which describes the response of an elastic body. Although not formally based on the principles governing an elastic body, ShIRT is associated with an elastic-like behaviour due to the Laplace operation term maintaining smoothness in the curvature of the deformation field.

The smoothness coefficient strength, τ, and node spacing are the principal inputs to ShIRT. By default, the smoothness coefficient is not static but automatically adjusted between iterations in an 'adaptive mode'. The node spacing refers to the number of pixels between the nodal points in the final iteration of the registration. ShIRT uses a multiscale approach, starting at a coarse node spacing and reducing this value towards the specified node spacing. A displacement is calculated for the nodal points and the displacements for pixels in-between calculated by bi-linear interpolation. ShIRT has been used locally for many years and has proved robust and versatile. The default parameters are a nodal spacing of 4 and an adaptive smoothness coefficient (~30 for abdominal MRI images [63]) – these parameters have been optimised to be applicable to a wide variety of medical images.

In summary, the main characteristics of ShIRT, as used in this thesis (other options exist) are:

- **Similarity metric:** Sum of square differences in intensity at every pixel.
- **Optimisation strategy:** Linear approximation of displacements at nodal points in parameter space through minimisation of the similarity metric. A solution is provided by differentiation with respect to the nodal displacements to form a set of solvable simultaneous linear equations.

---

[3] The Laplace operator has been written in its continuous form but should strictly be written in its discrete matrix form to operate on a discrete deformation field.

- **Deformation model and regularisation:** Bi-linear interpolation of displacements between the nodal points and regularisation of the displacements through a Laplace operator to control the curvature in the resulting displacement field – suppressing sharp changes in displacement.

- **Multiscale approach:** ShIRT uses an iterative approach for each linear approximation. In the first iteration, ShIRT uses a coarse nodal spacing and the spacing is gradually reduced upon convergence at each scale. The nodal spacing is reduced to an amount specified by the user (4 pixels by default).

- **Convergence criteria:** Convergence is confirmed, both within each stage of the multiscale approach and on the final result, when the average displacement vector falls below 0.1 of a pixel/voxel[4].

Arguably, ShIRT's main advantage over many other registration programs is that it can be applied, to good, robust effect without the time consuming, careful selection of appropriate registration parameters. Moreover, the computational simplicity of ShIRT's similarity metric and optimisation strategy (iteratively linear approximated deformation field) makes convergence quick compared to most other algorithms (e.g. ANTs) [92].

ShIRT was extensively tested during the previous PhD for the application of movement analysis in abdominal cine-MR images similar to those used during this current PhD. Assessment on deformations imposed on clinical images found that ShIRT accurately matched the imposed deformations where the deformation was not too large (<~10 pixels on a 512x512 image). This has implications for movement/time between frames in the dynamic MRI but the work supported the use of ShIRT for the registration of different time points in abdominal dynamic MRI sequences. The effects of noise were also explored to find that ShIRT copes effectively with noise and explicitly the noise levels typically encountered in the MRI images of this project are comfortably within tolerance.

On the basis of this background it was not necessary to complete another in-depth assessment of ShIRT's suitability for image analysis in this current PhD. ShIRT was adopted for the remainder of this work.

---

[4] The option exists for convergence to be reached based on the maximum displacement being <0.1 pixels as opposed to the average displacement. The user also has the option to set different convergence criteria including those based on the similarity metric.

Brief comparison of ANTs and ShIRT

Although, this project has used ShIRT as the main choice of registration algorithm, others have been explored during the PhD, namely, The Advanced Normalization Tools (ANTs). This sub-section is not intended to offer an in-depth comparison but communicates a limited qualitative experience of using both registration algorithms. ANTs is a large open source registration project and is regarded as one of the world leading registration toolkits [96]. ANTs contains a choice of several different deformation models including elastic, fluid and diffeomorphic. Its use required significant preliminary effort to gain familiarity with the large number of different parameters and inputs before it could be used effectively. Selection of suitable values for each of the inputs required significant investment. This was in stark contrast to the ease with which a first successful registration was accomplished using ShIRT. Once a suitable set of parameters for ANTs was selected, it proved less reliable and commonly took 10 times longer to converge for the 2D images presented in Figure 2.1. The literature suggests that with more time and further optimisation it is likely ANTs would be able to achieve a more accurate registration but ShIRT displayed other advantages (convergence time, ease of use, local expertise, MATLAB interface) and its performance proved more than adequate for the problem presented.

2.4   Review of image processing in abdominal imaging

The knowledge assimilated in previous sections is useful for discussion of the different image processing techniques applied to the complex anatomy of the abdomen. Accurate computational movement analysis of the whole abdomen is recognised as a difficult challenge and the related literature is sparse [86, 97, 98, 99, 100]. Complications are introduced by highly mobile organs, deformability of objects such as the bowel, large differences in relative movements between objects and large (mostly discontinuous) sliding motion occurring between adjacent structures. Coping with sliding motion is critical to this project and is discussed in a separate sub-section, Section 2.4.1.

The literature referring to abdominal registration is primarily limited to renal or hepatic applications [69]. These are coherent structures that lack many of the properties that make the intestines a challenge for image registration. Mani and Arivazhagan (2013) have produced a comprehensive review of different image registration techniques and categorised registration applications into different parts of the anatomy [70]. Several papers detailing abdominal registration techniques are mentioned but the focus of all the papers is on the kidney, liver or

prostate with none attempting to apply registration to the bowel [70]. These organs are less mobile, less deformable and structurally dissimilar to the bowel (the main organ of interest to this PhD); therefore registration techniques to these structures are less applicable and are not discussed further.

Several have attempted to create bespoke abdominal registration algorithms. One example is Freiman et al. (2012) whose algorithm focused specifically on addressing the problem that many of the organs in the abdomen can move independently of one another [72]. The registration technique was tested on abdominal CT and diffusion weighted MR images and good results were claimed relative to previously applied techniques [72]. Osorio et al. (2010) developed a non-rigid registration technique based on Fourier analysis that was claimed to be appropriate for highly deformable regions such as the abdomen [85]. Lausch et al. (2011) developed a registration technique for dynamic contrast MRI abdominal images. Their algorithm attempted motion correction in images with changing intensities resulting from contrast agents [101]. The bespoke registration algorithms reviewed were not readily available/accessible and were all produced for specific purposes that do not encompass the work and requirements of this PhD. Creation of our own bespoke registration algorithm was an initial consideration but ultimately ShIRT combined with image processing was a preferred, more feasible option for this specific challenge.

Registration has been used to assess small bowel motility by looking at the displacement of the bowel wall as it contracts in a dynamic MR image i.e. looking at the bowel cross-section [84]. Image registration was applied to a small section of bowel to analyse the motion of the wall rather than the abdominal contents as a whole and specifics of Odille et al.'s technique were deemed not relevant to this project. Despite the differences in application, there are overlapping concepts. For example, the authors note problems with bowel segments moving through the 2D image plane; this is a feature observed in our cine-MR images. The group claim their methods can detect a difference between temporal intensity changes due to in-plane motion and through-plane motion. It must be noted that some of the through-plane motion in their study was due to contrast solution propagating through the plane which is not applicable to this PhD's cine-MR images. Their technique was tested preliminarily on both *in silico* and real patient data with a proposal that the next stage of development should be towards 3D imaging with a parallel computing, 3D registration solution.

In summary, there is little relevant literature regarding registration techniques that have been applied to specifically assess bowel motion within the abdomen and none that have been applied for abdominal adhesion detection (other than work by Medical Physics in Sheffield [63]). A moderate number of publications detail highly specialised registration algorithms aimed at other organs in the abdomen. Odille's (2012) registration approach to measure small bowel motility is the only paper reviewed where registration has been applied to the bowel itself and some aspects of Odille's work are applicable to this project [84].

2.4.1 Coping with sliding geometries

A discontinuous displacement of two adjacent sliding objects, such as the abdominal contents against the abdominal wall, challenges registration algorithms [86, 97, 99, 100, 102]. The literature has primarily focused on the creation of specialist registration algorithms with appropriate mechanisms to adequately cope with and accommodate the sliding motion [86, 97, 98, 102]. For example, Kiriyanthan et al. (2016) utilise a custom-made motion segmentation tool to identify the discontinuity and sharpen the deformation field in that region [102]. They presented preliminary results showing a more accurate replication of the motion discontinuity for the liver sliding against the abdominal wall when compared to methods previously described in the literature. However, one of the ambitions of this PhD is to interrogate the sliding motion itself, which is a different challenge to most of the cases referenced above. Creation of a bespoke registration technique to accurately report displacements in sliding geometries, as well as addressing the other challenges presented by abdominal imaging mentioned previously, was discounted as an effective strategy for this PhD.

Fluid registration was expected to accommodate the sliding boundary more accurately due to the relaxation in the smoothness constraints acting on the deformation field. However, without custom modifications it is unlikely to be accurate enough to provide a measurement of the sliding itself for distinguishing subtle reductions in sliding. Acknowledging the greater suitability of fluid registration for sliding geometries, the concept of using displacement information derived from a fluid-like registration to segment the abdominal contents could be relevant and has been explored in Chapter 6, Section 6.5.

Others have attempted to cope with sliding using segmentation techniques. Pace et al. (2011) used a combination of segmentation and a bespoke registration algorithm specifically to cope

with sliding organs in the thorax and abdomen during respiration. Their technique revolves around segmentation of abdominal CT images isolating the liver, kidneys, spleen and spine while the other organs, such as the intestines were discarded (masked out). The registration was then performed with a set of constraints imposed on the deformation model for improved preservation of the discontinuity; greater correspondence was quantitatively demonstrated [86]. However, not all of their registration constraints are applicable to the bowel thus the usefulness of their algorithm in our context was unclear.

A handful of publications have recognised the diagnostic potential in measuring the sliding motion between anatomical structures. Amelon et al. (2012) and Ding et al. (2009) have developed methods to measure the sliding motion between lung lobes [103, 104]. They first separate the lobes using a specialist, automated segmentation algorithm based on the airway tree and vascular tree generated from CT images [105]. The movement of each lobe is then analysed independently from one another using image registration and the deformation fields subsequently recombined to form a complete assessment of motion in the lung. The relative differences in motion at the sliding interface were then analysed to quantify the inter-lobe sliding. Implementation of a similar method, developed independently, is the primary focus of this PhD and is covered in the next chapter.

2.5 ShIRT and sliding geometries

In most applications the smoothness parameter applied to the deformation field is important to ensure a stable registration. However, in the case where motion is discontinuous it enforces a resistance preventing it from conforming to sharp changes (discontinuities) in displacement, thus preventing the registration from accurately reporting the actual motion which occurred. This concept is illustrated in Figure 2.6 where an artificial, perfect discontinuous fault has been introduced. A rectangular section of an MR image (highlighted in red in Figure 2.6) was stretched relative to the rest of the image which remained fixed. The amount of movement and shear is known, therefore allowing comparison with the registration result. Two frames with different stretch applied to the rectangular section were registered using ShIRT. The magnitude of the smoothing parameter was varied to create different motion profiles across the discontinuous motion boundary, displayed in the graph in Figure 2.7.

(a) *(b)*
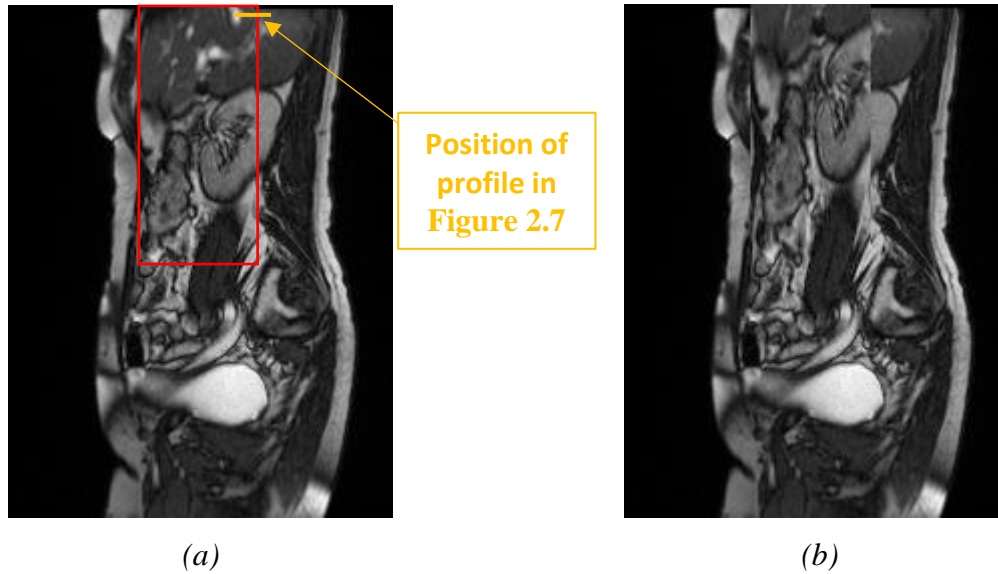
Figure 2.6: Sagittal MRI slice showing images with a stretched rectangular region relative to the surrounding image [3]. The displacement at the top of the red rectangle in (a) was 2 pixels and at the bottom of the red region there was a 0 pixel displacement. (b) shows the final frame stretched by 50 pixels. The yellow line at the top of (a) indicates the location of the displacement profiles in Figure 2.7.
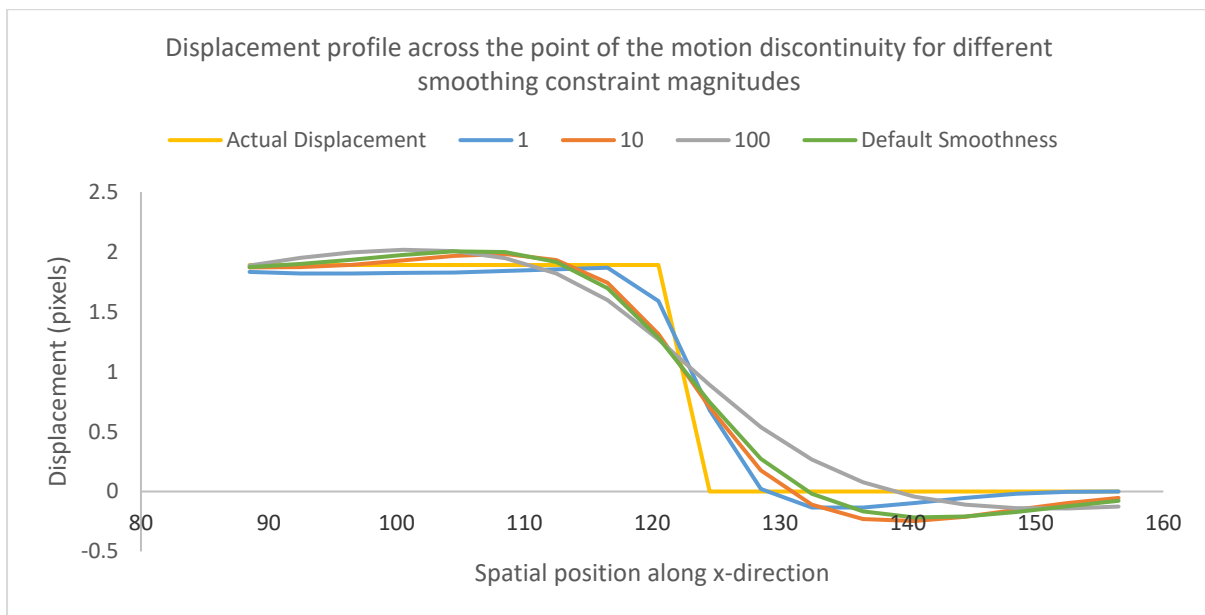
Figure 2.7: Graph showing the deformation profile across the sliding boundary shown in Figure 2.6 with different smoothing magnitudes. (The numbers in the legend correspond to the magnitude of the smoothness constraint).

It is apparent in Figure 2.7 that the more the smoothing factor (τ) is relaxed (smaller magnitude) the more the deformation field is able to conform to the discontinuous motion. Despite this, the actual displacement field cannot be accurately reported by the registration algorithm regardless of the smoothness constraint applied. With a relaxed smoothness parameter of magnitude 1, the discontinuity (which is across 1 pixel) was spread over approximately 10 pixels.

Discontinuities in clinical images may be less abrupt, but as shown in Figure 2.7, this is still not achievable by modifying the smoothness parameter in ShIRT. A smoothing factor of less than 1 could be implemented to further conform to the discontinuity but as expected for such low values the resultant deformation field becomes erratic as shown in Figure 2.8. The deformation generated in Figure 2.6 was both simple (a uniform elastic stretch) and small in magnitude, and represents an idealised case. In more complex images with localised deformations, using such a relaxed smoothness constraint would likely result in a poor registration elsewhere in the image. Manual control of the smoothness parameter τ, also prevents the use of ShIRT's default adaptive smoothness functionality, which, given its proven record, is undesirable.
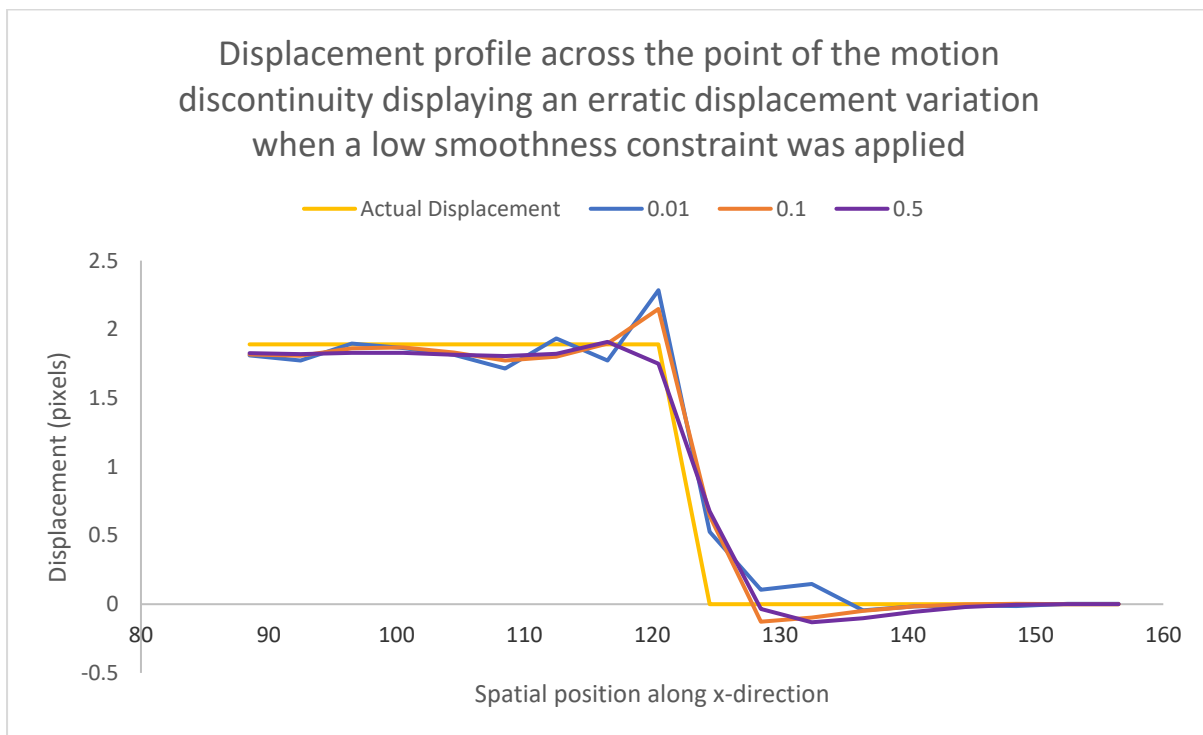
Figure 2.8: Erratic behaviour of the registration algorithm across the sliding boundary in Figure 2.6 when a smoothness constraint <1 is applied to an idealised scenario

Fundamentally, it is not possible to identify a single smoothness constraint that can both accurately accommodate the discontinuous motion and produce a reliable registration elsewhere. This precipitated a search for an alternative approach to determine the relative displacement between sliding objects.

2.6 Discussion of previous work in the context of image processing

The knowledge gained in Chapter 1 and the theory discussed in this chapter has implications for the approach taken to characterise the resistive effects of adhesions on motion of the abdominal contents. This section uses the principles discussed to identify pitfalls in the approach of the previous PhD and proposes solutions to inform the direction of the project.

Previous work has shown the ability of image registration to aid detection of anomalous movement patterns. The main evidence for this has resulted from promising ROC curves generated from semi-idealised *in-vitro* and *in-silico* data supported by preliminary clinical application [63, 6]. Some success was demonstrated in the identification of gross adhesive pathology (EPS) from abnormal motion signatures. In EPS, a large 'block' of abdominal contents was observed to move en masse throughout the respiratory cycle. The reason for pursuing diagnosis of this condition was that the difference between normal and abnormal movement is pronounced and therefore potentially easier to detect. A processing protocol was implemented in the form of AbsCAT (described in Chapter 1), which:

- Selected 2 frames at opposite ends of the respiratory cycle from a dynamic MR image sequence (i.e. the frames between which maximal abdominal excursion had occurred)
- Registered the two frames to quantify the movement which had occurred
- The movement of the abdominal contents was then displayed in the form of arrows/vectors displaying the magnitude and direction of the movement and/or contours depicting the magnitude of the movement

Several problems have been identified with AbsCAT's approach; outlined below:

1) **Problem:** Movement of objects in/out of the imaging plane:

   The abdominal cavity is a 3-dimensional volume and although during the respiratory cycle the predominant motion of the abdominal contents is superior–inferior there is still some lateral–medial movement. Objects moving laterally will appear/disappear in/out of the 2D sagittal imaging plane. Selection of frames at either end of the respiratory cycle maximises the displacement of objects superiorly/inferiorly but also laterally/medially; thus creating maximal disparity in the number of matching objects contained in both images. This contravenes one of the fundamental assumptions made by image registration algorithms (discussed at the start of Section 2.3): 'The same objects must be present in both images being registered'. Consequently, the resulting deformation field is likely to contain

movement signatures which are false and do not reflect the actual motion which has taken place (i.e. the object moving out of the imaging plane). This is a problem with imaging a 3D object in 2D generally, as highlighted by Odille et al. (2012) [84], but it is exacerbated by the methodology of the previous PhD by selection of frames at either end of the respiratory cycle.

Proposed Solutions: Focus on the perimeter of the abdominal cavity and register consecutive frames

The abdominal wall and other areas bordering the abdominal cavity almost always remain in the sagittal imaging plane. An object tethered to the outer perimeter of the abdominal cavity should therefore also largely remain within the imaging plane. Therefore, to combat the effects of out of plane motion, adhesions to the outer boundary of the abdominal cavity should be selected for interrogation. Added justification for this approach is provided by the fact that the anterior abdominal wall is the most common site of adhesion formation [30]. Furthermore, if abdominal surgery is planned (e.g. adhesiolysis) it is important to be aware of any bowel loops adhered to the abdominal wall to avoid complications such as bowel perforation during incision. This approach will not completely remove the issue of out of plane motion but should reduce its impact for 2D analysis.

Registration of consecutive frames is likely to further reduce the effects of out-of-plane motion. By considering frames only ~0.4 seconds apart, objects with a lateral/medial motion component gradually disappear/appear over several frames. Although still a source of incorrect motion interpretation, this lessens the severity of anomalous signatures in the deformation field and allows for some degree of capture of the component of motion within the sagittal slice being interrogated.

2) **Problem:** Ability of the registration algorithm to replicate large motions:

Assuming objects remain in the imaging plane between both images, if the displacements occurring between the two images has been very large the registration algorithm may not converge to a correct solution. If two objects are particularly distant, the registration algorithm is less likely to identify and match corresponding objects. This is particularly difficult in the abdominal cine-MRI where several objects are similar in appearance (i.e. structure, intensity and contrast). The registration is more likely to converge to a local minimum requiring a smaller deformation. As mentioned in Section 2.3.2, ShIRT was

found to struggle with large deformations (>10 pixels) during tests performed in the previous PhD. A rough estimation of the excursion in the upper abdomen was made in a single cine-MRI recognised to have a large amount of movement. An excursion in the upper abdomen of 23 pixels between maximum inhalation and exhalation was measured. This amounts to a movement of approximately 4 pixels between frames[5].

Proposed Solution: Registration of consecutive frames

An approach of registering consecutive frames should be sought to limit the displacement of objects between registrations, making convergence to a correct solution more likely.

3) **Problem:** Inaccurate reporting of actual movement which occurred:

AbsCAT selected images at either end of the respiratory cycle for registration. This approach means the abdominal contents have been maximally displaced between the two images. If points 1) and 2) above were not problematic and the registration algorithm did manage to provide a mapping from one image to match the other accurately, it would do so in a way that did not necessarily reflect the true path each object had taken to get from point A in image 1 to point B in image 2. The actual, real-life movement that has taken place in the abdomen through the respiratory cycle cannot be confidently inferred from the resulting registration map. Figure 2.9 illustrates this point by plotting the actual path of a bowel loop throughout the respiration (green) alongside the path most likely plotted by the registration algorithm (red).
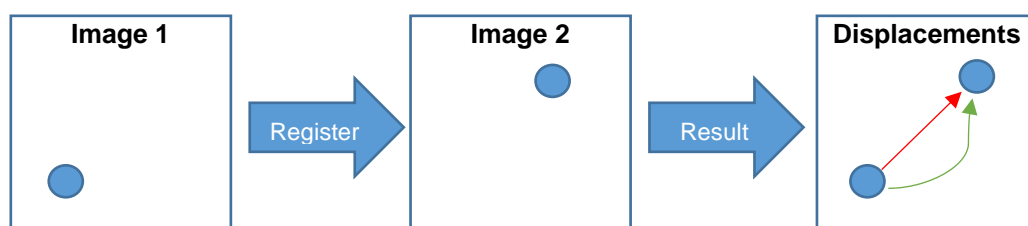
Figure 2.9: Diagram depicting a scenario where the registration has successfully matched the two images but has failed to replicate the actual path moved by the object between the two images. Actual Path = green arrow, incorrect registration path = red arrow.

---

[5] Estimation of movement between maximum inhalation and exhalation was made by selecting like points in the upper abdomen (using MATLAB). To approximate the movement between frames the excursion of 23 pixels was divided by the number of frames (6 frames) between the maximum inhalation and exhalation.

Proposed Solution: Registration of consecutive frames

Given a sufficient temporal resolution in the cine-MRI, it is possible to observe the path taken by objects throughout the respiratory cycle. Registration of each frame to its proceeding frame permits more accurate recreation of the path of the abdominal contents.

4) **Problem:** Inaccurate analysis of sliding geometries

Sliding geometries present a problem for most registration algorithms by presenting a region that does not comply with the smoothness/curvature constraints imposed on the deformation field. In the abdomen, the abdominal contents slide against the perimeter of the abdominal cavity with different modes of motion, as depicted in Figure 2.10. This type of motion system is analogous to the movement discontinuity discussed in Section 2.4.1 resulting in the registration algorithm poorly reporting the actual movement occurring around the sliding interface.

Figure 2.10: Typical abdominal MR image with the principal modes of motion highlighted either side of the sliding boundary

Proposed Solution: Segmentation of the abdominal cavity from its confines

Instead of attempting to accommodate the sliding motion in order to achieve a more accurate registration, the focus was changed to develop a method specifically designed to interrogate the sliding motion itself. In order to calculate the visceral slide, it is essential to quash the effects of the registration algorithm's smoothness constraint in the region of sliding. Relaxing the smoothness parameter would be one option but as shown in Figure

2.8, this is unlikely to be achieved without impacting the stability of the registration in the rest of the image. Another method to achieve this is segmentation of the abdominal contents from the remainder of the image based on the sliding boundary itself. Figure 2.11 shows the application of an ROI to segment the abdominal contents.

Figure 2.11: Example of a region of interest drawn to segment the abdominal contents from its surroundings

Once separated, the motion in each of the individual regions can be analysed independently without interference from the other region. Subsequently, a more accurate calculation of the amount of sliding at the interface is made possible, as described by Amelon et al. (2012) [103].

2.7 Summary

Sagittal abdominal MR images are complex, containing many different structures and, therefore, pose an image processing challenge. Movement analysis of such complex data is particularly challenging since movement out of the imaging plane and motion discontinuities are observed. The literature is markedly barren in terms of similar image processing applications in the abdomen. However, a handful of noteworthy contributions for coping with sliding geometries in other anatomical areas, particularly in the lung lobes, have been highlighted. An introduction and review of the principles and techniques of image

segmentation and image registration has precipitated a different approach to that taken in the previous PhD. The previous AbsCAT approach suffered from numerous limitations, namely:

1) Large degrees of out of plane motion
2) Large movements between registered images, leading to unsuccessful registration
3) Inaccurate replication of the actual path taken by abdominal structures due to only considering end points of the respiratory cycle
4) Failure to cope with sliding geometry at the abdominal wall and the rest of the abdominal cavity perimeter

A method combining image segmentation and registration has been proposed to alleviate these issues; an approach also sanctioned by the literature [103, 104]. These suggested improvements have been combined to formulate a new image processing method described in Chapter 3.

Chapter 3

Visceral slide analysis for the detection of abdominal wall adhesions

3.1 Introduction

In the healthy abdomen the contents slide smoothly against the perimeter of the abdominal cavity (abdominal wall, back muscles etc.) during respiration – a process termed visceral slide. This chapter outlines the methodology taken to produce an image analysis workflow aimed at quantifying the visceral sliding motion at the interface between the abdominal contents and the structures surrounding the abdominal cavity.

The move towards a visceral slide analysis technique represents a shift away from the processing methodology implemented in the previous PhD in the form of AbsCAT (described in Section 1.5). The knowledge assimilated in Chapter 1 and principles discussed in Chapter 2 culminated in the rationale described in Section 2.6 and suggested changes to the approach taken. The visceral slide quantification technique subsequently described through this chapter represents a refinement aimed at the detection of more subtle abnormalities while combating some of the pitfalls encountered during the previous PhD.

3.1.1 Mathematical Background

Before describing the refined technique, some concepts on which the technique are based need to be introduced. The principal aim of the technique is to quantify the sliding of the abdominal contents against the abdominal wall. Image registration and segmentation are employed to achieve a quantitative description of the movement in the dynamic image and these have already been introduced in Chapter 2. The specific mathematical entity which is calculated to

quantify sliding is the displacement gradient tensor. A brief introduction to the relevance of the tensor follows.

An introduction to tensors, stress and strain

The order of a tensor depends on the number of basis components. Displacement vectors that represent movement can be recognised as first order tensors. In three-dimensional space these have three basis components, typically *[x, y, z]* (relevant to unit vectors *[$\hat{\underline{i}}$, $\hat{\underline{j}}$, $\hat{\underline{k}}$]*), that together describe the magnitude and direction of the vector. This thesis is concerned with second order tensors relating to stress and strain, which, in three dimensional space, have nine components. If considering the forces acting on an elemental cube in Cartesian space, they result in three components of stress acting on each face of the cube. For the x-face this would could be denoted: σ_{xx}, σ_{xy}, σ_{xz}, where the first subscript refers to the face on which the stresses are acting and the second subscript the Cartesian component of the stress. When considering the stresses acting on the whole cube they can be represented as a 3x3 matrix (or second order tensor) which fully describes the forces or stresses on/in the cube.

Using the displacement gradient tensor

The displacement gradient tensor is a second order tensor which characterises the local deformation of a material in response to applied stresses by examining the derivatives in displacement between neighbouring points. In two dimensions, the displacement field at any point has horizontal and vertical components *u(x,y)* and *v(x,y)* and the displacement gradient tensor, *ε*, has four components: two relating to tensile strain and two shear strain components. The displacement gradient tensor is shown in Eq 3.1.

$$\begin{bmatrix} \dfrac{\partial u}{\partial x} & \dfrac{\partial u}{\partial y} \\ \dfrac{\partial v}{\partial x} & \dfrac{\partial v}{\partial y} \end{bmatrix} = \begin{bmatrix} \begin{array}{c} Horizontral \\ Tensile \\ \varepsilon_{xx} \end{array} & \begin{array}{c} Horizontal \\ Shear \\ \varepsilon_{xy} \end{array} \\ \begin{array}{c} Vertical \\ Shear \\ \varepsilon_{yx} \end{array} & \begin{array}{c} Vertical \\ Tensile \\ \varepsilon_{yy} \end{array} \end{bmatrix} \qquad Eq\ 3.1$$

Where *x* and *y* give the spatial position and ε_{xx} the strain between the x-component along the x-axis, ε_{xy} the strain between y-components along the x-axis etc.. It is the shear components (ε_{xy} and ε_{yx}) of the displacement gradient tensor that are used as the quantifiable parameter to describe the visceral sliding which has occurred.

If a continuous vector field describes the displacements which have occurred in the image, the displacement gradient tensor calculated from this field fully describes the strain which has been imposed across the entire image. The principal advantage of using tensors to describe the strain is that it allows determination of the strain irrespective of rotation: for example, two observers looking at a strain field from two different perspectives will report the same magnitude of strain. This concept is highlighted by an analytical derivation of the displacement gradient tensor for a specific vector field in Appendix 4.

The implementation described in this chapter

If the deformation in the image was described by a continuous function, the displacement gradient tensor components could be formed as a series of equations exactly describing the strain in the image (such as in Appendix 4). However, discretisation of the images and a lack of an exact analytical description of the deformation, necessitate approximations in the calculation of the tensor. In this implementation, the differential between neighbouring vectors has been used to approximate the displacement gradient tensor derivatives at each point in the image.

The flow diagram in Figure 3.1 outlines the mathematical process of calculating the displacement gradient tensor and the magnitude of shear strain along the abdominal wall.
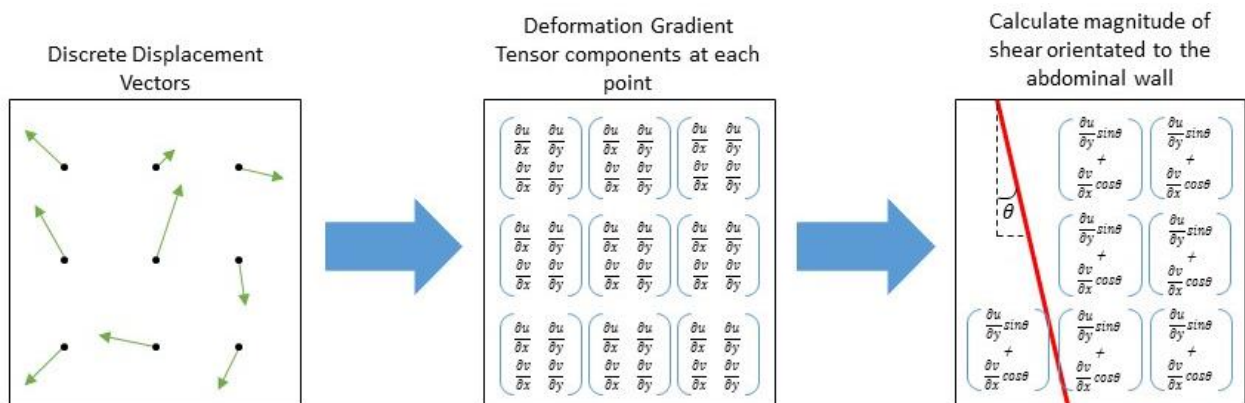
Figure 3.1: Outline of the calculation of the displacement gradient tensor and the component of shear aligned with the boundary extracted from a known displacement field. Shear expression is expected along the boundary. Please see the subsequent sections for a detailed description of this process.

Note: The author would like to note the distinction between shear and shear strain. Calculations of shear in this thesis refer to the differential in the displacement components perpendicular to the length between neighbouring nodes and is quoted in pixels. Shear strain

is a dimensionless quantity. In this thesis, shear strain pertains to the shear per nodal spacing. If using ShIRT, this is the displacement difference in pixels per node spacing of 4 pixels. As shear strain is defined as shear per nodal spacing and the shear values have been calculated between nodal points, shear strain and shear are analogous in the context of this thesis.

The Method section below describes the entire processing method step-by-step, amplifying the details of the process in Figure 3.1.

3.2 Method: Determining visceral slide

This method incorporates the principles discussed in Chapter 2 (image segmentation and registration) to determine the sliding motion at an interface between two sliding objects.

The analysis software was developed in MATLAB (version 2014b, MathWorks Inc.). The final product of the technique is the calculation of quantifiable shear as an analogue for the amount of sliding. Thus, the terms sliding and shear are used interchangeably, although a discussion regarding their interchangeability is covered in the main discussion chapter in Section 6.6. The method developed to calculate the shear naturally splits into 7 main components which will be described individually then summarised as an overall workflow, these are:

1. Pre-processing
2. Segmentation of the sliding regions
3. Image registration to acquire movement information
4. Calculation of the displacement gradient tensor
5. Calculation of the 'boundary shear/tensile strain'
6. Overlaying strain information on cine-MR images
7. Summation of shear/tensile strain across all frames

3.2.1 Pre-processing

Throughout the PhD each patient scan typically contained 5-7 sagittal slices (and 4-6 transaxial slices) with 30 frames in the dynamic image sequence for each slice (see Section 1.4 for details of the scanning protocol). The MR image files were provided in the DICOM (Digital Imaging and Communications in Medicine) image format. DICOM is a standardised medical imaging file format implemented to facilitate viewing, handling and transference of medical images [106]. DICOM files consist of two parts:

1) A header, containing metadata about the patient, imaging device and scanning parameters

2) The image data, containing the pixel/voxel intensities.

Before performing operations on the files, anonymisation and a series of pre-processing steps were completed. Most data were received on physical media (DVD) and once extracted onto the computer the following procedure was followed:

1. The files were reorganised so all images from the same patient and all frames from the same slice were grouped together in a sensible hierarchical folder structure.

2. The DICOM files invariably required the '.dcm' extension to be added and a MATLAB function *add_dcm_extension.m* was created to operate on the hierarchical file structure for each patient.

3. All folders containing the images were automatically renamed based on DICOM header information (acquisition time and slice orientation) using a MATLAB program *rename_folders_sag_trans.m*. The image files (the cine-MRI frames) were rarely ordered in the correct chronological order. A program was written (*rename_dicom.m*) to extract the order and rename the images according to their frame number e.g. 001.dcm.

4. Data would sometimes arrive not fully anonymised. Great care was taken to ensure all patient identifiable information was removed from every image file. A program was written in MATLAB specifically to do this: *anon_dcm.m*. This ensured a fully anonymised file replaced the original.

5. Finally, a video was created for every slice so the movement in the abdomen could be visualised. As the DICOM image files are now named according to their chronological order, their names were used to generate a video using *createvideo.m*. The framerate of the video can be altered as one of the inputs to the function. The creation of the video is essential for visualising motion in the image sequence to aid segmentation described in the next section.

The main visceral slide analysis program asks the user to select the folder containing the images to be processed and an output folder for the results generated. The program expects the files to be in chronological order and named as described above.

3.2.2   Segmentation of the sliding regions

Image segmentation refers to the process of separating different portions or regions in the image. Several methods of image segmentation have been discussed in the Section 2.1. A semi-automatic, registration based segmentation process was developed and implemented for the visceral slide processing technique, using custom code written in MATLAB. The aim of this segmentation procedure is to separate the abdominal contents within the abdominal cavity from the structures surrounding the cavity (for all images in the cine-MRI sequence). This requires the user to manually place ROI vertices around the abdominal cavity at the sliding interface on the first frame of the dynamic image series. To do so the user must combine information from the structural anatomy and movement from the cine video produced in step 5 of the pre-processing procedure. Figure 3.2 shows the positioning of ROI vertices around the abdominal cavity in the first frame of a typical left paramedian sagittal slice.
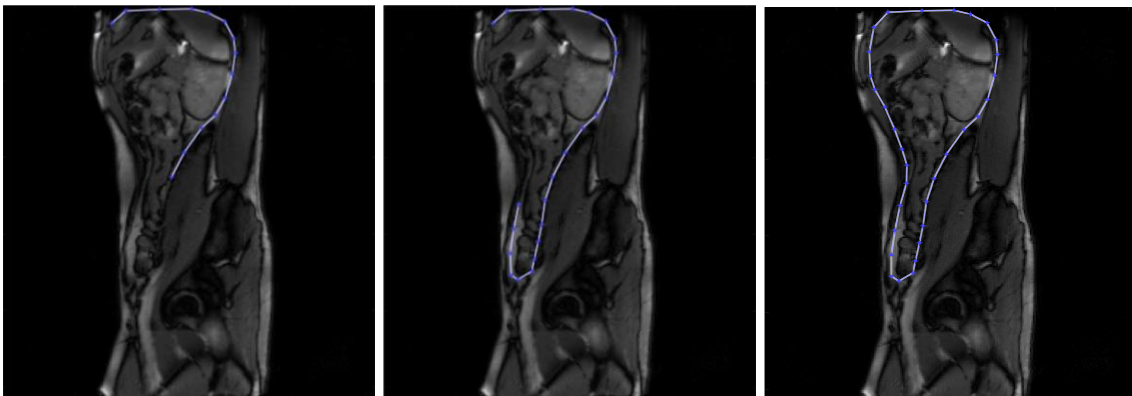
Figure 3.2: Example showing an ROI being drawn around the abdominal cavity in a left paramedian sagittal slice to separate the highly mobile abdominal contents from their relatively stationary surroundings.

Once the ROI is closed, the user is given the opportunity to edit the positions of the vertices before accepting. Once accepted, the program registers frame 1 to frame 2 (using ShIRT) and uses the deformation field to warp the ROI vertex positions to match the new position of the sliding interface in frame 2. The user is then given the opportunity to edit the ROI vertex positions in frame 2 before accepting the ROI. The accepted ROI vertices for frame 2 are then warped to frame 3 and so on. This process is repeated for all frames (usually 30 frames) in the time series.

This is the only user input required and the remainder of the operations described below are performed automatically.

Masking

An image mask is used to keep a region of the image unchanged, while setting all other pixels to an intensity of zero. The abdominal ROIs are used to create 2 masks for each frame; one keeping objects contained inside the ROI (the abdominal contents), the other its inverse, only retaining detail outside the ROI (abdominal surroundings). The two masks are applied to their respective image frames to produce two new sets of images. An example of the procedure is shown for a single frame in Figure 3.3.
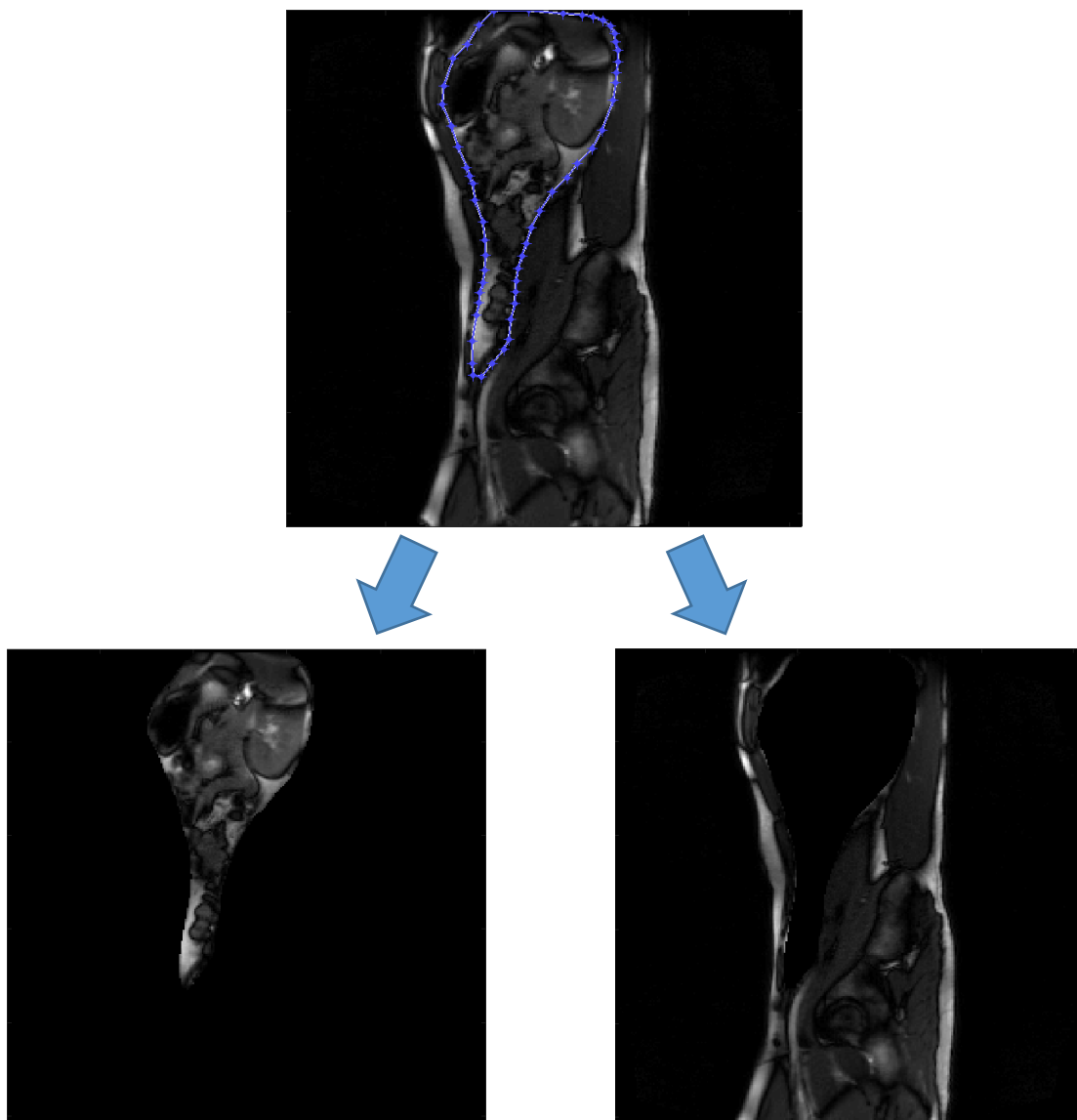
Figure 3.3: Example of the masking procedure which uses the ROI to produce two new sets of images: one containing the abdominal contents the other the abdominal surroundings

3.2.3 Image registration procedure

Two sets of masked dynamic image sequences have now been created, allowing for separate determination of the movement in each region without interference from the other. The vast majority of image registration was performed using ShIRT but the code has been constructed so that any registration algorithm could be easily incorporated. The ShIRT registration used the following default parameters:

- Node spacing = 4 pixels

- A particular smoothness constraint (τ) was not enforced and the default was an adaptive smoothness constraint to suit the problem presented.

Consecutive frames of the 'abdominal contents' images were registered (frame 1 → frame 2 etc.) to produce a deformation field corresponding to the movement between each frame. The same procedure was applied to the masked images of the 'abdominal surroundings'. The result is two sets of time varying deformation fields describing the movement across 30 frames within each of the respective regions.

Despite the registered images only containing detail from the unmasked region of the image, the deformation fields span across the whole image, including where the pixels are set to zero. This is shown by the green vectors spanning into the red zones in Figure 3.4. Thus, the masks produced in the segmentation process (Section 3.2.2) were re-applied to their respective deformation fields for each frame (mask for image 1 applied to deformation field corresponding to the registration of frame 1 → frame 2). This removed all the green vectors in the respective red regions in Figure 3.4, setting their value to zero and leaving only those vectors within the respective masks.
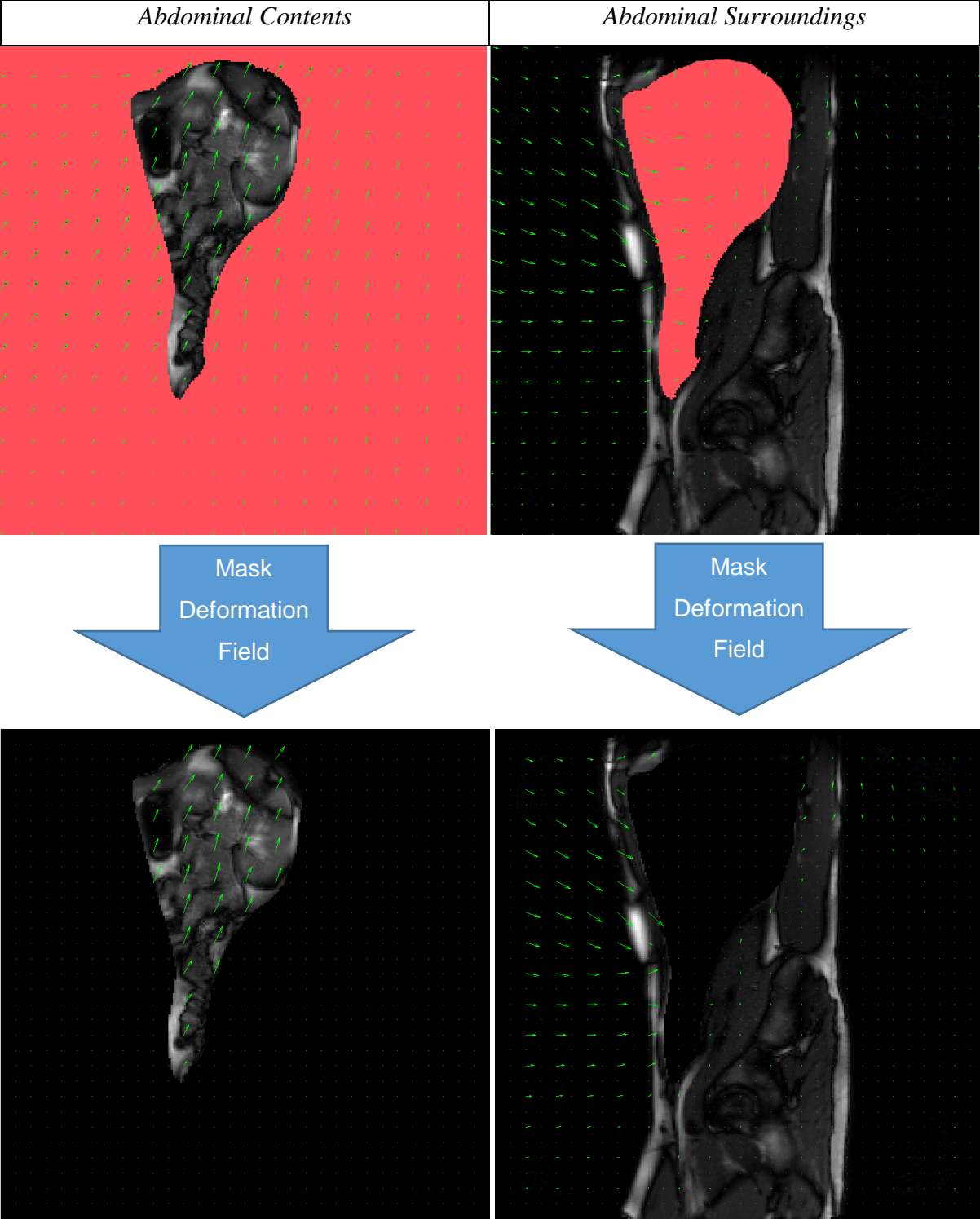
Figure 3.4: Deformation fields (green arrows) after registration of consecutive frames for abdominal contents (left) and abdominal surroundings (right). The red regions highlight the area outside the mask for each image and show the deformation field spreading into these regions. The deformation fields are themselves masked to produce two new deformation fields (bottom images).

The two masked sets of deformation fields were then recombined by summation to produce a full deformation field across the whole image for each frame. The result of this process is depicted Figure 3.5.
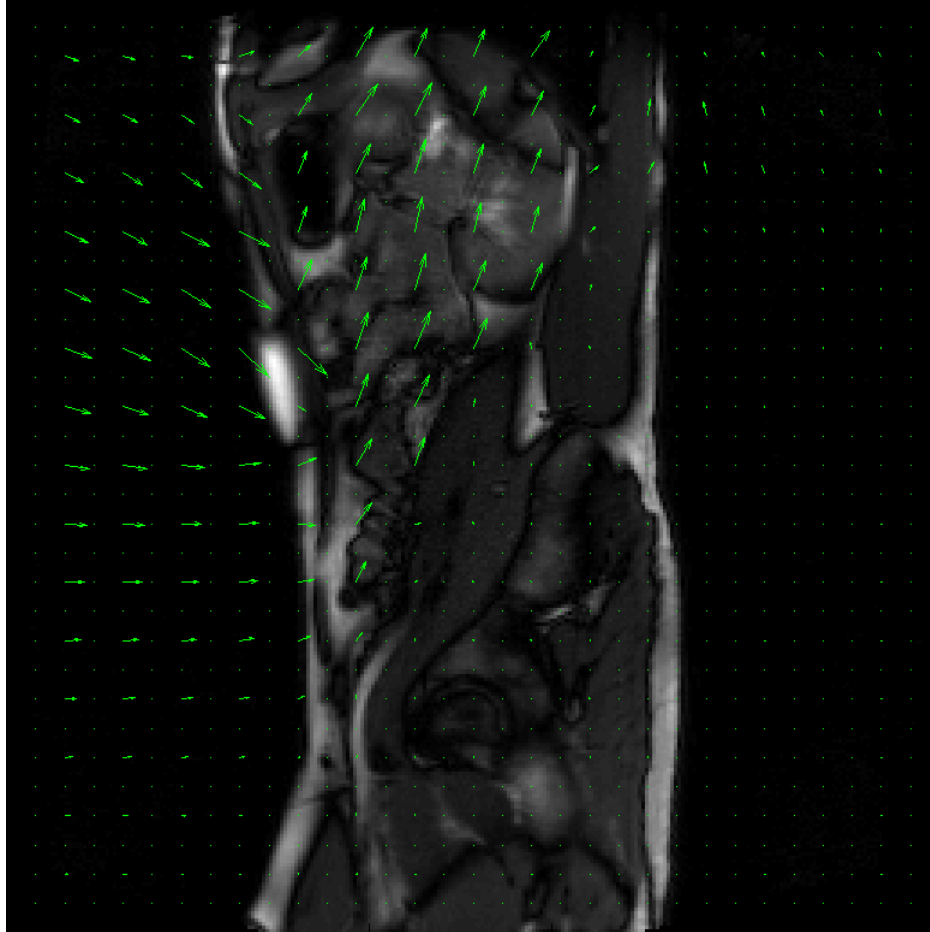
Figure 3.5: Combined deformation field from both the abdominal contents and surroundings shown in Figure 3.4 to produce a full deformation field describing motion across the whole image. A discontinuity in the displacement field is apparent at the ROI boundary.

The end of this process has produced a single set of time varying deformation fields describing the motion across all frames in the series.

3.2.4   Calculation of the displacement gradient tensor

The aim is to quantify and analyse the sliding motion which occurs around the edge of the abdominal cavity, and for this purpose the shear components of the displacement gradient tensor were calculated. The 2D displacement gradient tensor, *T*, has been described at the start of this chapter in Eq 3.1 and is repeated below for convenience.

$$
\begin{bmatrix}
\dfrac{\partial u}{\partial x} & \dfrac{\partial u}{\partial y} \\[2ex]
\dfrac{\partial v}{\partial x} & \dfrac{\partial v}{\partial y}
\end{bmatrix}
=
\begin{bmatrix}
\begin{array}{c} Horizontral \\ Tensile \\ \varepsilon_{xx} \end{array} & \begin{array}{c} Horizontal \\ Shear \\ \varepsilon_{xy} \end{array} \\[4ex]
\begin{array}{c} Vertical \\ Shear \\ \varepsilon_{yx} \end{array} & \begin{array}{c} Vertical \\ Tensile \\ \varepsilon_{yy} \end{array}
\end{bmatrix}
\qquad Eq\ 3.1
$$

Where *u* is the displacement along the *x* direction, *v* displacement along the *y* direction and *x* and *y* correspond to the spatial position. The components of the displacement gradient tensor are determined by calculating each of the derivatives over the deformation field. This is achieved by interrogating the linear difference in the vector component values along each direction between every nodal point in the deformation field.

The diagrams in Figure 3.6-3.10 demonstrate the displacement gradient tensor calculation procedure schematically. Figure 3.6 shows a simplified portion of a deformation field showing the displacements occurring around the interface between the two sliding regions.
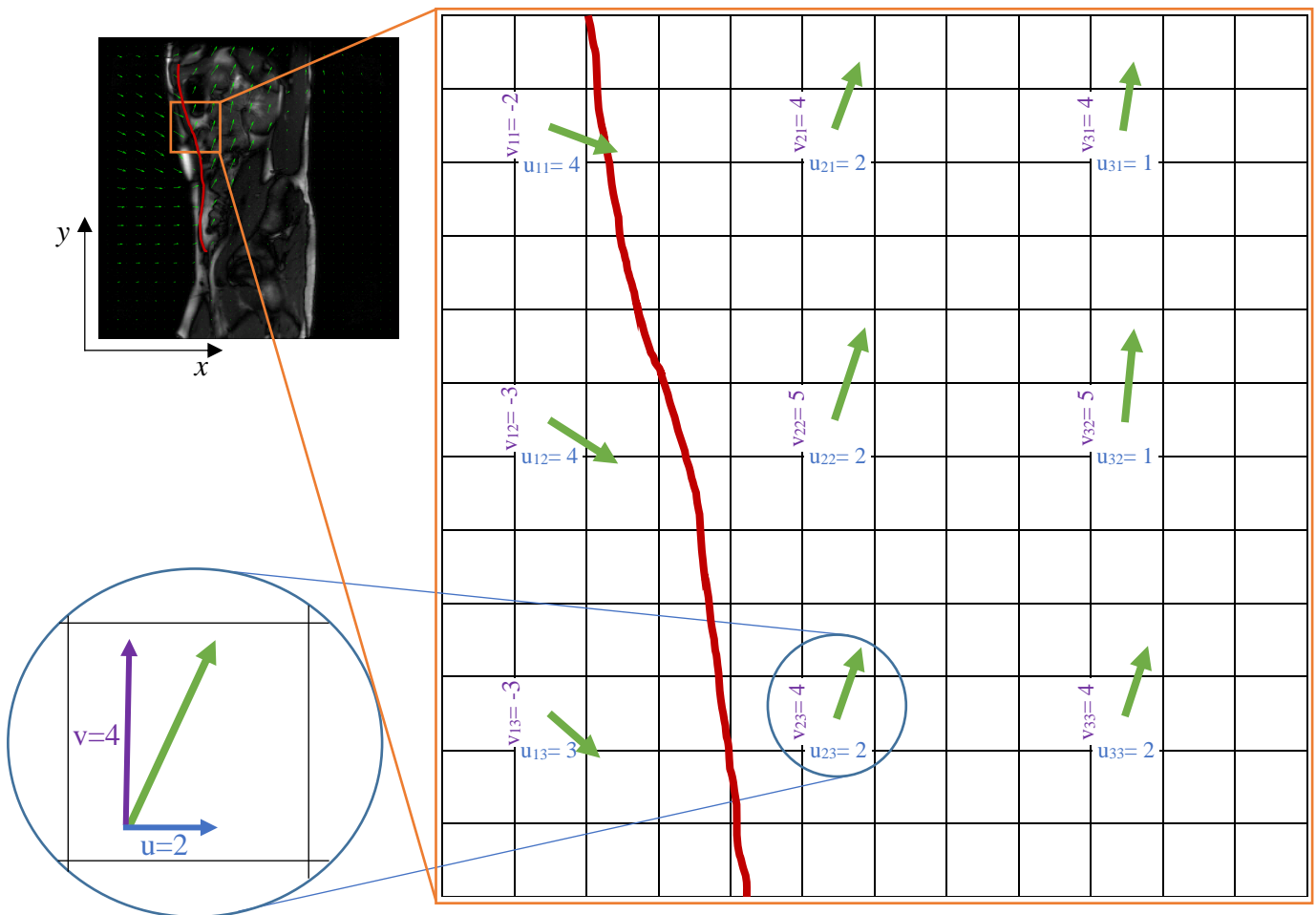
Figure 3.6: Simplified schematic of the displacements occurring around a small portion around the interface (red line) between sliding regions in the abdomen with example values assigned to the vector components

For the pixels shown in Figure 3.6 the horizontal tensile strain field is calculated by taking the linear difference between horizontally neighbouring *u* values (equation is colour coordinated to match values in Figure 3.7):

$$Horizontal\ tensile\ between\ columns = \left(\frac{\partial u}{\partial x}\right)_{11} = u_{21} - u_{11} = 2 - 4 = -2$$

$$\left(\frac{\partial u}{\partial x}\right)_{21} = u_{31} - u_{21} = 1 - 2 = -1$$

$$\dots \left(\frac{\partial u}{\partial x}\right)_{mn} = u_{i+1,j} - u_{ij}$$

Where u_{ij} is the horizontal component of the displacement at the ith and j^{th} position in the displacement field (i = column/x nodal position, j = row/y nodal position) shown in Figure 3.6. The positions of the tensor components have been designated by '*m*' and '*n*' rather than '*i*' and '*j*' in recognition that the image pixel that they lie in is different to the location of the displacement field arrows (see Figure 3.7 below). The other components of the displacement gradient tensor are calculated similarly:

$$Horizontal\ tensile\ between\ columns = \left(\frac{\partial u}{\partial x}\right)_{mn} = u_{i+1,j} - u_{ij}$$

$$Horizontal\ shear\ between\ rows = \left(\frac{\partial u}{\partial y}\right)_{mn} = u_{i,j+1} - u_{ij}$$

$$Vertical\ shear\ between\ columns = \left(\frac{\partial v}{\partial x}\right)_{mn} = v_{i+1,j} - v_{ij}$$

$$Vertical\ tensile\ between\ rows = \left(\frac{\partial v}{\partial y}\right)_{mn} = v_{i,j+1} - v_{ij}$$

Figure 3.7 shows the four resulting displacement gradient tensor components for the simplified example displacement values shown in Figure 3.6. The result of each displacement gradient tensor component has been superimposed on the same grid of pixels as Figure 3.6 shown as blue, purple, orange and green text in Figure 3.7.
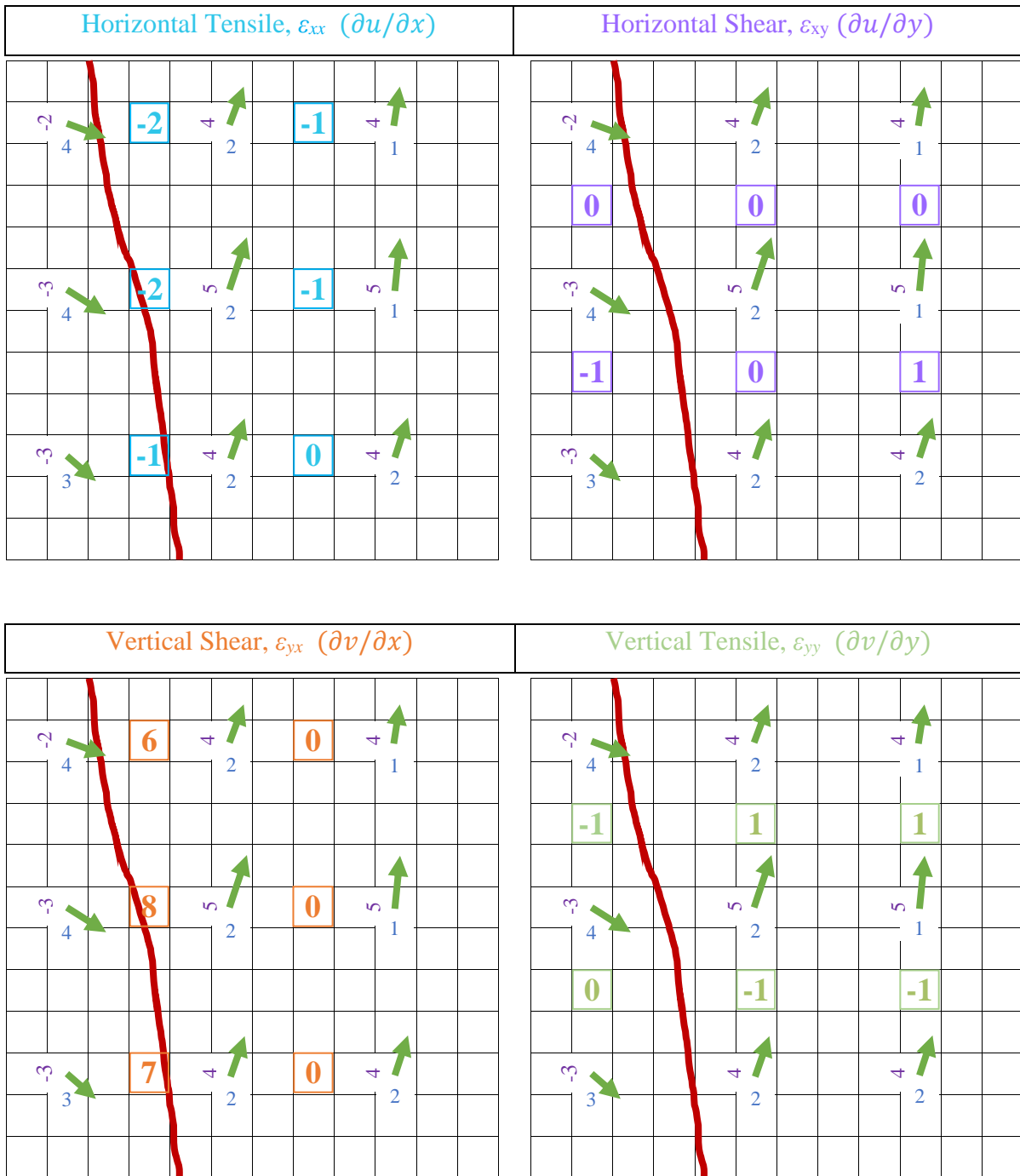
Figure 3.7: Schematic of the same image region as in Figure 3.6 with each of the four grids containing the values calculated for each of the displacement gradient tensor components

As can be seen in Figure 3.7, each of the tensor values were appropriately positioned half way between the deformation field vector values used in its calculation.

3.2.5   Calculation of 'boundary tensile/shear strain'

The calculation of the displacement gradient tensor (described in the previous section) provides information on the shear/tensile strain occurring relative to the image's Cartesian axes (in the *x* and *y* direction). However, the interface at which the sliding is occurring is rarely aligned with these axes and therefore the actual amount of shear/tensile strain occurring along/across this boundary is a combination of the shear/tensile strain components of each Cartesian axis.

The tensile strain along the boundary and shear strain across the boundary are calculated from Eq 3.2 and Eq 3.3 respectively:

$$\text{Tensile strain aligned with boundary} = \left| \frac{\partial u}{\partial x} cos\theta \right| + \left| \frac{\partial v}{\partial y} sin\theta \right| \qquad \textit{Eq 3.2}$$

$$\text{Shear strain aligned with boundary} = \left| \frac{\partial u}{\partial y} sin\theta \right| + \left| \frac{\partial v}{\partial x} cos\theta \right| \qquad \textit{Eq 3.3}$$

The absolute values of shear/tensile strain are taken because it is the magnitude of the shear irrespective of the displacement direction at the interface between the sliding regions which is of interest. θ is the angle of the particular portion of the boundary in question relative to the y-axis. The angle of the boundary from vertical is calculated by interrogating the ROI vertex positions and deriving the equation of the straight lines which link them. The angle relative to the y-axis is calculated using Eq 3.4:

$$\theta = tan^{-1}\left(\frac{x \; step \; between \; vertices}{y \; step \; between \; vertices} \right) \qquad \textit{Eq 3.4}$$

As shown in Figure 3.7 the spatial positions of the horizontal and vertical tensile/shear components are not overlapping, if the spatial positions of the two components from Figure 3.7 were placed on the image matrix together the result is as shown in Figure 3.8.
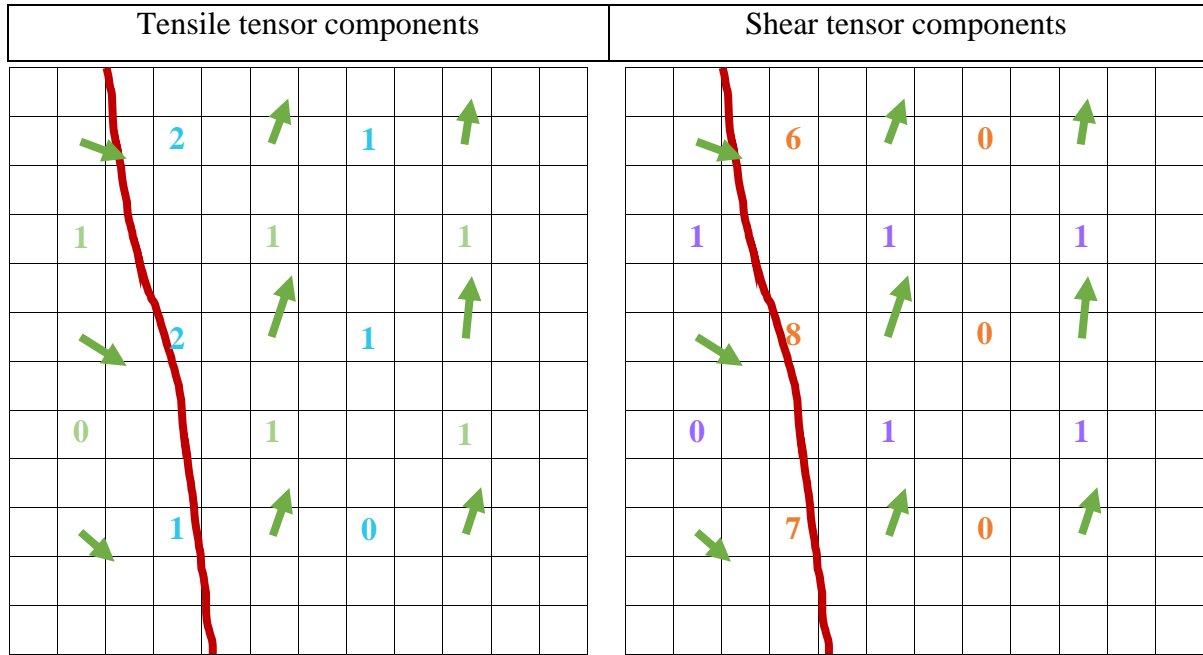
Figure 3.8: Horizontal and vertical tensile (left) and shear (right) superimposed on the same image pixel space for the simplified example in Figure 3.6. The absolute values of the components are shown as it is these that are used for the boundary tensile/shear calculations.

The lack of spatially overlapping horizontal and vertical shear (and tensile strain) components required Eq 3.2 and 3.3 to be operated on all combinations of nearest neighbours. The resulting 'boundary shear matrix' is depicted in Figure 3.9 using the same example numbers as Figure 3.6 – Figure 3.8 with an approximation of $\theta = 12°$ for the angle of the boundary across the entire example matrix (as shown).

Figure 3.9: Exemplification of the calculation of the tensile and shear strains around the boundary for the same set of example values as in Figure 3.6–Figure 3.8. A constant boundary angle of 12° has been assumed throughout this region.

3.2.6 Overlaying strain information on MR images

To increase the usefulness of the tensor component images they are overlaid on top of the original MR images. However, because the deformation field contained information at nodal points (nodal spacing = 4 pixels) and these points were used to compute the tensor components, the displacement gradient tensor also only contained a value at every 4th pixel[6]. When superimposed onto the original images this leaves gaps. In order to effectively overlay the strain information over the anatomy these gaps were filled by propagating (copying) the tensor values. For display purposes, the absolute tensor component values are used. Propagation of each component of the displacement gradient tensor (from Figure 3.7) forms the matrices presented in Figure 3.10.

---

[6] Although ShIRT does describe a continuous deformation field by interpolation between the nodal points, using the interpolated values was not appropriate for this task. This is discussed further in the discussion section.

Figure 3.10: Propagated matrices for each of the displacement gradient tensor components to fill in voids between tensile/shear values to effectively overlay the tensile/shear information over the MRI image.

This process creates a separate matrix for each tensor component (Eq 3.1) from the linearly approximated first order derivative of the displacements in Figure 3.8. The propagation of these values into the empty pixels is based on the nearest neighbouring value, to cover the image space. This process is repeated for every frame to produce time varying values for each component of the displacement gradient tensor. The displacement gradient tensor component matrices for each frame can be displayed as shown in Figure 3.11. In the images, the

68

magnitudes of strain components have been assigned to a colour map: red = high shear/tensile strain, blue = low shear/tensile strain. The range of the colour map shown in Figure 3.11 is normalised to the maximum within each component. The overlaid colour map is given some transparency so both shear values and underlying anatomy can be viewed concurrently.
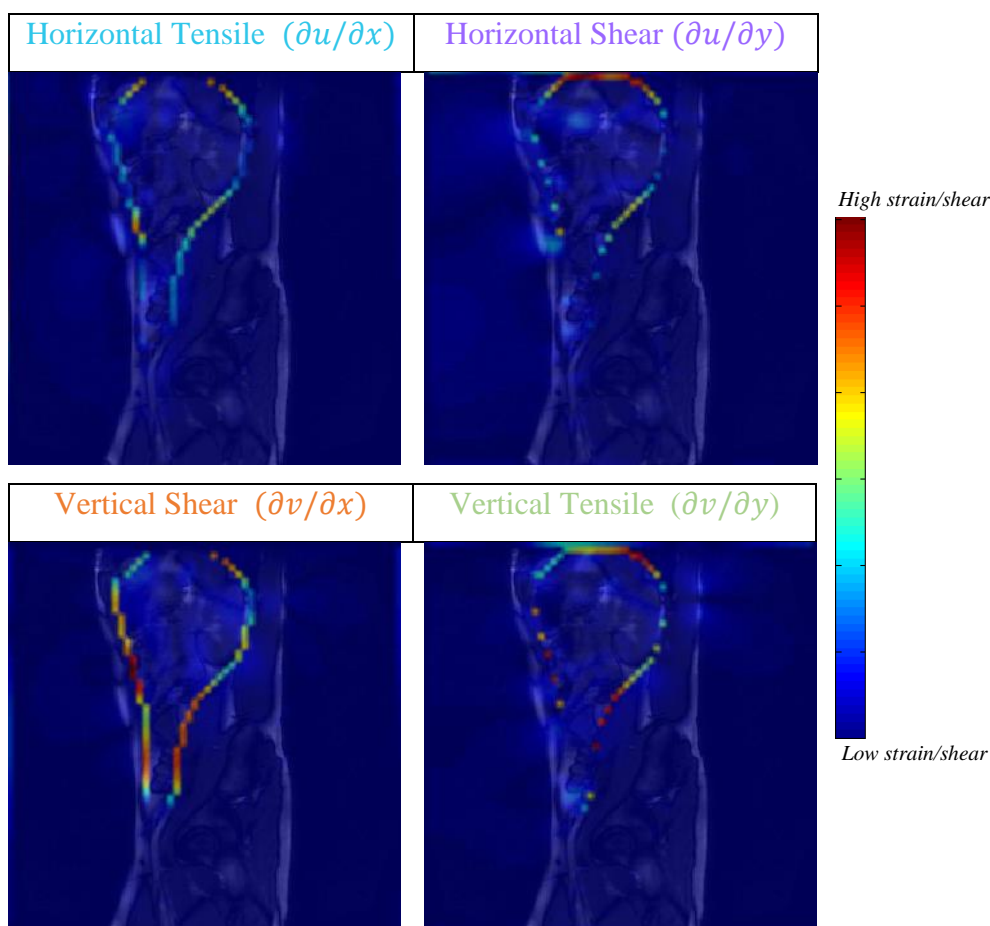
Figure 3.11: The tensile and shear components of the displacement gradient tensor for a single frame overlaid on the corresponding MRI image. A colour map has been applied to the tensile/shear values, red=high magnitude, blue=low magnitude. The values are all normalised to the maximum within each image.

Note: the colour bar in Figure 3.11 above is the same for all shear related images and has not been included in all subsequent figures.

A similar process is followed to permit overlaying the 'boundary shear/tensile' matrix (i.e. aligned with the ROI boundary) on the MR images. Using the values generated in Figure 3.9, the boundary tensile and shear strain values are propagated by duplicating the values into the empty spaces as shown in Figure 3.12.
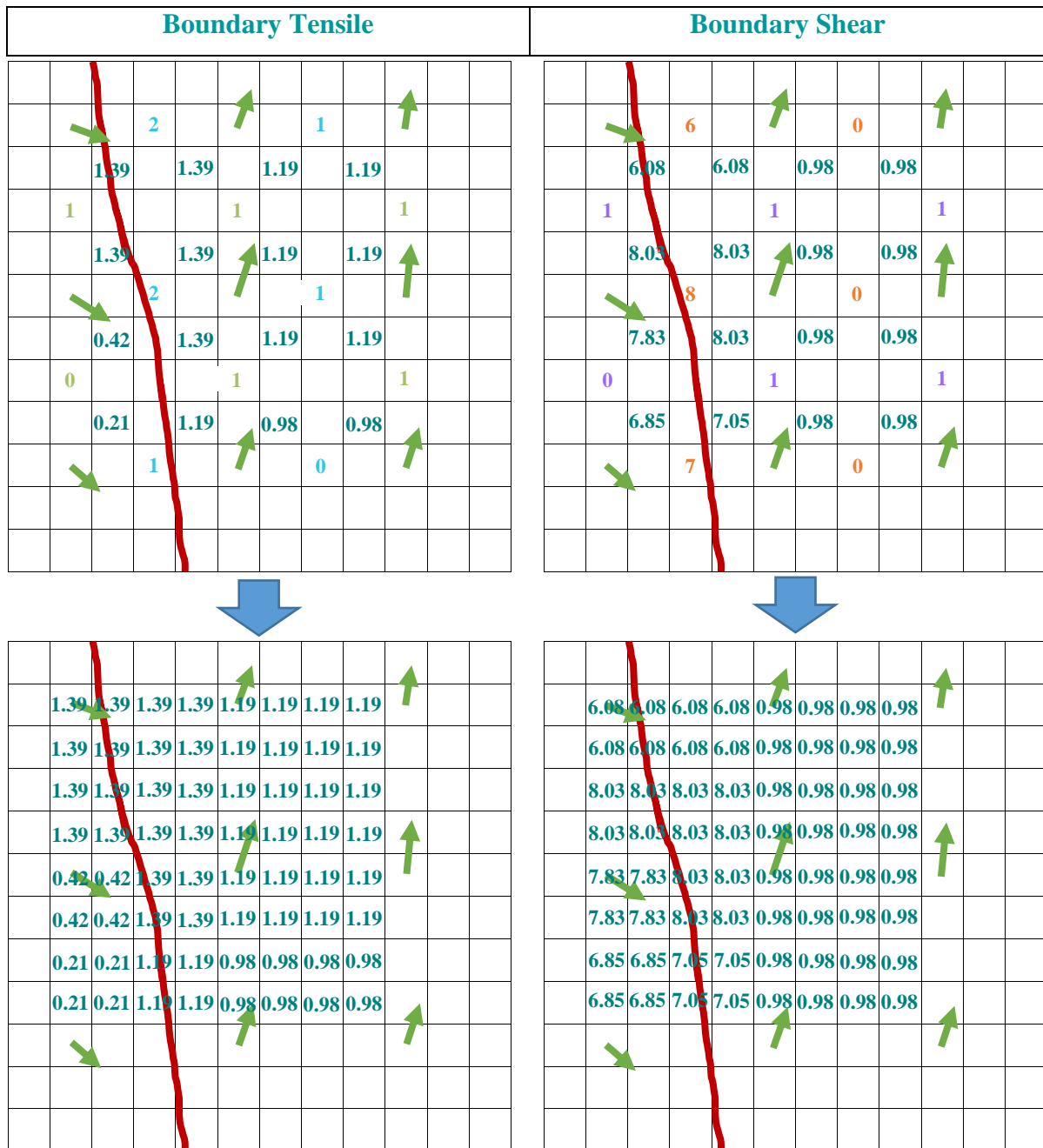
Figure 3.12: Propagation of the boundary tensile and shear strain values to fill gaps in the matrix to produce an effective overlay for the MRI image. (For convenience and clarity the top two diagrams have been copied from Figure 3.9 to provide context for the propagation)

The method used to propagate the boundary shear matrix effectively shifts the centre of gravity of the area associated with that tensile/shear strain value by 0.5 pixels to the left and 0.5 pixels upward on the image from its original position (visible on Figure 3.12). When considered in the context of the structures within the image this shift is relatively minor and is not expected to affect interpretation.

3.2.7 Summation of the shear/tensile strain

The method described thus far has produced a matrix (for each of the components of the displacement gradient tensor and boundary shear/tensile strain) for each frame of the dynamic series of images: i.e. time varying shear/tensile strain fields. Arguably it is the cumulative shear (or lack of it) across all frames that is important for identifying adhesions. Consequently, in order to present the reporter with a simple, clear visualisation of the areas which have reduced shear/sliding, a single depiction of the sliding across all frames was sought.

The position of the boundary changes between frames. A shear summation procedure was developed to map the shear corresponding to a particular place on the sliding boundary to the same place on the subsequent frame. The deformation fields from registrations of the 'abdominal surroundings' were applied to the shear/tensile strain images. These deformation fields were free from interference from the sliding objects of the abdominal contents. Explicitly, the deformation field describing movement from frame 1 to 2 was used to warp the shear/tensile image generated from the displacements between frames 1 and 2 to the shear/tensile image generated from frames 2 and 3[7]. After warping, the shear values for the first two frames spatially match and the matrices are summed. The resulting summed shear image is then warped using the displacement map for frame 2 to 3 to match the position of the shear values in frame 3. The shear values are again summed to produce a summed shear matrix for the first 3 frames. This process of warping the summed shear image and adding the shear of successive frames is continued for all frames in the dynamic sequence. The result is the construction of a single image depicting total shear strain over the respiratory cycles captured.

The summation procedure is applied to all components of the displacement gradient tensor and the 'boundary shear/tensile strain' to produce a set of summed images, shown in Figure 3.13 and Figure 3.14. The spatial position of the summed shear matches the final frame in the dynamic MRI and it is this frame that the summed shear strain is overlaid. The resulting summed boundary shear image in Figure 3.14 (shear strain calculated relative to the orientation of the boundary) is the principal output of the visceral slide quantification technique. These images are the primary focus of subsequent work and are intended to be the main diagnostic aid for detection of adhesions. The summed boundary shear has been termed a '**sheargram**' and will be referred to as such throughout the remainder of this thesis.

---

[7] The deformation field associated with frame 1 describes the displacement of objects in frame 1 to match frame 2, therefore the spatial position of the shear/strain values calculated from this deformation field correspond to frame 1. Hence, the deformation field from frame 1 to 2, to warp shear of frames 1 to 2 to shear of frames 2 to 3.
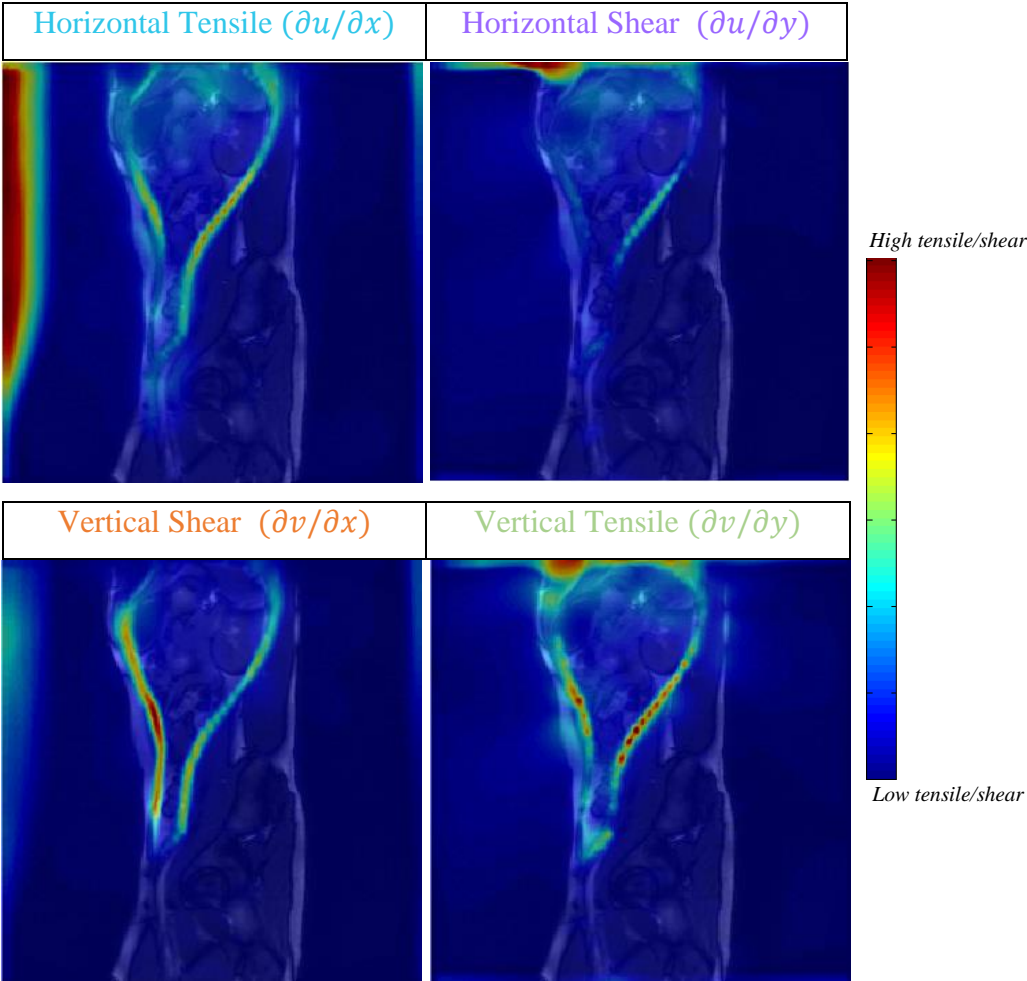
Figure 3.13: Example of summed displacement gradient tensor components
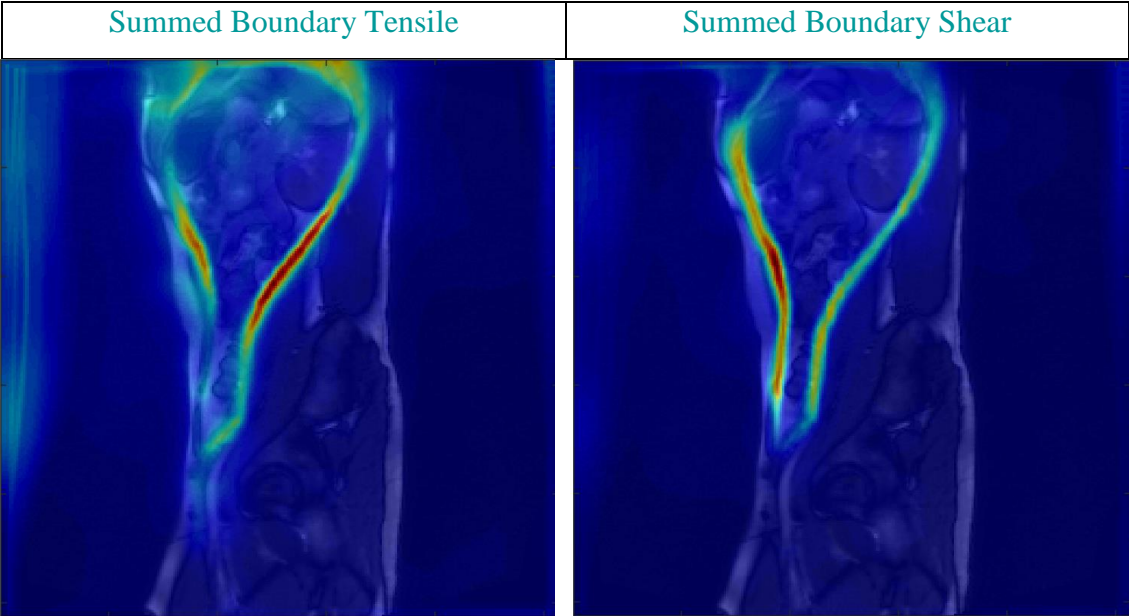
Figure 3.14: Summed boundary tensile strain and boundary shear strain. The summed boundary shear is referred to as a 'sheargram'.

3.2.8   Summary of Method

Figure 3.15 summarises the seven elements of the visceral slide quantification technique.
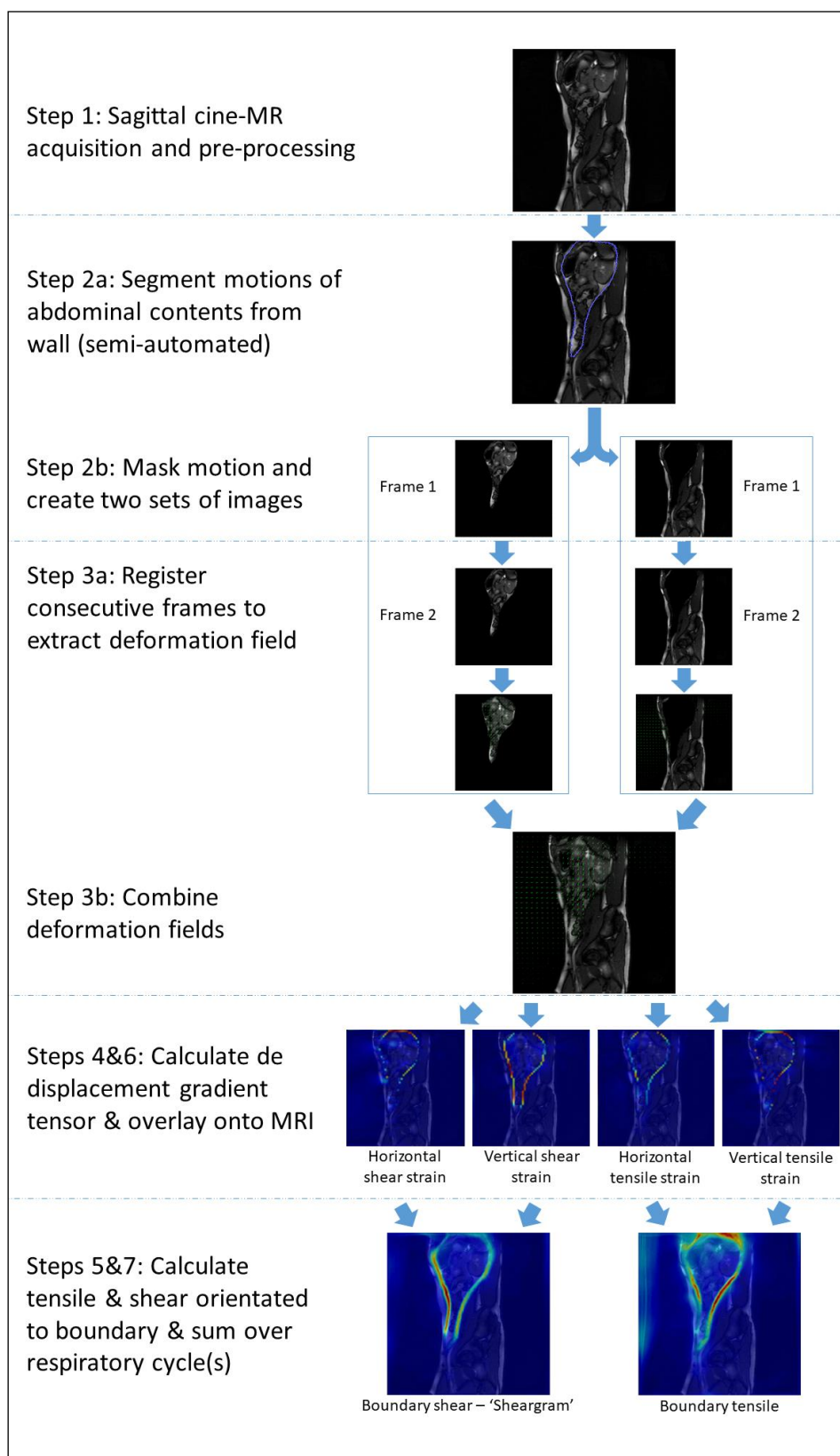
Figure 3.15: Flowchart summarising the steps of the visceral slide processing procedure

3.3 Discussion

Section 2.6 outlined the underlying reasons for pursuing a method to measure the sliding around the perimeter of the abdominal cavity and this will not be repeated here. This discussion aims to:

1. Demonstrate the visceral slide quantification technique correctly calculates the displacement gradient tensor by comparison to a simple analytical example.

2. Examine and clarify the rationale behind each aspect of the chosen methodology described in this chapter.

3.3.1 Comparison to an analytical case

Comparison to an analytical case is valuable because it allows the method to be exercised against a known reference. By way of example, an abdominal MR image was chosen and GIMP 2.8 used to impose a constant vertical shear across the width of the image. A set of 6 images were produced with a shear of 10 pixels (-5 pixels along the left image edge, 0 at the centre and +5 pixels along the right edge) imposed between each frame – as shown in Figure 3.16. The sets of sheared images were then rotated at different angles (0°, 25° and 45°) to produce two rotated sheared images. Figure 3.16 shows examples of the sheared images that were processed.
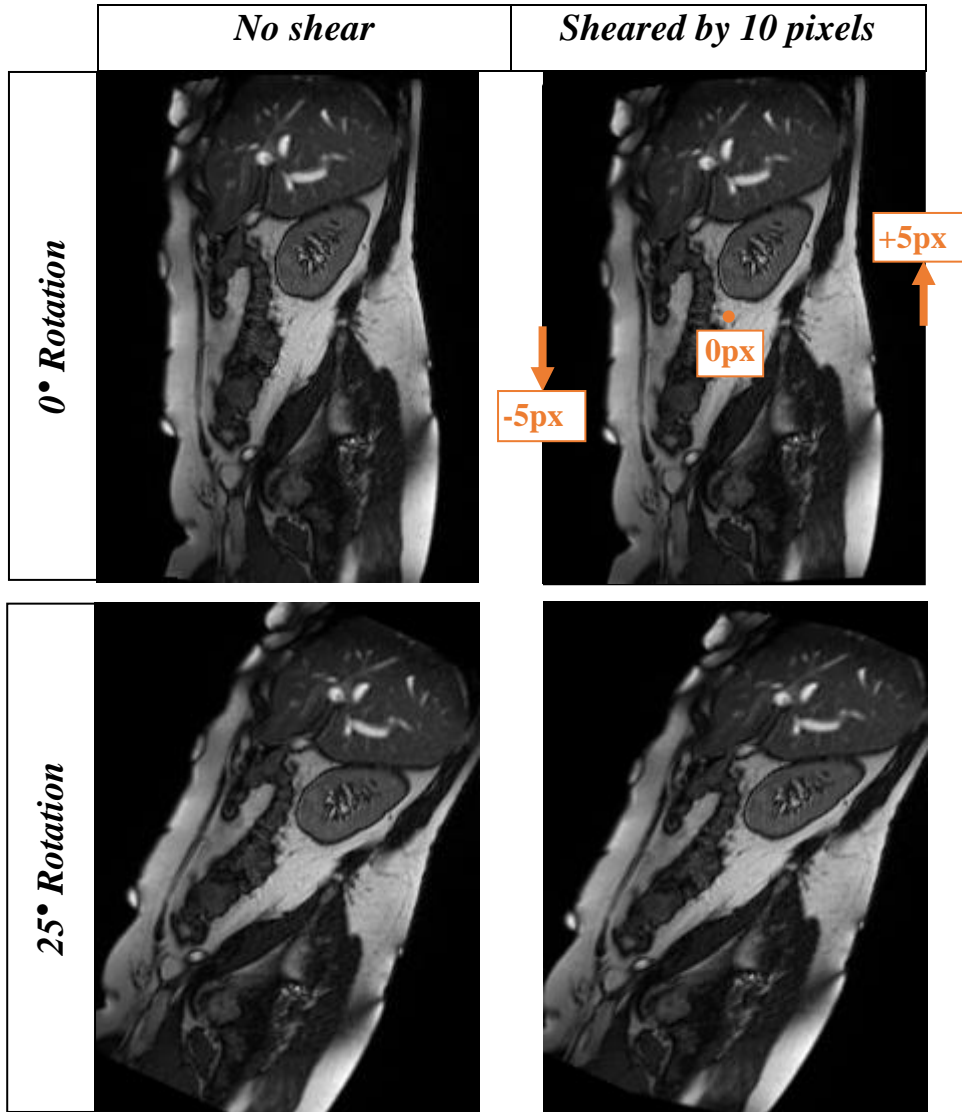
Figure 3.16: Examples of images to be processed that had a uniform shear across the image at different angles.

The displacement gradient tensor for these images was derived analytically and this derivation is shown in Appendix 4. The images were then processed by the visceral slide quantification technique described in this chapter and the displacement gradient tensor output from the processing was compared to the analytical calculation. From Appendix 4, the displacement tensor for this system which describes strain in the images in Figure 3.16 is:

$$T = \begin{bmatrix} \dfrac{\partial u}{\partial x} & \dfrac{\partial u}{\partial y} \\[2mm] \dfrac{\partial v}{\partial x} & \dfrac{\partial v}{\partial y} \end{bmatrix} = 0.05208 \begin{bmatrix} cos\theta sin\theta & -sin^2\theta \\[2mm] cos^2\theta & -sin\theta cos\theta \end{bmatrix} \qquad \text{Eq 3.6}$$

The displacement gradient tensor is multiplied by 0.05208 to account for the difference in magnitude of shear between the images and analytical derivation in Appendix 4[8] (the magnitude is 0.05208 times less in the images).

Results

In the images in Figure 3.16 the displacement gradient tensor components should be constant across the image domain. Consequently, the analytical calculations for each of the rotations results in a single value for each of the displacement gradient tensor components. The result of the processing gives a value for the displacement gradient tensor components at every point in the image. To achieve a single value for the tensor components an average value was taken over an area indicated by the example in Figure 3.17[9].
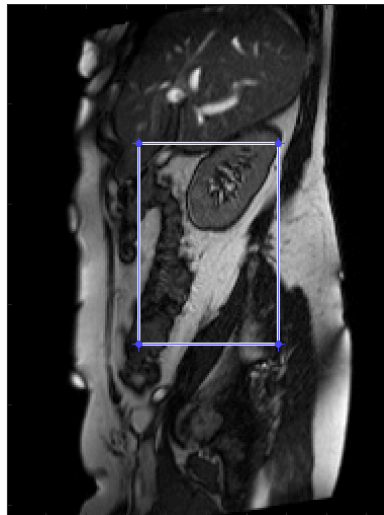
Figure 3.17: Example of the region used to calculate the average shear produced by the visceral slide quantification technique (drawn on an image with 0° rotation)

---

[8] The analytical calculation considered a vector field changing in magnitude with the value of x along the x-axis. Multiplication by 0.05208 arises because a shear of 10 pixels has been applied over 192 pixels (width of the images), therefore the size of the vector along x is 10/192 (0.05208) multiplied by x.

[9] The region selected was central as this excluded any anomalous shear generated at the edges of the images due to objects disappearing out of the image space as a result of the applied shear distortion.

The average value for each tensor component is given in Table 3.1, adjacent to the theoretical analytical results.

Table 3.1: Visceral slide processing results compared to the analytical results for the images with a constant shear at different rotations

Rotation	Processing Results	Analytical Results
0°	$T_{0°} = \begin{bmatrix} -0.00002 & 0.00002 \\ 0.05208 & 0.00002 \end{bmatrix}$	$T_{0°} = \begin{bmatrix} 0 & 0 \\ 0.05208 & 0 \end{bmatrix}$
25°	$T_{25°} = \begin{bmatrix} 0.0204 & 0.0093 \\ -0.0430 & -0.0200 \end{bmatrix}$	$T_{25°} = \begin{bmatrix} 0.0199 & -0.0093 \\ 0.0428 & -0.0199 \end{bmatrix}$
45°	$T_{45°} = \begin{bmatrix} 0.0259 & 0.0263 \\ -0.0263 & -0.0259 \end{bmatrix}$	$T_{45°} = \begin{bmatrix} 0.0260 & -0.0260 \\ 0.0260 & -0.0260 \end{bmatrix}$

The processing results closely matched the tensor components calculated analytically. The difference in sign observed in some of the components in Table 3.1 can be attributed to the inversion of the y-axis in MATLAB's coordinate system relative to the analytical case's coordinate system. Differences in agreement corresponding to $< 1/10$ of a pixel were observed in all cases. It can therefore be concluded that the technique developed generates sensible measurements for the displacement gradient tensor.

The remainder of this discussion offers critique of and justification for each component of the processing method described.

3.3.2 Segmentation

The reasons why a segmentation procedure is necessary for the sliding geometry in the abdomen is to accommodate discontinuity in motion (covered in Section 2.4). Several methods were considered ranging from completely manual to fully automated. This section discusses why this particular segmentation method was implemented and its advantages and disadvantages over other potential methods.

Manual segmentation naturally benefits from the experienced eye of the user but involves locating and re-drawing the ROI in every frame in the dynamic sequence. This was considered too time consuming, impractical and would most likely result in less consistency compared to

the other methods. A fully automated method was also not strongly considered. Despite the advantages of removing intra- and inter-operator variability and decreasing processing time, the complexity of the segmentation (relying on both movement and structural information) and wide variability between patients meant that off-the-shelf, fully automated methods were unlikely to be reliable. Intensity based segmentation methods (e.g. intensity threshold, region growing) are not well suited to the images due to the wide ranging, constantly changing intensity levels across the whole abdomen. In many cases image intensity and contrast do not provide the information necessary to identify the sliding boundary and amalgamation of movement information from the dynamic video is required. It is difficult to incorporate these elements into a bespoke, fully automated segmentation tool. Such an approach was considered impracticable in the timescale of the PhD and therefore partial human input was considered to provide the most cost effective solution.

A fully automated registration approach could be achieved by a specially adapted registration algorithm capable of coping with displacement discontinuities at sliding boundaries. Such registration algorithms used in the research environment have been discussed in Section 2.4 and have been developed for their own specific purpose/application [97, 102, 86, 98]. To the author's knowledge the algorithms are not freely available and development of our own registration algorithm was not considered an effective, feasible solution within this PhD. Generally, such bespoke algorithms developed for a specific application tend to be less versatile and lack robustness in situations which stray away from their expected input. The abdominal MR images under interrogation in this project often contain complexities (such as out-of-plane motion, differing degrees of noise, movement artefacts) which present difficulties for registration algorithms and are difficult to account for in a bespoke algorithm.

The dependency of the shear strain result on correct segmentation necessitates implementation of a robust technique while providing an element of control for the user. The semi-automated segmentation protocol that has been implemented involves subjective positioning of the ROI and currently lacks well-defined rules for its placement. One example of this is how sharply the abdominal contents are contoured. It is generally preferential to draw a smooth boundary without sharp changes in direction because the angle of the boundary affects the (boundary) shear calculation. Therefore, sharp changes in boundary angle that are poorly aligned with the direction of abdominal movement can artificially reduce the shear. As a result, in some cases it is better to 'softly' contour the abdominal cavity to create a smoother delineation at the

expense of perfectly contouring the anatomy. An example of such a scenario where a protrusion on the abdominal wall causes an artificial reduction in shear is shown in Figure 3.18.
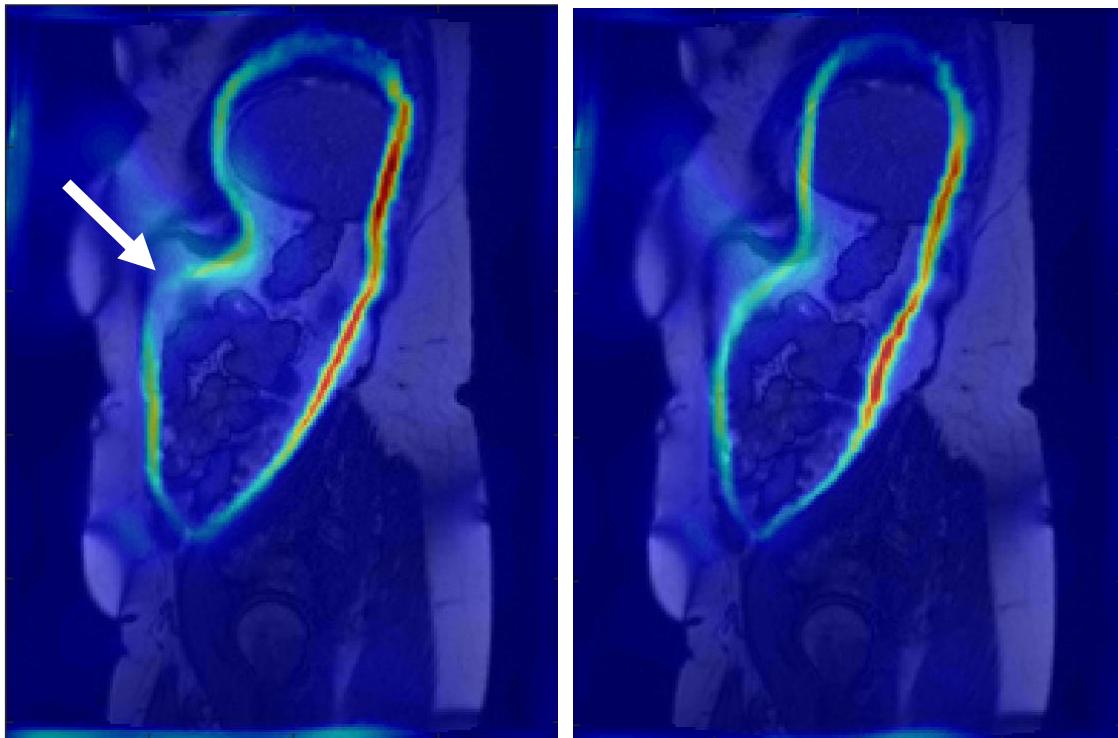
Figure 3.18: Example where contouring a protrusion on the abdominal wall can create an artificial reduction in shear (indicated by the white arrow) and a softer contouring is preferred.

Nonetheless, at the current stage of development the semi-automated approach described is fit for purpose and was considered a reasonable compromise between development time, processing time, accuracy and consistency.

3.3.3   Masking procedure

Two different methods of masking the images were considered:

1) Using the masks for every frame to create two series of images of the abdominal contents and its surroundings (as described in the method in Section 3.2.2).

2) The masks could be supplied as an input to the registration algorithm. This method uses a single mask, e.g. the mask for frame 1, as an input for the registration command to register frame 1 to frame 2 (therefore not utilising the mask from frame 2 in the registration procedure).

When using a mask during registration it is most frequently applied as part of the registration process as proposed in Method 2. This could offer marginal improvements in computation time as the process of producing two new sets of masked images (Method 1) would no longer be necessary. Method 2 applies a single mask to both consecutive frames being registered and therefore relies on the assumption that the movement between the frames is small enough for the same ROI to apply to both images. As more clinical images were examined it became apparent that this assumption was not consistently held. An extreme example of such a case is shown in Figure 3.19 where the positions of the sliding boundary in two consecutive frames of a cine-MR imaging sequence are considerably different.
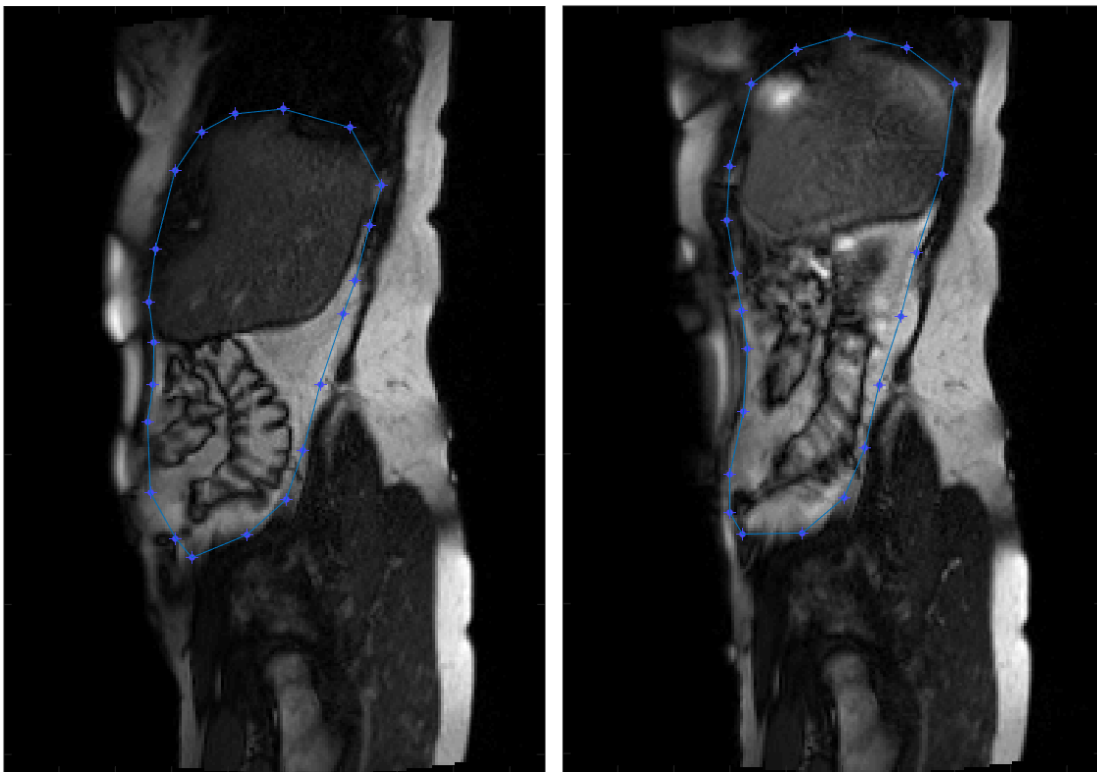
Figure 3.19: An example where a single mask is unsuitable for segmentation due to a large amount of movement of the sliding boundary between two consecutive frames.

In contrast, Method 1 relies on no such assumption. The ROI corresponding to each frame is used in the registration and therefore the masked images should, theoretically, contain the same objects/detail (with the exception of out-of-plane motion). This satisfies one of the main assumptions made by the registration algorithm – the objects in one image are present in the other image. This method proved more reliable and was therefore adopted within the workflow.

3.3.4   Registration procedure

The registration of consecutive frames was chosen as the preferred registration procedure to limit the effects of out of plane motion and to achieve as accurate a registration as possible. This potentially permits detection of more subtle abnormalities which were beyond the capabilities of the approach of the previous PhD.

The merits of ShIRT and the reason for it becoming the primary registration algorithm for this work has been covered in Chapter 2 (Section 2.3), but to summarise:

i)   The local research group developed the algorithm and therefore a wealth of experience and support was available

ii)   It was extensively tested and approved for abdominal movement assessment in the previous PhD on similar types of images

iii)   Its robustness, ease of use and convergence speed were strong positives over alternative algorithms

The ShIRT registration parameters used for all registrations within the visceral slide processing method were the default, tried and tested settings that have proven robust for a wide variety of medical images [71, 92, 93, 63, 94, 95]. This combined with their testing and implementation in the previous PhD make these parameters the logical choice. In subsequent tests described in Chapters 4 and 5, ShIRT was found to produce reliable results. Although brief experimentation into changing the nodal spacing and lambda was performed, an in-depth investigation into changing the parameters was not considered necessary.

Performing the registration on the masked images, with black regions in place of the masked area (see Figure 3.3 and 3.4), allows the registration algorithm to only be driven by accurately aligning the region containing detail. The black areas contain no distracting information and can be warped without biasing the cost function and is effective for accurately defining the motion in each of the regions separately. Recombination of the two masked deformation fields forms a complete, representative description of the motion which has occurred between the frames. Chapter 4 investigates the accuracy and suitability of the registration method on synthetic data.

3.3.5   Calculation of the displacement gradient tensor

Calculating the displacement gradient tensor permitted a mechanism to mathematically quantify the amount of sliding occurring along the perimeter of the abdominal cavity. The calculation is based on the premise that shear is a quantifiable analogue for the sliding motion of the abdominal contents against the perimeter of the abdominal cavity. As such, throughout this chapter the terms shear and sliding have been used interchangeably. However, the extent to which this assumption holds is debatable and is discussed in detail in the final discussion chapter (Chapter 6).

The shear values were calculated by taking the difference between neighbouring displacement values at the nodal points of the image registration without considering other nearby values. This method makes no attempt to maintain a smooth tensile/shear strain field which may be expected in physical objects/models. This approach was necessary because taking neighbouring values into account would negate the effects of segmenting the images: the segmentation's principal purpose is to remove the effects of the registration algorithm's smoothness constraint around the region of the sliding boundary. Just as the registration algorithm would have artificially under-estimated the shear at the sliding boundary due to smoothing the displacement across the discontinuity, building nearby displacements into the shear strain calculation would have the same effect. The result of this would be particularly stark as the neighbouring nodal points either side of the boundary are relatively devoid of shear/changes in displacement.

As shown in Figure 3.10 the shear values between nodal points in the registration were propagated to fill the pixels in the image space rather than interpolated. Interpolation of the shear values would incorporate assumptions about the system (e.g. a gradual, linear change in displacement between the nodes). The discontinuity, and therefore sharp rise in shear, at the sliding interface is likely to correspond to a single shearing point across 1 or 2 pixels rather than change gradually over the full separation between the nodes. The exact pixels between the nodes at which the motion discontinuity occurred is impossible to determine. By duplicating/propagating the single shear value it maintains the discontinuity as a sharp rise/drop in shear at each of the nodes either side of the sliding boundary. The resolution of where the sliding boundary exactly occurs is reduced and no attempt to pinpoint its exact location between the nodes is made, but the crucial information regarding the shear profile is conserved.

Propagation of the shear values created a shear matrix of equal size to the original MR image; necessary to overlay the shear information onto the anatomy to give context to the data. Propagation created a wider band of shear values which is also more visible and easier to interpret than a single row of pixels with a high shear.

3.3.6 Calculation of boundary shear

The sliding occurs along the perimeter of the abdominal cavity and it is appropriate to calculate the shear orientated to the locally varying orientation of the sliding boundary rather than calculating the shear orientated to a fixed, global coordinate system, as is the case with the components of the displacement gradient tensor. The re-orientation combines both components of shear (and tensile strain) into a single value for easier interpretation.

The decision was made to only consider the magnitude (ignoring direction) of the shear between nodal displacement points. By only considering the magnitude, it allowed for the production of a clear, simple depiction of the amount of sliding at the boundary: an absence of shear irrespective of sliding direction is the proposed diagnostic metric for adhesion detection. The incorporation of sliding direction of the abdominal contents could be considered in the future but the advantages of this additional information are not clear. Incorporating direction into the sheargram would complicate the data displayed and likely distract the reporter rather than augment its diagnostic capability.

3.3.7 Summation procedure

The time varying shear/tensile strain across the dynamic image sequence does theoretically contain the necessary information to observe which areas are sliding and which are not. This may be useful on its own but would require close examination of all frames to determine which areas are/are not sliding over the whole respiratory cycle – for interpretation, it critically lacks simplicity. A clearer visualisation of the shear across the whole dynamic image sequence was required which condensed the shear information into a single image depicting the total amount of shear at every point, across all frames. To achieve this, the position of the interface between the two sliding regions needed to be matched for all frames.

The method chosen utilises the deformation fields resulting from registration of consecutive frames of the abdominal surroundings. One advantage of this approach is that an additional round of computationally intensive registrations is not needed as the information required has already been determined.

Two methods of summation were considered and their comparison forms one of the experiments discussed in Chapter 4. The summation technique chosen needed to robustly track the abdominal wall and remain fixed where necessary e.g. the posterior wall. Therefore, freeing the registration from the complex movement within the abdominal contents was necessary. The abdominal surroundings are relatively fixed and lack internal structures which move relative to one another and are therefore devoid of internal localised motion. This provides less of a challenge for the registration algorithm and produces a more reliable, robust result.

The chosen summation method has demonstrated fallibility in certain situations; particularly where large translations of the sliding boundary are observed between frames. Figure 3.20 shows two examples of the summation procedure failing to successfully overlap the shear profile in every frame. However, these cases were only encountered occasionally. In these extreme cases the movement was often so fast that severe motion blur would render the scan potentially non-diagnostic. There is little chance of these shear artefacts resulting in incorrect diagnosis as they are easy to identify and would result in that portion of the sheargram being discounted.
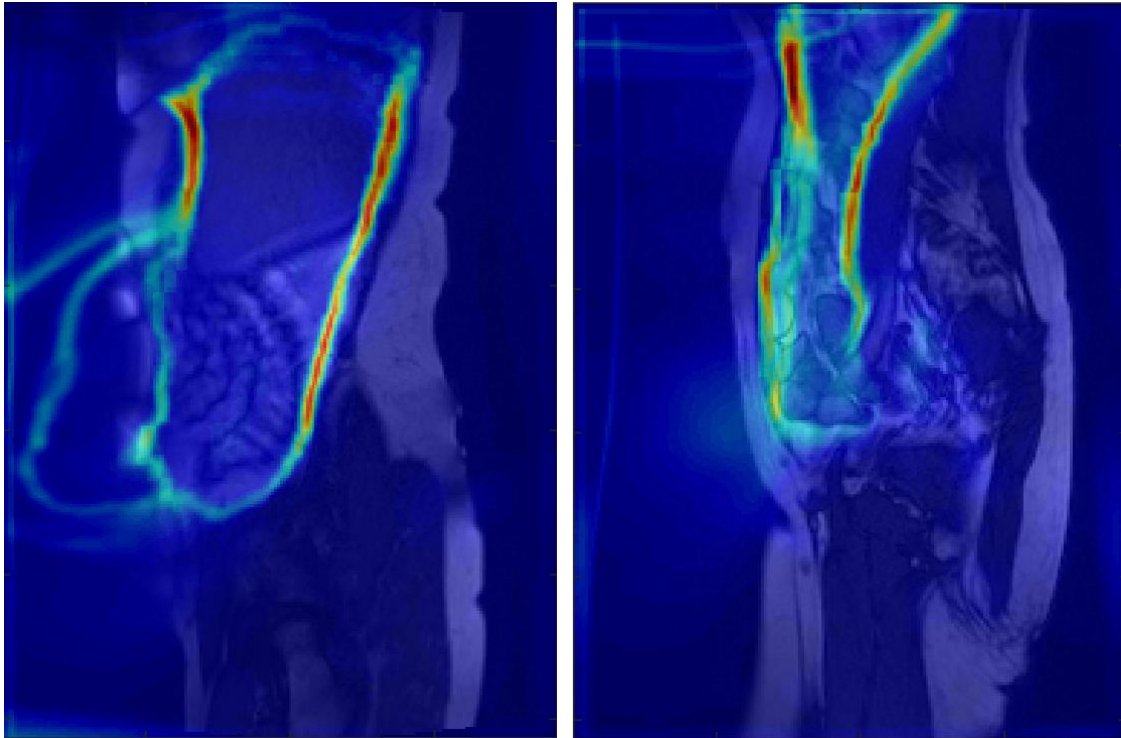
Figure 3.20: Two examples showing the appearance of the sheargram when the summation technique fails to register one or more frames correctly

3.3.8   The role of tensile strain

Although the tensile strain is calculated as part of the visceral slide processing procedure, experience has found it to be of little use. Initial justification for its calculation argued that: where an adhesion was present to the abdominal wall the forces present from respiration would 'tug' at the adhesion and result in an increased tensile strain component. However, as more experience was gained with clinical data such a correlation with adhesive pathology was not noted and it proved to be of limited use. Its inclusion in the processing procedure description has been included for completeness but the sheargram is the principal focus for the remainder of this thesis.

3.4 Summary

Movement of the abdominal contents resulting from respiration is captured by cine-MRI. The abdominal contents normally slide unimpeded against the abdominal wall and other structures adjacent to the abdominal cavity. This chapter has described the development of a technique to interrogate the sliding interface in cine-MR images. The hypothesis for its use as a diagnostic aid focusses on reduced sliding possibly corresponding to a potential adhesion to the abdominal wall.

85

The technique separates the abdominal contents from its surroundings and applies image registration (ShIRT) to consecutive frames in each of the regions independently. The abdominal anatomy in each region is tracked as it is displaced during respiration. Performing the registration independently in each region allows for more accurate determination of the movement of the anatomy around the sliding interface. The technique quantifies the sliding at the interface between the two regions by calculating shear strain. Shear strain is derived from displacement maps provided by the image registration and involves calculation of the linear difference in displacement between neighbours. These shear values form the components of the displacement gradient tensor in 2D. The shear components of the tensor are used as a quantifiable analogue for sliding. The shear values are displayed as an overlay on the original MR images to give anatomical context. Finally, the shear values are tracked with the underlying anatomy and summed over all frames to produce a single image representing the magnitude of cumulative shear on the perimeter of the abdominal cavity – a 'sheargram'. It is the sheargram which is intended to form the primary aid for diagnostic interpretation of the cine-MR image sequence.

A discussion and justification has been offered for the methodology adopted for each component of the visceral slide quantification technique. The next chapter applies the technique to a series of tests to confirm its ability to measure shear in sliding geometries and investigate its limitations.

Chapter 4

Validation of the visceral slide quantification technique

The previous chapter detailed a technique to calculate the displacement gradient tensor and shear along a boundary where a motion discontinuity is present. The discussion in Chapter 3 provided justification for the final implementation of the technique. This chapter assesses that final implementation using a series of experiments to test its accuracy and robustness.

Six different tests were conducted ranging from simple in-silico experiments to clinical images. The purposes of these experiments were to:

i.   clarify the technique could correctly measure shear in simplified systems while demonstrating the requirement for segmentation

ii.   determine if this shear could indicate adhesive regions

iii.   provide information on reproducibility and the approximate error associated with the technique

This chapter is arranged into sections with each describing an investigation into a different characteristic of the visceral slide processing technique. Specifically, the experiments and tests were:

1. Shear accuracy in idealised in-silico sliding geometries
    Calculated shear was measured against known values in idealised environments which included rigid sliding objects and simple deformations.

2. Artificial introduction of shear
    Two experiments using idealised and real patient data tested whether the methodology of the technique is capable of introducing artificial shear where none should exist.

3. Shear accuracy in a semi-idealised in-vitro model

   Images captured of a sliding geometry were used to manually measure shear by landmark placement which were then compared to the result generated by the technique.

4. Adhesion detection in a semi-idealised in-vitro model

   A simulated adhesion was added to the above in-vitro model to create a resistance to sliding motion. Application of the visceral slide measurement technique sought to test 'proof of concept' regarding its capacity to detect adhered regions.

5. Repeatability in processing

   This is the first of two tests related to reproducibility in the sheargram. Two different cine-MRI scans were processed five times each and the differences in the sheargrams analysed.

6. Effect of ROI position

   This is the second test related to reproducibility. An ROI was systematically translated away from the sliding boundary on a sagittal cine-MRI and the effects on the resulting shear observed.

7. Shear summation procedure accuracy

   The sheargram relies on summation of the shear in each frame by spatially matching points on the sliding boundary across all frames. The accuracy of two different methods to spatially matching manually landmarked points between frames were compared.

The above experiments provide information on how the technique performs in different scenarios and provides measures for its accuracy in idealised cases. Each of the experiments are described and discussed individually. The results and discussions are then summarised at the end of the chapter.

4.1 Shear accuracy in idealised in-silico environments

4.1.1 Introduction

Highly idealised computer-generated movements were applied to an abdominal sagittal MR image. The known in-silico distortions provided an exact reference against which the inherent accuracies and inaccuracies in the technique could be evaluated under idealised conditions. Two types of movement tests were produced:

1. **Translation Shear Accuracy:** A uniform, bulk translation of a central portion of the image while the remainder of the image was left stationary.

2. **Stretched Shear Accuracy:** A central region was stretched to create a simple locally varying deformation with respect to the rest of the image.

4.1.2 Method

1. Translation Shear Accuracy

A representative paramedian sagittal MR image was selected. A central region spanning the full height of the image was displaced superiorly by 2 pixels between each frame. 10 frames were produced, amounting to 11 images including the original. Portions of the image translated beyond the image edge were copied to the bottom. Figure 4.1 below shows the region on the original image and the last frame translated by a total of 20 pixels.
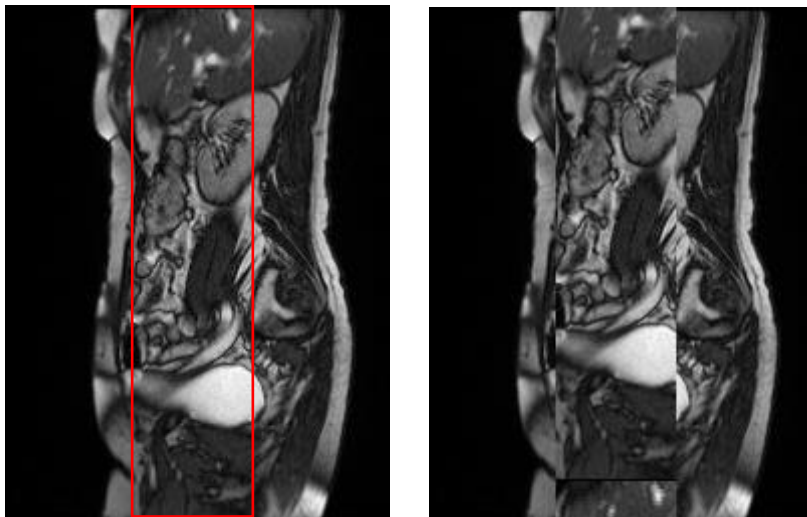
Figure 4.1: First and last frames showing the in-silico bulk translation of a section of a 192x256 sagittal MR slice. The red rectangular region indicates the region translated and this is the same as the ROI used to analyse shear in the experiment. Wraparound was used for pixels moved beyond the image edge.

The motion between each frame was tracked with and without implementing segmentation of the displaced region.

2. Stretched Shear Accuracy

The same sagittal MRI slice from experiment 1 was used to produce a second set of idealised images. A rectangular section was cut out (highlighted in red in Figure 4.1) and stretched. The stretching was performed in GIMP 2.8 using a cubic interpolation of the pixel intensities. The remainder of the image outside the rectangular region remained fixed in the same position. The

stretch was implemented by anchoring the bottom of the rectangle and, effectively, pulling from the top. 26 frames were produced with the total stretch increased in increments of ~2 pixels between each frame. This created a discontinuity in 'motion' of adjacent pixels at the edge of the rectangular section. The result of the technique can be compared to the actual shear values present in the system. Figure 4.2 shows the images of two stretched frames.
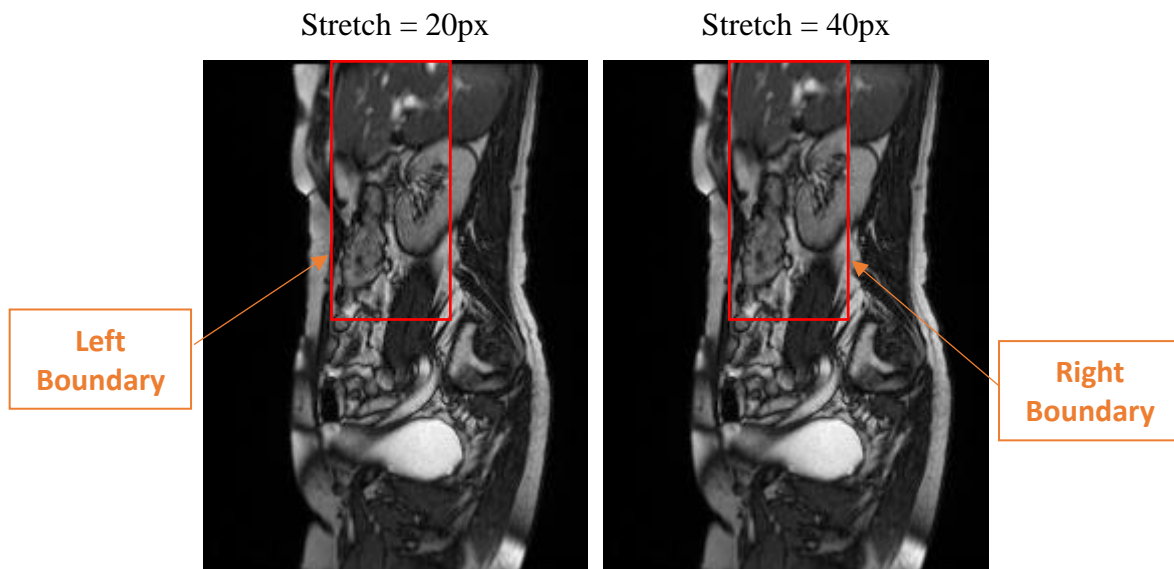
Figure 4.2: Examples of synthetically stretched sections of a 192x256 MR image [3] indicated by the red region. The red region also indicates the location of the ROI drawn for processing.

4.1.3   Results and Discussion

1. Translation Shear Accuracy

Figure 4.3 below shows the sheargrams (summed shear over all frames) with and without segmentation for the translation experiment.

| With Segmentation | Without Segmentation |
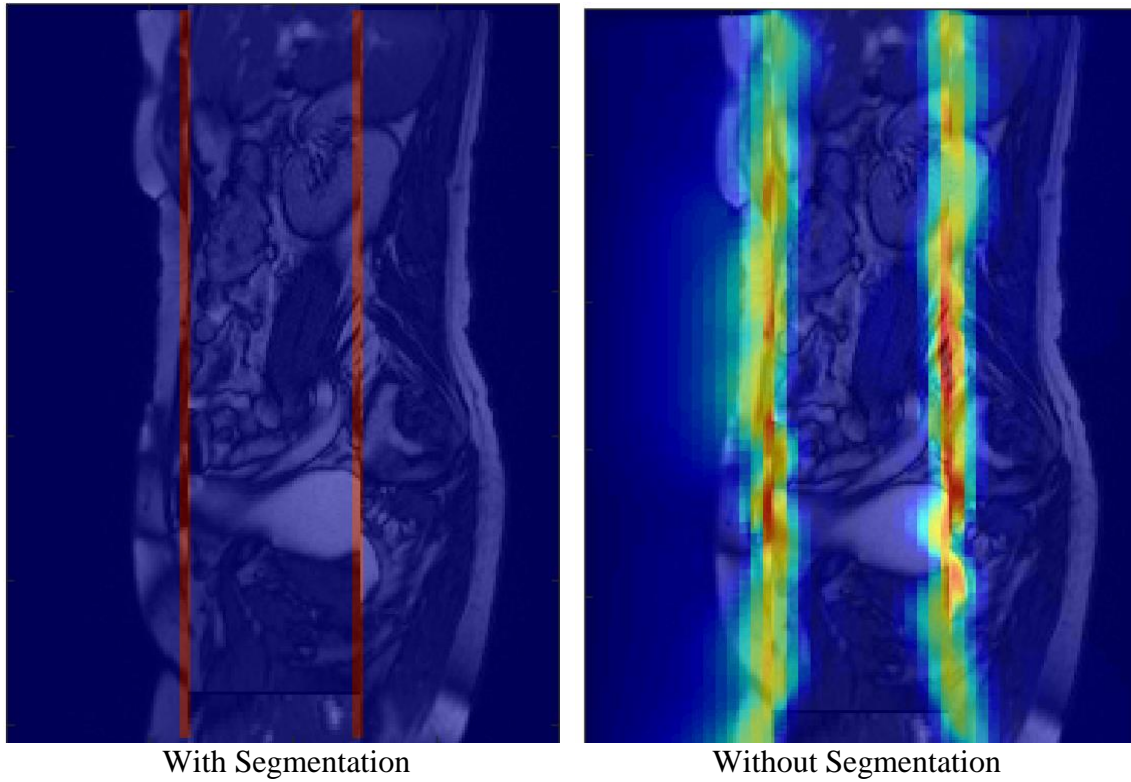
Figure 4.3: Sheargrams depicting the summed shear over all 11 frames with and without segmentations

Figure 4.4 plots the actual total shear which occurred in the system (along the right boundary) alongside the shear calculated along the boundary in each of the two sheargrams in Figure 4.3.
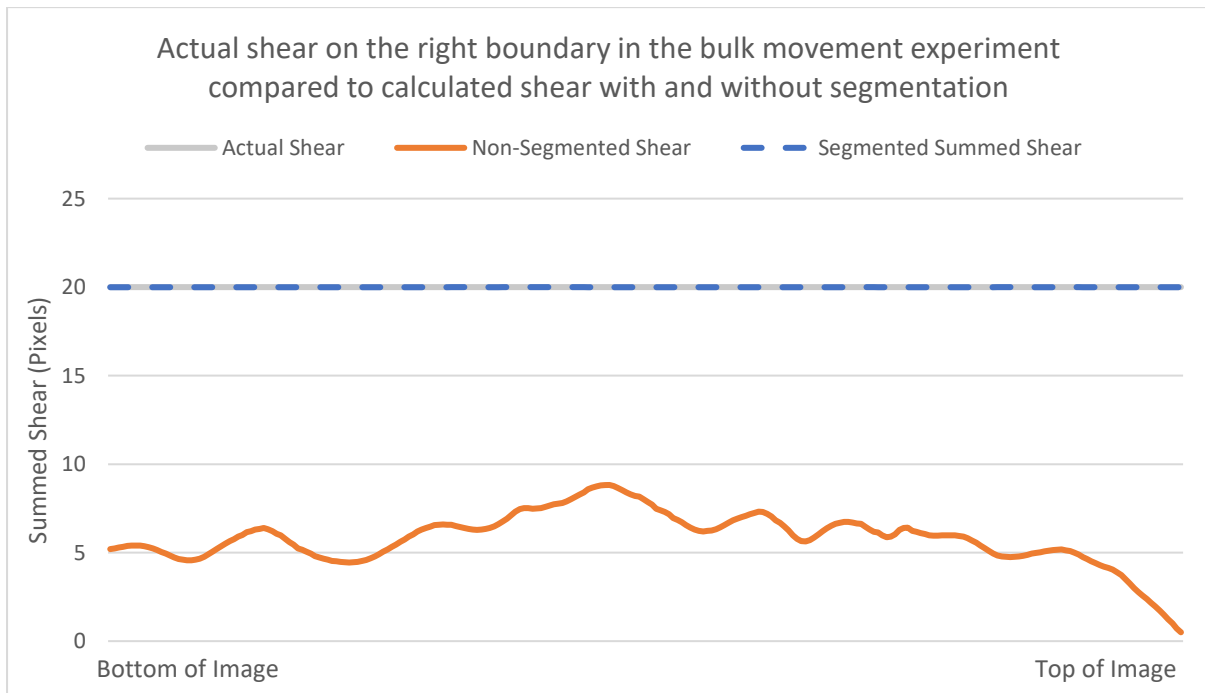
Figure 4.4: Actual shear along the sliding boundary of the bulk movement experiment compared to shear calculated with and without segmentation

The sheargram in Figure 4.3 and graph in Figure 4.4 show an exact match between actual shear and calculated shear using segmentation. A consistent value of 20.0 pixels was achieved from top to bottom along the sliding boundary. Without segmentation of the translated region, the shear profile was more diffuse and therefore did not accurately report the actual shear profile in the system. The average shear value for the non-segmented results was 5.8 pixels, less than 30% of the actual value of 20 pixels.

The imposed global translation meant that, when segmentation was used, the underlying registration problem was solvable using only rigid registration techniques. For this undemanding deformation, the technique was capable of exactly measuring the applied sliding when using an appropriately segmented region. This test indicates that the technique is fundamentally capable of accurately determining shear.

2. Stretched Shear Accuracy

Five frames of the stretched MRI were quantitatively analysed at evenly spaced intervals through the image sequence. The graph in Figure 4.5a shows a typical example of a result replicated across all frames analysed. The plots in Figure 4.5a compare the shear results achieved along the sliding boundary with and without segmentation. Figure 4.5b shows the result of the summed shear across all frames compared to the actual total shear.

(a) Comparison of actual shear to calculated shear at both edges of the stretched region, with and without segmentation of the moving region for a shift of 1.73 pixels at the top of the image

(b) Comparison of total summed shear compared to actual summed shear across the whole stretched MRI image sequence
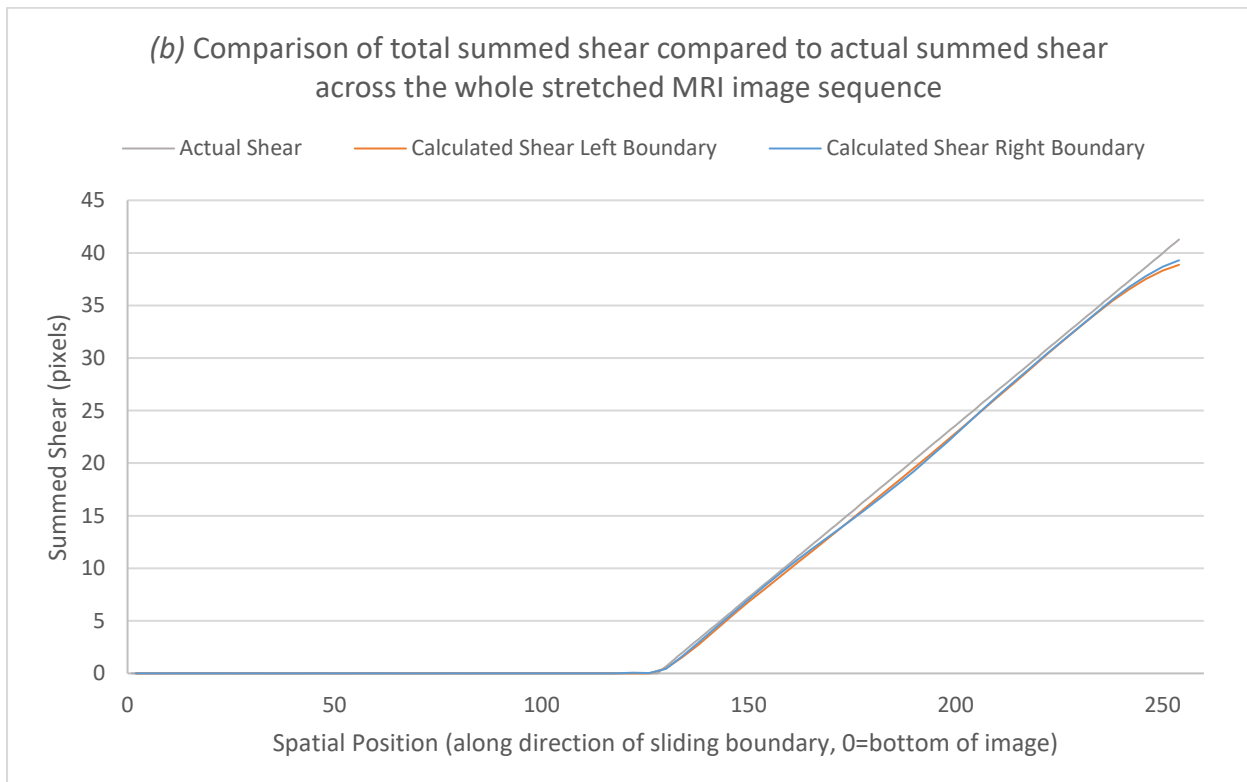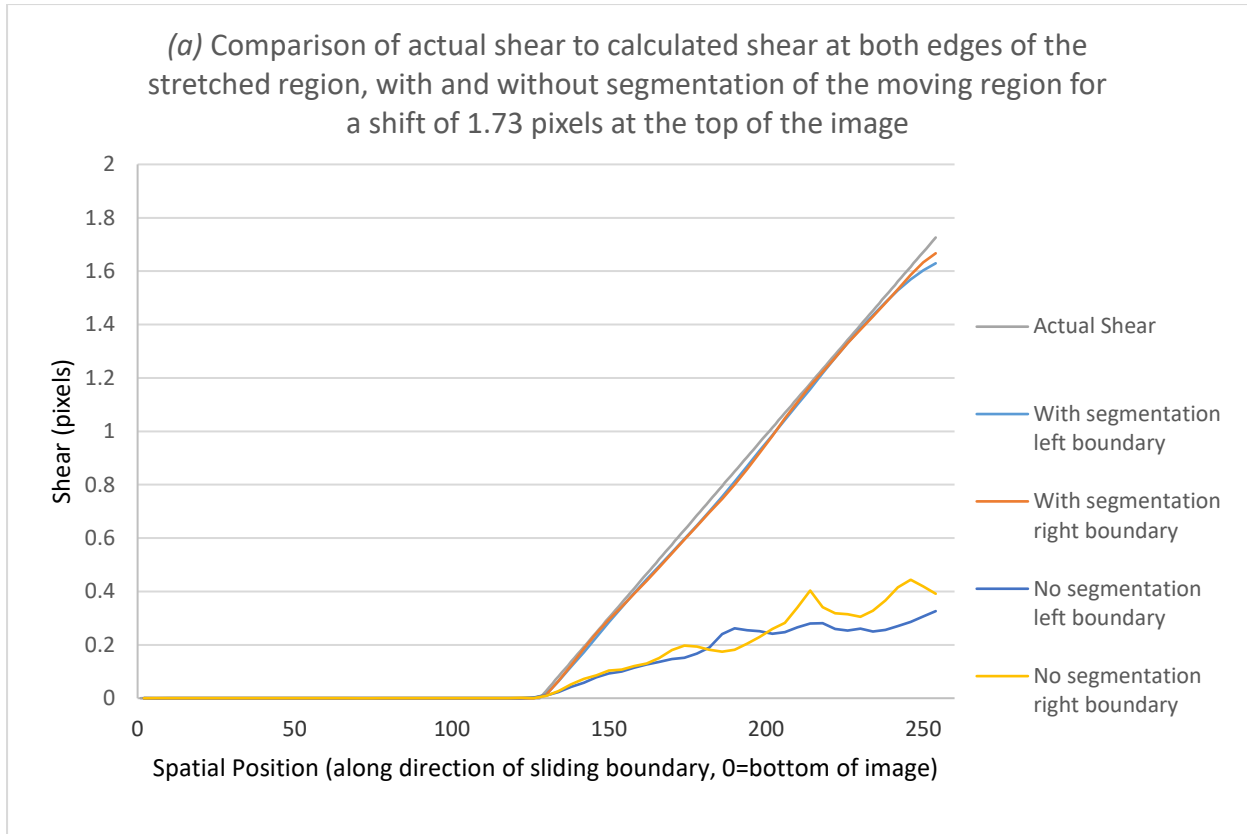
Figure 4.5: a) Comparison of results with and without the use of segmentation in a single frame [3].
b) Comparison of the summed shear across all frames with segmentation implemented

93

Figure 4.5a shows a close match between actual shear and calculated shear is produced when segmentation is implemented and shear is grossly underestimated when no segmentation is applied. The largest discrepancy in the results acquired by segmentation is observed towards the right of the graph (corresponding to the top of the MR image). The summed shear calculation in Figure 4.5b shows a similar pattern as the result for the individual frame (in Figure 4.5a). The largest discrepancy in Figure 4.5b was 2.4 pixels, corresponding to a percentage difference of 5.8% on the left boundary. In Figure 4.5a, similar percentage differences were calculated, with a percentage difference of 5.6% at the top of the image. This deviation may be attributed to detail being stretched outside the image space resulting in their new location being unknown to the registration algorithm. Excluding the uppermost extremities of the image, the discrepancy reduces to 1.05 pixels (4.7%) around the centre of the stretched region. These figures can be compared to a percentage discrepancy of the order of 70-80% when segmentation is not implemented. The stretched shear accuracy test incrementally increases the complexity relative to the translation in experiment 1. This test demonstrates the accuracy of the technique in a highly idealised environment in the presence of a simple, but spatially varying deformation. However, the simple nature of the deformation (uniform stretch) limits the extent to which the reported accuracies can be extrapolated to 'real-world' cases containing more complex deformations.

Section 2.5 discussed ShIRT's application to sliding boundaries without segmentation with varying magnitudes of smoothness constraint. The effect of the smoothness constraint on the shear at the boundary can also be observed and compared to the result of the technique with segmentation. Figure 4.6b shows the shear profile across the image taken at the position indicated by the yellow line at the top of the image in Figure 4.6a. The shear spikes are at pixel number 64 and 123 but the spike's width spans 8 pixels as the profile was sampled every 4th pixel (to match the nodal spacing of the image registration).

(a)
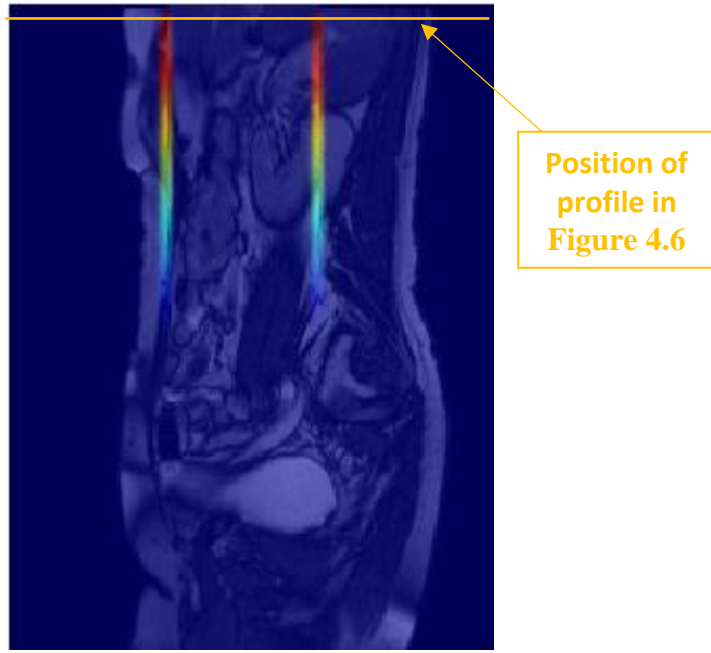
Figure 4.6:(a) shows the sheargram (when segmentation is used) from a single frame of the stretched MRI slice with the gold line indicating the profile used to plot (b). (b) compares the actual shear profile highlighted in (a) to the result with segmentation and without segmentation using different smoothness contraint values given by the numbers in the legend (default smoothness constraint is ~30 for the cine-MR images in this thesis).

95

The numbers in the legend labelling the curves on Figure 4.6b correspond to the magnitude of the smoothness constraint imposed on the non-segmented attempts. Section 2.5 highlighted that a smoothness constraint magnitude of <1 leads to an erratic deformation field and this range was therefore not included in Figure 4.6b. A close match between the shear profile produced from the segmentation is observed compared to ShIRT without segmentation for all smoothness constraints. This clarifies the need for particular methods to accommodate movement discontinuities when interpreting high shear.

The evidence presented throughout this section provides justification for the segmentation and registration approach taken (described in Chapter 3) to accurately measure shear in a discontinuous system.

4.2 Shear accuracy in a semi-idealised in-vitro model

4.2.1 Introduction

Moving on from highly idealised in-silico testing, this section describes a physical, practical challenge for the sheargram technique. A specific sliding geometry was created where a piece of sponge was inserted into a glass syringe and compressed. The aim was to confirm the performance of the technique in a less idealised setting.

4.2.2 Method

A roughly cylindrical piece of sponge was cut and detail was added to its surface in the form of pen markings. The sponge was inserted into a 100ml glass syringe. On the exterior of the syringe two paper strips (with regular markings) were applied to create a 'fixed wall' to contrast with the motion of the sliding sponge. A picture of the syringe and sponge in situ is shown in Figure 4.7a.
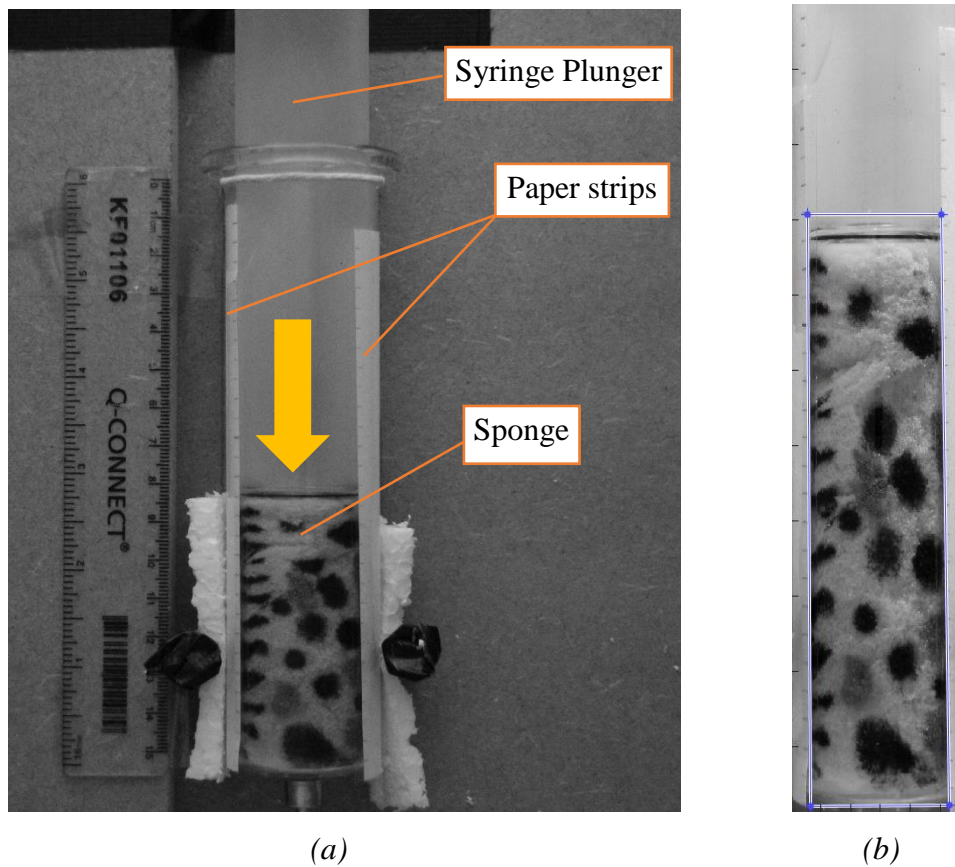
Figure 4.7: (a) Image of the experimental set up of the syringe fixed on a wooden board as the sponge was plunged to compress a sponge patterned with pen markings. (b) The ROI used for processing.

The plunger was used to gradually compress the sponge and to create an effective sliding motion relative to the stationary paper walls. As the sponge was compressed frontal images were captured with a standard DSLR camera (Cannon EOS 1100D) using a remote capture button to avoid inadvertent movement in the camera's position. The plunger was compressed by hand by approximately 2 mm between each image. The images were captured in monochrome on the lowest resolution setting on the camera (2256 x 1504 pixels). The images were cropped so only the portion containing the syringe remained. The cropped images were then processed by the visceral slide quantification technique (ROI shown in Figure 4.7b).

The result of the processing was compared to a manual estimate of shear gained through careful examination of the images by eye. The left hand side of the sponge (intentionally) contained regular pen markings to aid the operator in identifying corresponding points between images. By manually tracking the objects' positions immediately either side of the boundary (on the paper and sponge), an estimate of the shear could be calculated. It was the visual measurement of the sliding along the left sliding boundary that was compared to the processing result. Four frames were manually analysed to determine an estimation of shear along the left boundary.

97

4.2.3 Results and Discussion

Figure 4.8 shows two of the shear profiles calculated by the technique (blue line) compared to the manually interpreted shear (orange crosses).
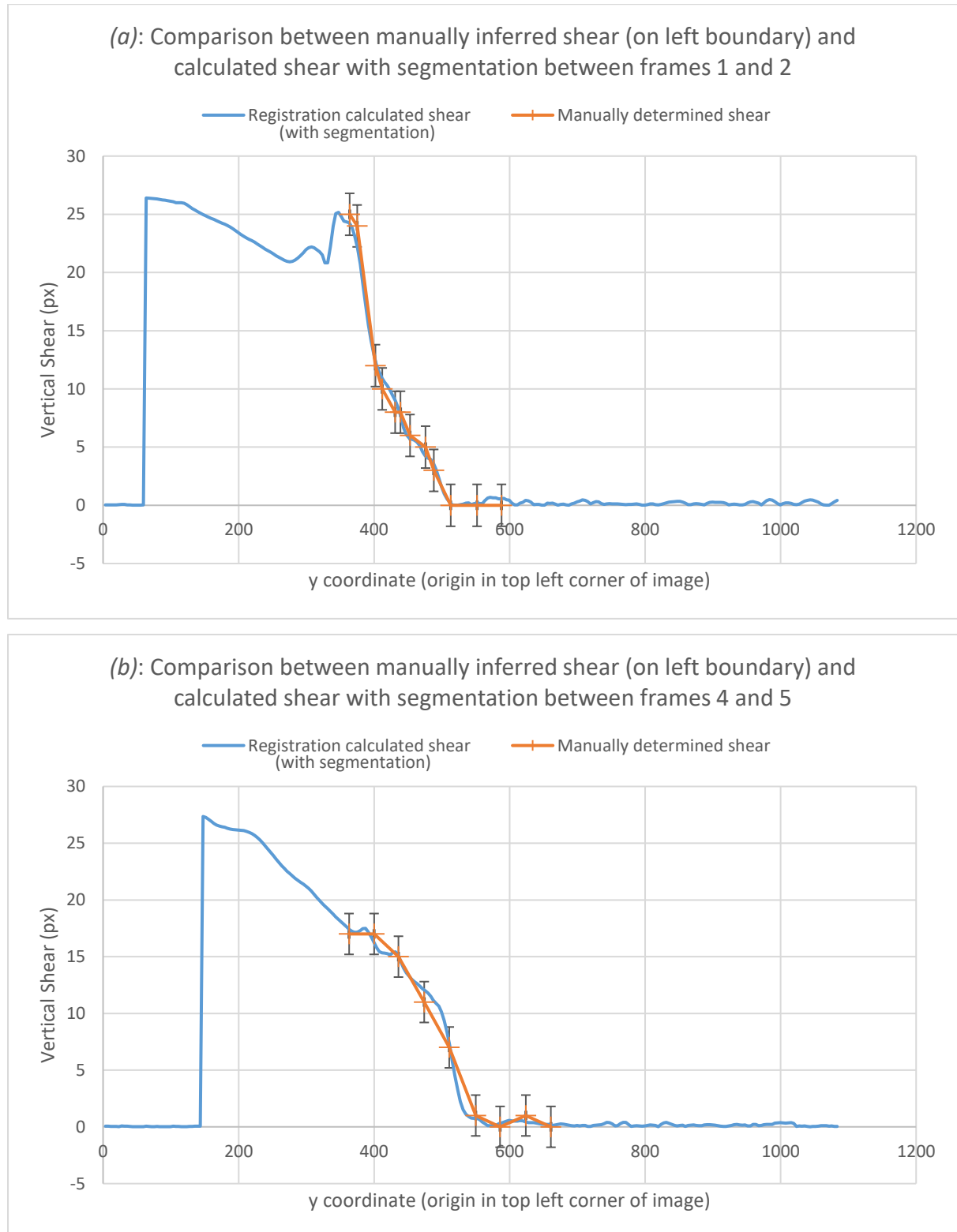
Figure 4.8: Shear determined manually (orange) along the left edge on two frames compared to shear calculated by the visceral slide quantification technique (blue).

The shear in the system is not known and must be inferred from visual interpretation of the images (by selecting reference points on the image by eye). Regular markings on the left of the sponge and markings on the paper boundary (see Figure 4.7) helped to select like points between frames but the process is still associated with an error, which must be taken into account when comparing the sheargram results. The error bars in Figure 4.8 were determined by manually judging the shear along the left sliding boundary between two frames 10 times and observing the variation. The standard deviation of the 10 repeated measurements at each point was calculated and the average of two standard deviations used for the error bars. A period of at least 3 days was left between each set of repeated manual shear measurements to lessen the impact of immediate memory. This error may compromise an in-depth quantitative analysis of accuracy but does allow a coarse comparison.

The manual results (orange) are only displayed for the region of sponge that was sliding and therefore do not run the length of the image/graph. In this region, the technique matched the manually interpreted shear within error for almost every point in every frame analysed. There were two positions (out of 38) in which the calculated shear lay outside the error bounds but both these points only marginally missed the error extremities by <0.1 pixels and are not a major concern.

The complexity of this in-vitro system remains relatively simple compared to the abdomen but presents a more realistic, less idealised challenge than the in-silico MR image experiments in Section 4.1. However, as the system becomes less well defined, the amount of shear which has occurred is not known and is harder to determine. A trade-off exists between complexity and the challenge presented by the experiment i.e. the more complex the system, the harder it is to obtain values for the 'true' deformation/shear to compare against the sheargram. This in-vitro syringe model acts as a stepping-stone towards the clinical situation by including non-uniform deformation and localised variations in sliding motion but maintains adequate simplicity so that shear measurements may be inferred to compare against the sheargram result.

This test has demonstrated the ability of the technique to accurately measure shear in the presence of more complex, irregular, localised movements. However, despite showing success, some aspects of the visceral slide quantification technique's methodology have not been challenged. For example, the syringe remained stationary throughout the frames meaning the shear summation process was not tested and the shape of the sliding boundary (i.e. a straight

line of the paper on the syringe walls) meant ROI placement was trivial. Nonetheless, this experiment has provided further evidence for, and confidence in, the underlying shear calculation process.

4.3 Adhesion detection in a semi-idealised in-vitro model

4.3.1 Introduction

The previous tests have focused on whether the implementation of the visceral slide quantification technique is measuring shear correctly. In this experiment, proof of concept for adhesion detection was sought. This experiment develops the physical syringe in-vitro model further to incorporate a simulated adhesion.

4.3.2 Method

This experiment used the same in-vitro syringe model and experimental set-up as described in Section 4.2.2. An adhesive piece of double-sided sticky tape was added to the inside of the syringe to create a localised resistance to the sponge's 'motion'. This set of images were then processed using the visceral slide quantification technique. The results could then be compared to the results of the previous experiment (Section 4.2.3), where the sponge's motion was un-impeded, to ascertain whether the adhered region was detected.

4.3.3 Results and Discussion

Figure 4.9a and Figure 4.9b show the syringe test object with the sponge uncompressed and in its final compressed position, respectively. Figure 4.9c and Figure 4.9d depict the shear summed over the whole compression sequence for the un-adhered acquisition and the acquisition with the double-sided sticky tape inserted, respectively.

(a)   *(b)*   *(c)*   *(d)*
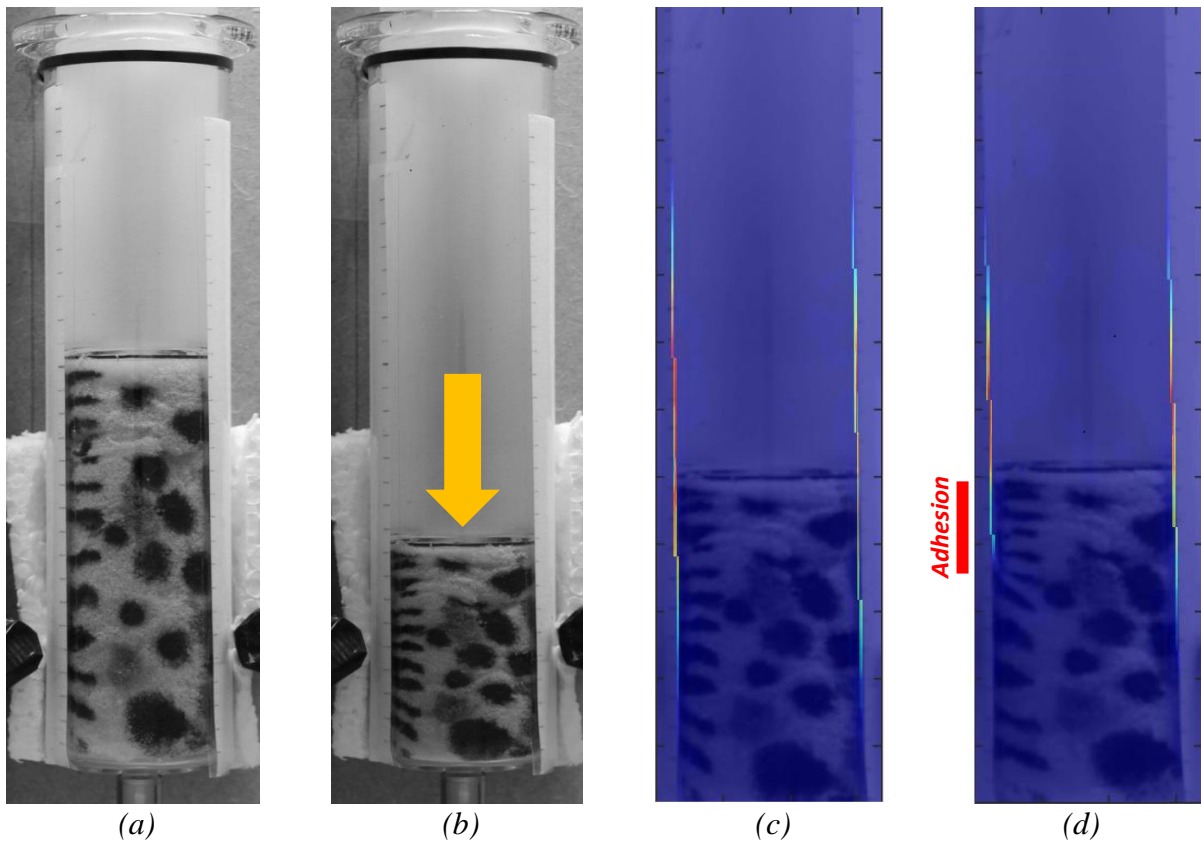
Figure 4.9: Syringe test object displaying a) uncompressed sponge, b) compressed sponge, c) shear result without adhesion, d) shear result with adhesion (indicated by red block) [3]

The difference in shear between Figure 4.9c and Figure 4.9d indicates that the presence of the adhesion has had an impact on the appearance of the sheargram. Comparison of the left boundary shows a sufficient reduction in shear at the site of the 'adhesion' to raise awareness of its presence. The small amount of shear observed at the site of the adhesion may be attributed to the weakness in bonding between tape and sponge as a small amount of slippage occurred. Comparison of the two sheargrams also indicates a subtle reduction in shear on the opposite wall to the adhesion. Close examination of the images and registration deformation field reveals that this is not a failing in the shear calculation but that the presence of the adhesion also influenced the sponge's compression at the right hand boundary. The region below the adhesion remained largely uncompressed and resulted in some sponge moving laterally into this uncompressed space rather than sliding vertically down the right hand boundary.

The experiment has been successful in its aim to demonstrate proof of concept that the sheargram is capable of detecting a localised resistance to sliding motion.

4.4 Artificial shear introduction

4.4.1 Introduction

This experiment investigates whether the process of segmentation and subsequent analysis of motion in different portions of the images separately generates artificial shear or exaggerates the actual shear which occurred.

4.4.2 Method

Two tests were undertaken using images containing idealised and complex motion to assess artefactual shear introduction:

Idealised motion

An idealised system without shear was generated by imposing a specified vertical translation to an entire sagittal MR image. Rows of pixels being translated outside of the image space (at the top of the image) were copied to the bottom row of the image. As all pixels were moving upwards together no shear was present in the image sequence. A triangular portion of the image was segmented and the region observed for the introduction of any shear. Using a triangular region allowed assessment of each of the vertical and horizontal axes and a boundary at an angle.

Complex motion

A region of interest was drawn in a stationary portion of two clinical cine-MRI sequences which contained movement elsewhere. The area surrounding each of the segmented stationary regions was also not moving, therefore no shear should be present around the perimeter of the segmented region. This is a less idealised example as there is complex movement in the vicinity of the ROI. The purpose of the first experiment was to confirm that implementation of the technique was not responsible for introducing shear; this experiment tests how well it copes in the presence of noise and movement elsewhere in the image space.

Quantification of the amount of artificial shear induced by the presence of an ROI was sought to help gauge its significance. To achieve a quantified value of the shear induced by the ROIs, first the scans were processed without any ROI present. The resulting sheargrams contain information on the amount of shear that would be calculated if the ROI was not present. The shear values generated in the presence of the ROI were first interrogated by examining the

shear around the ROI perimeter[10]. The same pixels in the sheargram without the ROI were also examined and used as a 'background shear'. The background shear was then subtracted from the shear calculated with the ROI in place, to give a value for the increase in shear when the ROI was added to the processing.

4.4.3   Results and Discussion

It is important to confirm whether artefactual shear is introduced by the process implemented in the visceral slide quantification technique.

Idealised motion

The ROI and sheargram for the first experiment (vertical translation) are shown in Figure 4.10.

<center>(a)   (b)</center>
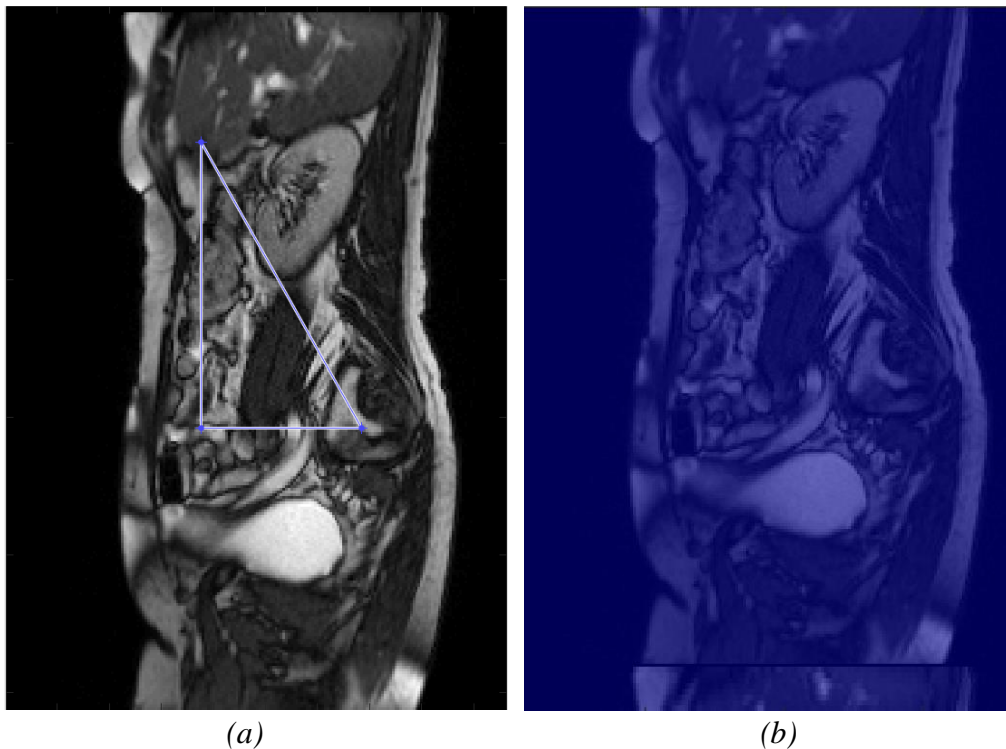
Figure 4.10: (a) Region drawn on the MR image and (b) the resulting sheargram depicting no shear

No shear was detected around the boundary of the region in Figure 4.10: the maximum summed shear across all frames was negligible (0.0004 pixels). This test confirms the absence of any fundamental flaws in the shear calculation process that introduces shear where none exists.

---

[10] Specifically, the shear around the perimeter of the ROI was interrogated by searching for the highest shear value along a line perpendicular to the ROI boundary (+/- 5 pixels either side of the ROI line). This achieved a maximum shear value for every point on the ROI boundary. The process was repeated on the same pixels in the sheargram produced when no ROI was used.

Complex motion

The second experiment was performed on two clinical images shown in Figure 4.11. The regions (orange) are positioned in stationary areas of the image where there should be no shear.

(a) (Example 1)   *(b) (Example 1)*

High tensile/shear

Low tensile/shear

(c) (Example 2)   *(d) (Example 2)*
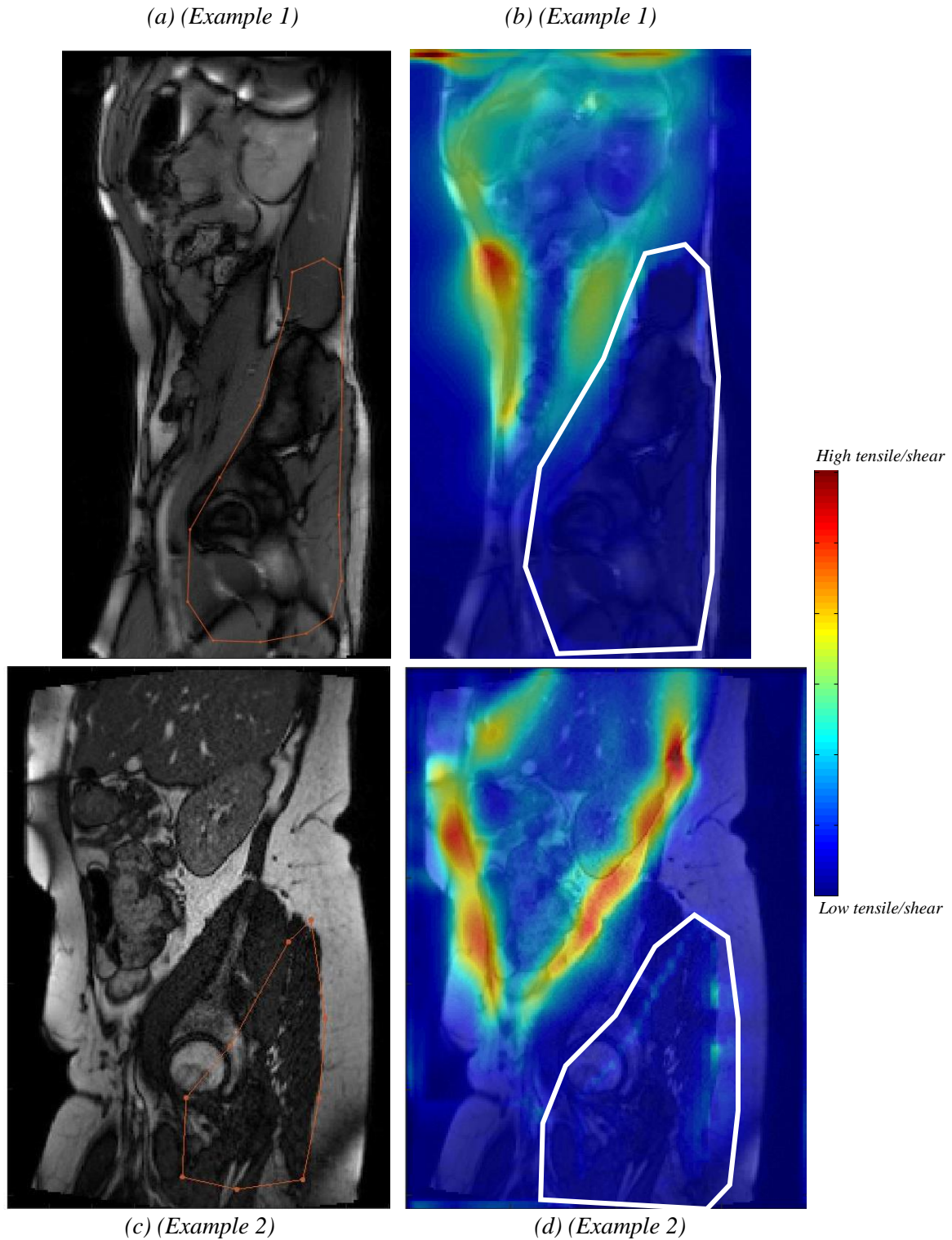
Figure 4.11 Images showing the locations of ROIs drawn in stationary areas of two clinical cine-MR images (a and c) and their accompanying sheargrams with the vicinity of the ROI marked by the white line to investigate whether the ROI artificially introduces shear. Note: the diffuse high shear (red/yellow areas) around the abdominal cavity are not the focus of this test.

The resulting sheargrams did not involve segmentation of the abdominal contents creating a more diffuse shear pattern around the abdominal cavity. Qualitatively, minimal shear was artificially induced around the perimeter of the regions as shown in Figure 4.11b and Figure 4.11d. In both examples a faint outline of induced shear is visible around the ROIs – within the white highlighted area.

The quantitative analysis calculated the increase in shear as a result of the presence of the two ROIs shown in Figure 4.11a and Figure 4.11c. The histograms in Figure 4.12a and b show the distribution of shear increase observed around the perimeter of the ROIs in each example case.

In the first example (Figure 4.11a and Figure 4.11b), the mean shear induced (ROI shear minus background) was 1.8 pixels and the standard deviation 1.6 pixels. From Figure 4.12a the vast majority of pixels around the ROI had a raised shear of between 0 and 3 pixels (317/371 pixels, 85%). In the second example (Figure 4.11c and Figure 4.11d) the mean shear increase was 1.5 pixels with a standard deviation of 1.3 pixels. Figure 4.12b also shows the vast majority (271/297, 91%) of pixels had an artificially induced shear of <3 pixels in the second example. When the example scans in Figure 4.11 are processed 'correctly', i.e. by drawing an ROI around the abdominal cavity, the average maximum shear around the perimeter of the abdominal cavity was 58 and 24 pixels in example 1 and 2 respectively. These figures place the shear increase in the presence of an ROI in the stationary region into perspective relative to the typical shear observed in cine-MRI scans; i.e. the presence of an ROI boundary can introduce artificial shear but the increase in shear is small when compared to the typical shear calculated in clinical sheargrams.

(a): Example 1
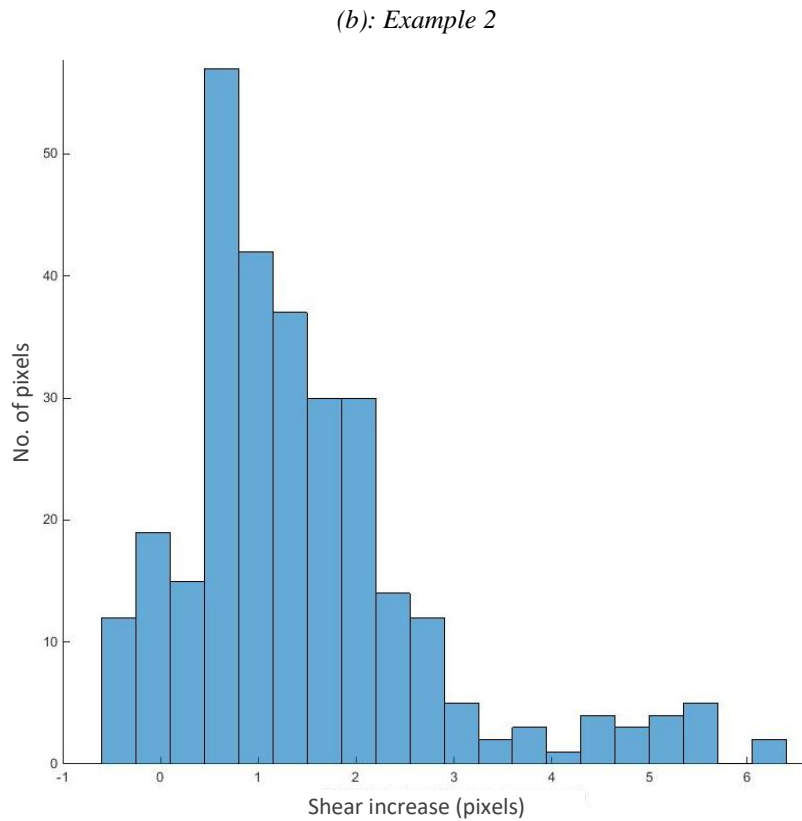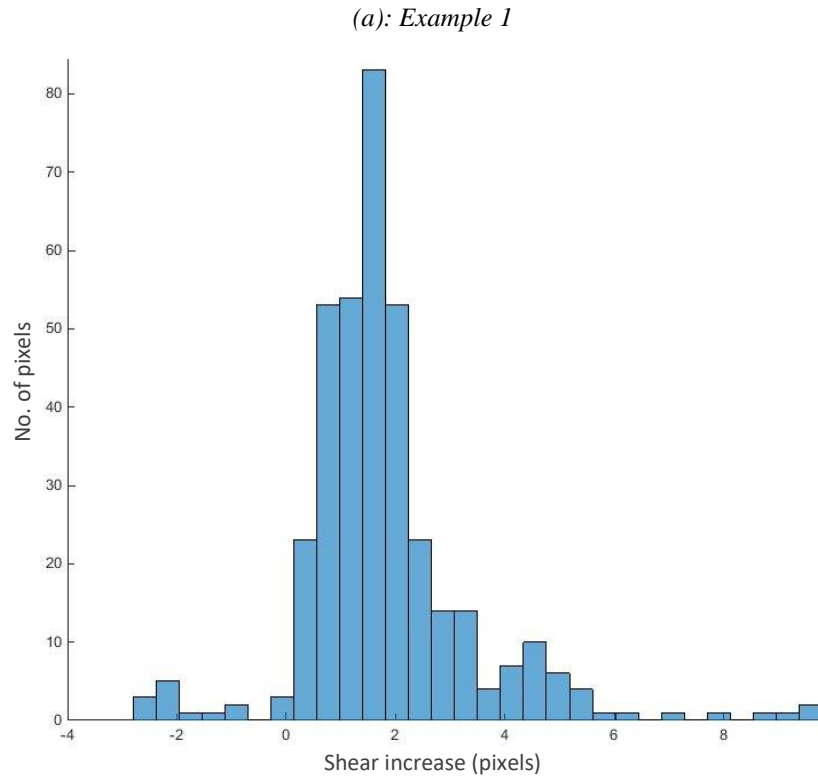
(b): Example 2

Figure 4.12: Histograms showing the amount of artificial shear introduced around the ROI perimeter in a stationary portion of (a) Example1 and (b) Example 2. The histograms provide a distribution of shear increase by linking the increase to the number of pixels with that shear increase.

The primary reason for the observed increase in shear around the stationary ROIs is explained by the lack of an ROI around the abdominal cavity causing a diffuse shear pattern to spread into the vicinity of the stationary ROI. The smoothness constraint in the registration algorithm causes the displacements calculated to spread further from the natural sliding boundary leading to the wider shear distribution observed in Figure 4.11b and d. When the displacements meet the boundary of the ROIs, their propagation is halted more abruptly. This leads to a sudden cut-off in displacement rather than the natural decline observed elsewhere and results in a larger perceived shear. Other factors, such as changing signal intensity between frames and noise also contributed to a shear increase and are the cause of the localised increases in shear to the posterior of the ROI in example 2.

Considering these points, the small amount of introduced shear that has been observed is to be expected. The amount of shear is small relative to the shear in the system with 85% and 91% of the shear induced being <3 pixels. Whether this amount of artificially induced shear will be the same around the sliding boundary is not possible to determine. However, the evidence presented in the highly idealised in-silico tests suggest that when the ROI is perfectly positioned the shear can be accurately measured. The information presented indicates that the process used to calculate shear could potentially lead to errors in shear measurement but it is unlikely to significantly affect the result.

4.5 Repeatability in sagittal abdominal cine-MRI

4.5.1 Introduction

The synthetic tests offer insights into the abilities of the technique but in order to understand its capabilities for its intended purpose it must be tested on clinical images. A brief investigation of the potential for artefactual shear to be introduced on clinical images has already been described. This test aims to determine the reproducibility of the processing method as a whole as an indicator of its reliability and robustness: two essential characteristics relevant to its potential as a clinical tool.

4.5.2 Method

Two sagittal cine-MRI slices were processed five times each. Both slices contained surgically confirmed adhesions to the abdominal wall of differing subtlety: Scan 1 contained a gross adhesion, Scan 2 a subtle adhesion. The presence of adhesions in both scans permitted analysis

of the variability in shear observed in the adhered areas. For Scan 1 four of the processed results were produced over the course of two consecutive days while the other was processed a year before. Two of the processing runs for Scan 2 were performed a year prior to the other three. The sheargram is the principal diagnostic output of the technique and it was the reproducibility in the sheargram (i.e. summed shear over the whole dynamic image sequence) that was assessed. The resulting repeated sheargrams were compared both qualitatively, by comparison of their appearance, and quantitatively.

Quantitative comparison between two sheargrams may not be achieved via simple subtraction of the shear in one image from the other. The exact spatial position of the shear changes with the user-defined ROI position. The small spatial mismatch requires a post-processing solution, which was sought through two approaches:

1. **Image registration and subtraction:** The sheargrams were registered (non-linearly using ShIRT) to one another so their shear profiles overlapped. A whole image subtraction of the registered sheargrams could then be performed to achieve an image displaying the differences in shear between repeated processing results.

2. **Regional Analysis:** The sliding boundary was split into several regions/ROIs and the average shear values in each region compared. The regions were drawn in MATLAB and the ROI positioning process ensured continuity between regions around the perimeter of the abdominal contents (i.e. there were no gaps between the ROIs). Scan 1 was split into 11 ROIs and Scan 2, 13 ROIs. The sizes of the regions were roughly the size of an adhesive area in each scan. The regions used for each scan are shown in Figure 4.13.

Scan 1 *Scan 2*
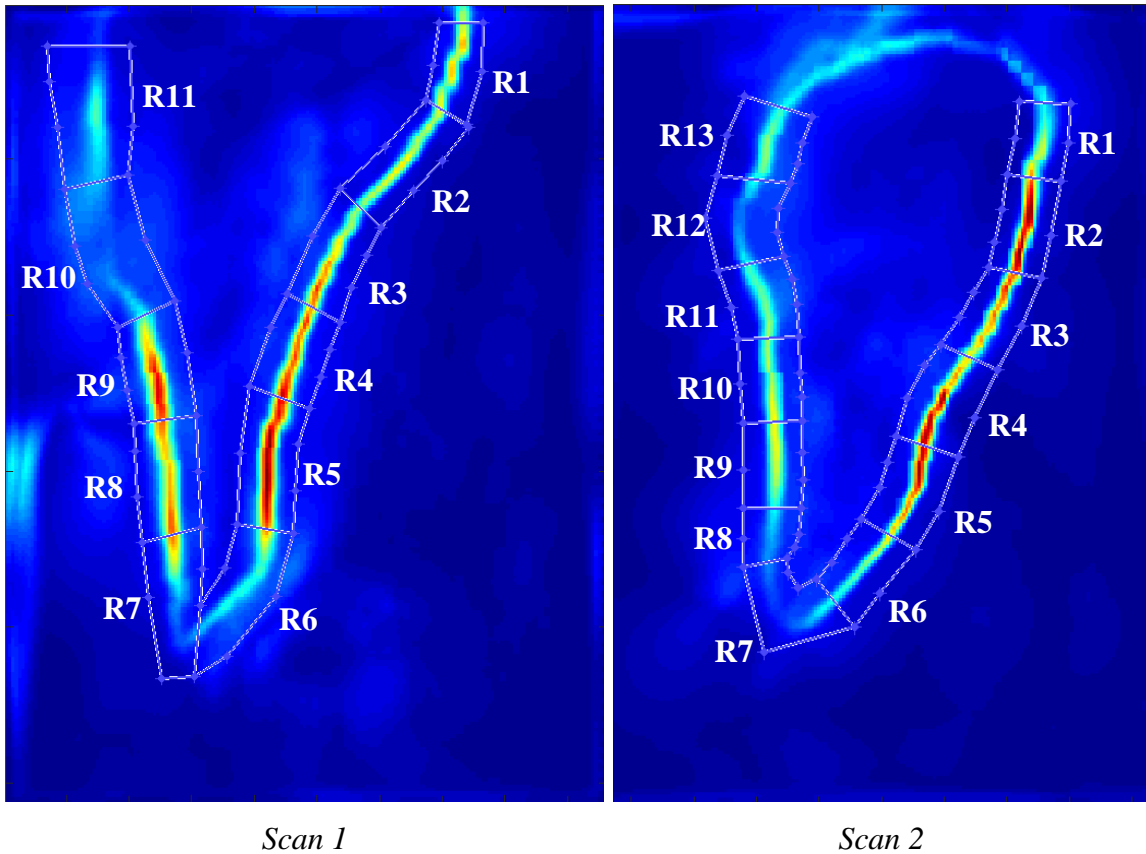
Figure 4.13: Regions used to quantitatively analyse each of the two sets of sheargrams

4.5.3   Results

4.5.3.1   Qualitative Sheargram Comparison

A qualitative comparison compares the appearance of the repeated sheargrams side-by-side. Five sheargrams resulting from repeated processing of the two different scans are shown in Figure 4.14 and Figure 4.15.
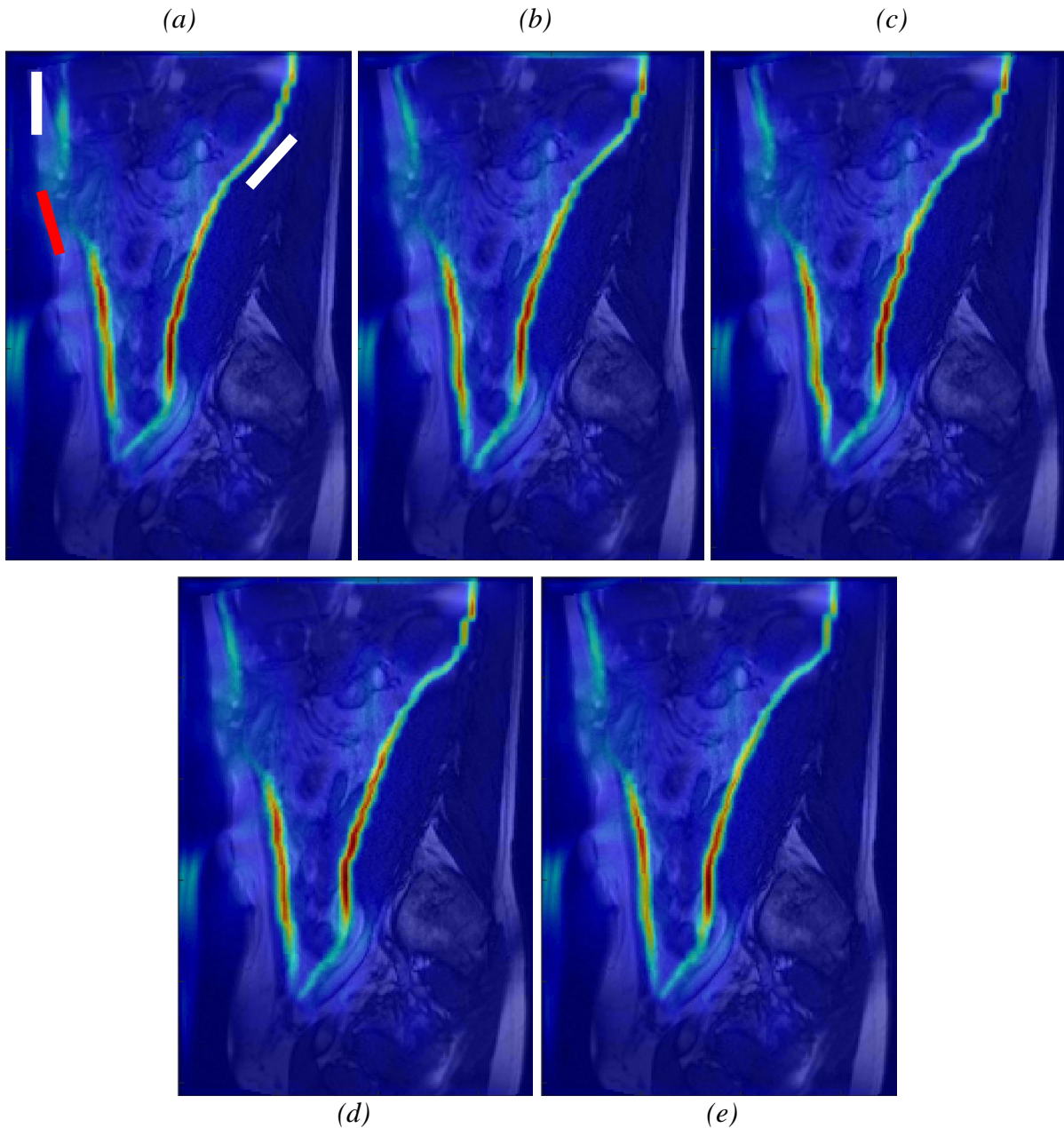
Figure 4.14: Five sheargrams showing the results of five processing runs of Scan 1. The first sheargram (a) was produced over one year prior to the others. On the first sheargram the red bar highlights the location of an adhesion, the white bars indicate areas of increased discrepancy

Similarity of the repeated sheargrams in Figure 4.14 is apparent; all offering a similar interpretation. Minor differences between the sheargrams are only visible under close inspection. A sharp drop in shear at the site of the adhesion (red bar in Figure 4.14) is present in all sheargrams.
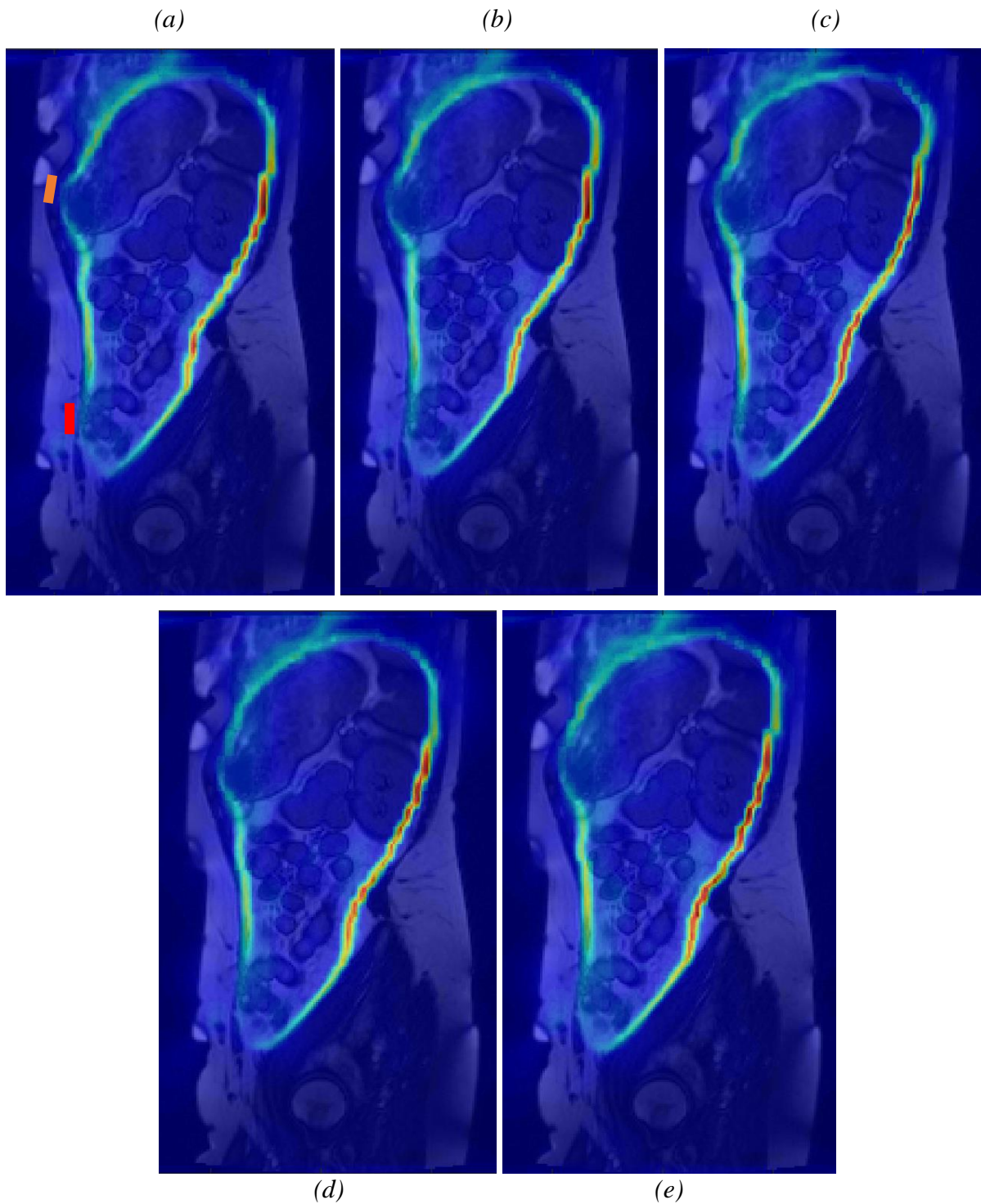
Figure 4.15: Five sheargrams resulting from repeated processing of Scan 2. The first two sheargrams (a and b) were produced over 1 year prior to the other three. The location of a surgically confirmed adhesion is indicated by the red bar in the first sheargram, the orange bar corresponds to a possible adhesion.

Figure 4.15 also shows a similar shear pattern in all repeated sheargrams performed on Scan 2. The drop in shear at the surgically confirmed adhesion (red bar) is less obvious than for the adhesion in Scan 1 but is present in all sheargrams.

4.5.3.2   Quantitative Sheargram Comparison

Quantitative comparison aims to produce a measure of the difference between the two sets of five repeated sheargrams shown in Figure 4.14 and Figure 4.15. As stated in the method (Section 4.5.2) two approaches for quantitative comparison were attempted and the results for each are communicated separately.

Image registration and subtraction:

An example of a difference image, after image registration and subtraction of two sheargrams, is shown in Figure 4.16.
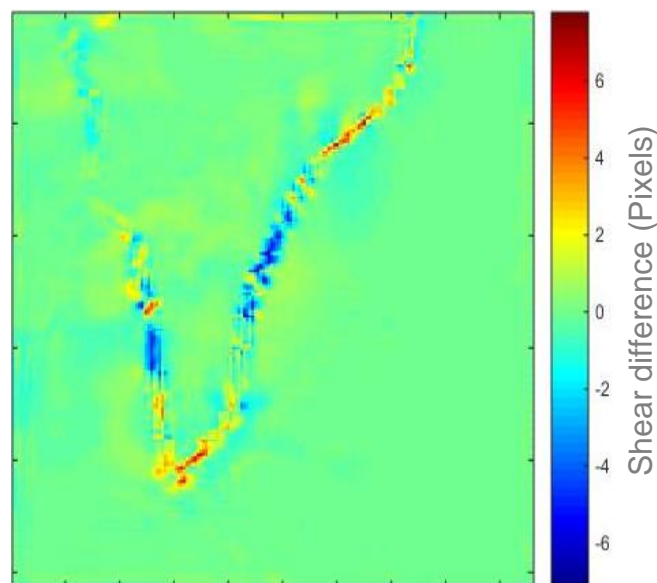
Figure 4.16: Image depicting the difference in shear values between two of the processing runs

Image subtraction gives the difference between every pixel in two sheargram images and can be used to identify the areas of largest discrepancy around the sliding boundary. Detailed description of these results is not appropriate due to their questionable significance – discussed in detail in the discussion, Section 4.5.4.2.

Regional analysis:

Both scans were split into the regions shown in the method section, Figure 4.13. The average shear in each region was calculated for each of the five processing runs and the maximum difference in average shear in each region used as a metric for similarity. These results are represented in Figure 4.17. The shade of each block indicates the average shear (across all five processing runs) and the thickness of each block is proportional to the range of average shear observed between the processing runs.
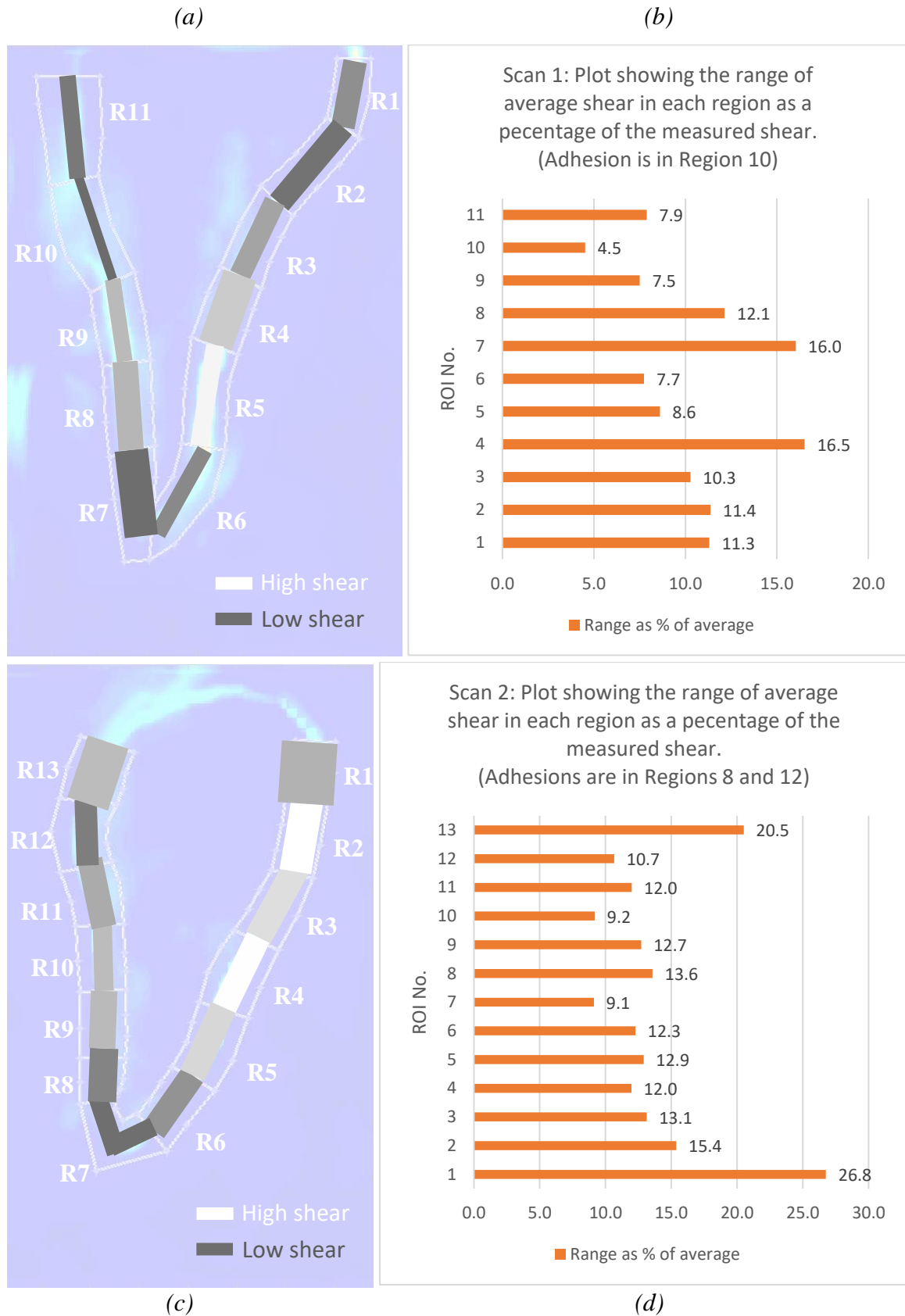
Figure 4.17: Images and graphs indicating the range in shear observed in each of the ROIs. The graphs in (b) and (d) show the range in average shear between the processing runs as a percentage of the shear in each region. Figures (a) and (c) show the percentage range overlaid on the original sheargram: the width of the bar in each region is proportional to the percentage range; the shade of grey is proportional to the average amount of shear in each region (white = high shear, dark grey = low shear)

113

In Scan 1 the maximum range in average shear occurred in region 4, which in absolute shear, was 3.4 pixels. However, most regions exhibited a much smaller variation bringing the average range to 1.7 pixels. When converted to a percentage of the average shear in that region, the maximum difference between processing runs was 16.5%, with most regions remaining under 11%. The average range as a percentage of the regional average shear was 10.4%. In Scan 2, the difference range was larger, averaging at 2.6 pixels. The maximum difference between processing runs was 4.8 pixels in region 1. The average percentage difference as a percentage of the average shear in each region was 13.9% and the maximum percentage difference was 26.8% in region 1. Regions containing adhesions exhibited lower than average discrepancies in shear.

4.5.4   Discussion

4.5.4.1   Qualitative discussion

When reporting, the sheargram is judged qualitatively, therefore the reproducibility in the qualitative assessment is arguably the most important. For Scan 1, the two areas in which small differences in shear are observable are highlighted in white in Figure 4.14a. Small deviations in the position of the ROI is the likely cause of the small differences in these regions. In all repeated sheargrams, the reduction in shear at the adhesion site is apparent and the diagnostic outcome would be the same in all instances.

For Scan 2, the drop in shear in all repeated sheargrams would result in the surgically confirmed adhesion being identified. However, differences in the magnitude and severity of the drop in shear can be observed between the repeated sheargrams: Sheargram 1 has a more severe drop than Sheargram 3. Although the differences were not great enough to affect detection of *this* adhesion, the variability observed in the lower abdomen region indicates that for an even subtler adhesion, this is a conceivable possibility.

The area marked by the orange bar in Figure 4.15 is a suspected adhesion (previously undetected before an expert radiologist's examination of the sheargram) but is not surgically confirmed. The drop in shear in this region is consistent and although subtle, it remains large enough in all cases to draw the attention of the reporter. Similar to the surgically confirmed adhesion (red bar), the magnitude of the drop at the suspected adhesion (orange bar) varies between sheargrams: sheargrams 3 and 5 exhibit slightly larger shear values than Sheargrams

1 and 2. This difference may be attributable to a difference in the ROI position: a sharper contour of the abdominal cavity and more abrupt change in boundary angle is observed, particularly in Sheargram 1 compared to Sheargrams 3 and 5.

The sheargrams presented in Figure 4.14 and Figure 4.15 offer reassurance that the processing technique is robust enough to not alter the sheargram enough to change clinical opinion. Scan 2 presented a challenging subtle adhesion which was detected on all sheargrams. The small differences in shear may be mostly attributed to differences in the ROI at those specific locations. It should be emphasised that this test has only been performed on two cine-MRI scans and although this offers some evidence to support the reproducibility of the technique, it would benefit from further exercises to confirm its reproducibility. To some extent Chapter 5 provides additional supporting evidence for the technique's reliability on clinical data.

4.5.4.2 Quantitative Discussion

Although qualitative assessment of reproducibility is consistent with how the sheargrams are interpreted and reported, the assessment of reproducibility is itself subjective. Attaching a figure to the variability of the processing technique improves objectivity in the reproducibility assessment.

Image registration and subtraction:

Although this method provides a clear picture of the differences between two sheargrams, it can be shown to exaggerate this difference. For instance, consider a sheargram registered to another sheargram then registered back to its original position and subtracted from the original. Figure 4.18 shows the original sheargram (Figure 4.18a) next to the re-registered sheargram (Figure 4.18b) and the two sheargrams overlaid on top of one another with the original given a green colour channel and the re-registered sheargram a red channel – where they overlap in magnitude therefore results in yellow (Figure 4.18c). Figure 4.18d shows the result of subtracting the re-registered sheargram from the original sheargram to produce a difference image similar to that shown in Figure 4.16. Figure 4.18e shows a histogram of the difference values in Figure 4.18d for pixels in the vicinity of the sliding boundary.
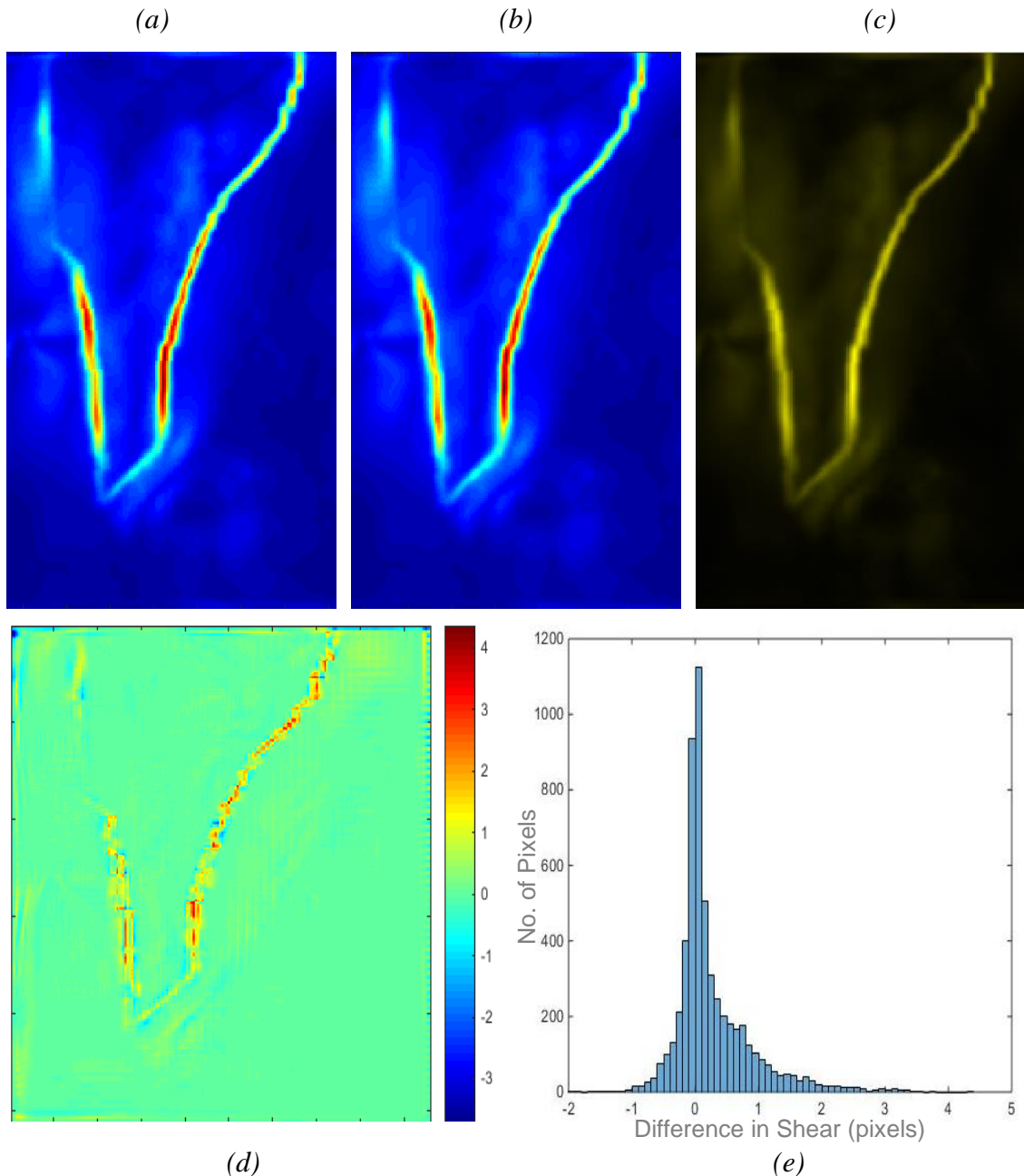
Figure 4.18: (a) Original sheargram; (b) Sheargram that has been registered to another sheargram and re-registered back to the original in (a); (c) The original and re-registered sheargrams overlaid with green and red channels (so overlap is coloured yellow); (d) Image depicting the differences between the original and re-registered sheargrams; (e) histogram of the difference in shear around the abdominal perimeter in (d).

Figure 4.18a, b and c show the re-registered sheargram to be almost identical to the original; by eye there is no discernible difference between the two. Despite the apparent similarity, the difference image in Figure 4.18d and the spread of difference shown in Figure 4.18e indicates notable differences between individual pixels. The average percentage difference between in individual pixels between the two sheargrams (only considering pixels within +/-5 pixels of the sliding boundary) was 3% with a maximum difference of 24%; for comparison, the average

percentage difference between two different sheargrams registered to one another was roughly 8%. These figures suggest that the analysis method is prone to introducing large discrepancies making any assessment of the actual differences between sheargrams difficult. The average difference introduced together with the spread of difference values shown in Figure 4.18e does not give a representative account of the actual observed differences in the sheargrams. The regional analysis method for quantification of the differences (discussed below) therefore takes precedence.

Regional Analysis:

Figure 4.17 allows conclusions to be drawn regarding the reproducibility in shear that can be expected across a significant portion of a sheargram. Quantitatively comparing the shear in larger elements around the perimeter of the abdominal cavity recognises the fact that it is not the individual pixels which are inspected when viewing the sheargrams but trends over larger portions of the sheargram.

The regions containing adhesions resulted in an average or below average discrepancy between processing runs. These regions are arguably the most clinically important and it is reassuring that the discrepancy in these regions was not inflated and the amount of shear was mostly replicated across repeated sheargrams. This provides some evidence for consistency in adhesion detection.

Regions 4 and 7 in Scan 1 exhibited a considerably larger error than other regions. Region 7 can be attributed to large differences in the ROI placement. The path for ROI boundary placement in this region was ill-defined due to a lack of landmarks and the point at which the ROI met the abdominal wall was not important due to the lack of structure in this region. The larger maximum difference observed in region 4 is difficult to attribute to a particular aspect of the processing technique as the ROIs were consistently drawn between processing attempts. However, deeper interrogation revealed that two of the processing runs had a small but consistent difference in the ROI position, present in all 30 frames. The accumulation of the difference over the whole imaging sequence was enough to produce the largest difference in this scan. This was potentially exacerbated by the fact that this was an area of high shear, therefore leading to a larger absolute difference in shear. Re-inspection of this region in the original sheargrams between Figure 4.14d and Figure 4.14e does reveal a noticeable difference, supporting this quantification.

The largest discrepancies, across both scans were observed in regions 1 and 13 in Scan 2. As with region 7 in Scan 1, the large differences in region 13 can be attributed to relatively large differences in ROI placement. The position of the sliding boundary was challenging to determine in this region due to out-of-plane motion and ambiguity in its edge. The discrepancy observed in region 1 of Scan 2 may be attributed to an accumulation of small differences in ROI position over the whole imaging sequence, as with region 4 in Scan 1. The two processing runs exhibiting the largest difference in region 1 (therefore accounting for the largest 4.8 pixel, 26.8% discrepancy across both scans) had similar initial ROI placement in this region. However, examination of all subsequent ROI positions throughout the imaging sequence reveals a small but systematic difference.

A large difference in ROI position was expected to produce a different result in shear but this experiment has uncovered that small, consistent differences can also significantly impact the shear profile. This finding affects practice, and consistency is required when adjusting the ROI placement across all frames. It provides evidence and impetus for pursuing a more consistent segmentation method, relying less on subjective human input. Further attempts to characterise the effect of ROI position are made through a more systematic investigation in the following sub-section (Section 4.6).

Quantitative characterisation of the error/reproducibility in the sheargram was an aim of this chapter but it is difficult to conclude with a single figure for reproducibility from this experiment. Firstly, only two scans have been processed and this lacks the power to be considered a representative sample of all scans: dynamic MRI abdominal scans vary considerably in shape, presence of pathology and magnitude of visceral slide generated by the individual. Secondly, the method of regional analysis is only one way of tackling the problem. There are many potential tests and measures which could be performed to obtain different results for the reproducibility; as demonstrated by the brief investigation into comparing the difference in every pixel of the sheargram. This experiment has determined that considerable variation between different regions of the sheargram may exist when reprocessing scans, therefore a single measure is unlikely to apply to all regions. For these reasons, this analysis has intentionally quoted a conservative, worst case measure of the differences observed: the maximum difference between the five processing runs in each region. From the evidence available in this experiment an approximate figure for the range of expected discrepancy in

shear across a considerable region of the image may be considered to be roughly 2±2 pixels in absolute shear values or 12±9% as a percentage of the average shear in a particular region (based on the overall average across both scans and ±2 standard deviations about that mean). These figures may be considered large enough to conceivably affect judgement in the region of a potential adhesion. However, all three regions containing an adhesion in this study exhibited smaller variation, providing some reassurance that this may be less likely around adhered areas. Additionally, as stated, this is a conservative estimate and these figures should not be taken as a rule but a rough approximation of the potential uncertainty in the shear that could be encountered. This is likely to be dependent on the ease of ROI placement in individual scans and therefore a much larger reproducibility study would be required to achieve a reliable estimate of the difference to be expected. Such a study was not considered feasible or necessary at the expense of other advancements at this stage of development.

This experiment has not made any attempt to assess inter-operator variability. This thesis aims to demonstrate proof of principle through processing with a single highly experienced operator prior to undertaking investigations into more detailed characteristics of the technique's efficacy. Nonetheless, a brief inter-operator comparison has been performed in the main discussion chapter (Chapter 6) to give an impression of this attribute.

4.6 Effect of ROI position

4.6.1 Introduction

The positioning of the ROI is the only component of the processing method requiring human interaction and therefore generates variability. The position of the initial ROI is expected to affect the final shear values calculated. It is important to determine the precision in ROI placement required to produce consistent shear values. This information is useful for making a judgement on the reliability of the technique and is a necessary component for assessing its clinical potential. The investigation described below assessed the change in shear along the, predominantly vertical, abdominal wall as a result of translating the ROI horizontally.

4.6.2 Method

An initial ROI was manually drawn around the abdominal contents and 8 more ROIs were generated by shifting the whole region +/- 4 pixels in the horizontal (x) direction. A new sheargram was generated for each ROI position. Sample points at every 20 pixels along the abdominal wall were examined – indicated as red horizontal lines in Figure 4.19a.

119

4.6.3 Results and Discussion

A comparison of nine sheargram profiles at one of the locations across the abdominal wall boundary is shown in Figure 4.19b. Figure 4.19c shows the maximum shear in each profile plotted against the ROI position.
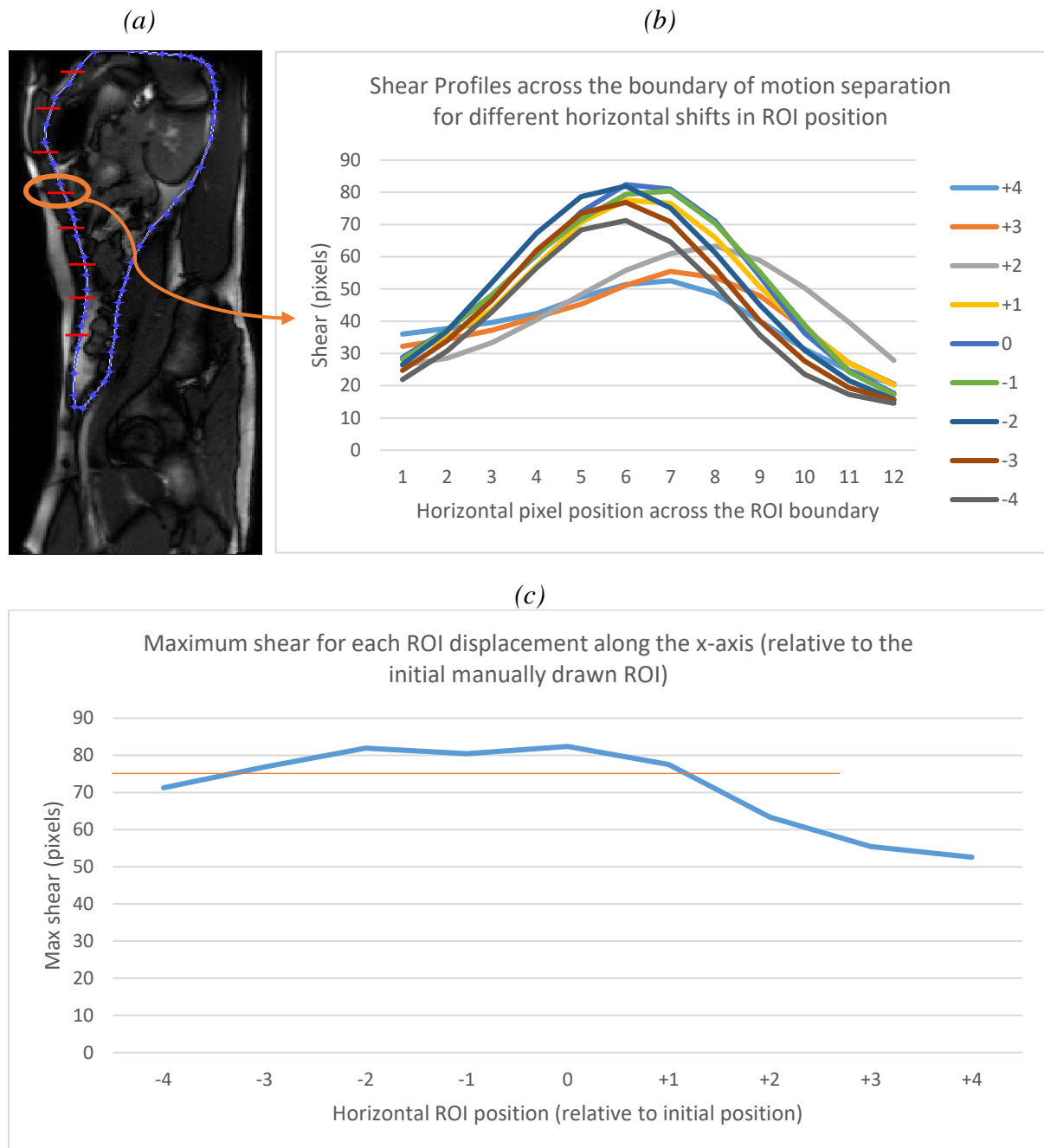
Figure 4.19: Comparison of shear results with a shift in ROI position. (a) shows the points along the abdominal wall which were sampled, (b) the shear profiles across the abdominal wall (along a red line in (a)), (c) the variability in maximum shear of the profiles in (b) with ROI position, orange line indicates a drop of 10% of the maximum shear.

It is apparent from the shear profiles in Figure 4.19b that the ROI position does influence the shear calculated. However, at most of the sampled points there is a range of ROI positions which result in a 'similar' shear profile. In Figure 4.19b and c, a shift in ROI position of between -3 and +1 (a range of 5 pixels) produces a drop in maximum shear of <10%, relative to the maximum shear achieved across all ROI shifts (orange line in Figure 4.19c = 10% drop). A range in ROI shift of 4 pixels was seen to produce a drop in shear of <10% in 5 of the 8 sampling points and 11%,17% and 22% at the remaining sampling points. The three sampling points with a larger response to a change in ROI position were the three lowest points in the lower abdomen. The reason why the lower abdomen is more sensitive to changes in ROI position is unclear, but this is a finding worthy of consideration when drawing the ROI.

These results highlight the importance of achieving a consistent and appropriate ROI position. Examination of the ROI position from the repeatability experiment (in the previous section) provides an idea of the variability in ROI placement. The two most disparate ROIs for Scan 1 have been superimposed on the MRI image in Figure 4.20.

Figure 4.20: ROI positions of the two most disparate ROIs from the repeatability experiment. The orange ROI is from the processing run which was undertaken over 1 year prior to the others.

The orange and blue ROIs display a gap of greater than 4 pixels in two locations: at the upper and lower extremities of the abdominal wall. The lowest extremity of the abdominal wall is of little importance in this example due to a lack of abdominal contents in this area and less attention was given to this area. After re-examination of the sliding boundary in the upper abdomen, the orange ROI (the processing run performed >1 year prior to the others) was in error and is an example of the human error present within the processing technique. Apart from the two areas mentioned, all five ROIs were within 3 pixels of one another around the remainder of the perimeter of the abdominal cavity. This implies this level of consistency in ROI placement is possible but also draws attention to the risks of relying on human interaction. (Note, other risks and challenges are acknowledged when using alternative mechanisms to human interaction.)

The observed changes in shear profile and drop in maximum shear (Figure 4.19) as a result of shifting the ROI position indicates the importance of identifying the correct location of the sliding boundary. This is recognised as a drawback of the current implementation of the technique. As shown in the repeatability experiment, drawing the ROI by eye is capable of consistently replicating the position to within 3 pixels of one another, at least in this example. However, the potential errors introduced by human interaction will always remain and, as shown in the lower abdomen, the ROI occasionally needs to be more precise as a shift of 3 or 4 pixels is capable of generating differences in shear in the order of 20% (at the most extreme). A more consistent, less subjective, more automated ROI positioning method is earmarked for future developments. This could focus on identifying the boundary which produces a maximum shear profile. Potential options have been tentatively explored and are discussed in the discussion chapter – Chapter 6.

4.7 Shear summation procedure accuracy

4.7.1 Introduction

The accurate summation of the shear in each frame to produce a single picture of shear across the imaging sequence is essential for interpretation. The summation procedure requires spatial matching of like points along the sliding boundary between consecutive frames. Two different shear summation procedures were implemented and tested on clinical data during the development phase of the technique. This section assesses the accuracy of both methods.

4.7.2 Method

The two implemented methods were:

1) Registration of a 'boundary region': The position of the ROI perimeter in every frame was used to generate a mask encompassing only the boundary itself (+/- 3 pixels). This produced a series of images with only a thin band around the ROI perimeter remaining, as shown in the example in Figure 4.21a. Consecutive 'boundary image' frames were then registered and the resulting deformation maps used to overlay like points on the sliding boundary between frames.

2) Registration of the abdominal surroundings: This was the method adopted and described in Section 3.2.7 – using the deformation map acquired from the registration of the abdominal surroundings to track the position of the boundary.

(a)   *(b)*
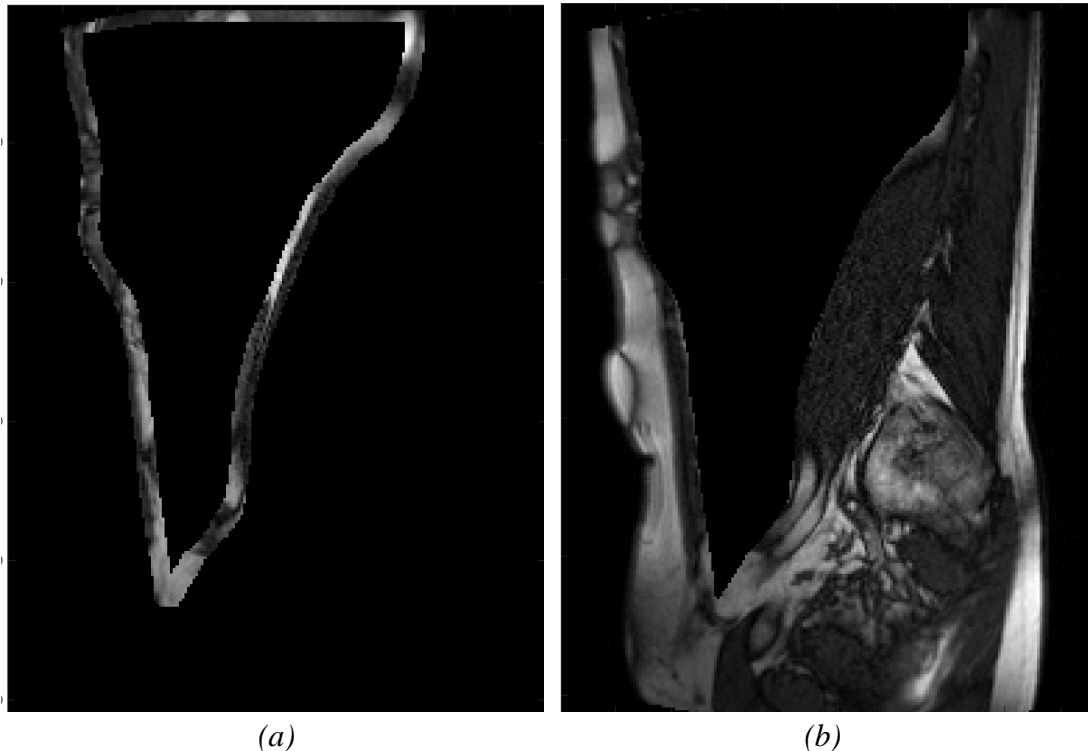
Figure 4.21: Images showing (a) boundary masked image and (b) the masked image of the abdominal surroundings for the same sagittal slice

The reasoning behind producing a masked region which only maintained detail around the sliding boundary (Method 1) was to aid the registration algorithm by reducing interference from other areas in the image. Method 2 incorporated a greater amount of detail at only one side of the boundary providing more information to the registration algorithm.

The accuracy of the two summation techniques was quantitatively analysed on a typical patient with large abdominal motion and abdominal wall motion. A series of landmark points (corresponding to 12 of the ROI vertices) were tracked by eye throughout the cine-MR series of images. The landmarked points were chosen for their proximity to easily identifiable anatomy to aid reproducibility and consistency in picking the same points between frames. The landmarked points are shown in Figure 4.22.
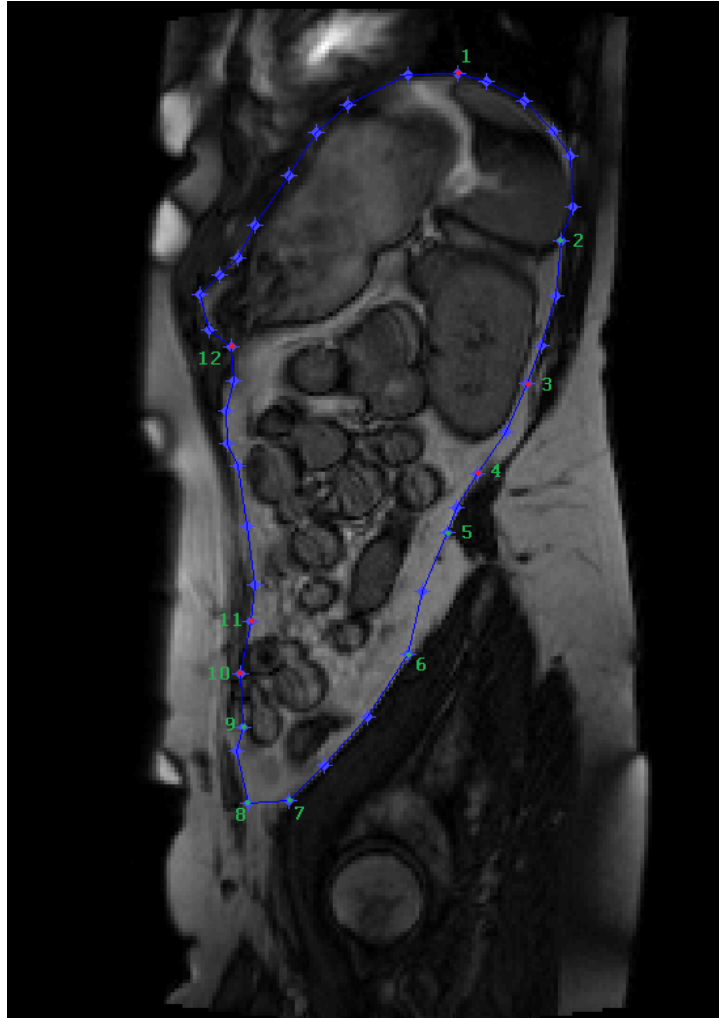
Figure 4.22: Positions of the landmark points used to compare the accuracy of the two summation techniques

The positions of the landmarked points after registration for both summation techniques (Methods 1 and 2) were compared to the positions marked by eye in every frame. Eq 4.1 to 4.3 were used to calculate the distance separating the two:

$$x_{eye} - x_{sum} = x_{diff} \qquad\qquad Eq\ 4.1$$

$$y_{eye} - y_{sum} = y_{diff} \qquad\qquad Eq\ 4.2$$

$$\sqrt{\left(x_{diff}^2 + y_{diff}^2\right)} = xy_{diff} \qquad\qquad Eq\ 4.3$$

Where x_{eye} is the x coordinate of the landmark point determined by eye, x_{sum} is the x coordinate determined by the summation technique, x_{diff} is the difference in x position between the two and xy_{diff} is the overall distance between the points.

4.7.3   Results and Discussion

The average xy_{diff} was calculated for each of the 12 landmark points across all frames to produce Figure 4.23. The horizontal lines correspond to the overall average discrepancy for all the points. The error bars correspond to the standard deviation of the average discrepancy across all frames.
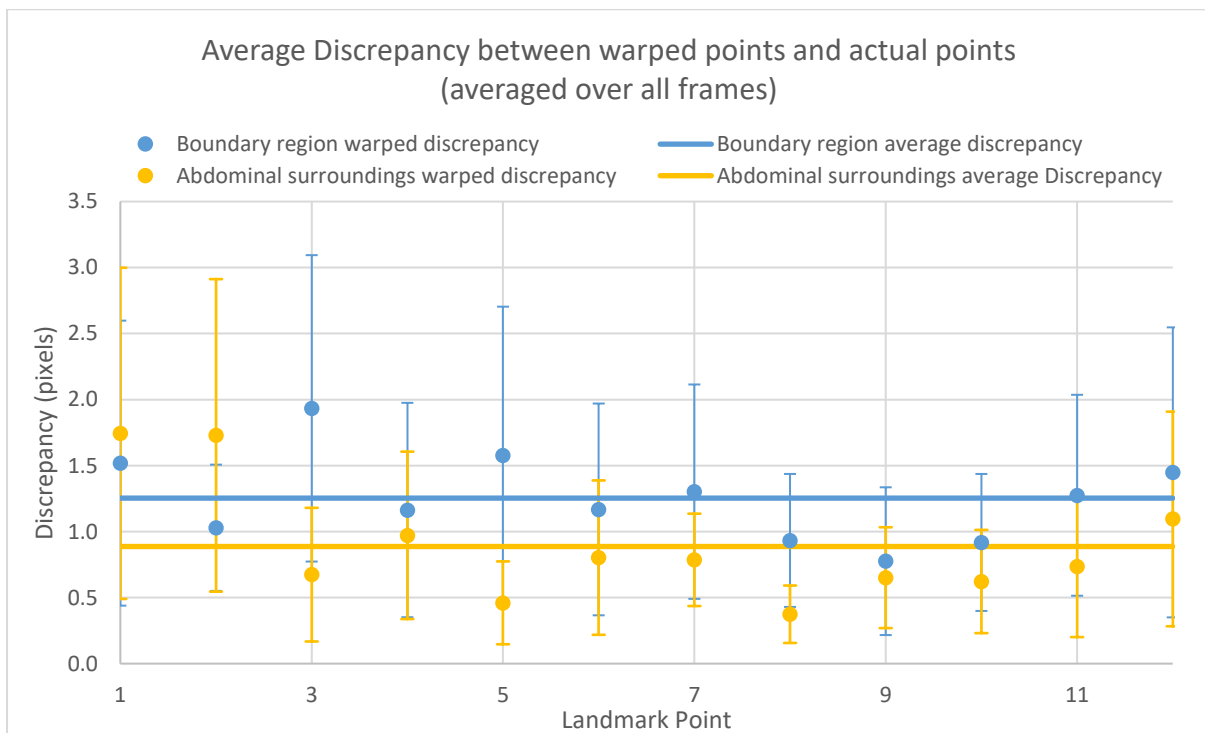
Figure 4.23: Graph showing the average discrepancy between the positions for each of the landmark points determined by eye and the position determined from both the summation techniques.

Both techniques matched the landmarked positions closely but Figure 4.23 shows the summation technique using the abdominal surroundings for registration (Method 2) produced

a closer match for 10 out of 12 points. Moreover, the two points (points 1 and 2) for which it had a larger discrepancy are in regions of the image which are considered less important for the analysis – the abdominal wall being the primary focus (points 8-12). The region around point 1 lacked detail exterior of the ROI (see Figure 4.22) and may explain why Method 2, which used the abdominal surroundings, had the poorer results in this area. The error bars in Figure 4.23 indicate that the spread in the discrepancy values was also lower in the summation technique for the abdominal surroundings for all points except 1 and 2. This suggests that not only did the second summation technique produce smaller average discrepancies but it was also more consistent and precise across the frames.

The close match to the eye-balled landmarks also provides reassurance regarding the accuracy of the implemented summation technique. The uncertainty in positioning the landmark may be considered to be greater than 1 pixel and therefore the difference between the summation technique and landmark position agreed within this uncertainty.

This quantitative comparison of the two summation techniques was performed in addition to using the two techniques in conjunction for a period of ~10 patients. Observations noted that Method 2 (utilising the abdominal surroundings) was consistently more robust than Method 1 (utilising the boundary region). Method 1 more frequently resulted in artefacts in the summed shear profile which were characteristic of miss-registration of one or more frames around the boundary, such as those shown in Figure 3.20 at the end of the previous chapter. This was particularly noticed in cases with larger amounts of abdominal wall movement. The abdominal surroundings summation technique only rarely had a similar artefact in extreme cases of large, fast abdominal movement between frames.

MR imaging artefacts can also present problems for shear summation. MR imaging artefacts are frequently visible in the abdominal wall and can disrupt the deformation field in that region leading to poor tracking of the sliding boundary. This occurs only when the artefacts are severe and fluctuate in spatial position between frames. Utilisation of the boundary region rather than the whole abdominal surroundings would reduce the amount of artefact present within the registered images and therefore most likely reduce their effects. However, with the other advantages of the using the abdominal surroundings, this was considered a necessary trade-off.

4.8 Summary and conclusion

A discussion for each experiment has been offered in each respective section throughout this chapter. In this section a summary of each of the characteristics is offered and the pertinent findings consolidated.

4.8.1 Accuracy of shear calculation

In-silico experiments confirmed the visceral slide quantification technique was capable of accurately determining the shear in highly idealised systems. With the ROI drawn exactly along the sliding boundary, the shear calculated matched the shear in the system for a simple translation movement and closely matched the shear in an elastically stretched section. These results were in stark contrast to the gross underestimation of shear observed without using segmentation.

The technique's ability to accurately calculate shear was also supported in the less idealised in-vitro experiment. A close match between calculated shear and the manually determined shear was observed. Proof of concept for adhesion detection was also demonstrated through the correct localisation of a piece of double-sided sticky tape placed inside the in-vitro syringe model.

These experiments indicate that under idealised conditions the technique is fundamentally capable of accurately determining the shear in a system.

4.8.2 Artificial introduction of shear

An idealised experiment involving only uniform bulk movement identified that no artificially induced shear was detected around the segmented region. In a non-idealised scenario using a clinical cine-MR image, analysis of the shear in a segmented stationary region was shown to potentially introduce artefactual shear around the ROI boundary. One major cause of this was diffuse displacement elsewhere in the image which spread to the boundary of the segmented region. Once at the ROI boundary a sudden drop in displacement was observed leading to an increase in shear. Changes in intensity and image noise could account for some of the artefactual increases in shear around an ROI boundary. The amount of shear induced around an ROI placed in a stationary area (without a sliding interface) was small compared to the shear observed around a sliding boundary. This still raises the question of whether artefactual shear

is being introduced when the ROI is correctly positioned around the abdominal cavity. This has not been attempted on clinical examples but the in-silico and in-vitro tests support an accurate calculation of shear and therefore this was considered less of a concern.

4.8.3 Reproducibility

The sheargrams resulting from five repeated processing attempts on the same two cine-MRI scans were all considered visually similar and the diagnostic interpretation of all sheargrams was the same. Quantitative analysis was performed by splitting the abdominal perimeter into regions. The range in the difference in average shear in each region was used as a conservative estimate of the variability between processing. Due to the limited data (two cine-MRI scans) reliable figures regarding the general repeatability cannot be concluded, but as a rough guide a range of shear was approximately 2±2 pixels which corresponded to a difference of 12±9% as a percentage of the shear in the respective region.

The shear profile was affected by ROI position in the repeatability experiment. A systematic investigation into ROI position in one cine-MRI scan found a drop of <10% over a ROI position range of 5 pixels in 5 out of 8 sampling areas along the abdominal wall. As a rough guide, a 4-pixel wide buffer was considered to produce shear of similar enough profile and magnitude.

4.8.4 Shear Summation

Shear summation in the highly idealised in-silico example with a stretched region produced the same percentage error as found in each frame, indicating that no or very little additional error was introduced by the summation procedure. However, for this highly idealised example, without a mobile boundary, this was expected.

Two different summation techniques were implemented and discussed and the technique chosen has been justified. The average discrepancy between the position of manually landmarked points and the chosen summation technique's calculated location was less than 1 pixel. The error in manually positioning landmarks between frames is larger than 1 pixel and the technique was therefore considered to accurately track the points.

4.8.5 Conclusion

The tests outlined in this chapter have provided insights into the underlying behaviour and limitations of the visceral slide quantification technique. It has proven capable of accurately determining shear in idealised and semi-idealised cases. Proof of concept has been demonstrated through simulated adhesion detection in a semi-idealised in-vitro syringe model and via the detection of surgically confirmed adhesions in two clinical examples (processed during the reproducibility experiment). The sheargram was found to be sensitive to ROI placement and this was found to limit the reproducibility. As a rough ballpark figure, the variability in the shear within regions around the abdominal perimeter could be considered $12\pm9\%$ as a percentage of typical shear values. An ROI placement range of approximately 4 pixels about the sliding boundary was considered acceptable for reproducing similar shear values. While a 4-pixel buffer was considered achievable in most cases for intra-operator variability, it does indicate a lack of robustness in the technique. This is one of the main limitations and is a suggested area for further work.

In summary, the evidence presented provides confidence that the technique could be of diagnostic merit and the next chapter explores a more comprehensive application to clinical images.

Chapter 5

Application to clinical images: a retrospective pilot study

5.1 Introduction

Chapter 3 detailed a technique developed to quantify the visceral slide of the abdominal contents against the perimeter of the abdominal cavity, with a particular focus on the abdominal wall. Chapter 4 has described a series of tests used to:

  i.   Confirm the technique was measuring shear at a sliding interface accurately
 ii.   Determine the accuracy and limitations of the method
iii.   Show that it can be applied to clinical data

Chapter 5 extends the clinical application of the visceral slide quantification technique to a significant patient cohort to assess its potential for its intended clinical purpose – to aid diagnosis of adhesions in cine-MRI. The success of the technique will be principally gleaned from how well the visceral slide measurement produced results that correlated with clinical findings.

Access to cine-MRI scans for 52 patients was available through collaboration with the adhesions research group at Radboud UMC, Nijmegen and Rijnstate Hospital, Arnhem in the Netherlands. The cine-MR images were acquired as part of the patient pathway for adhesiolysis as it aids decision-making for intervention. All patients provided consent to enable their images to be used for research purposes (Local Review Board File No. 2016-2610).

The series of dynamic images (in both sagittal and transaxial orientations) are reported similarly at both Rotherham (UK) and Arnhem (Netherlands): the radiologist reviews the cine-MR images as moving videos (without any image processing) to reach a decision. Both centres

use the same model of scanner resulting in similar scanning protocols and comparable image appearance. The results of this pilot study are therefore relevant to both centres. Details of the scanning protocol parameters for the patient scans in this pilot study are as described under the Nijmegen heading in Table 1.2, Section 1.4.

5.2 Method

The visceral slide analysis technique has already been described in Chapter 3 and tested synthetically in Chapter 4. The method described below solely pertains to the process undertaken to analyse a retrospective cohort of 52 patients. The flow diagram in Figure 5.1 outlines the principal steps involved.
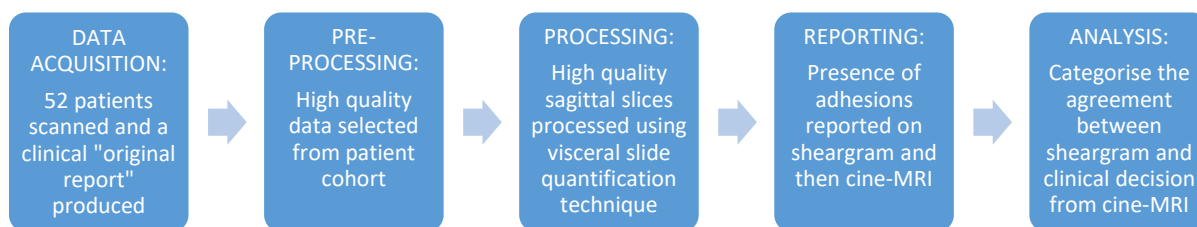
Figure 5.1: Flow diagram depicting the overall methodology adopted for the pilot study

The patient cohort consisted of 52 individuals who had been referred to Radboud UMC, Nijmegen for undiagnosed abdominal pain with suspected adhesions. The 52 patients were randomly selected from a pool of 106 at the time of study commencement. As part of the clinical investigation they all underwent a cine-MRI examination.

The anonymised patients were assigned an identification number from 1 to 52. Each patient had both sagittal and transaxial slices acquired. Only the sagittal slices were considered and processed in this study as the visceral slide quantification technique is only designed to operate on sagittal images. The total number of sagittal slices from all 52 patients amounted to 341, with each slice consisting of 30 frames in the dynamic sequence. It is worth noting that at least one sagittal slice for every patient did not contain any movement and was repeated in all patients. This is to give the patients a practice run at the bearing down breathing procedure. Consequently, the total number of usable sagittal slices (341) quoted is reduced to 281 unique slices. Of the 281 unique slices, a subset of high quality images was identified and used to test

the visceral slide technique. The following section describes what is meant by high quality data and the filtering process undertaken.

5.2.1 Pre-processing: selecting high quality data

Visible sliding motion is important for effective processing, so cine-MR image sequences were first examined for adequate intra-abdominal respiratory movement. The dynamic image sets were converted to video files to facilitate examination of intra-abdominal movement. Videos for all 341 sagittal slices were reviewed and given a score from 1-4 using the following categorisation criteria:

1. Barely any motion due to respiration, or completely unusable for any other reason (e.g. respiratory motion too fast between frames).

2. Very small amount of motion due to respiration and/or <1 respiratory cycle completed during the scanning period.

3. Significant motion induced by respiration and >1 respiratory cycle completed during the scanning period.

4. Good motion induced by respiration and close to or greater than 2 respiratory cycles completed during the scanning period.

These criteria were used as a guide for scoring movement quality and this was helpful to inform judgement regarding the images' suitability for processing. The complexity of factors, including presence of imaging artefacts, meant the decision was ultimately left to expert judgement. Although a definitive decision on an integer from 1-4 was always assigned to each image sequence, for cases which were considered between integer scores (or were difficult to judge without processing the image first to observe any difficulties encountered), a comment was added such as "score 3 (possible 4)". Scores of 3 or 4 were considered 'good quality data' and were subsequently processed and analysed. 141 of the 281 unique dynamic image sequences were deemed to be of high quality (score 3 or 4).

Each dynamic sagittal cine-MRI was judged for suitability twice. In the first instance the slices were assessed in order from patient 1 to patient 52. The second assessment was performed over 1 week after the first and used a random number generator to select the order. Once the two sets of scores were collected, those cine-MR images which were given the same score on both passes were assigned that score; those which had a disagreement were reviewed a third time

and a final decision was made. During the process of making a final decision the comments of whether an image sequence lay between two integer scores were taking into account (e.g. "score 2 (possible 3)"). All sagittal dynamic image sequences were ultimately assigned a single suitability score. Figure 5.2 shows a flow diagram clarifying the image grading procedure.

Figure 5.2: *Flow diagram showing the procedure taken to give a quality score to every sagittal slice*

5.2.2 Reporting

The primary assessment in this pilot study was to establish whether the visceral slide processing technique produced results which correlated with clinical findings and clinical judgement. The visceral slide image processing technique described in Chapter 3 was applied to only the high quality data. All 141 selected dynamic image sequences were processed by the same expert operator and reported by two reporters. The principal output of the visceral slide processing technique is the sheargram and it alone was correlated to clinical judgement.

Training

A training dataset was produced to ensure both reporters were familiar with the sheargram, facilitating its appropriate interpretation. The training dataset consisted of 10 cine-MR sagittal slices with their corresponding sheargrams. It incorporated a variety of cases, including:

- Sheargrams which accurately portrayed sliding in healthy volunteers
- Cases where the sheargram successfully detected surgically confirmed adhesions
- Cases where artefacts were present in the shear profile – Figure 5.3 shows an example included in the training dataset where an MRI imaging artefact has interfered with the image registration process to produce an anomalous reduction in shear.

Within the training dataset a description/explanation was provided after the images had been reviewed by the trainee. The descriptions justified why the sheargrams were considered normal

or abnormal and highlighted any shear artefacts and the reasons for those artefacts. During the study, if a drop in shear could be attributed to an imaging artefact this was designated as an artefactual reduction in shear by the reporter and was not reported as a possible adhesion.
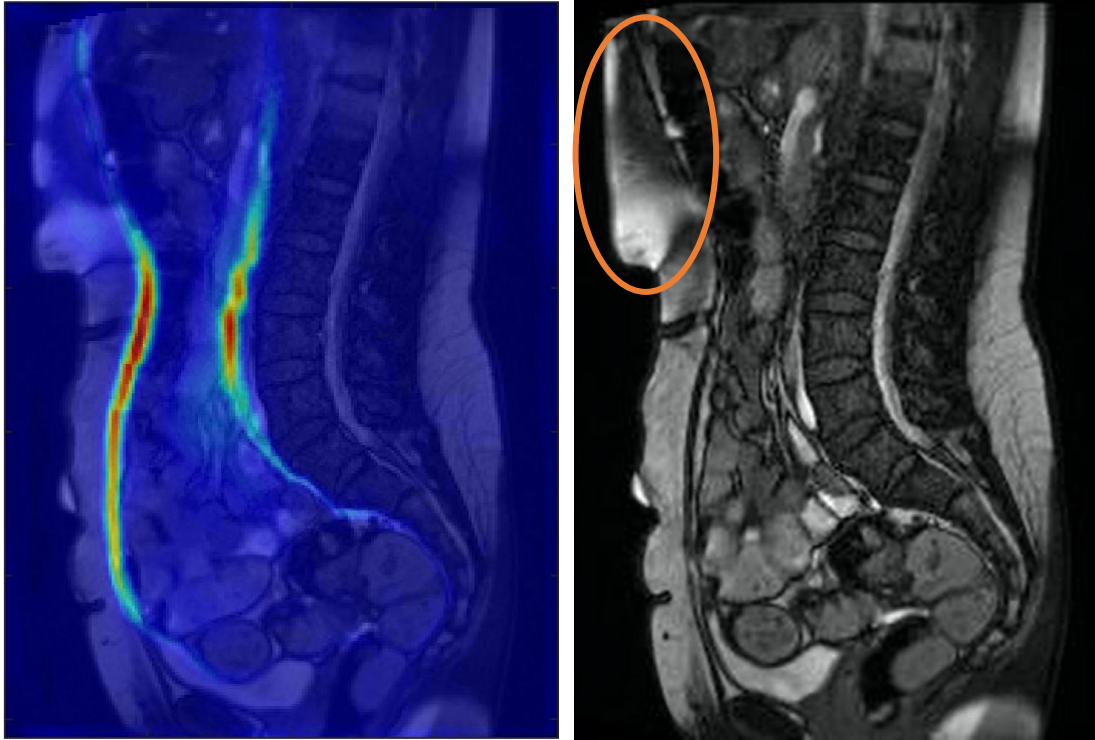
Figure 5.3: *Sheargram from the training dataset with an artefactual shear reduction due to an MRI artefact (circled) in the abdominal wall which moved with the intra-abdominal organs*

Reporting procedure

Two reporters were selected to examine all 141 sagittal image sequences with sheargrams. In order to achieve a balanced assessment of the degree of agreement, each reporter was an expert in interpretation of each of the two components of the reporting procedure: One a technical expert in the image processing technique with an understanding of the underlying clinical context and the other a consultant radiologist who originally reported all 52 patients. In addition to the two reporters' judgements on whether the sheargram agreed with clinical observations/judgement, a decision was made as to whether the sheargram agreed with the original report. This provided three separate adjudications on whether the sheargram was providing clinically accurate and relevant information. Each reporter was blinded to the other's reporting results.

The reporting of each slice involved the following procedure:

i. The sheargram was observed first. A subjective judgement was made on whether the sheargram showed a significant enough drop in shear for there to be an expected adhesion at that site.

ii. The reporter categorised the decision into one of three options:

    i. **'Yes'** – I expect there to be an adhesion present

    ii. **'No'** – the sheargram depicts a typical shear pattern of a healthy individual

    iii. **'Equivocal'** – for instances where interpretation is not straightforward enough to provide a categorical 'yes/no' answer

iii. The cine-MR sagittal video was then reviewed and a decision made as to whether an adhesion was present in that slice.

iv. The cine-MR decision was categorised using a similar scoring system as in step 2 – yes, no or equivocal.

Both the technical expert and radiologist made a judgement on each sheargram and the radiologist judged each cine-MRI. The original report was assigned the same categorisation ('yes', 'no' or 'equivocal') based on the description in the report. An equivocal adhesion was designated from the report when the description cited, for example, '… possible adhesion…'.

5.2.3 Analysis

Both the radiologist's and technical expert's judgement on the sheargram ('yes', 'no', 'equivocal' adhesion observations) were compared to the radiologist's report on the cine-MRI. The radiologist's clinical judgement of the presence of an adhesion on the cine-MRI was considered the 'gold standard' for this study.

From the 'yes/no/equivocal' scoring system described above, there are 9 possible combinations of outcomes. Each combination was assigned a number termed the 'Classification Number' – summarised in Table 5.1. The 9 different agreement categories can also be grouped into broader classification groups of agreement as shown in Table 5.1.

Classification Number	Adhesion inferred from original report/final clinical decision	Adhesion inferred on Sheargram	Broad agreement classification
Table 5.1: Classification of the different agreements that can occur between sheargram and clinical decision on cine-MRI and their associated broad agreement classifications (taken from [4])			
1	Yes	Yes	**Agreement** (True positives/negatives)
2	No	No	
3	Equivocal	Equivocal	
4	Equivocal	Yes	**Partial Agreement**
5	Equivocal	No	
6	Yes	Equivocal	
7	No	Equivocal	
8	Yes	No	**Disagreement** (False positives/negatives)
9	No	Yes	

This agreement categorisation system permitted quantitative assessment of how well matched the sheargram was to the report and final clinical decision. The cases where an equivocal judgement was made on the original report or on the final decision by the radiologist, have been greyed out in Table 5.1 and were excluded from the analysis. An equivocal clinical judgement indicates that the diagnosis was unclear and the presence of an adhesion was unknown. These cases do not offer a clear comparison for the sheargram and their inclusion would be inappropriate for assessment of correlation between sheargram and adhesion presence. There was one final clinical decision by the radiologist which was equivocal and two equivocal original reports. This reduces the total number of sagittal slices used for comparison to 140 and 139 for the final clinical decision and original report respectively.

5.2.4   Statistical Assessment

Through the exclusion criteria imposed, the original cohort of 281 sagittal slices (52 patients) has ultimately reduced to a cohort of 140 slices that were processed and analysed. This number was still large enough not to hinder statistical inference of the study. If agreement between the sheargram and radiologist were by chance (i.e. the probability of agreement was 0.5), three standard deviations about the mean of a binomial distribution with n=140 would be placed at 88/140 slices or 62.8% agreement. Any agreement above 62.8% may therefore be considered statistically significant to a p-value of 0.01.

5.3 Results

To reiterate, the purpose of this pilot study was to assess the extent to which the sheargram (visceral slide quantification technique) agreed with clinical opinion as a means of determining its potential as a diagnostic aid for cine-MRI abdominal wall adhesion detection. Consideration of the three broad agreement classifications in Table 5.1 provides a coarse overview of the level of agreement, as displayed in Figure 5.4. It was the radiologist's sheargram judgement (not the tech expert's) that was compared to the original report. This was because the radiologist in this pilot study was the same radiologist who had previously reported the scans (0.5–3 years earlier) and therefore it was most appropriate that his opinion should have greater authority.
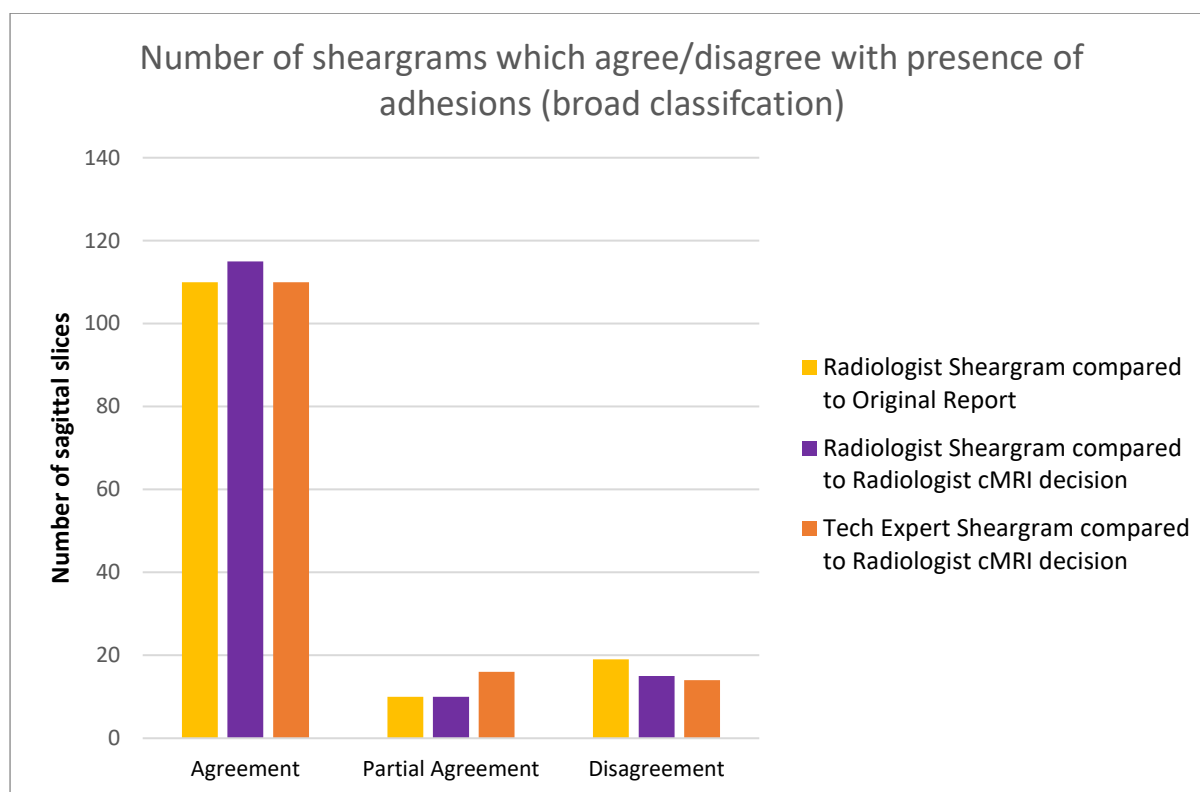
Figure 5.4: *Overview of the level of agreement between the sheargram and clinical decision/original report for both reporters in the pilot study (some information duplicated from [4])*

The distribution in Figure 5.4 indicates that, in general, the sheargram matched the original report and the radiologist's judgement in the large majority of cases. The percentage of the number of sheargrams which agreed with the radiologist's final decision was 82% for the radiologist and 78% tech expert. 79% of the radiologist's sheargram interpretations agreed with the original report. The percentage of cases where the sheargram failed to correlate with the clinical judgement was 11% (15/140) for the radiologist and 10% (14/140) for the tech expert.

The technical expert had a higher proportion of partial agreements. There were more disagreements of the sheargram to the original report than the radiologist's final adjudication. This indicates that after observing the sheargram and making a final decision on the presence of an adhesion, in some cases the consultant radiologist had altered his opinion to align with what the sheargram was displaying.

Deeper interrogation of the underlying constitution of the broad categories for the agreement between the sheargram and the radiologist's final decision is presented in Figure 5.5.
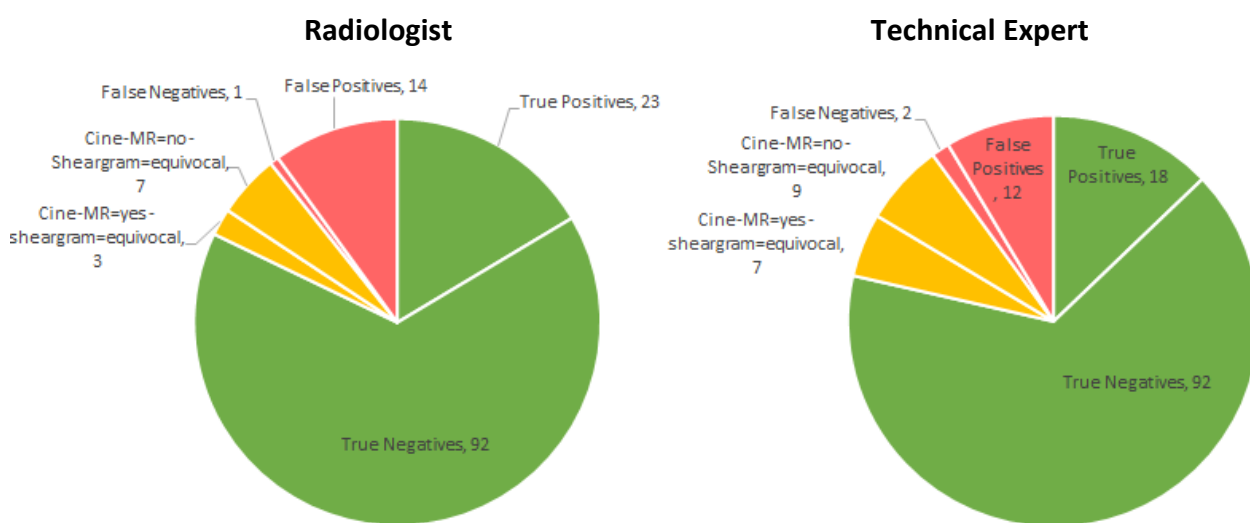
Figure 5.5: Correlation between the sheargram and clinically inferred adhesions on the cine-MRI for each of the two reporters represented as pie charts. The numbers on the charts are the number of sagittal slices (total sagittal slices = 140) (taken from [4])

Only considering the definitive conclusions, i.e. excluding any equivocal cases (i.e. excluding the yellow portions in Figure 5.5), allows the production of three 2x2 contingency tables shown in (Table 5.2 to 5.4) summarising the definitive agreement for each of the three comparisons.

Table 5.2: True and false positives/negatives resulting from the **Radiologist's** sheargram interpretation compared to the **Original Report**		
	Orig. Report = Adhesion	Orig. Report = No Adhesion
Radiologist Sheargram Positive	20	17
Radiologist Sheargram Negative	2	90

Table 5.3: True and false positives/negatives resulting from the **Radiologist's** sheargram interpretation compared to the **Radiologist's final clinical decision**		
	Final decision = Adhesion	Final decision = No Adhesion
Radiologist Sheargram Positive	23	14
Radiologist Sheargram Negative	1	92

Table 5.4: True and false positives/negatives resulting from the **Technical Expert's** sheargram interpretation compared to the **Radiologist's final clinical decision**		
	Final decision = Adhesion	Final decision = No Adhesion
Tech Expert Sheargram Positive	18	12
Tech Expert Sheargram Negative	2	92

The green highlighted cells of Table 5.2 to 5.4 show true positive and true negative figures while the red cells show the number of false positive and false negative cases. The total number of cases differs between the two reporters due to the increased number of equivocal sheargrams (omitted from Table 5.2 to 5.4) made by the technical expert, as seen in the distribution in Figure 5.4. The vast majority of sagittal slices deemed to contain no adhesions were correctly identified on the sheargram, leading to specificities of 87% for the radiologist and 88% for the tech expert, when excluding all equivocal results. However, these percentages become 81% (92/113) for both reporters when considering equivocal sheargrams as positive identification of adhesions. Sensitivities of 96% and 90% were recorded for the radiologist and tech expert respectively (again, without considering any equivocal findings). This corresponded to 1 adhesion which was not identified on the sheargram for the radiologist and 3 that were missed by the tech expert. If considering equivocal sheargrams as positive adhesions, the percentages of correctly identified adhesions remains at 96% (26/27) for the radiologist and increases to 93% (25/27) for the technical expert.

There were also 12 cases where the radiologist's final decision on the presence of an adhesion changed relative to the original report. The constitution of the 12 changes are shown in Figure 5.6 below.
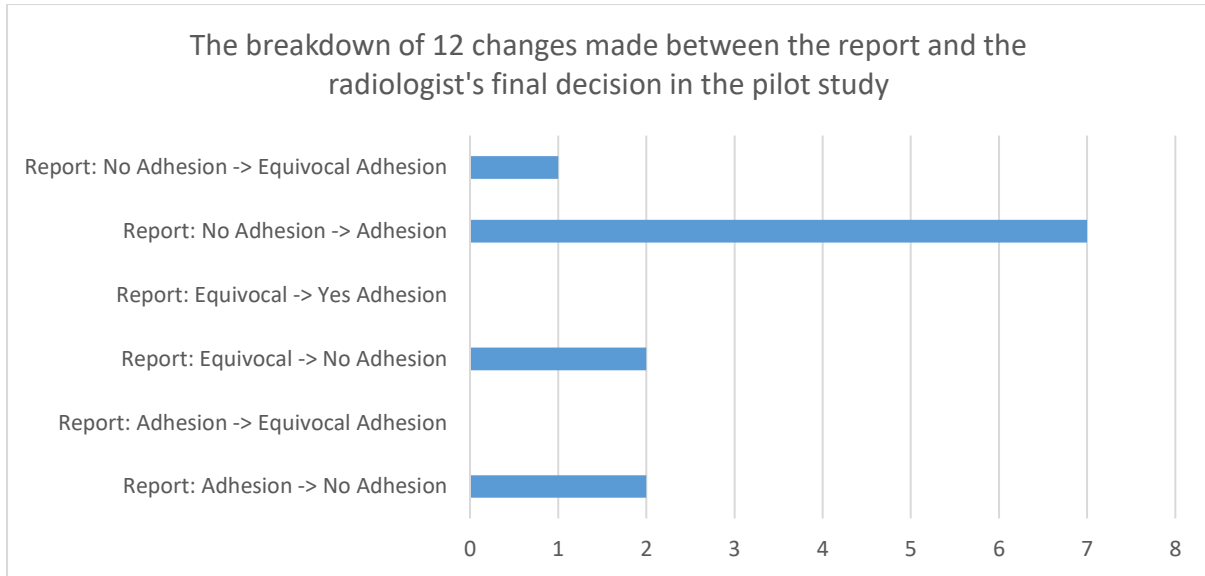
Figure 5.6: The breakdown of 12 changes made between the report and the radiologist's final decision in the pilot study [4].

In 2 cases a region previously reported as having an adhesion was adjudicated to not contain one after review of the sheargram. The sheargram potentially raised awareness of adhesions in 7 regions where they had previously not been reported.

5.4 Discussion

This study is the first clinical proof of principle relating to the visceral slide measurement technique and builds an understanding of its potential as a diagnostic aid. The fundamental question related to this exercise is: "is the technique an effective aid to diagnosis?". This discussion considers several important factors to characterise its effectiveness as a diagnostic aid and is arranged under these headings:

1. **Accuracy:** First and foremost, the sheargram must correlate with the correct answer. In this pilot study, what proportion of cases did the sheargram agree with clinical opinion?

2. **Robustness:** How often does the sheargram fail, where did it fail and what were the reasons for any discrepancies?

3. **Influence:** Does it have an effect on clinical diagnosis and is this evidenced in the pilot study?

4. **Limitations:** What are the problems with the current sheargram implementation and what drawbacks have been revealed in this pilot study?

5. **Reporting Efficiency:** A decrease in reporting time is desirable. Is there evidence to support increased efficiency with the use of the sheargram?

A discussion on these core points is followed by a critical appraisal of the methodology undertaken in this pilot study.

The radiologist's clinical judgement made in this pilot study was considered to supersede that in the original report. The original report incorporated information from dynamic transaxial images (routinely included in the clinical scanning protocol, see Section 1.4) but these were not considered in this pilot study. This study intended to see how well the sheargram matched what was observed in the clinical images. The appearance of the sheargram is based solely on information present within the sagittal slice and it is therefore appropriate that it be compared to a clinical judgement of the sagittal slice alone. The bulk of the analysis therefore focuses on comparison of the sheargram to the radiologist's expert opinion on the cine-MRI (not the original report).

5.4.1   Accuracy: how well did sheargram observations correlate with clinical findings?

In general, the results indicate good agreement between the interpretations of the sheargram and cine-MRI across both reporters. Figure 5.4 displays a clear overview of the level of agreement in absolute numbers of sagittal slices. The large number which were considered to agree compared to the other broad classifications is both striking and encouraging. The combination of complete and partial agreements accounted for 89% (125/140) of cases for the radiologist and 90% (126/140) for the tech expert. These figures give an indication of the level of good agreement achieved between sheargram and clinical judgement, however, a definitive figure of agreement is dependent on the interpretation of an equivocal judgement on the presence of an adhesion. An equivocal region on a sheargram has still drawn the attention of the radiologist. There is therefore justification for an equivocal judgement on the sheargram to be more closely associated with a 'yes' than a 'no'. Considering an equivocal sheargram as a 'yes', results in the radiologist correlating the sheargram to clinical opinion in 84% (118/140) of cases with the tech expert also achieving a correlation of 84% (117/140). A chi-squared calculation comparing this result (84% agreement) to a distribution which assumes agreement by chance, results in a p-value of <0.00001 for both reporters. The low p-value confirms statistically significant results and the high correlations indicate that the sheargram is generating movement signatures that represent the underlying physiology and pathology.

Examination of Table 5.2 to 5.4 gives an indication of the level of agreement without considering any cases with partial agreement (i.e. not considering sheargrams reported equivocally). They reveal percentages for correctly identified adhesions on the sheargram (sensitivity) of 96% (23/24) and 90% (18/20) for radiologist and tech expert respectively. In the worst case, considering positively identified adhesions with an equivocally reported sheargram as incorrect correlation, this figure drops to 85% (23/27) and 67% (18/27) for the radiologist and technical expert respectively. As discussed, however, it may be unfair to consider equivocal areas on the sheargram as a failure to identify an adhesion as they still draw the reporters' attention to a particular area. Therefore, if considering equivocal sheargrams as positive identification of an adhesion, the sensitivity remains at 96% (26/27) for the radiologist but increases to 93% (25/27) for the tech expert. These encouraging figures indicate a strong correlation between adhesions and a drop in shear on the sheargram. Only one positive adhesion decision was not identified on the sheargram by the radiologist and two were not identified by the tech expert. Figure 5.7 shows two true positive examples with sharp reductions in shear matching the location of adhesions identified by the radiologist's examination of the cine-MRI.
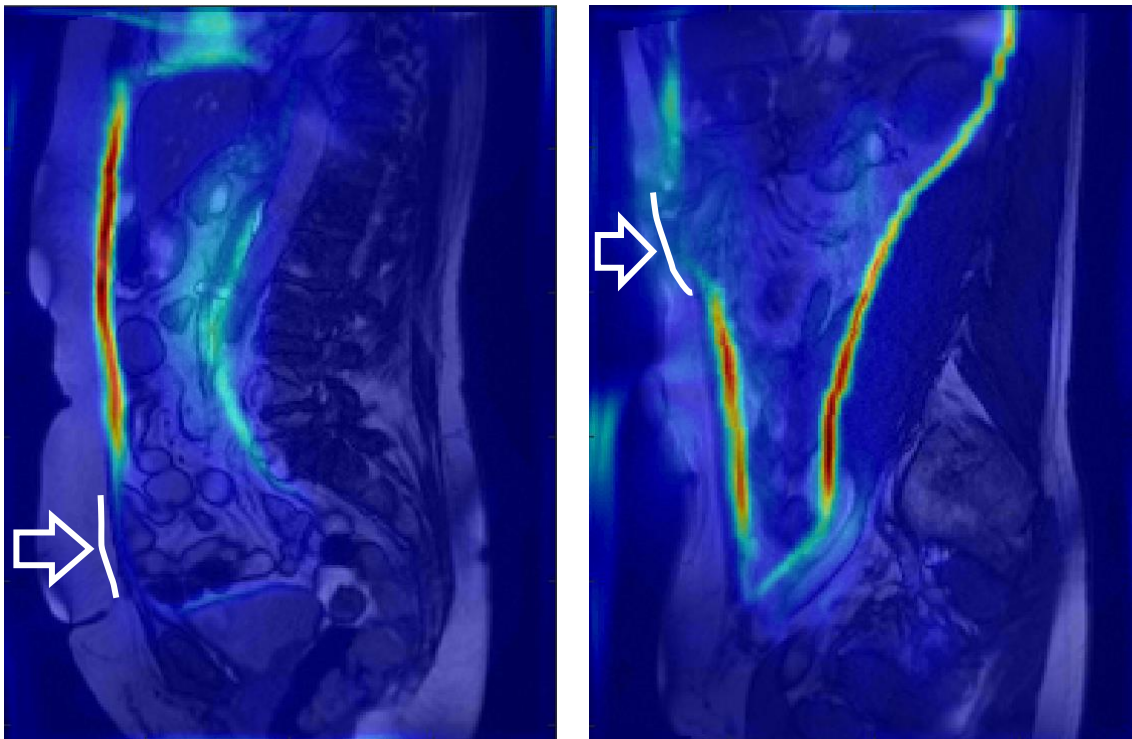
Figure 5.7: Two examples of adhesions which were positively identified on their respective sheargrams. White arrows and lines indicate location and extent of each adhesion (taken from [4])

It is also important to determine the number of normal cases correctly identified by the sheargram (i.e. specificity). The specificity was 81% (92/113) for both reporters when considering equivocally reported sheargrams as positive identification of an adhesion (therefore incorrectly correlating with the diagnosis of a normal slice). The technique therefore apparently exhibited a higher sensitivity at the expense of a lower specificity. Figure 5.8 shows two examples of healthy slices which correctly correlated with an absence of adhesions.
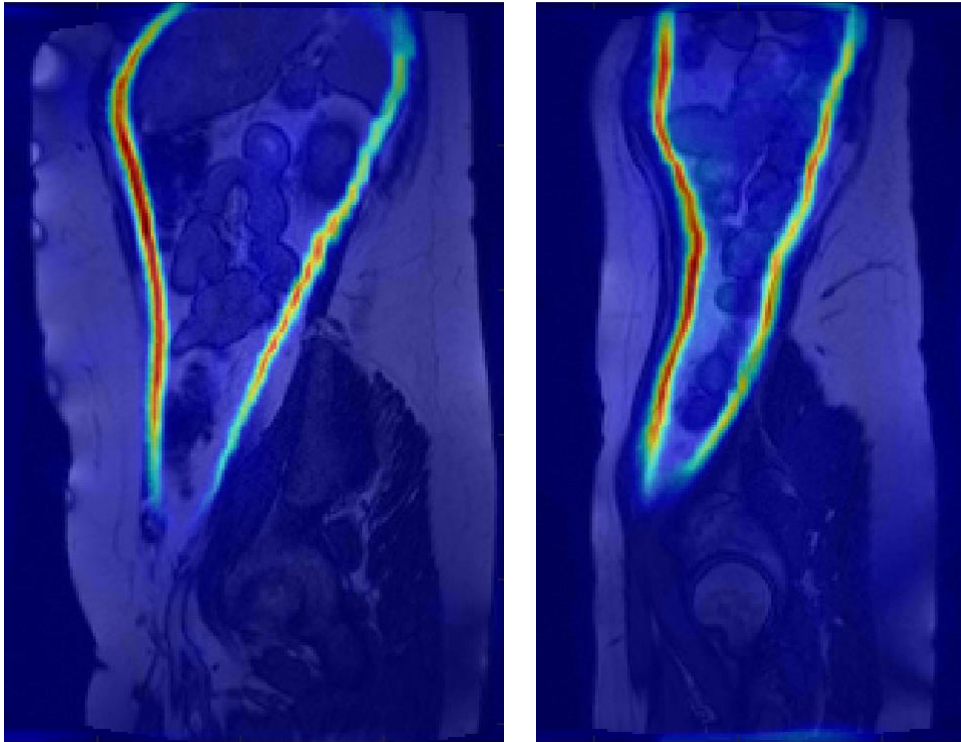
Figure 5.8: *Two examples of healthy sagittal slices which were identified as such on the sheargram (from [4])*

Section 5.4.1. Key Points:

- 84% of scans were considered to correlate with clinical opinion for both the radiologist and tech expert. If agreement were by chance this would correspond to a p-value of <0.00001.

- 96% and 93% of positively identified adhesions correctly correlated with sheargram interpretation for the radiologist and technical expert respectively (i.e. sensitivity).

- Only a single positive adhesion was not visible on the sheargram from the radiologist's judgement while an additional second false negative judgement was made by the tech expert.

- 81% of healthy slices were correctly judged to be so on the sheargram by both reporters (i.e. specificity).

5.4.2 Robustness: Where did it fail and what were the reasons for failure?

Figure 5.9 shows the single false negative which was identified as such by both reporters.
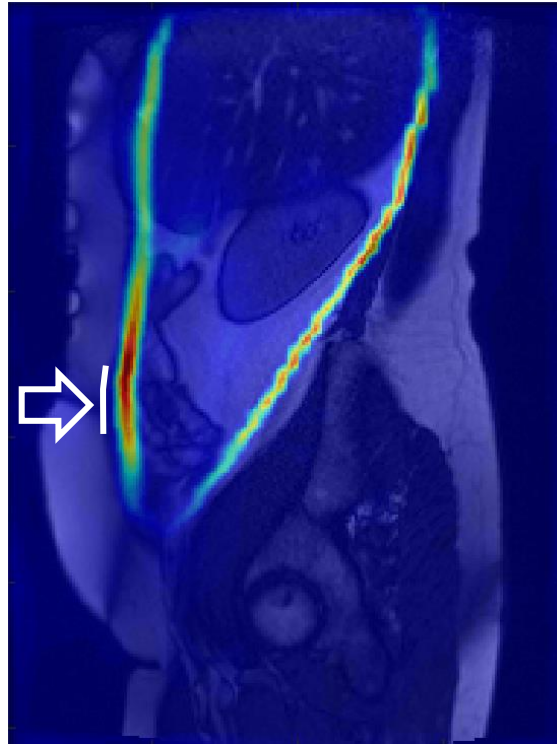
Figure 5.9: The false negative sheargram identified by both reporters during the pilot study. The identified adhesion was located at the position indicated by the white markings at an area of high shear (taken from [4])

The false negative in Figure 5.9 was attributed to a large degree of out of plane motion occurring at the abdominal wall. Whereas the portion adhered to the abdominal wall can be distinguished by eye, there is a large degree of motion taking place in the surrounding area and the adhered object itself moves out of plane for approximately half the image sequence. It is therefore unsurprising that the calculated shear does not reflect the presence of an adhesion.

Figure 5.10 shows the additional false negative case reported by the tech expert (the radiologist reported the sheargram as a positive adhesion).
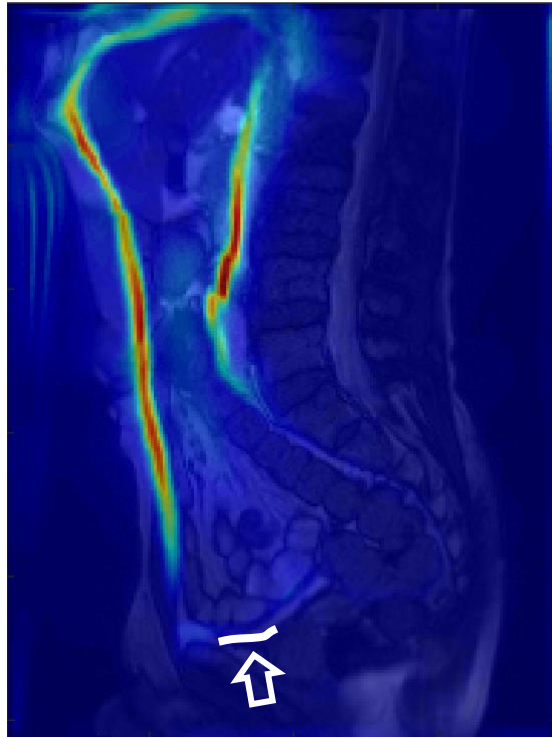
Figure 5.10: The additional false negative identified by the technical expert but not the radiologist [4].

The case in Figure 5.10 can be explained by a difference in interpretation of the definition of 'abdominal wall adhesion'. Both reporters agreed that there is a drop in shear and that there is an adhesion to the pelvic floor close to the abdominal wall. However, the tech expert noted that the drop in shear was in a region without adjacent organs/bowel (only fat) and therefore considered the absence of structure to contribute to the shear drop and did not consider this region for an abdominal wall adhesion. The radiologist noted that there was a bowel loop close enough to the abdominal wall and that the drop could be the result of an adhesion to the pelvic floor close by.

From Table 5.2 to 5.4, the most common error in sheargram reporting, accounting for 93% (radiologist) and 86% (tech expert) of discrepancies, was the reporting of adhesions on the sheargram in areas which were found not to contain adhesions i.e. false positives. This reflects the sheargram's bias as a diagnostic aid and its designed purpose to alert the radiologist to areas containing suspected adhesions. A high sensitivity is favoured over specificity: it is better to draw the attention of the radiologist to suspicious areas which are subsequently deemed to be healthy than miss potential adhesions.

Section 5.4.2. Key Points:

- Robustness has been demonstrated as only one false negative sheargram was identified by both reporters, with only a single second false negative identified by the tech expert.

- A favourable skew towards sensitivity over specificity is exhibited as very few adhesions were missed.

5.4.3 Influence: Did the sheargram influence decisions?

The consultant radiologist chosen for the pilot study is not only an expert at cine-MRI adhesion reporting but is also the same radiologist who had previously reported this 52 patient cohort. The consultant radiologist originally reported the scans between July 2012 and November 2015: at least 6 months prior to this pilot study and therefore was not influenced by recent memory. Involvement of the same reporter adds pertinence to the changes of opinion between the original report and this pilot study as the influence of inter-operator variability is eliminated. It offers greater insight into the level of influence of the sheargram in affecting the clinical decision. Figure 5.4 shows a difference between the number of sheargrams which agreed with the original report and the radiologist's final decision in this pilot study. This signifies that the radiologist had altered his clinical opinion between the original report and after reviewing the sheargram. Moreover, the majority of clinical decision alterations resulted in alignment with the sheargram. Further investigation, shown in Figure 5.6, reveals the consultant radiologist altered his diagnosis/opinion relative to the original report on 12 occasions. In 10/12 cases the radiologist changed his opinion to agree with the interpretation of the sheargram. The remaining two sagittal slices, where the original report agreed with the sheargram but the radiologist's final decision disagreed, were from the same patient. On one, the sheargram matched the original report of an adhesion and on the other the sheargram agreed with an equivocal adhesion on the original report. Although it has not been used in any of the analysis, the technical expert also made a judgement on the cine-MRI (without the sheargram) and reported both these sagittal slices as equivocal. The implication is that the cine-MRI scans for this particular patient were hard to interpret and assessment of adhesions was difficult and unclear.

All 7 cases where a new adhesion was identified compared to the original report (on Figure 5.6), agreed with the judgement made on the sheargram: 5/7 sheargrams were reported as 'yes', 2/7 cases had 'equivocal' sheargrams. This implies that the sheargram positively influenced

the clinical decisions made by the radiologist and even a relatively small shear reduction, which was considered 'equivocal', still drew attention to previously unidentified adhesions. Although, without surgery these additional adhesions cannot be categorically confirmed and, as mentioned previously, the original report was recorded after reviewing both sagittal and transaxial slices. The exclusion of transaxial slices in this pilot study could account for some of the alterations encountered.

Overall, the sheargram appeared to aid/influence the radiologist to make more informed decisions on the presence of an adhesion to the abdominal wall. However, its fallibility, exemplified by the two changes made opposing the sheargram interpretation, are a reminder that the technique is a diagnostic aid and must still incorporate significant examination by the radiologist.

Section 5.4.3. Key Points:

- In 10/12 cases the radiologist changed his diagnosis/opinion to align with the sheargram
- 7 potential new adhesions identified after examination of the sheargram
- Evidence suggests the sheargram is potentially capable of influencing clinical decisions

5.4.4 Limitations: what limitations been revealed?

Results so far indicate promise for the aided detection of adhesions to the abdominal wall using the sheargram. However, several limitations of the technique are apparent:

1. Approximately 50% of sagittal slices were considered unsuitable, 'low quality' scans
2. The sheargram is objective but it requires subjective interpretation by the viewer
3. The technique is confined to detecting adhesions to the perimeter of the abdominal cavity and only the abdominal wall has been assessed in this pilot study

Point 1 highlights a significant issue with data quality. The centres involved have not had opportunity to refine their scanning protocols which is likely to have contributed to the large proportion of poorer quality data. The primary reason for the unsuitability of the images was patient compliance. The vast majority of low quality scans could be attributed to a lack of respiratory motion (128/140). Without intra-abdominal motion, no sliding occurs between the abdominal wall and intra-abdominal organs, therefore no meaningful results can be obtained. A small number of cases breathed too fast (7/140). Despite producing the intra-abdominal

motion necessary, particularly fast respiration introduced motion blur within the frame acquisition time and large jumps in position between frames. The combination of these factors could cause failed registrations between frames. Whereas image artefacts could account for some other difficulties, these only culminated in rejecting the image as high quality in cases where there were other contributory issues with the scan.

The process of assessing the quality of the data has highlighted the importance of patient compliance and indicates a requirement for improvement in the cine-MRI scanning protocol. There are two ways to alleviate this problem:

    i.   Provide better training and instruction to the patient prior to scanning.

    ii.   Alter the scanning protocol to reduce its complexity and the participation required from the patient

Both of the above options are being investigated. A patient instruction video is under production by colleagues in Radboud UMC, Nijmegen showing the breathing and bearing down procedure expected from the patient, while changes to the scanning protocol are primarily aimed at making the breathing procedure less difficult (discussed in Chapter 6, Section 6.4).

Point 2 refers to inter-operator variability in sheargram interpretation. While the shear is a quantifiable parameter, the information is presented in an image requiring subjective interpretation. In the pilot study two reporters from differing backgrounds made a judgement on whether the sheargram pattern could indicate the presence of an adhesion. Their sheargram interpretation agreed in 85% (121/141)[11] of the total sagittal slices, partially agreed in 13% (19/141) and disagreed in 1.4% (2/141); clearly interpretation of the sheargram is not clear-cut. The most discernible difference between reporters is the tech expert's relatively large number of partial agreements compared to the radiologist. This reflects a characteristic difference between the reporters as the tech expert's tendency to report more equivocally may be attributed to the relative lack of clinical decision making experience.

The principal region responsible for partial agreements and differences was the lower abdomen (16/21). In healthy individuals a reduction in shear is often observed at the lowest extremities

---

[11] Note: 141 slices (instead of 140) could be included in the comparison between operators because we are not comparing the sheargram to the clinical decision and the single slice that was reported equivocally by the radiologist could be included.

of the abdominal wall, which can lead to an ambiguous judgement as to whether the reduction is typical/normal or sharp and severe enough to be considered pathological. Movement induced by respiration is generally smaller in the lower abdomen and leads to a reduction in the magnitude of shear. Therefore, if an adhesion is present this region is often subject to a lower 'signal to noise' ratio.

Partial disagreements are less of a concern than the two cases in which the reporters completely disagreed in their sheargram interpretations. One case is the sheargram previously shown in Figure 5.10 which resulted in a false negative for the tech expert and the other is shown in Figure 5.11.
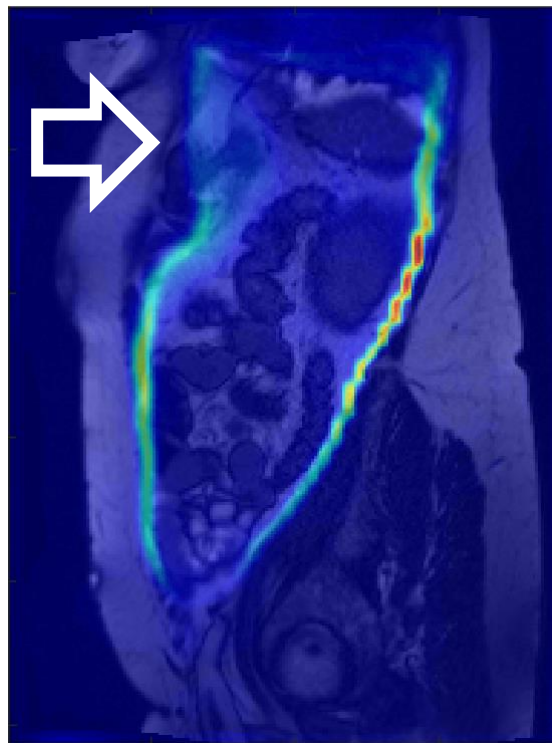
Figure 5.11: The second sheargram where the two reporters disagreed in their interpretation (location of disagreement indicated by the white arrow).

Figure 5.10 has already been discussed and the reason for the discrepancy was a difference in opinion of what constitutes an abdominal wall adhesion: The radiologist determining the bowel loops were close enough to the abdominal wall to be associated with the drop in shear, the tech expert deeming the lack of structure adjacent (only fat) to the abdominal wall meant this region should not be considered for adhesions. In Figure 5.11 the technical expert reported the drop in shear in the upper abdomen contradicting the verdict of the radiologist. The difference

resulted from the radiologist drawing upon clinical knowledge and disregarding the area in question due to identifying the structures (or lack of structures) involved as a region not of interest for adhesion formation.

Greater objectivity would benefit the technique. However, implementation of a simple quantification and threshold detection mechanism would not suffice: the shape of the ROI, potential effects of MRI artefacts and location of the shear drop all need to be considered. There may be potential to apply a machine learning algorithm to a training dataset but this is considered a possibility for future work and beyond the scope of this PhD.

Point 3 highlights a fundamental limitation of the visceral slide quantification technique. The technique was designed to help with the detection of adhesions to the perimeter of the abdominal cavity. The adaptation of the technique towards detection of intra-abdominal adhesions, deeper within the abdominal cavity is theoretically possible. For example, drawing regions of interest around individual objects (e.g. a bowel loop) could permit calculation of the relative motion, or sliding, between the bowel loop under interrogation and the objects surrounding it. Areas around the bowel loop which were found to contain reduced sliding could be candidates for adhesions. Ultimately this was not considered feasible due to the typically larger amounts of out of plane motion taking place away from the perimeter of the abdominal cavity. The limitation is effectively a result of dynamically imaging a 3D object in 2D. The technique developed may have some merit in aiding adhesion detection at the abdominal wall interface but in order to make further advancement, imaging in 3D is a necessity. The next chapter (Chapter 6) tentatively explores image analysis in pseudo-dynamic 3D abdominal MR images.

Section 5.4.4. Key Points:
- Improvement in patient compliance is highlighted as a necessity for the sheargram and cine-MRI interpretation with only 50% of scans deemed 'high quality'.
- Sheargram interpretation of reporters completely agreed in 85% of cases and completely disagreed in 2/141 cases – interpretation would benefit from greater objectivity.
- Out of plane motion imposes a fundamental limitation of 2D analysis. Detection of adhesions deeper in the abdomen will require 3D pseudo-dynamic imaging.

5.4.5   Reporting efficiency: has the sheargram helped decrease reporting time?

One of the important metrics for judging whether a technique has aided diagnosis is its effect on reporting time. This pilot study aimed to assess the potential for the technique to aid diagnosis and reporting time should be considered a relevant metric. A limitation of the pilot study is that it did not officially record the reporting times, however, anecdotally, review of the sheargram was typically <30 seconds and was considerably shorter than the examination time of the sagittal cine-MR images.

If the sheargram proves reliable in future studies and gains the trust of the reporting clinician, a reduction in examination time is likely. A positive sheargram that pinpoints suspicious regions could negate the need for detailed examination of the entire abdominal cavity perimeter; whereas negative sheargrams may result in the expectation of no adhesions and a less in-depth review of the abdominal perimeter. However, the author acknowledges the technique is some distance from achieving this level of functionality.

5.4.6   Critique on pilot study methodology

Grading of the cine MR images

The method chosen to randomly select 52 patients and then subsequently select a subset of high quality data from this cohort is entirely justified for the aim of this pilot study. Selecting patients at random in the first instance provided a representative sample in terms of the quality of the images. This allowed a judgement to be made on the proportion of data which may be considered 'high quality', i.e. perfectly adequate for processing. In this cohort 50% of dynamic sagittal slices were judged to be high quality. Selection and processing of only high quality data permitted a good test of the technique under real, but suitable conditions. At this stage of development, it is first necessary to test the technique on suitably high quality data, free from any aberrations introduced by challenging processing and interpretation of low quality data. To test the technique on poor quality data at this stage would be a distraction and complicate the assessment of whether the technique had *potential* to help identify adhesions, possibly making it difficult to draw conclusions. However, the fact that this analysis has been performed on data considered to be of high quality should be kept in mind when interpreting results. Protocol modifications to improve the fraction of suitable images is a priority but subsequent investigations should also clarify the limitations of the technique on lower quality images.

The methodology used for the scoring procedure (scoring each scan twice and reviewing the scans in a different order) recognises that human judgement often drifts as more images are viewed and more experience is gained. The aim of viewing the images in a different order in each scoring session was to reduce 'drift' in the usability scores across the dataset. Although subjective, this scoring procedure proved consistent. After both passes of scoring the quality, 253 of the 341 sagittal dynamic image sequences were found to agree without the need for a third review. In all cases where disagreement between the two passes was observed the score difference was 1. Moreover, in most of these disagreements (59/88) the difference may be considered less than 1 if, for example, on the first pass a score of "score 3 (possibly 4)" was received and on second pass "score 4" was given.

An alternative to the approach taken would be to mathematically quantify the amount of motion occurring in the abdomen. One consideration was to register every frame and calculate the average displacement across all nodes (or pixels) within the abdominal cavity. However, the images would still require a review by eye to assess for artefacts and respiratory motion (as opposed to pelvic thrust, for example) and, given the reasonable consistency shown by the expert eye, such an implementation was not considered necessary.

Reporter training

The reporters' correct interpretation of the sheargram is paramount if the sheargram's ability to help detect adhesions is to be accurately assessed. The training dataset of 10 sheargrams (with accompanying cine-MRs) reviewed by both reporters prior to commencing the pilot study addressed this requirement. The cases were specially selected to cover a wide range of possible scenarios, priming the reporters to recognise the effects of MRI artefacts (see Figure 5.3), out-of-plane motion and large, fast abdominal wall excursions. Additional sheargram patterns reflecting the presence or absence of adhesions were also included. The 10 examples for training were thought to be adequate without becoming too time consuming, and the scenarios presented covered the vast majority of situations encountered within the pilot study.

The technical expert was the developer of the visceral slide measurement technique and therefore has a deep understanding of the process used to generate the sheargram. The radiologist was provided with a simplified description of the sheargram generation procedure and was only exposed to the training dataset of 10 patients. The disparity of the reporters' knowledge and experience of examining sheargrams permits deeper insights into the difficulty

of sheargram interpretation. Although the requirement for greater objectivity is acknowledged, the two reporters' sheargram interpretation only disagreed in 2 cases. This implies that only a small amount of training was required to understand and interpret the sheargram without requiring a deep understanding of the technique.

Reporting and analysis method

The reporting procedure was intended to reflect how the sheargram might be used clinically i.e. in conjunction with the cine-MRI to draw attention to suspicious areas. The use of the sheargram in this way in the pilot study makes conclusions more relevant to its clinical implementation.

The classification system for deciding whether an adhesion was present (in both the sheargram and final decision) would ideally be a binary choice – 'yes', an adhesion is indicated or 'no', an adhesion is not indicated. However, in reality a single diagnostic procedure is often unable to offer a clear-cut diagnosis and for this reason the third 'equivocal' grouping was offered to reporters. The results and analysis are less 'clean' but it allowed the views of the reporters to be more accurately categorised rather than forcing a decision which would not normally be possible with the information available. Ultimately, classification of the sheargram result and clinical decision permitted the quantitative comparison and analysis shown in Table 5.1. It was this which formed the basis for most of the quantified data relating to the sheargram's correlation to the final clinical decision.

The analysis method has treated each slice as an independent entity; however, an argument could be made for slices to be grouped or clustered as some belong to the same patient. The data within the groups could potentially demonstrate greater correlation with one another and lead to bias in the statistics. For example, if the technique works in a single patient with 8 slices, but fails in one patient with 4 slices, it would show an 8/12 agreement but only 50% agreement on a per-patient basis. An in-depth look at the agreement distribution within each patient reveals: 63% of patients had agreement between sheargram and cine-MRI in all their slices; 34% had one disagreement and 3% had two disagreements. The patient-by-patient analysis shows almost all patients included in the study had 0 or 1 disagreement – therefore the agreements/disagreements were spread evenly rather than being concentrated in certain patients, indicating little influence from the 'clusters'. This implies that the likelihood of two slices belonging to the same patient leading to a disagreement is no more than two slices

originating from different patients. Consequently, while there was potential for clustering to be present within the data, the patient origin of the slice does not appear to be a contributory factor for agreement and it was appropriate for the analysis method to treat each slice independently.

The results principally revolve around comparing the sheargram to clinical interpretation of cine-MRI scans. It should be recognised that surgical confirmation is considered the true gold standard for diagnosis of adhesions. However, in the absence of surgical confirmation in the vast majority of patients scanned, clinically judged cine-MRI serves as a practical alternative. Use of cine-MRI as a diagnostic comparison tool is also supported by a recent in-house study conducted in Nijmegen. The study found high correlation between cine-MRI findings and surgically confirmed adhesions (further details were not available for inclusion in this thesis as the results are under review for publication).

5.5 Summary

This chapter has demonstrated and discussed the potential usefulness of the visceral slide quantification technique in a retrospective clinical pilot study. The pilot study included a cohort of 52 randomly selected patients who had been referred for abdominal pain with suspected adhesions. The following bullet points summarise the methodology taken:

1. The 281 unique sagittal cine-MRI slices were filtered so only those suitable for processing were selected, leaving 141 images (50%).
2. Processing produced a sheargram for all 141 sagittal slices.
3. An expert radiologist and technical expert reviewed all sheargrams and cine-MR slices. The original report of the cine-MRI was also available for comparison.
4. A judgement was made as to whether an adhesion was indicated on the sheargram and whether an adhesion to the abdominal wall was present in the cine-MRI.
5. Data analysis compared the degree of correlation between sheargram interpretation and the clinical decision on the cine-MRI made by the radiologist.

Each of the metrics proposed for an effective diagnostic aid have been addressed. The principal metric, **accuracy**, has been evidenced through the sheargram's strong correlation to expert clinical opinion:

- The results indicate good agreement between the sheargram and clinical decision as displayed in Figure 5.5.

- 84% of scans were considered to correlate with clinical opinion for both reporters (compared with 79% sheargram correlation with the original report).
- 96% and 93% of positively identified adhesions correctly correlated with sheargram interpretation for the radiologist and tech expert respectively.
- 81% of healthy sagittal slices were correctly identified by both reporters.

Robustness is indicated as there were only two cases where a positive adhesion was not visible on the sheargram. The technique exhibited a high sensitivity but a lower specificity. However, given that the aim of the technique is to be a diagnostic aid, wrongly drawing the attention of the radiologist to healthy regions is preferable to missing adhesions.

The **influence** of the sheargram has been evidenced through the radiologist altering his decision on the presence of an adhesion on 12 occasions relative to the original report. On 10/12 cases the sheargram agreed with the change made, suggesting that it influenced the decision making process. As a result, 7 additional adhesions were identified in the pilot study relative to the original reports.

Despite encouraging results, several **limitations** have been highlighted. Differences in judgement between reporters were observed, highlighting the subjective nature of sheargram interpretation. Differences in correlating the sheargram to clinical opinion could mostly be attributed to the relative lack of experience of the technical expert resulting in a tendency to report more equivocally. The inability to analyse adhesions away from the abdominal wall is a fundamental limitation of the 2D sheargram technique and a move to 3D imaging is proposed.

The pilot study has not effectively quantified the effects on **reporting efficiency** but a reduction in reporting time is a likely outcome and this should be investigated more thoroughly in future studies.

The evidence raised by the pilot study has indicated that the visceral slide measurement technique is well placed to become a future diagnostic aid for cine-MRI interpretation of the abdominal wall. The results build confidence in the technique and signify that further investigation is deserved. However, fundamental limitations of imaging in 2D cannot be ignored and the need for a 3D analysis is acknowledged and explored in the next Chapter.

Chapter 6

Discussion

This thesis has described the application of image segmentation and registration to measure sliding of organs around the perimeter of the abdominal cavity for detection of adhesive pathology. This analysis technique represents a shift from the approach of previous work and the reasons for this have been discussed and justified. Validation of the implemented technique has been sought through tests investigating certain characteristics and its clinical potential has been ascertained through a pilot study.

This chapter brings together the considerations of previous chapters but also offers some more general, fundamental concepts and explores alternative image processing options. It is organised under the following discussion points:

1. Summary of previous discussions
2. Is the sheargram necessary?
   a. Comparison with AbsCAT
3. Clinical potential of the technique
   a. Inter-operator variability
4. MRI acquisition
5. Alternative approaches to segmentation
6. Shear as an analogue for sliding
7. Presentation of the sheargram
8. Feasibility of 3D analysis

6.1 Summary of previous discussions

The structure of adhesions is not visible on current imaging modalities. The principal diagnostic technique for their detection remains an invasive laparoscopic procedure; which

itself can cause further adhesion formation. A non-invasive method for adhesion detection does not exist and would benefit effective patient management. Cine-MRI is an imaging technique which has produced some success and this project sought to aid detection of adhesions through image analysis of the movement in these dynamic images. Previous work attempted the use of image registration to detect gross adhesive pathologies. This thesis has described a refinement to the image processing approach for the detection of more common, subtle pathology. Much of the reasoning behind the change in approach and many of the aspects of the visceral slide measurement technique have already been discussed in detail. Chapter 2 recognised challenging features within the abdominal cine-MRI images which are not readily accommodated by an 'off-the-shelf' image registration algorithm, namely:

1. The presence of a motion discontinuity as a result of sliding around the perimeter of the abdominal cavity

2. Large and localised displacements

3. Motion of objects out of the imaging plane

The proposed solution was to register between consecutive frames and segment the abdominal contents from its surroundings so that the motion in each region could be analysed separately. Development of these features formed the visceral slide quantification technique in Chapter 3.

ShIRT was the registration algorithm of choice in the previous PhD and it remained the principal algorithm for the visceral slide quantification technique. ShIRT was justified for this problem because of:

- local expertise and experience

- its extensive testing in relation to abdominal images during the previous PhD

- its proven robustness, convergence speed and ease of use.

Chapter 3 tested and critiqued each aspect of the analysis method which culminated in the following salient points:

- The segmentation method was a practical implementation, utilising the power of the human eye while being facilitated by registration of the ROI position between frames. However, reproducibility tests in Chapter 4 highlighted differences in the sheargram resulting from changes in ROI position. Ultimately, human interaction introduces subjectivity, inconsistency and is responsible for >80% of the total processing time. As a result, this was one of the main areas highlighted for improvement. Some potential alternative approaches are explored in Section 6.5 of this chapter.

- The use of ShIRT to register consecutive frames of the segmented regions (rather than frames at either end of the respiratory cycle) was considered an essential approach to counteract the issues highlighted at the end of Chapter 2 and the above-mentioned points (1-3).

- Discrete approximations were used to calculate the displacement gradient tensor and determine the shear strain orientated along the sliding boundary. The approximations were considered a necessary compromise to achieve quantification of shear. It was noted that the visceral sliding of the abdominal contents against the abdominal wall is the major focus of this PhD. The quantity calculated using the displacement gradient tensor is *shear*, which has been used as an analogue for sliding throughout this thesis. The extent to which this is true is considered in Section 6.6 of this discussion chapter.

- Summation of shear over the whole dynamic image sequence was considered crucial for effective data interpretation. Utilising the deformation fields from the registration of the abdominal surroundings for summation was considered robust but did occasionally fail in the presence of large, fast respiration/abdominal wall excursion. Chapter 4 included a comparison of two potential summation techniques and the method adopted proved superior.

- Tensile strain was also calculated but experience proved this information had no correlation with known adhesions and was considered to be of little use.

The series of experiments in Chapter 4 confirmed the technique was fundamentally capable of determining shear through idealised in-silico and in-vitro experiments. The sheargram was found to be reproducible with repeated processing of the same scan through qualitative assessment. However, quantitative differences in shear were observed. A rough approximation quoted for the variation in shear was 2±2 pixels or, as a percentage of the shear in a region, 12±9%. The position of the ROI was thought responsible for the majority of differences in shear. An estimated tolerance in ROI placement of <4 pixels was quoted as a rough guide for an acceptable range. The reproducibility was considered acceptable for a research tool under development; but these findings stress the importance of the robustness of the technique, particularly if considering its application in a clinical setting.

Application to a sizeable cohort of clinical data (140 sagittal slices) resulted in a high sensitivity (>93%) for adhesion detection, indicating that a drop in shear corresponded to adhesions. However, a large number of reductions in shear were found to be false positives (12-14 cases),

resulting in a lower specificity of 81%. A high true negative rate was observed as a high shear almost invariably correlated with a lack of adhesions. The skew towards sensitivity over specificity was considered favourable for the technique's role as a diagnostic aid - only one adhesion was not detected on the sheargram (by the radiologist). The pilot study confirmed the potential of the technique to become a diagnostic aid.

The issue of out of plane motion has reoccurred throughout this thesis and also featured in the results of the pilot study – it was the cause of the only missed adhesion by both reporters. A direct solution to out of plane motion is to image and analyse movement in 3D. A sizeable portion of this discussion chapter (Section 6.8) is devoted to considering the possibility of adhesion detection using a 3D analysis.

The majority of evidence has indicated that the visceral slide quantification technique is capable of detecting adhesions to the abdominal wall. The discussion points proffered throughout this thesis predominantly pertain to the characteristics and capability of the visceral slide measurement technique. This final discussion will now consider some more fundamental questions and explore alternatives to the implemented methodology.

6.2 Is the sheargram necessary?

As previously identified, the main aim of this project was to aid the reporter of abdominal cine-MRI images for the detection of adhesions. Cine-MRI has shown promise to become a non-invasive diagnostic technique for adhesions as shown in the literature [20, 31]. These publications have caused a handful of centres to adopt the technique for research purposes and in the process it has become part of the patient pathway in these centres. This project was inaugurated due to reports that cine-MRI was subject to high inter-operator variability and local comments regarding the difficult, time consuming nature of the report [32]. However, with evidence generally indicating a high correlation between cine-MRI and surgically confirmed adhesions, (without the sheargram) it raises the question: Is the sheargram necessary?

Two experienced radiologists have been involved during the course of this PhD and both acknowledge that reporting adhesion cine-MR scans is a time consuming challenge and requires extended periods of concentration. Comments from both radiologists have been supportive of the sheargram technique, citing that it could help identify abdominal wall

adhesions more easily. For less experienced radiologists undertaking training in adhesion cine-MR reporting, the value of the sheargram could be of greater merit. The usefulness of the sheargram to facilitate training and to increase efficacy in reporting by less experienced radiologists, is an area identified for future work. A quote from one radiologist, experienced in cine-MRI adhesion reporting, is included to support the remarks above:

"As the study is a dynamic one it requires much more training to analyse than the conventional static images radiologists are accustomed to. The sheargrams will facilitate training and aid in diagnosing adhesions. Intelligent reading by computer software is a fast upcoming feature in radiology as has been mentioned at the latest RSNA meeting by the CEO of Philips medical systems (2016). CAD (computer aided diagnosis) will greatly influence the daily practice of radiologists."

The pilot study in Chapter 5 noted the radiologist making 12 changes in clinical opinion (between original report and the pilot study, see Figure 5.6). This provides evidence that the sheargram influenced decisions and helped to identify a greater number of adhesions, even at this early stage of implementation.

The comments from the radiologists and the changes in clinical opinion observed in the pilot study indicate that the sheargram could aid the radiologist.

A secondary factor is whether the sheargram adds any value to existing tools. Prior to this PhD, AbsCAT had already been created and a comparison of the information produced by each should indicate whether the sheargram adds any additional information.

6.2.1   Comparison with AbsCAT

AbsCAT was aimed at the detection of gross adhesive pathology, namely EPS. As discussed in Chapter 1, this PhD changed focus to attempt detection of more subtle abnormalities. This led to the creation of the visceral slide quantification technique and the sheargram. AbsCAT and the visceral slide quantification technique are designed to operate on the same cine-MRI data and therefore can be directly compared. Three clinical examples that contained substantial adhesions were taken from the pilot study in Chapter 5 and processed by AbsCAT. The AbsCAT results are shown above the corresponding sheargram result for each of the three examples in Figure 6.1.

Example 1   *Example 2*   *Example 3*
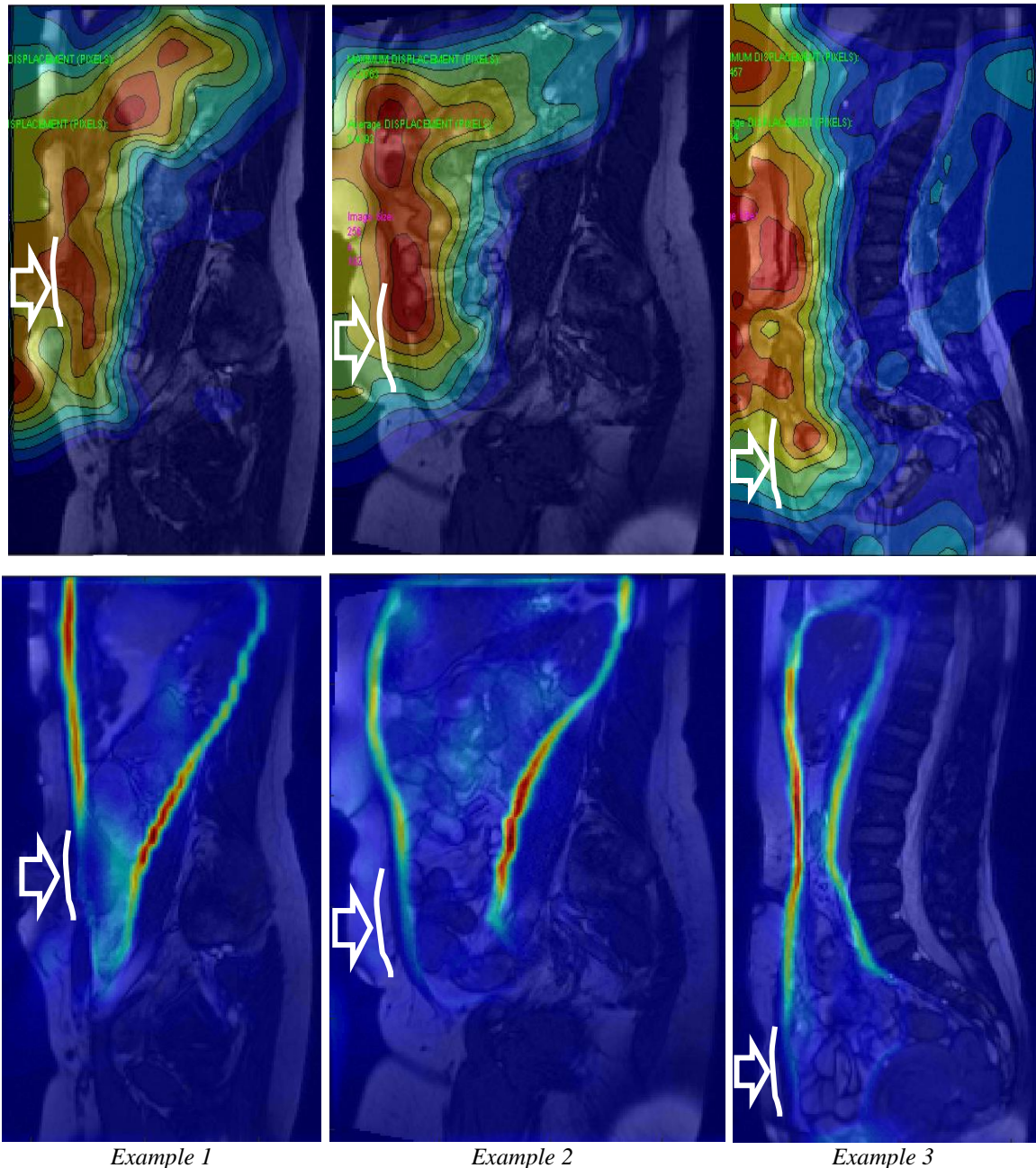
Figure 6.1: Comparison of a set of 3 results on different patients from AbsCAT (top row) and the visceral slide quantification technique (bottom row)

The adhesions in each of the examples were identified on the sheargrams. The drop in shear on example 2 is less stark but still shows a large enough reduction to draw the attention of the reporter. AbsCAT did not correlate a reduction in movement magnitude with any of these adhesions. Movement of the abdominal wall, and therefore with it the abdominal contents, was the cause of the large movement signatures in the anterior region and around the adhered areas. This is not a surprising result: the two tools are designed for different purposes. Nonetheless, it is reassuring that the sheargram clearly adds sensitivity for the detection of subtler adhesions as was the intention from the outset.

6.3 How the sheargram relates to clinical practice

The previous section concludes that the sheargram could be of benefit for aiding diagnosis but does not cover the extent to which it could impact on clinical practice more generally. Clearly, at this stage of development, the technique needs to address the following before it is likely to be welcomed into clinical practice:

- its reliance on a single expert operator
- the impractical processing time required
- its focus on a subset of adhesions to the abdominal wall
- a lack of conclusive characterisation of the sheargram's reliability.

Despite such shortcomings, there is sufficient evidence to extrapolate and consider its future potential, highlighting areas requiring improvement to move closer to a workable clinical tool.

There is evidence that the technique has merit in aiding detection of adhesions to the abdominal wall and it has been suggested that it could particularly benefit less experienced, training radiologists. However, to have a wider impact on clinical practice any technique would need to detect adhesions deeper in the abdomen. If a patient presented with symptoms which led to suspected adhesions the clinician would query, "are adhesions present or not?". Currently the sheargram is not capable of answering such a query as it is only capable of assessing a small subsection of the abdominal cavity: its perimeter. Moreover, its efficacy has only been tested with regard to the abdominal wall. Application of the analysis of shear between adjacent structures within the abdominal cavity was considered, but out of plane motion would ultimately lead to a lack of confidence and limit the number of cases where it could be applied reliably. Analysis deeper within the abdomen would require a 3D solution.

Time pressures in the clinical setting limit the effort that can be devoted to a processing task and encourages efficiency. To process a single sagittal slice takes a well-practiced user roughly 10 minutes. There are typically 5-7 slices for each patient, meaning a single patient takes approximately one hour to process. This is not practicable in a clinical setting. Roughly 80% of the processing time can be attributed to the segmentation process. The semi-automated segmentation implementation has served a valuable role but was developed as a research tool for proof of concept. Modifications would be necessary if it were to be translated to the clinic. A full commitment to developing such a method was considered beyond the scope of this PhD but some progress has been made and is discussed in Section 6.5.

Only a single operator is currently trained in sheargram processing and clearly, if used in a clinical setting, processing would need to be performed by different operators. The segmentation process is the only user input required. The inter-operator variability must be small if the technique is to succeed. The current operator possesses knowledge of the underlying mathematics of the technique which aids the drawing of a suitable ROI. The extent to which this information is a requirement to perform successful processing is not known but is not thought to be crucial. This thesis has not attempted a formal, in-depth investigation into the inter-operator variability. However, given its importance in adjudicating its usefulness in the clinic, an inter-operator test involving a short training session (without imparting knowledge of the underlying maths) is presented in the following section.

6.3.1   Inter-operator variability

A brief discussion on the inter-operator variability of sheargram interpretation was offered in Chapter 5, Section 5.4.4. The discussion offered here pertains to inter-operator variability in the processing procedure. The subjective nature of the ROI placement has been highlighted as a problem which may influence robustness and the training of other operators. At this stage of development, a thorough investigation into inter-operator variability was not considered vital but it is an important consideration if the work is to progress. In recognition of its impending future importance, a brief investigation was undertaken to expose any inconsistencies between operators.

Two operators were trained on the processing procedure using four sagittal cine-MRI slice examples. Both operators were clinical scientists familiar with abdominal anatomy and image processing but without a specific understanding of the visceral slide quantification technique. The training involved observing an expert process two scans, processing two scans themselves under supervision, then finally processing two further scans unsupervised. Explicitly, the inter-operator variability experimental procedure involved the following steps:

1. Operator observed an expert process a median sagittal slice
2. Operator processed a median sagittal slice under supervision
3. Operator observed an expert process a paramedian sagittal slice
4. Operator processed a paramedian slide under supervision
5. Operator processed two scans, one median and one paramedian, without any guidance or supervision to be used for inter-operator comparison.

The training offered did not constitute a full training programme; nevertheless, it was practical given time constraints (training + processing exceeded 1.5 hours). Variability was gauged from qualitative comparison of the sheargrams.

The two sheargrams for each operator are shown next to the expert operator's results in Figure 6.2: the top row shows the results for the median sagittal slice (Case 1), the bottom row shows the results from a paramedian sagittal slice (Case 2).
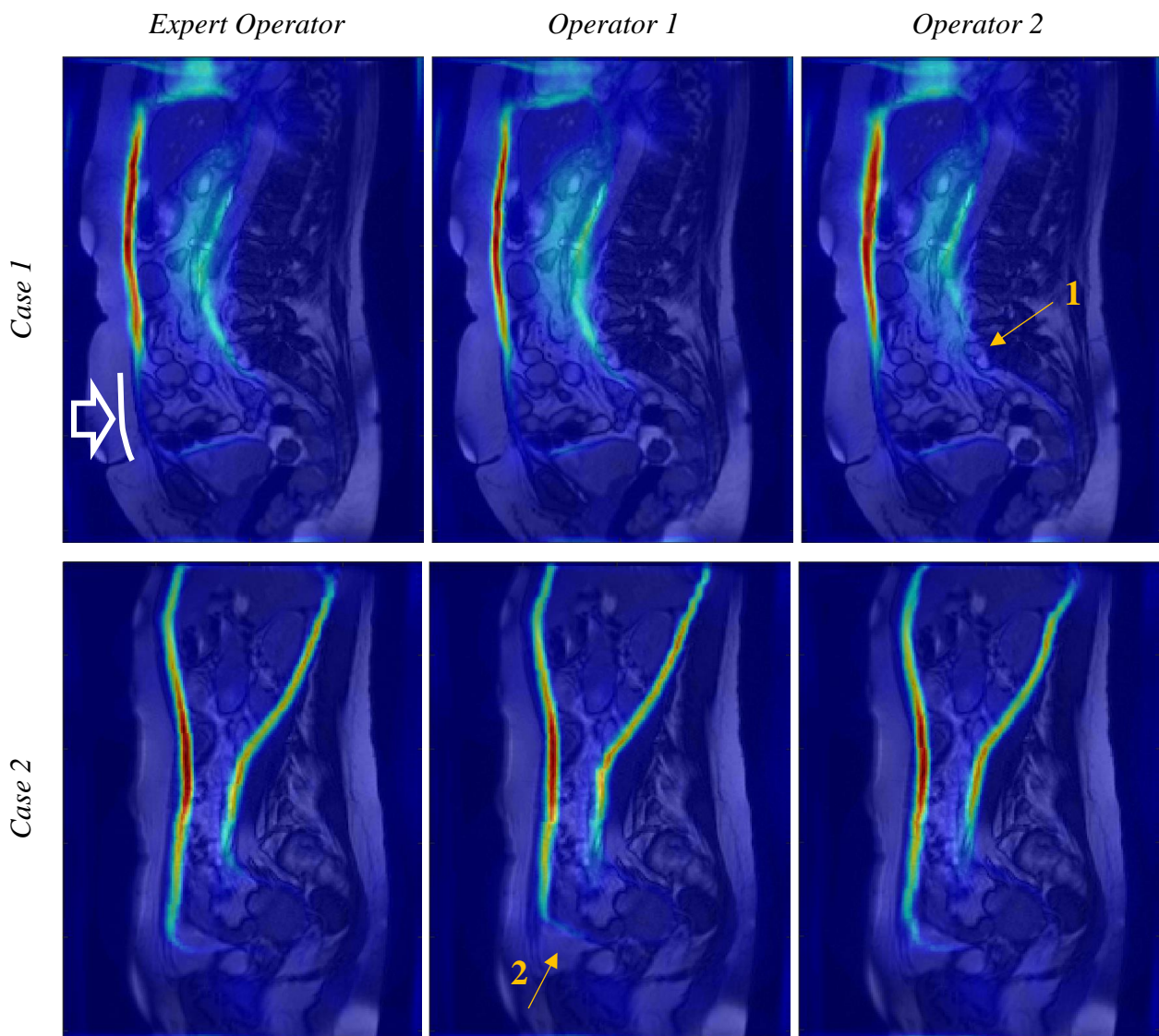
Figure 6.2: Sheargrams for the two cases used for the inter-operator variability test. Top row is case 1 and contains an adhesion to the lower abdominal wall. The large white arrow shows the location of the adhesion. Bottom row is case 2 and has no adhesions to the abdominal wall. The small gold arrows indicate the locations of observable differences between operators' sheargrams.

The sheargrams for both cases in Figure 6.2 have a similar appearance across all operators. No area stands out as being particularly different that would alter interpretation. One way of viewing inter-operator variability is as a signal to noise ratio: the signal of an adhesion should be strong enough to be seen through the noise introduced by differences in processing between operators. The clear drop in shear at the adhesion (white arrow) in Case 1 is immediately apparent across all operators and clearly exceeds the 'noise' introduced by different operators.

Some minor differences between operators are observable: highlighted by the gold arrows in Figure 6.2. Arrow 1 shows a reduction in shear relative to the other two operators and is attributed to Operator 2 including two stationary objects attached to the spine within the abdominal contents – mistaking them for bowel loops. The lack of movement of these objects (correctly) resulted in a shear reduction relative to the other operators. This highlights the difficulty and ambiguity in deciding what should be considered as abdominal contents: a degree of anatomical knowledge and experience of MRI image interpretation is required. The difference observed at Arrow 2 corresponds to a difference in ROI position in a region without detail. Operator 1 drew the line to contour the nearest section of bowel; operator 2 and the expert opted to draw the ROI more horizontally to the abdominal wall. This represents a minor mistake in the case of operator 1: a bowel loop (not visible in Figure 6.2) appeared in the imaging plane later in the dynamic image sequence and the ROI placed by operator 1 cut this object in two. However, due to the small number of frames where the object appeared this has not had a major impact on the result of the sheargram.

This exercise has highlighted some of the challenges in training others to process abdominal cine-MRI, with implications for training requirements and future developments:

1. The need for improved definitions of what should be included as abdominal contents. This is difficult to address due to the complexity of features in the abdomen, different areas imaged (different sagittal slice positions) and variability between patients. The current implementation attempts to combine movement information from the cine-MRI video and basic anatomical knowledge but this task can prove challenging. Greater automation in the segmentation technique could partially alleviate this.

2. The need to thoroughly review all frames in the cine-video before completing the ROI to avoid situations such as that highlighted by Arrow 2. Although the user changes the ROI between frames, dramatic changes from one frame to the next are not desirable for accurate registration i.e. it is important to draw an appropriate ROI in the first instance.

More extensive training could reduce instances of these cases but the time and attention required by the operator means mistakes are inevitable.

3. The current developmental version of the user interface was usable but could be improved. The operators were only provided with a small amount of training (2 observations and 2 practice runs) and both produced results comparable to the expert operator. However, the operators were both timed and took an average of 16 minutes and 18 minutes to segment each sagittal slice. There are two ways to improve on this inefficiency: improve the user interface for defining the ROI and/or increase the automation in the segmentation. In this developmental stage neither have been thoroughly investigated but potential mechanisms for improvement are discussed in Section 6.5 and in the conclusion (Section 7.3.2).

6.4 MR acquisition

Optimisation of the MRI scanning protocol was not a focus of this PhD as almost all of the images analysed were acquired prior to the project's commencement. However, developments made during the course of the PhD influenced discussions on changes to the scanning protocol at Rotherham District General Hospital. Two features were discussed and influenced an ethics application for a volunteer study: introduction of higher temporal resolution and the need for comparison between bearing down and breathing deeply. The intention was to use evidence gained from the volunteer study to support scanning protocol optimisation for both research and clinical practice. The volunteer study was not completed during the PhD and is therefore not discussed.

Higher temporal resolution

Prior to this PhD, images acquired in Rotherham used an image matrix size of 512 x 512 rather than a smaller 192 x 256 matrix. This higher spatial resolution increases the acquisition time of each frame and therefore compromises the temporal resolution of the dynamic sequence (512 x 512 = 0.8 seconds per frame, 192 x 256 = 0.4 seconds per frame). The visceral slide quantification technique relies on accurate registration between sequential frames and a higher temporal resolution was beneficial to:

1. Reduce out of plane motion between frames to lessen anomalous registration deformation field artefacts from objects suddenly appearing/disappearing.

2. Reduce the magnitude of displacement between frames for greater registration reliability.

3. Increase ability to replicate the actual paths taken by objects in the abdomen throughout the dynamic series.

The previous PhD also highlighted inaccuracies in registration for large deformations and cited the need to limit the movement between frames [6]. As a result of the arguments provided above, the volunteer scanning protocol was altered to include a higher temporal resolution scan (192 x 256, 0.4 seconds per frame) as well as the original clinical scan for comparison.

Bearing down vs deep breathing

The instruction to 'bear down and breathe normally/deeply' during the MR scan is currently given to patients at both Rotherham and Nijmegen. The inclusion of this instruction is based on the following statement in Lienemann et al.'s (2000) paper [20]:

"In the first three patients, as part of a pilot study, the cycle in the midsagittal position of the abdomen was acquired twice: First, the patients were asked to increase intraabdominal pressure by straining and to subsequently relax. Then, they were asked to breathe deeply while performing the same cycle. The decision about which type of induced visceral slide to use ultimately was based on only the visual facts...
In the pilot study, we found that an increase in intraabdominal pressure caused by straining proved to be superior to that due to respiratory excursions alone."

Evidently, the choice of 'bearing down' is based on qualitative, visual analysis of 3 participants. After reviewing several hundred cine-MRI scans and having undergone the procedure as a volunteer, the 'bearing down' procedure is suspected to be detrimental to patient compliance. To breathe deeply while bearing down is difficult in practice and may hinder diaphragmatic motion in some subjects. Often movement in the images would be a result of 'pelvic tilt' or 'pelvic thrust' where the patient moves their entire abdomen or body rather than creating an intra-abdominal motion through diaphragmatic excursion. Before changes can be made to the scanning protocol more concrete evidence regarding the effects of bearing down is required. The volunteer study aims to provide this evidence.

6.5 Alternative approaches to segmentation

A consistent conclusion throughout this thesis is that the visceral slide quantification technique would benefit from increased consistency and efficiency in the ROI placement procedure. The segmentation is complex as the operator is required to combine information of structure and motion. This makes implementation of a more automated procedure more challenging. Also, additional complication is added by the complexity of structure and inter-patient variability observed in the abdomen. For these reasons such an implementation was not considered within this PhD and the semi-automatic segmentation method employed was adequate for proof-of-concept. However, several methods of segmentation were tentatively explored. These mostly revolve around achieving an initial guess for the position of the sliding boundary on one frame that could then be warped to match the boundary in subsequent frames. Achieving a sliding boundary match in one slice was seen as the first step towards a fully automated technique to produce a suitable ROI for all frames. Even so, ROI placement for a single slice would itself save approximately 1/5 (~2 minutes) of the total processing time and potentially lead to greater reproducibility and consistency between operators.

The purpose of this section is to discuss the possibility of a more automated segmentation. Conceived techniques for achieving increased efficiency in segmentation are described and discussed in turn.

6.5.1 Segmentation of motion

Chapter 2, Section 2.4.1 mentioned the concept of achieving segmentation by analysis of the motion in the image. A technique proposed by Kiriyanthan et al. incorporated a motion segmentation within an iterative registration algorithm to preserve the motion discontinuity [102]. The group showed some preliminary success in abdominal images of the liver. While Kiriyanthan et al.'s work is directly relevant, it is still under development, can only cope with small displacements and would be difficult to reproduce. This was not the focus of this PhD and this route was not considered (particularly as the paper was published towards the end of this PhD). Instead, readily available tools were used to gain insight into the potential of using motion segmentation as a component of the visceral slide processing technique.

A picture of magnitude of motion can be obtained by registering each frame to its consecutive frame without imposing a mask. Both ANTs and ShIRT registration algorithms were used to

produce images of motion magnitude on the same cine-MRI slice. The ShIRT registration used the default parameters used throughout this thesis (node spacing of 4 and an adaptive smoothness constraint strength). The ANTs registration parameters used were:

- Cross correlation similarity metric with a regular sampling grid
- Diffeomorphic transformation
- Multiscale approach with five levels
- No pre-rigid registration step (as the images are consecutive and already aligned)

Upon summation of the magnitude of motion between each frame, images were produced from the results from each of the registration algorithms, as shown in Figure 6.3.

(a)   *(b)*
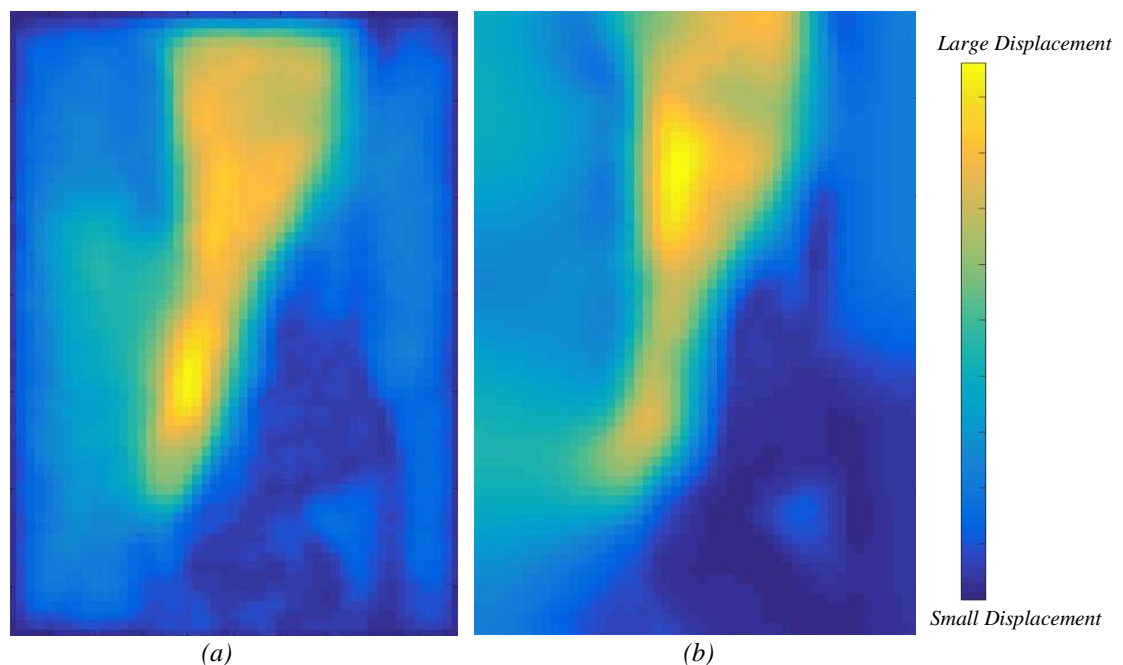
Figure 6.3: Images showing the summation of the displacement fields from registration of consecutive frames of a cine-MRI with: (a) diffeomorphic registration performed using ANTs and (b) default parameters in ShIRT

ANTs was selected as the primary tool in this investigation as relaxation of the smoothness constraint was expected to permit a sharper change in displacement and therefore a better defined cut-off at the edge of the moving region. This can be seen to be the case when comparing the ANTs registration (Figure 6.3a) to the registration using ShIRT (Figure 6.3b). In this experiment, ShIRT was only included for comparison purposes and to demonstrate the dependence and importance on registration algorithm/parameter selection.

A Canny edge detection algorithm [107] (built-in to MATLAB) was used on the motion images to identify an approximation of the sliding boundary position. The default lower and upper thresholds for 'edge strength' were used (determined by MATLAB based on the input data). The results are shown in Figure 6.4.

(a)   *(b)*
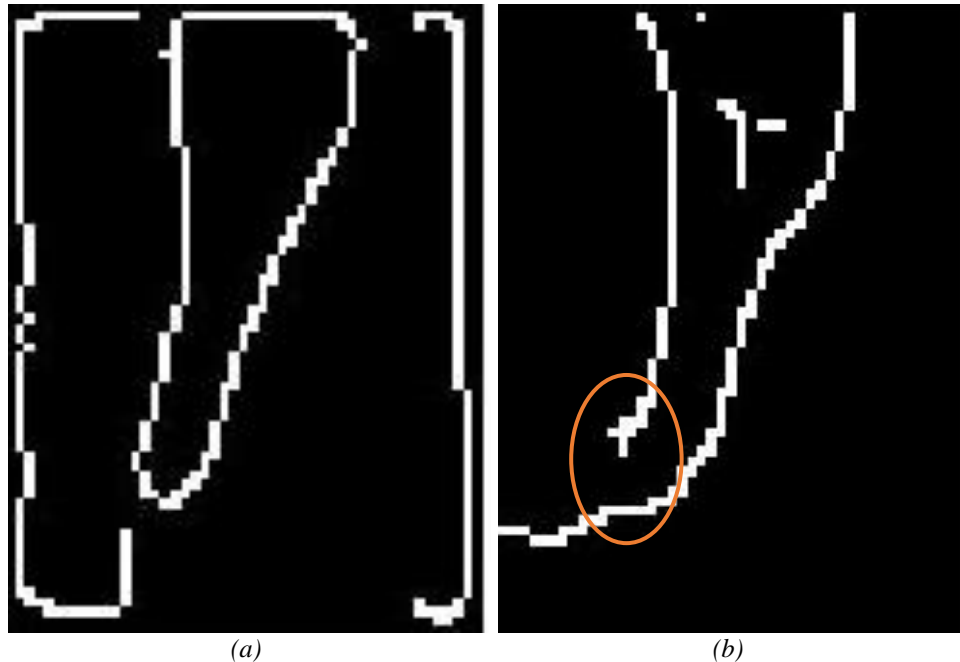
Figure 6.4: Result of a Canny edge detection on the motion images shown in Figure 6.3 [(a) = ANTs, (b) = ShIRT]. The orange oval highlights an area where the edge detection algorithm was unable to produce a closed loop on the result from the ShIRT registration.

The edge detection algorithm successfully identified a perimeter for the abdominal surroundings of the ANTs registration result (Figure 6.4a). The boundary identified was achieved fully automatically without the need for any user interaction and could be used to define a starting point for the ROI. The ShIRT registration did not result in a closed boundary as the edge corresponding to a portion in the lower abdomen was not detected, indicated by the orange oval in Figure 6.4b. As mentioned at the start of Chapter 2, this gap highlights a major drawback of edge detection techniques and points towards a lack of robustness.

The boundary in Figure 6.4 appears thick because the edge detection was performed on an image of the displacement at each node. A node spacing of four was used, meaning the images were a quarter of the resolution of the original images and the boundary is therefore four pixels thick. It should be noted the cine-MRI chosen was a 'favourable' example as large amounts of

motion within the abdominal contents could be observed. Less ideal images with less movement could present problems for this method.

Overlaying the result of the boundary in Figure 6.4a onto one of the cine-MRI frames produces the result in Figure 6.5.
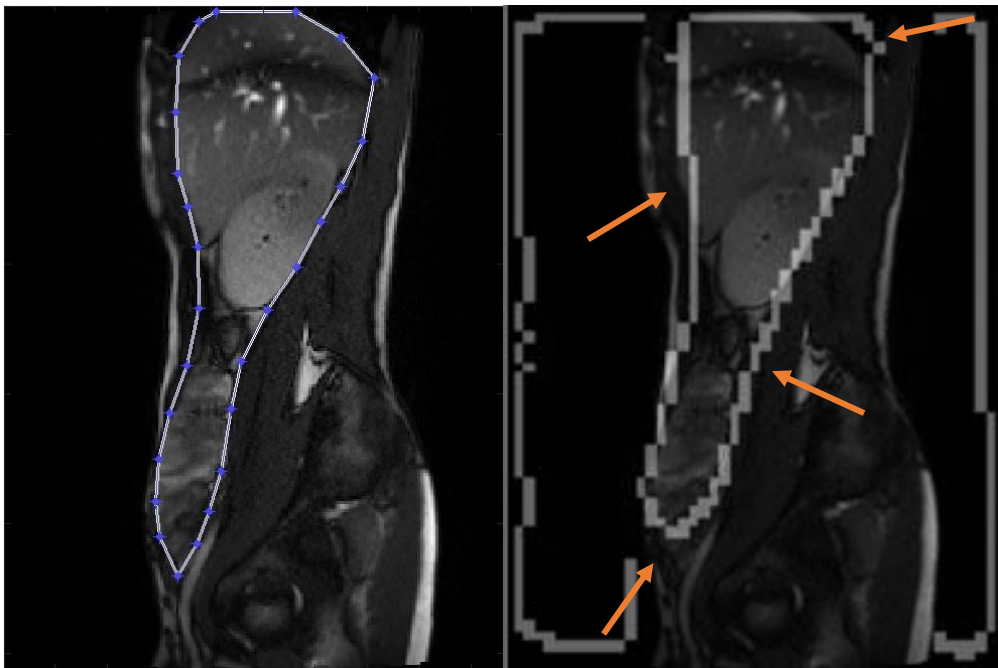
Figure 6.5: *ROI drawn manually compared to an automatic sliding boundary detection using segmentation of motion resulting from an ANTs registration. Results are overlaid on a frame of the original cine-MRI sequence. Orange arrows highlight areas where the automatic boundary deviates from the manual boundary.*

Figure 6.5 shows a good correlation between the edge detection result and the manually drawn ROI. A particularly close match is observed along the majority of the posterior portion of the sliding boundary and lower to mid abdominal wall. The areas highlighted by the orange arrows indicate apparent (but small) deviations from the manual boundary. A further problem which could be encountered is that the images of motion represent average motion over all frames. Therefore, the edge which is detected may not map to any particular frame. This could lead to the user having to modify all the calculated ROI vertex positions, resulting in no time saving over drawing the ROI manually. Overall, if similar results to those in Figure 6.5 were replicated across more patients, this initial estimate of the sliding boundary could reduce processing time.

This investigation has explored edge detection of the motion image, but given the pitfalls of edge detection, other segmentation algorithms such as intensity threshold techniques or region

growing may be more suitable options. Edge detection was explored as this could have potentially been easily implemented as a fully automated technique without the need for user interaction. The region of the abdominal contents in the images in Figure 6.3 do not display sharp changes in intensity; they are reasonably homogenous regions. For this reason, region growing techniques with a dynamically varying homogeneity criterion remains a possibility and may be a target for further investigation.

6.5.2 Image subtraction

Subtraction between frames should produce higher intensities in regions with movement (i.e. areas with larger variations in intensity) and low intensity in regions where objects are not moving (i.e. areas with little variation in intensity). A sharper drop in intensity at the sliding boundary may then be more easily segmented with automated techniques. Three methods of image subtraction were attempted in a single patient:

   a) Subtract each sequential frame from the previous frame;

   b) Subtraction of every frame from all other frames, covering all combinations of subtraction.

   c) Calculation of an average image and subtraction of the average image from all other frames.

Figure 6.6 shows the summation of the subtracted images for each of the methods (as well as the original image for comparison). In each method absolute difference in pixel intensities was taken and summed.

(a)   *(b)*

(c)   *(d)*
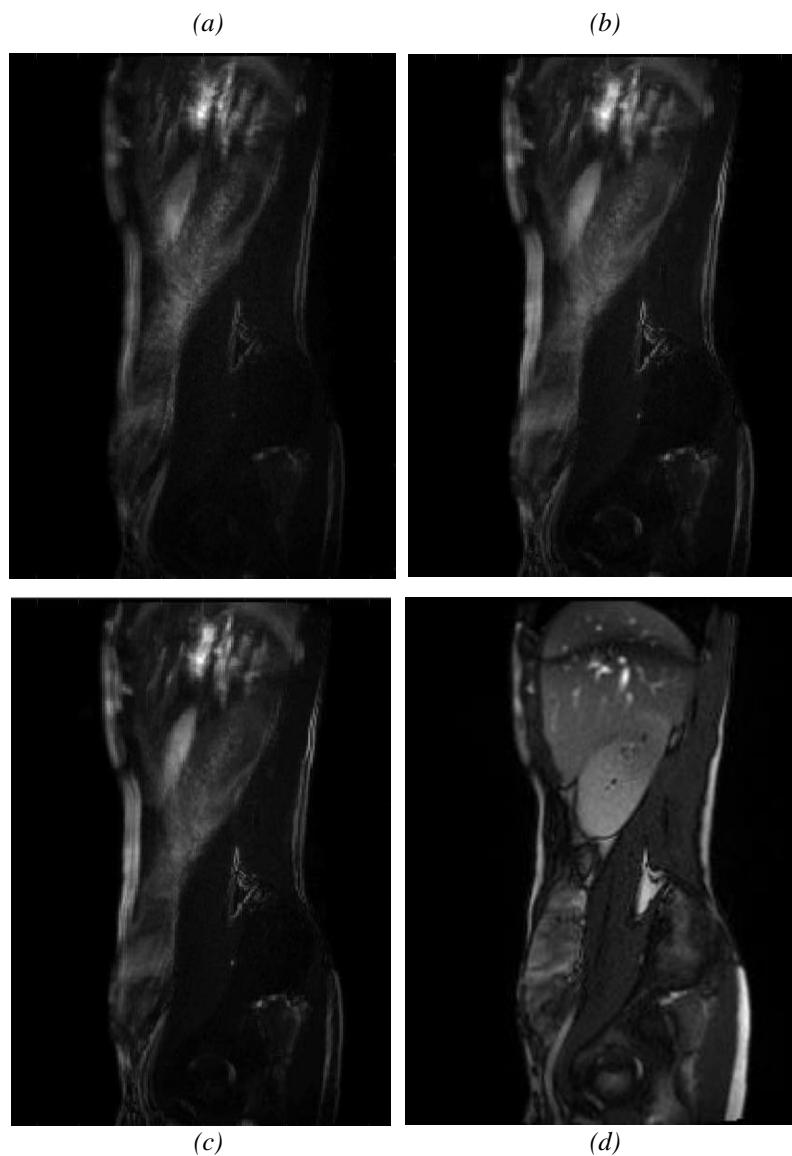
Figure 6.6: (a) summed image of image subtractions when subtracting consecutive frames, (b) summed image of subtractions resulting when every frame is subtracted from every other frame, (c) subtraction of an average image from all frames which were then summed; (d) an example of one of the frames from the original image-set.

Figure 6.6a, b and c are similar in appearance. Figure 6.6b presents a slightly larger difference in intensity between the mobile abdominal contents and its surroundings compared to the other two. On the posterior wall the sharp drop in intensity at the sliding boundary may be enough to apply an intensity threshold to automatically determine the boundary. On the anterior wall this may be more difficult as it itself moves and has a strong signal. The variation and lack of uniformity in the intensity throughout the abdominal contents also casts doubt over the robustness of applying such a technique to abdominal cine-MRI. Moreover, for this quick test a favourable cine-MRI case was chosen with large amounts of diaphragmatic excursion.

Images with less abdominal movement are likely to provide a greater challenge to process with this method.

The subtraction images do not present any obvious advantages for automatically distinguishing the sliding boundary relative to the original image. Although only a brief investigation, the results displayed in Figure 6.6 do not provide incentive for pursuing this method further.

6.5.3   Atlas based segmentation

An ROI drawn on one or more reference sagittal slice(s) could be registered to match the sliding boundary position in individual cases. Given the large variability in size and shape of individuals it is unlikely that a single 'atlas' ROI would suffice for the full range of individuals: a range of atlases would be more appropriate. An atlas for each of the sagittal slice positions in the patient (e.g. median, left paramedian etc.) would also be necessary. The number of different atlas ROIs required therefore adds complexity to implementation and usability. Nonetheless, a potential automated implementation could be possible if the location of the slice in the DICOM header were used to determine which atlas slice position is most appropriate. It is also possible that a similar point in the respiratory cycle to the atlas image may be required. The extent to which points in the respiratory cycle would need to match would need to be investigated. An automated approach for determining a similar point in the respiratory cycle may be necessary and could be achieved using a similar method to AbsCAT (described in Chapter 1, Section 1.5) where an overall vector was used to find frames at the extremities of the respiratory cycle. The user would still most likely be required to review and modify the ROIs produced, but improvements in efficiency and consistency are a possibility. Implementation of this technique would require significant time investment and could not be achieved within this PhD. This method should be explored as an option for further development.

6.5.4   Summary

Some potential techniques to increase automation in the segmentation procedure have been discussed. Two of the proposed techniques have already been tentatively explored. Using a summed displacement field over all frames of a cine-MRI has shown some potential to approximate the outline of the abdominal contents. The initial attempt described in this section had some inaccuracies but showed enough promise to suggest that, with refinement, it could increase processing efficiency. The brief investigation into the use of image subtraction

revealed it is unlikely to produce images suitable for automatic segmentation; particularly as the cine-MRI example used was a suitable candidate. A method for atlas based segmentation has been proposed. It involves the creation of a library of atlas ROIs for different slice positions and patient sizes that could then be registered to individual cases. It has been suggested as an area for potential development but the variability between patients remains a potential problem for its implementation. Segmentation of the motion and atlas based segmentation should be the primary targets for refinement in the segmentation procedure.

6.6 Shear as an analogue for sliding

Throughout the thesis the terms 'sliding' and 'shear' have been used almost interchangeably. However, the two do describe different types of movement/deformation. Shear describes a lateral shift between layers/elements of an object or between two objects; whereas for sliding to occur there must always be two de-coupled objects exhibiting motion relative to one another at an interface. The term shear may be more generally applied to include shear strain forces acting within an object. The experiment illustrated in Figure 6.7 exemplifies this difference.
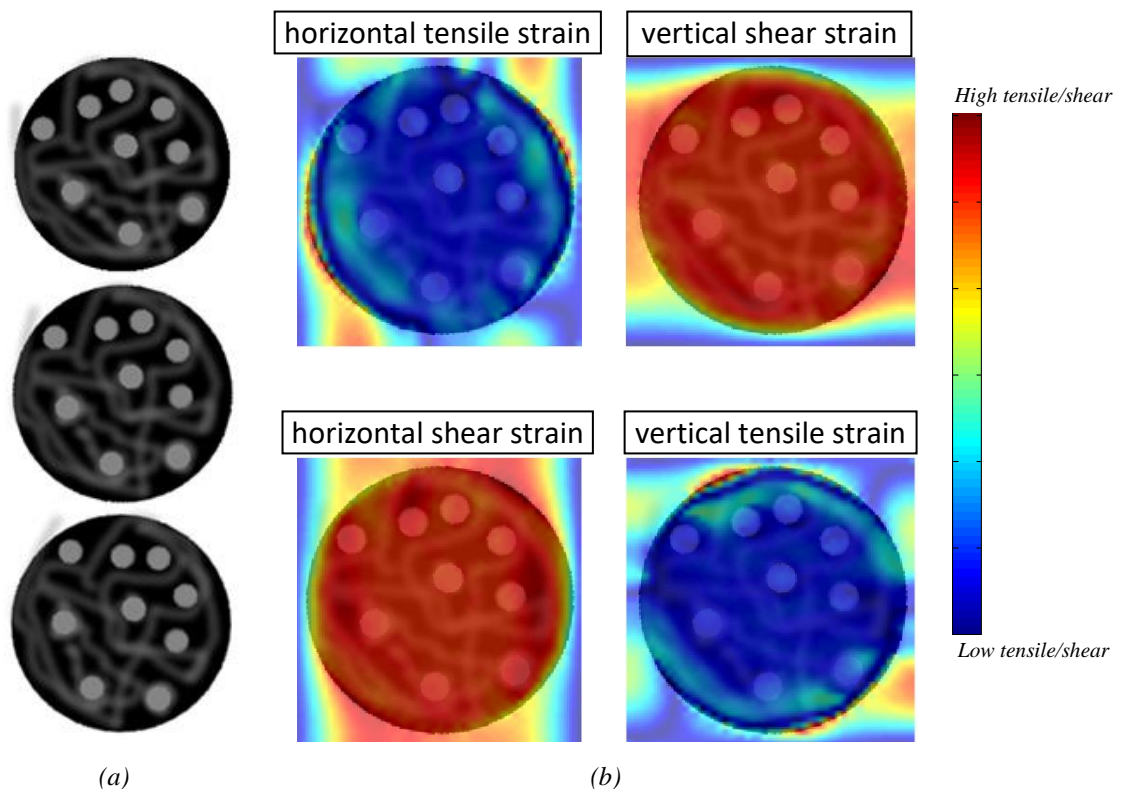
Figure 6.7: *(a) Shows three rotations of a disc with detail added onto its face; (b) shows images relating to each component of the displacement gradient tensor resulting from registration between two frames (produced by the visceral slide processing technique).*

The visceral slide quantification technique was applied to images of a rotating disc. The disc was rotated through 45° in 5° increments. Figure 6.7a shows three snapshots with a rotation of 15° between each image. Figure 6.7b shows that both tensile strain components of the displacement gradient tensor are minimal within the body of the disc and shear strain is present in both directions and uniform across the disc face. This is as expected: the displacement of the elements within the disc increases linearly with radial distance from its centre, as indicated in Eq 6.1 for the circumference of an arc. Therefore, there is a differential in movement between neighbouring elements as distance from the centre is increased, resulting in a quantifiable shear strain.

$$Displacement = \frac{2\pi r\theta}{360}$$ *Eq 6.1*

In the rotating disc system, no sliding has occurred and the two terms (sliding and shear) are clearly not analogous in this case. However, in the abdomen, sliding is occurring as the abdominal contents move unimpeded against the inner surface of the abdominal wall. In these types of systems shear and sliding may be thought of as analogous.

6.7 Presentation of the sheargram

Information rich data would be useless without it being appropriately displayed for human interpretation. This is especially true in the clinical environment where clarity is important to avoid potentially catastrophic consequences of an incorrect diagnosis and to comply with tight time constraints associated with radiological examination/reporting. A diagnostic aid must be efficiently interpreted by the radiologist, ideally reducing overall reporting time and increasing the proportion of correct diagnoses.

The display method chosen in the visceral slide quantification technique was to overlay the calculated shear data on an MR image using a semi-transparent colour map. The colour map ranged from deep blue for no shear to red indicating a high shear. This method of visualisation produced a simple, clear image which was well received by clinical colleagues.

The sheargram is normalised to the maximum shear in each sheargram and therefore, in terms of the absolute shear occurring, different sheargrams cannot be compared to one another.

Normalisation of all sheargrams to an absolute shear value would allow comparison of sheargrams but the amount of shear between cine-MRI slices varied dramatically making selection of a single value difficult. The value of comparing sheargrams is also unclear. Displaying the relative shear within each sheargram allowed for greater clarity in the pattern of shear around the abdomen and this was the principal feature assessed when reporting. The user could be made aware of the maximum shear in each sheargram but this was not considered essential.

The sheargram was used throughout this project but alternative visualisations were considered and briefly explored:

- Figure 6.8 shows a **three-dimensional surface plot** of the summed shear overlaid onto an MR image.
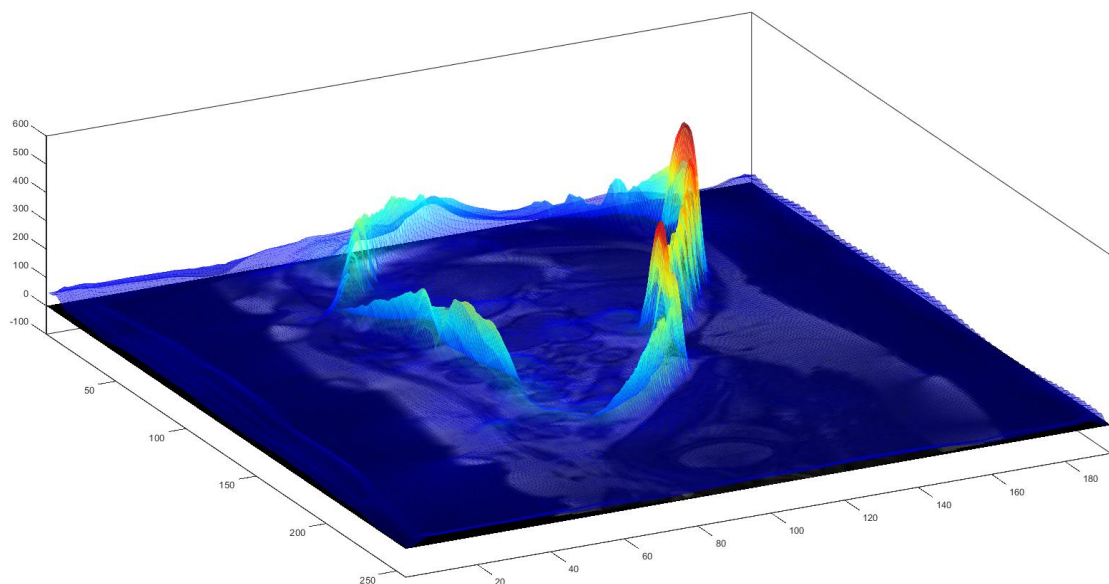
Figure 6.8: 3D surface plot representation of the sheargram

The extra dimension was considered superfluous for interpretation and made it more time consuming to assimilate the information. The user would be required to rotate and re-orientate the 3D image using a mouse in order to build a complete picture of the shear. This is in contrast to the 2D colour map representation where the information can be assimilated without the need for any interaction.

- A **one-dimensional representation** that plots position along the boundary against the maximum shear value selected from a perpendicular line to each boundary pixel. A

programme (written in MATLAB) produced an interactive interface to display a 1D graph of shear and place it in an anatomical context (this is the same program used for some of the analyses in Chapter 4). An example is shown in Figure 6.9.
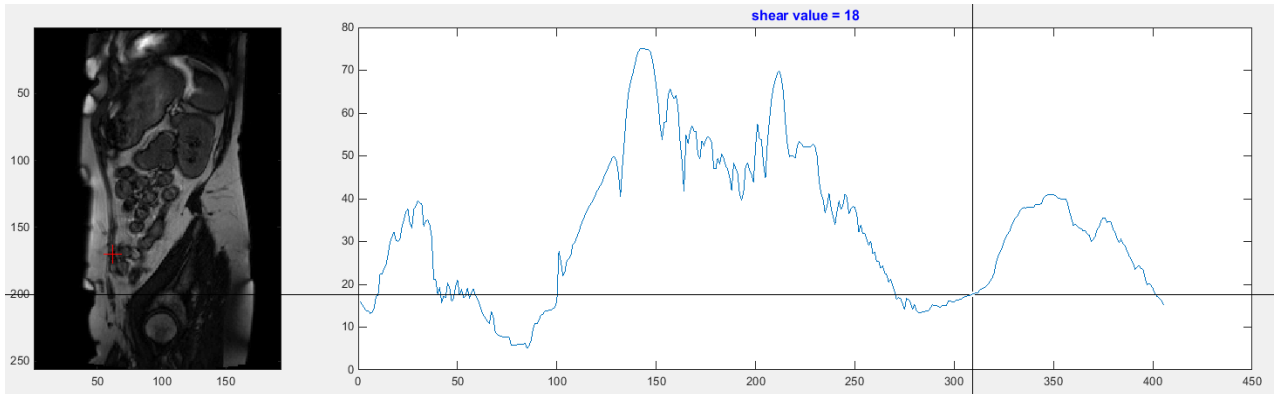
Figure 6.9: 1D representation of a sheargram showing the profile of the maximum shear around each boundary pixel. An interactive interface provides the user with the value of shear at a particular location and indicates the spatial coordinates in the image on the left with a red cross

A 1D representation has advantages as the graph makes it easier to determine actual quantitative values for the shear. The shape of the profile is immediately visible and areas of reduced shear can be identified with ease. However, there were two principal problems with this visualisation method. Firstly, at least for the quick implementation shown in Figure 6.9, only the maximum shear values at each location are displayed. The actual distribution of shear values is contained in a band spanning several pixels and a view of the whole band can influence interpretation. The second issue is that the shear information is no longer presented and immediately associated with the anatomy. To combat this problem, the graphical user interface correlates a point on the graph to the underlying anatomy with a mouse click. The position of the crosshairs on the graph corresponds to the red cross on the lower abdominal wall in Figure 6.9. However, even with this feature the user cannot immediately associate every value of shear with the anatomy as is the case with the sheargram.

In summary, the main advantage of representing the shear data in 1D is that actual values of shear are more apparent but this is at the expense of immediately being able to see all the information on a single image without the need for any user interaction. The 1D representation could be of use but given the success of the 2D colour map visualisation, it was not pursued further at this stage of development. A future improvement on the 2D colour map approach

could be to combine 1D and 2D into a single diagnostic aid figure. This could take the form of a 2D sheargram image displayed beside the 1D graph.

Progression to 3D imaging and analysis presents a greater challenge for data visualisation. The remainder of this chapter is devoted to discussion of 3D analysis and visualisation of the data.

6.8 Feasibility of 3D imaging and analysis

The requirement to move towards a 3D solution has reappeared on numerous occasions throughout this thesis. Out of plane motion occurring through 2D sagittal slices can only be solved by a dynamic 3D acquisition and analysis. This section describes a tentative attempt at 3D analysis to gain insight into its feasibility and the potential challenges that await. Specifically, several aspects of a 3D analysis methodology were attempted and assessed:

1. 3D abdominal MR image acquisition
2. Image registration accuracy in 3D
3. 3D movement analysis and determination of shear
4. Severity of out of plane motion
5. Visualisation of results

These aspects are addressed in turn and used to form a discussion of the feasibility of 3D imaging and analysis.

6.8.1   3D abdominal MR image acquisition

Current MRI technology is not capable of acquiring large 3D volumes (such as the abdomen) with adequate temporal resolution for dynamic imaging (~40 seconds per abdominal volume is required). The technology therefore only permits a pseudo-dynamic 3D image; capturing abdominal displacements at set points through the respiratory cycle during breath holds. A single volunteer undertook a pseudo-dynamic 3D MRI scan. The scan details were:

- Seimens Avanto 1.5 T scanner
- True FISP imaging sequence
- Acquisition time ~40 seconds (for each breath hold)
- Pixel size 1.56 x 1.56 mm
- Slice thickness 1.6 mm
- 128 coronal slices

- Matrix 320 x 320 pixels in each slice

- Flip angle 50°

- Echo time 1.54 msecs

Figure 6.10 shows the same slice at 5 different contiguous breath hold positions from maximum inhalation (left) to maximum exhalation (right).
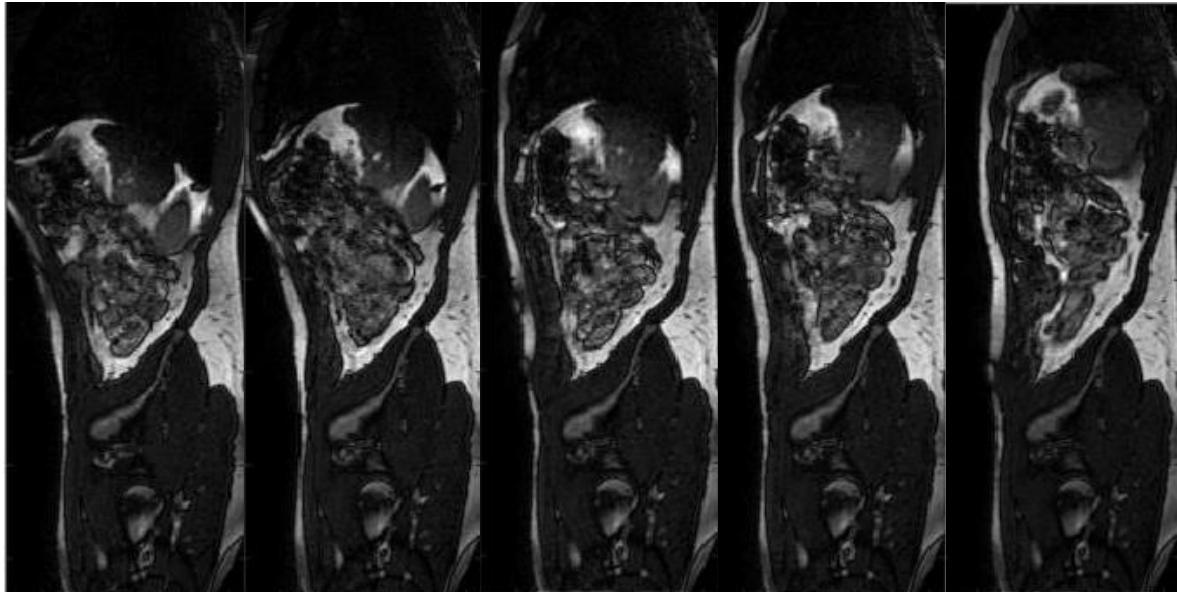
Figure 6.10: The same slice in five different 3D MRI breath hold acquisitions between maximum inhalation (left) and maximum exhalation (right)

The volunteer was unaided when choosing the graduated breath hold positions throughout the respiratory cycle. Eleven 'frames'/breath hold positions were captured to simulate a complete respiratory cycle: 5 breath holds between maximum inhalation to maximum exhalation, and 6 returning from maximum exhalation to maximum inhalation. Qualitative observation of the different breath hold images showed that consistent incremental graduations through the breathing cycle were not always achieved.

6.8.2 Image registration accuracy in 3D

For results of a 3D analysis to be meaningful, it is important to determine whether ShIRT is capable of successfully tracking movement of abdominal organs in 3D. The accuracy of ShIRT was tested by measuring the (post registration) discrepancy between corresponding landmarked points in two 3D images.

Method

Nineteen corresponding landmark points were identified throughout two 3D images of sequential breath hold positions. Two methods of image registrations were performed: one registering the entirety of the 3D images and the other separately registering 3D segmented abdominal contents and abdominal surroundings (the 3D equivalent of the visceral slide quantification technique). The positions of the points after applying the registration displacement map were then determined and the difference in landmarked positions between the two 3D images calculated using Eq 6.2.

$$Diff = \sqrt{((x_2 - x_1)^2 + (y_2 - y_1)^2 + (z_2 - z_1)^2)}$$

Eq 6.2

Results

The graph in Figure 6.11 shows the distance between the landmarked points before and after the two deformation maps were applied to warp the point positions.
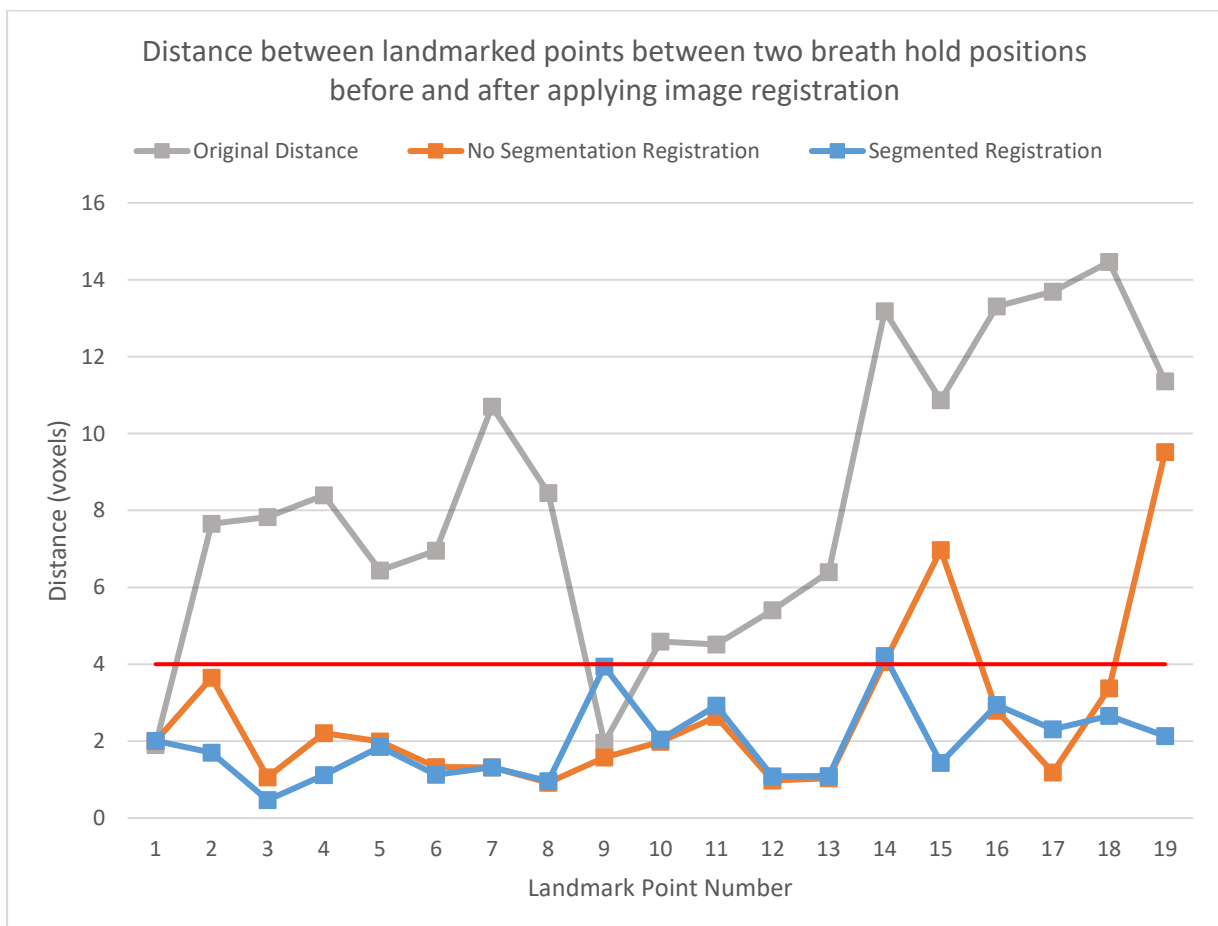
Figure 6.11: Plot showing the discrepancy between the landmark points before registration (grey) and after registration using both registration methods (without segmentation = orange and with 3D segmentation = blue). The red line indicates the approximate uncertainty in manually selecting 3D landmark points.

181

Selecting like points in 3D was challenging, particularly as much of the intestines deform between breath holds. The uncertainty in selecting like points in 3D was estimated to be 2 voxels in each image, therefore when considering placement of landmark points in 2 images, an estimate of the error in distance between landmarks was ~4 voxels – indicated by the horizontal red line in Figure 6.11. A more accurate registration was achieved when segmenting the abdominal contents (blue points in Figure 6.11). Almost all points were registered to within the 4-voxel tolerance. Two orange points (i.e. without segmentation) were above the red line (15 and 19) and both were close to the sliding boundary at the perimeter of the abdominal cavity. This supports a segmentation approach in the future and the next section explores the use of segmentation and registration in 3D to visualise movement and calculate shear around the abdominal perimeter.

6.8.3   3D movement analysis and determination of shear

Mapping the movement and/or shear across the entire abdomen rather than in specific slices, as in the 2D analysis, is the principal advantage and ultimate aim of moving to 3D. An attempt has been made to observe movement in 3D and produce an example of a 3D sheargram.

Method

The analysis method replicated the approach taken in 2D (described in Chapter 3): the abdominal contents were segmented from its surroundings and the two regions (volumes) were registered separately. The 3D segmentation and registration procedure is outlined below:

1. The 3D data was re-orientated into a series of sagittal slices (rather than coronal).
2. An ROI was drawn around the abdominal contents in one slice (slice 1).
3. Slice 1 was then registered to the neighbouring slice (slice 2) and the deformation map used to warp the ROI vertices from slice 1 to slice 2.
4. The user was given the option to edit the ROI vertex positions in slice 2.
5. The vertices in slice 2 were then warped to match the perimeter of the abdominal cavity in slice 3 and edited. This was repeated for all slices containing abdominal contents.
6. The ROIs were used to mask the image slices and create two images for each 3D dataset: the abdominal contents and abdominal surroundings.
7. The two 3D datasets of the abdominal contents were then registered, as were the abdominal surroundings to achieve two 3D deformation fields.
8. The resulting deformation fields were then combined to form a complete deformation field spanning across the 3D image.

The deformation field could be visualised as a vector field but also permits the determination of the 3D displacement gradient tensor, F_{3D}, in Eq 6.3 below.
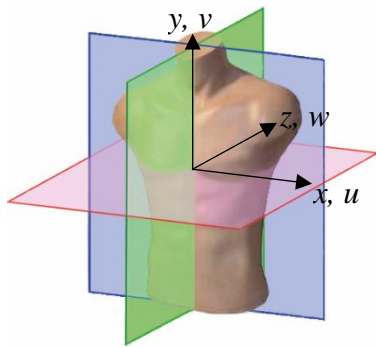
$$F_{3D} = \begin{bmatrix} \dfrac{\partial u}{\partial x} & \dfrac{\partial u}{\partial y} & \dfrac{\partial u}{\partial z} \\[2mm] \dfrac{\partial v}{\partial x} & \dfrac{\partial v}{\partial y} & \boxed{\dfrac{\partial v}{\partial z}} \\[2mm] \dfrac{\partial w}{\partial x} & \dfrac{\partial w}{\partial y} & \dfrac{\partial w}{\partial z} \end{bmatrix}$$

Eq 6.3

Where *u, v, w* correspond to the *x, y, z* components of the deformation field vectors. For the purposes of this proof of concept demonstration only a single component was calculated, highlighted in orange in Eq 6.3 ($\frac{\partial v}{\partial z}$, vertical shear along the z-direction). The majority of shear at the sliding boundary around the abdominal wall can be expected to be contained within this component and it should therefore give a representative impression of the appearance of a 3D shear analysis.

The shear $\left(\frac{\partial v}{\partial z}\right)$ was calculated between each nodal point across the image, producing a 3D block of shear values. This is difficult to interpret and for visualisation purposes, a surface describing the shear values around the sliding boundary was sought. This required a single value for shear at each point on the sliding boundary. The maximum shear within the vicinity of every voxel on the sliding boundary was extracted and a surface of the maximum values used as the '3D sheargram'.

Due to time constraints, only movement between two 'frames'/breath hold positions were analysed (despite 11 different breathing points being captured).

Results

The 3D segmented abdominal contents can be shown by plotting a series of contiguous sagittal ROIs, as displayed in Figure 6.12. The results of the 3D registrations can be displayed in several ways. Figure 6.13 shows a 3D vector field describing the movement between two breath hold positions.
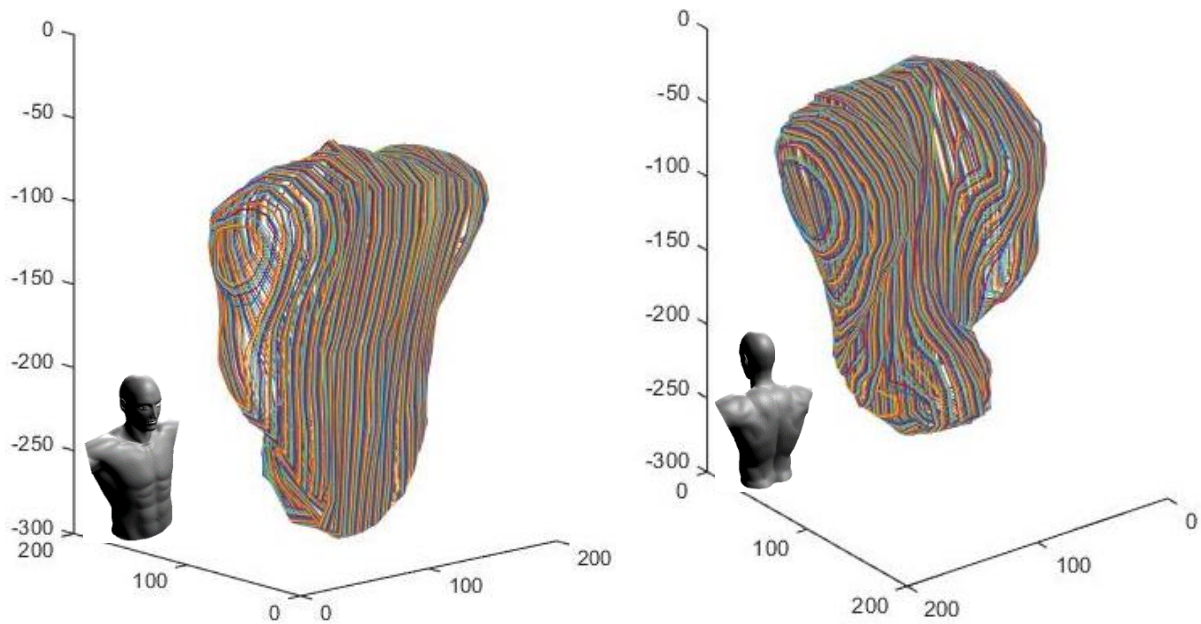
Figure 6.12: 3D ROI used to segment the abdominal contents from its surroundings
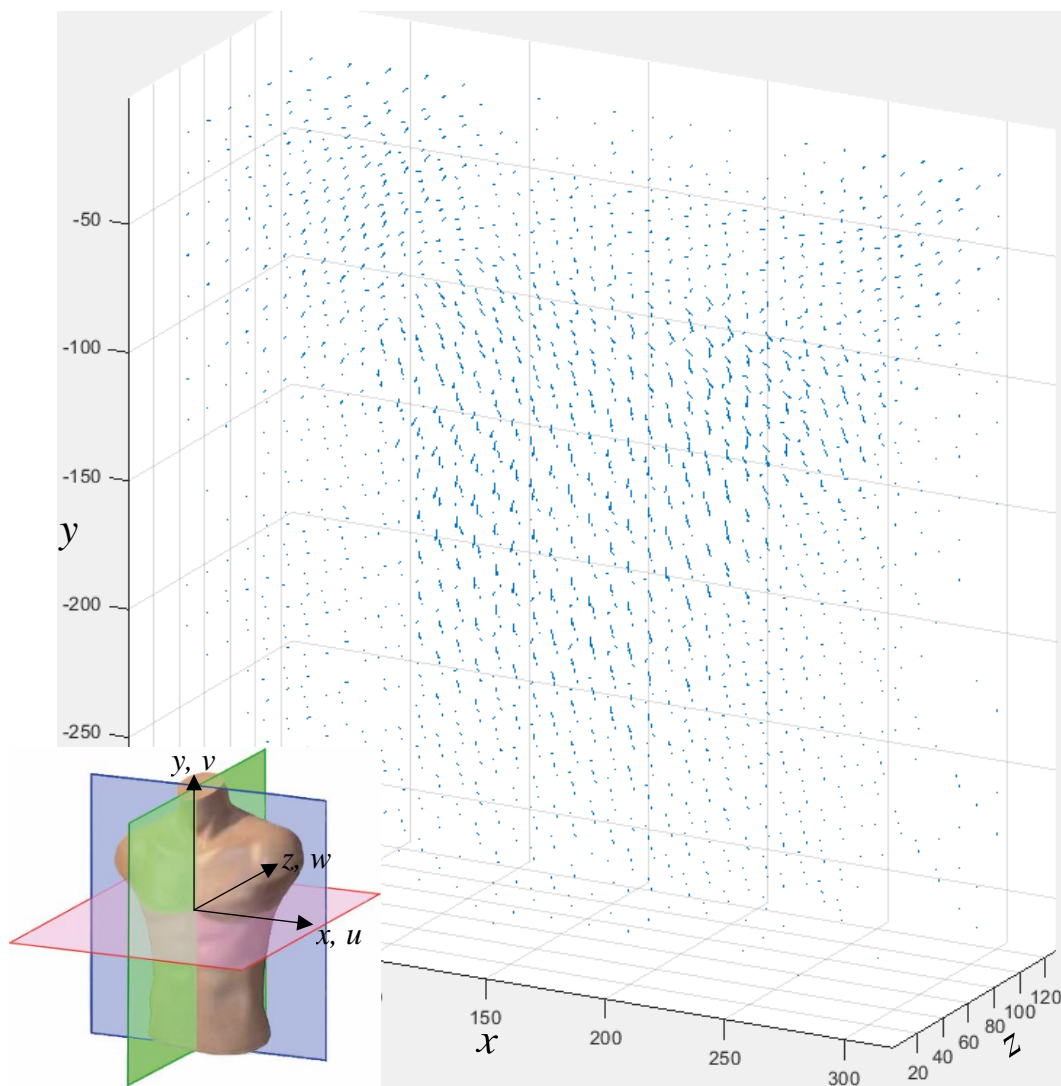
Figure 6.13: 3D vector field describing the displacements between two breath hold positions. The insert torso shows the approximate reference frame.

The vector field in Figure 6.13 shows the movement vector for every 4th node point. The large vectors mostly occur in the abdominal contents and the sudden reduction in vector magnitude corresponds with the sliding boundary. The display in Figure 6.13 has been optimised with respect to the best compromise between density of vectors and interpretability: if more vectors were included in the plot, the arrows became indistinguishable and if the plot were more sparsely populated, features of the field were difficult to see (e.g. the shape of the abdominal contents given by the edge of the larger arrows). Despite its appearance being optimised, Figure 6.13 remains challenging to interpret and a more appropriate method of displaying 3D movement is required.

The shear of the y-component of the vectors along the z-axis $\left(\frac{\partial v}{\partial z}\right)$ around the perimeter of the abdominal cavity can be plotted as a 3D point cloud with the colour of the points corresponding to the magnitude of the shear $\left(\frac{\partial v}{\partial z}\right)$. The point cloud in Figure 6.14 consists of every point around the perimeter in every 4th sagittal slice to display the 3D shear around the abdominal perimeter.
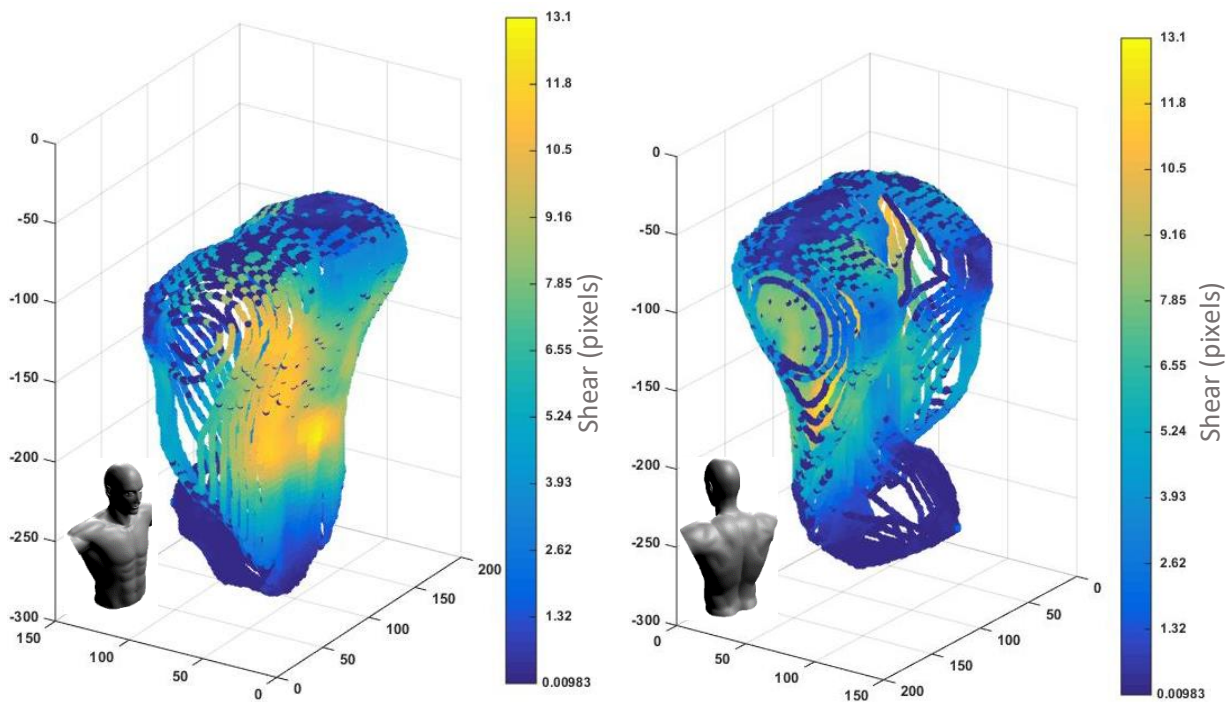
Figure 6.14: Anterior and posterior views of a 3D sheargram example showing the $\left(\frac{\partial v}{\partial z}\right)$ component of the displacement gradient tensor around the perimeter of the abdominal cavity

185

The highest shear was observed along the abdominal wall while little shear was observed deep in the pelvis – similar observations to those made in 2D. However, little importance should be assigned to the actual shear values because it is only between two points in the breathing cycle and only the shear in the vertical direction is shown. The main purpose of producing the 3D sheargram shown in Figure 6.14 was to give an indication of its appearance and explore ways to visualise the data.

6.8.4   Out of plane motion assessment

Out of plane motion has been cited as a problem throughout this thesis. Analysis of movement in 3D permits quantitative assessment of the degree of movement occurring through the sagittal imaging plane. The out of plane motion is derived from the x-component of the displacement vectors shown in Figure 6.13. Figure 6.15 shows a 3D shape of the abdominal contents with the colour indicating the maximum out of plane motion occurring in each sagittal slice.
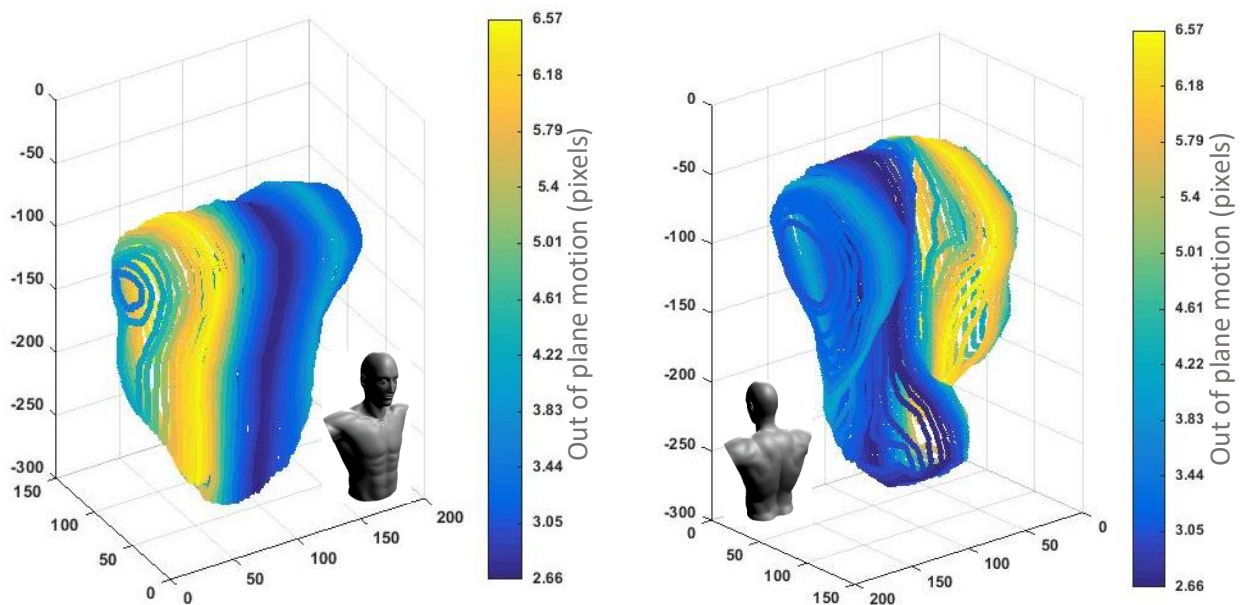
Figure 6.15: Anterior and posterior views of a 3D plot of the maximum out of plane motion in each slice (each sagittal slice was assigned a single value)

Observations made during data processing in Chapter 5 saw greater out of sagittal plane movement away from the midline and Figure 6.15 supports this observation. The midline shows the lowest out of plane motion with increasing out of plane movements either side. In this example, larger out of plane motion was observed in the right paramedian and right lateral images than the left. The movement information presented in Figure 6.15 covers a small

proportion of the respiratory cycle (between two sequential breath hold points), even so, the data does indicate that significant out of plane motion is occurring. It is fair to assume that the out of plane motion will be larger when considering the difference between maximum inhalation and exhalation and therefore provides further evidence for a move to 3D analysis.

6.8.5   Visualisation of 3D data

Experimentation in 3D has revealed difficulties regarding the visualisation of results. Interpretation of the 3D sheargram surface (Figure 6.14) has been accomplished using a traditional computer interface, but an information data stack that is truly 3D, such as a 3D vector field (Figure 6.13), presents a greater problem. Analysis in 3D aims to show movement information throughout the abdomen and, clearly, the information in Figure 6.13 needs to be presented with greater clarity. The computer monitor merely presents projections of 3D data, whereas technologies are emerging that offer stereoscopic visualisation in 3D. One such example is virtual reality (VR) technology, which was selected as a potential medium to enhance visualisation and interpretation of such complex data.

VR headsets offer the wearer stereoscopic vision, head tracking and positional tracking in a virtual 3D environment. These features create an immersive experience and potentially offer advantages for data interpretation. VR is a product of the gaming industry and to effectively interface with the technology requires a game engine. Unity [Unity Technologies, San Francisco, USA] was selected as a suitable gaming development environment. The 3D vector field was exported from MATLAB into a format readable by Unity (.dxf). The exported objects could then be imported into a 3D virtual environment ready to be viewed in a VR headset. The headset chosen was an Oculus Rift [Oculus VR, Menlo Park, USA] as it offered a high quality VR experience and mature development tools.

The 3D sheargram data and 3D vector field were imported into Unity. Figure 6.16 shows screenshots of the vector field and sheargram being viewed in the Unity environment and Figure 6.17 shows a screenshot of views when wearing an Oculus Rift headset (from one eye).
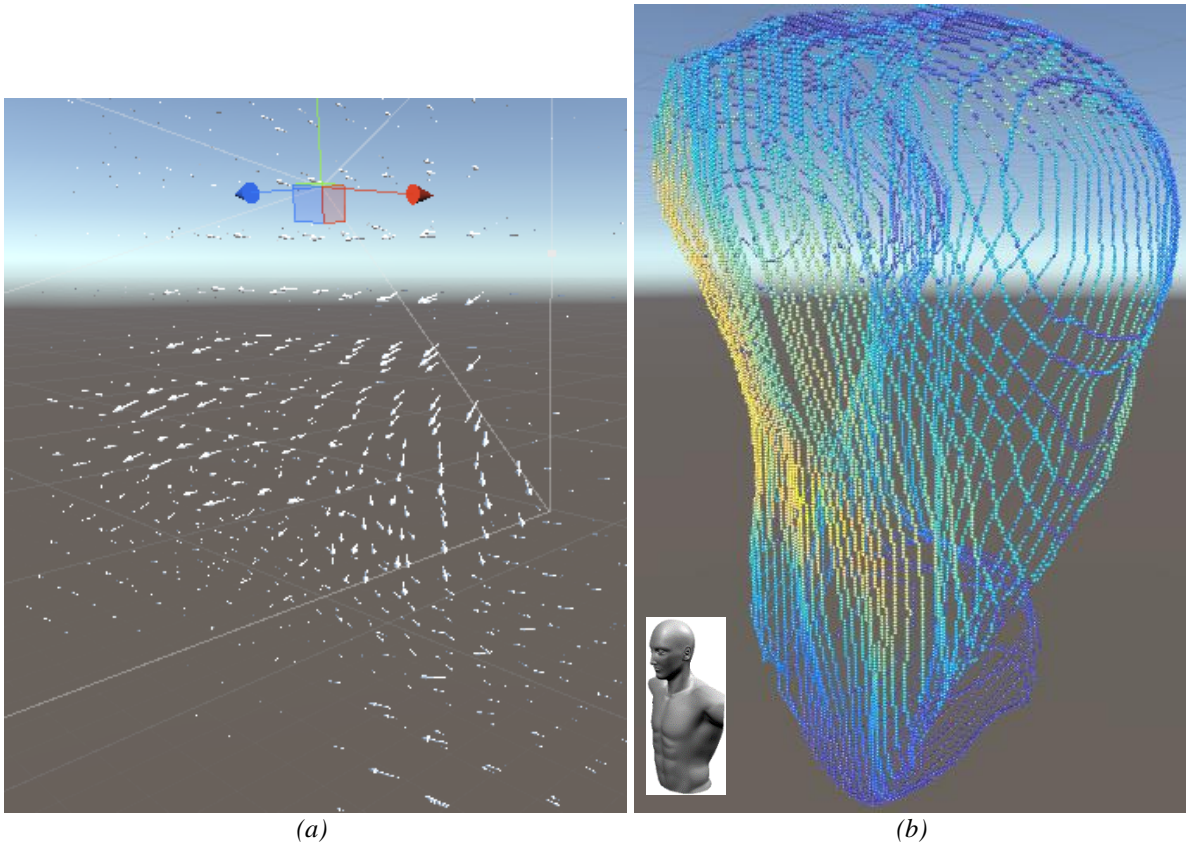
Figure 6.16: Screenshot of (a) the vector field and (b) the 3D sheargram viewed in the Unity development environment

(a)

(b)
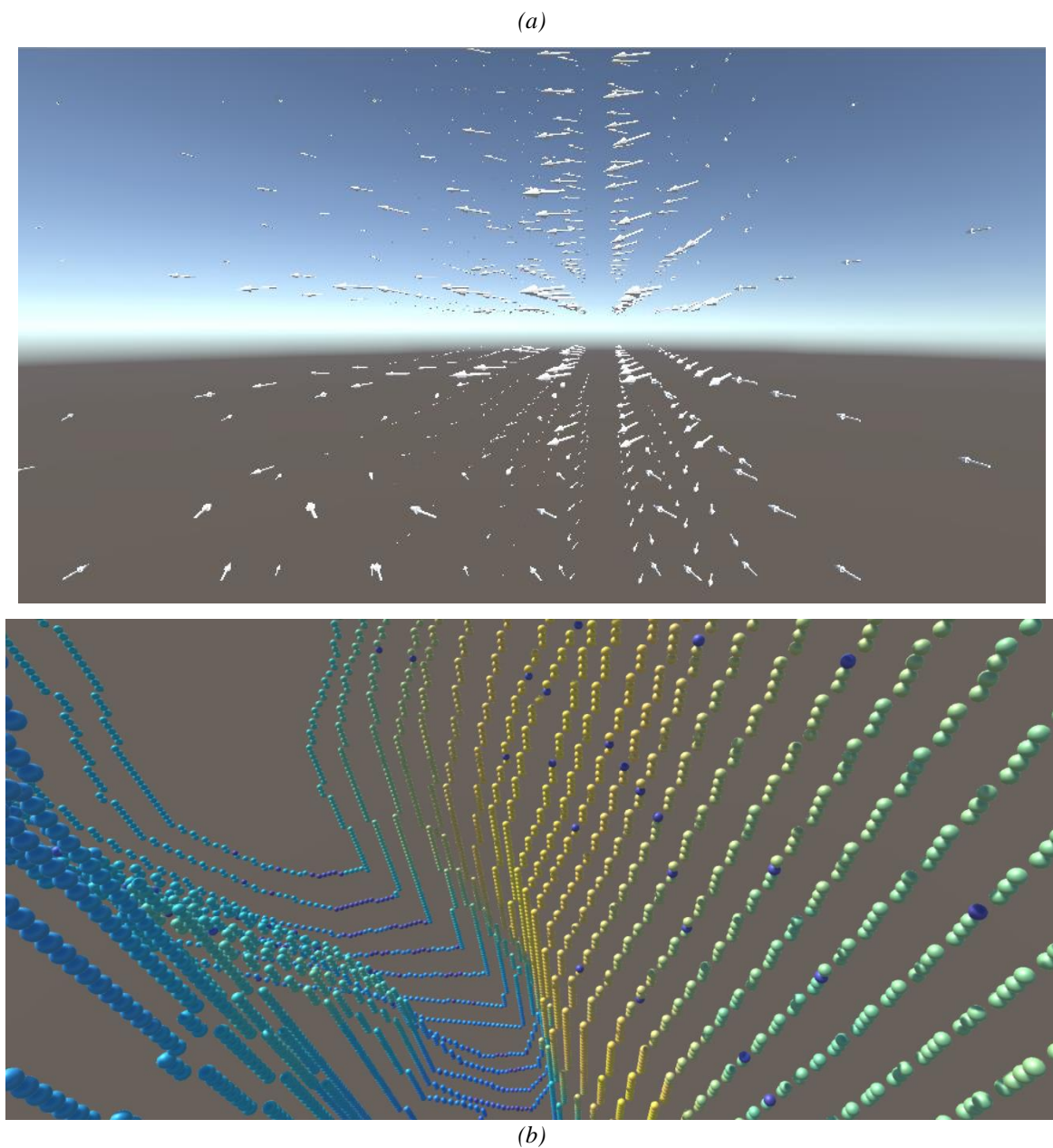
Figure 6.17: Views of (a) the vector field and (b) the 3D sheargram with a user wearing the Oculus Rift VR headset.

The views in Figure 6.17 place the wearer of the headset inside both the vector field and 3D sheargram. The combination of head tracking and stereoscopic vision creates an immersive experience, which is lost in the screen-captures presented in Figure 6.17. The addition of depth perception and sense of being 'in' the data could influence interpretation but currently the value of such features is unclear. Virtual reality also offers new possibilities for interacting with the data: travelling through the data is possible rather than passively observing it from outside and the ability to interact with the data via hand movements and gestures may be of benefit.

6.8.6 Discussion

The decision to analyse motion on the perimeter of the abdominal cavity was a strategy for focusing on objects fixed in the sagittal plane to reduce the effects of out of plane motion (see Section 2.6). The main driving force behind a 3D analysis is that it enables the possibility to analyse movement deeper within the abdominal cavity, away from its perimeter. The ultimate aim would be to provide a comprehensive adhesion detection tool across the entire abdomen and this can only be realised with a successful 3D approach.

This explorative 3D exercise was undertaken to gauge the feasibility of a 3D analysis workflow. Despite the limited time available for development in 3D, this explorative work managed to calculate and display movement and shear in a 3D abdominal MRI. Consequently, a 3D analysis is certainly possible but it also reveals some challenges that must be overcome for the technique to be effective. Key points from the work include:

i.   The image acquisition would ideally contain breath hold positions at regular intervals through the respiratory cycle. The single volunteer was unable to achieve this. Memorising the previous breath hold point and producing a graduated increase/decrease in inhalation was noted as a difficult task. This problem could be alleviated with the aid of an instrument to track the participant's breathing in real-time so they could be informed of an appropriate place to hold their breath for each 3D acquisition. This is outlined in future work, Section 7.3.1.

ii.   The segmentation procedure used in this study is not practicable for 3D datasets. The complexity of the image slices and difficulty in forming a coherent 3D volume ROI makes segmentation a complicated task. To segment two 3D breath hold images took >6 hours. If the abdominal contents are to be segmented, the best option may be a machine learning approach or registration of a 3D atlas to each individual case. An alternative would be to use an adapted registration algorithm to cope with the sliding geometry and forego any segmentation.

iii.   Extension of the 2D analysis computer programme to analyse the deformation field in 3D is not expected to be particularly troublesome given the achievements of this short study. However, some aspects of the processing and analysis will require significant modification, for example, as explained in point ii, the approach for segmentation would need to be overhauled for 3D analysis.

iv. Visualisation of shear results in 3D has been achieved in Figure 6.14 and Figure 6.17b but requires refinement for easier interpretation. It should be reiterated: the shear data was only determined from one 'frame', producing a summed 3D shear surface has not been attempted and may present problems.

v. This study has given confidence that production of a time varying deformation field is possible. It is apparent that the challenge does not lie with data production but in its visualisation and post-processing to generate diagnostic signatures:

   a. Visualisation of movement deeper in the abdomen is essential to realise the full potential of 3D. Radiologists are able to assimilate a 3D block of MR/CT data and construct a picture of the anatomy through several years of training. Building a picture of movement (or lack of) from 4D MRI data is arguably more challenging. Undoubtedly the radiologist would need a diagnostic aid for such data. A 3D vector field has been viewed but is itself particularly difficult to interpret. A novel visualisation solution using a virtual reality headset has been explored but it requires more work and its value is uncertain. This is an important aspect to solve without an obvious solution.

   b. Visualisation covered in the previous point is only one part of the data interpretation problem. The data being presented to the reporter also needs to contain useful, diagnostically relevant information. Visualisation of a time varying deformation field as vectors presents too much information and is unlikely to be useful. Further post-processing is required to reveal diagnostic signatures. The post-processing approach necessary to produce diagnostic signatures is not clear. One example could be the determination of the derivative of the deformation field. This would quantify relative motion between neighbouring objects (i.e. neighbouring objects with matching trajectories could indicate an adhesion) but this alone is unlikely to produce reliable diagnostic signatures (especially if an elastic registration with a strong smoothness constraint were employed).

vi. Motion through the sagittal plane between two consecutive breath hold positions was observed and supports the pursuit of a 3D analysis.

This exploration into 3D analysis has been informative and has supported its feasibility, but it has also revealed the complexity of the problem and amount of work required. A 3D adhesion detection aid is suggested for a subsequent PhD.

6.8.7   2D or 3D

The proposal to develop the 3D work does not undermine suggestions for further developments in 2D, discussed previously in this chapter. It is possible that a combination of 2D and 3D analysis may provide increased diagnostic power. Each offers advantages and disadvantages that could complement each other e.g. poor temporal resolution in 3D vs high temporal resolution in 2D and out of plane motion in 2D is addressed in 3D. Developments in both 2D and 3D should be pursued for the work to progress.

6.9   Summary

The evidence presented through Chapters 3-5 has indicated that the visceral slide quantification technique developed in this PhD has the ability to accurately measure visceral sliding and produce diagnostic signatures for adhesion detection. The success demonstrated has provoked discussion of its usability in a clinical context. The technique is expected to have greatest impact in training and aiding less experienced individuals but has also shown some evidence to aid more experienced radiologists. To achieve wider impact on clinical practice the technique must be further developed to map adhesions throughout the abdomen rather than focussing only on the perimeter of the abdominal cavity. Other issues relating to reliability and robustness must also be addressed if the sheargram is to be useable in the clinic. This discussion has offered some ideas and presented some explorative work that could help to relieve these issues, including:

- Possible improvements to the MRI acquisition for improved patient compliance
- Potential segmentation methods to increase automation and consistency
- First steps into 3D imaging and analysis to gauge its feasibility

The 2D analysis has been placed in a wider context which supported further development. A move to 3D analysis has been mentioned throughout this thesis and the feasibility of 3D has been demonstrated. It is suggested that developments in both 3D and 2D should be pursued concurrently.

Chapter 7

Conclusion and future work

This chapter consolidates the findings of this PhD to produce a coherent message and pulls together the opportunities for future work mentioned throughout this thesis to form a clear path for the next steps of this project.

7.1 Conclusion

7.1.1 Thesis overview

The work presented in this thesis builds on the efforts of a previous PhD, the principal output of which was a workflow (using image registration) aimed at the detection of gross adhesive pathology – EPS (encapsulating peritoneal sclerosis). **Chapter 1** introduced the clinical background and previous work. The focus of this thesis was translational and aimed to develop a diagnostic aid for abdominal adhesions based on movement in cine-MRI images.

Chapter 2 laid the theoretical and technical foundations and used this knowledge to make the case for a different image processing approach (compared to the previous PhD). This involved focussing on detection of adhesions around the perimeter of the abdominal cavity with particular focus on adhesions to the abdominal wall. This represented a shift away from detection of gross adhesive pathology towards more subtle adhesions.

Chapter 3 developed a visceral slide quantification technique to interrogate sliding at the interface between the abdominal contents and its surroundings during respiration. Segmentation and image registration were used to quantify movement within the abdomen from dynamic MR imaging. The principal output of the technique is a sheargram which presents the magnitude of shear (or sliding) around the perimeter of the abdominal cavity

summed over all frames in the dynamic image. Each component of the methodology was justified through rigorous critique.

Chapter 4 tested the sheargram technique using a series of experiments to clarify its behaviour and suitability for adhesion detection. The method was capable of measuring shear in sliding geometries accurately and proved able to detect idealised experimental 'adhesions'. Reproducibility in the sheargram from repeated processing runs of clinical cine-MRI revealed that differences in shear could arise from discrepancies in ROI placement around the sliding boundary. However, the observed differences in the sheargrams were not enough to alter clinical opinion.

The pilot study presented in **Chapter 5** demonstrated the efficacy of the sheargram for adhesion detection in 141 sagittal cine-MR slices. A strong correlation between sheargram interpretation and expert clinical opinion of the cine-MRI was observed (84% of sagittal slices agreed). The sheargram boasted an impressive sensitivity for adhesion detection (>93%) but lower specificity (81%). It also potentially aided detection of adhesions; 7 adhesions were identified in the pilot study that were not highlighted in the original report. The pilot study confirmed the sheargram correctly reflected the sliding motion observed in clinical cine-MRI images. It provided evidence for pursuing the work further but the lack of information regarding its clinical usefulness (e.g. effect on reporting time/efficiency) was noted as a requirement for subsequent investigation.

Evidence supporting the visceral slide quantification technique's application has accumulated throughout this thesis, culminating in the pilot study which provided the most conclusive evidence for its potential as a diagnostic aid. The work in chapters 3 and 4 largely support the pilot study findings but also delve into the underlying characteristics of the technique and highlight areas of weakness. The reproducibility tests in Chapter 4 and a specificity of 81% (in the pilot study) indicate a weakness with robustness. For the technique to be clinically useful the clinician must be able to 'trust' the sheargram – arguably it lacks this reliability. The two reasons attributed to the lack of robustness are: the subjectivity in the segmentation procedure and out of plane motion. Chapters 5 and 6 have discussed the implications of imaging a 3D object in 2D and potential solutions have been proposed in Chapter 6. The remainder of this chapter re-iterates the limitations and converts these into a clear path for future work.

7.1.2   Hypothesis

The success of the PhD may be measured by the extent to which it has answered its hypothesis, namely:

Hypothesis: "The appropriate manipulation and analysis of image registration applied to cine-MRI can yield improved diagnostic signatures for detection of abdominal adhesions"

This thesis has successfully addressed this hypothesis and demonstrated that a combination of image segmentation and registration of dynamic images is capable of producing diagnostic signatures for abdominal adhesions.

7.2   Current limitations

Identifying the main limitations sets the scene for future developments, these include:

1. **Only adhesions on the edge of the abdominal cavity have been investigated and out of plane motion can produce anomalous shear:** Imaging a 2D cross-section of 3D anatomy results in a degree of movement through the imaging plane. This can result in anomalies within the image registration deformation field that affect the calculated shear. Crucially, out of plane motion prohibits an investigation of adhesions deeper within the abdomen. Being able to detect adhesions anywhere within the abdominal cavity is a future ambition and a key focus for future work.

2. **Subjective segmentation:** The user-defined ROI is prone to variability and this has been shown to affect the resultant sheargram. This is an important focus for further 2D development.

3. **Patient compliance in cine-MRI:** In the pilot study approximately 50% of sagittal slices were rejected as 'poor quality' images, mostly due to lack of diaphragmatic movement. 'Poor quality' does not always translate into 'non-diagnostic' but the lack of movement is likely to affect clinical efficacy and patient compliance needs to be improved.

4. **Lack of conclusive adjudication on clinical viability:** This thesis has mainly focussed on development and testing of a new image processing technique for adhesion detection. The success of this work enabled a viable pilot study which has provided a wealth of useful information on the potential of the sheargram. However, it has not conclusively answered questions regarding the technique's clinical viability and does

not constitute a clinical trial. This, among other clinically related goals, are discussed under a "route to clinical implementation" in the next section (7.3).

5. MRI image artefacts – Image artefacts were observed to disrupt the resulting shear profile in the pilot study. Image artefacts are likely to remain a problem and cannot be removed or easily accounted for using image processing. It is necessary to acknowledge this problem, but its solution is a task to be addressed by the wider MR imaging community and is not a realistic ambition for this project. This has not been addressed in the future work section.

7.3 Future work

Several distinct aspects of future work have already been identified. This section defines a clear strategy by prioritising the suggestions mentioned throughout the thesis. From the Limitations section, the principal areas highlighted for further work are ranked below.

1. Developments in 3D
2. Greater automation and robustness in segmentation
3. Greater patient compliance in cine-MRI acquisition
4. Using the developments of 1, 2 and 3 to move towards clinical translation
5. Other potential areas to explore

These are briefly reviewed in the order above.

7.3.1 Developments in 3D

The brief exploration into 3D analysis in Section 6.8 has revealed both its viability and associated technical challenges. A major limitation is the capability of MRI imaging technology. As MRI technology improves, it may be possible to acquire larger volumes in a shorter time to enable dynamic imaging rather than pseudo-dynamic, breath hold imaging. In the meantime, alternative approaches could circumvent imaging limitations:

-   Respiratory gating could be employed to combine images at specific points in the respiratory cycle to gradually build a 3D image. This would rely on the abdominal contents being reproducibly positioned from one respiratory cycle to the next. A preliminary study to investigate positional reproducibility of abdominal contents could be undertaken to gauge its feasibility.

- Respiratory gating technology could be used to enhance the pseudo-dynamic breath hold approach. Respiratory gating equipment, such as Anzai Medical's AZ-733VI [108], is capable of producing a live trace to pinpoint the current position in the breathing cycle. This could be used to inform the patient when to hold their breath and achieve breath holds at appropriate points through the respiratory cycle.

In Section 6.8, movement and shear information have been generated from breath hold images demonstrating its feasibility, but challenges arise in the presentation and interpretation of the data. Some attempts at visualising the data have been made, including the use of virtual reality, but more effective data presentation is still required. The amount of information presented to the operator is overwhelming and currently lacks clarity. Future work should first focus on producing diagnostic signatures through post-processing of the movement information. Once such signatures are identified the information presented to the reporter could be condensed for easier interpretation. For example, 'hot spots' of suspected adhesion locations could be highlighted in 3D. However, there are many hurdles to overcome before this end-point is realised and a separate PhD or post-doctoral research project aimed at development of 3D analysis is recommended.

7.3.2   2D segmentation procedure

One of the principal problems identified during testing of the visceral slide processing technique is the lack of robustness resulting from segmentation. Some different possibilities for increased automation in segmentation were suggested in Section 6.5. An atlas-based segmentation should be explored as first priority. Initial success at segmentation using motion in the image also provides impetus for further investigation. Additionally, a degree of human interaction is likely to remain a feature and alongside pursuing greater automation, attention should be given to enhancing the user interface used to define the boundary. The current 'click and drag' interface to move the ROI vertices is not efficient and could be improved. One example would be to use a large area 'brush' to 'push' several vertices at once.

7.3.3   2D cine-MRI patient compliance

The procedure expected of patients during a cine-MRI examination has been poorly adhered to and presents a problem for clinical implementation. Work is currently underway to promote patient compliance through improved patient understanding of what is required (a pilot video

is due to be trialled by colleagues in Nijmegen) but an investigation into the effects of bearing down should be the priority.

7.3.4 Route to clinical implementation

The pilot study has provided evidence for the potential of the sheargram to aid diagnosis and warrants further investigation. Any advancements in 3D and 2D are likely to impact on the route to clinical implementation, hence these are the priorities. Depending on the outcomes and successes of these technical developments, the suggested path towards clinical translation is as follows:

1. The usefulness of the sheargram for aiding radiologists in training is an area worthy of investigation. It has been suggested by experienced radiologists that this is where the sheargram may add the most value. This investigation could also be inaugurated at the current level of development without waiting for further developments in 2D and 3D.

2. Advanced versions of the 2D and 3D analysis should be incorporated into a new pilot study to confirm/disprove their combined ability for adhesion detection. This should inform on the efficacy of the technique and is likely to indicate some technical refinements. This is a preparation step towards a comprehensive clinical trial (below).

3. Refined 2D/3D image processing techniques should be assessed in a clinical study. The radiologist should report the cine-MRI unaided and aided by image processing and the reports compared to surgical findings. The study should assess the following:

   a. The sensitivity and specificity of cine-MRI diagnosis with and without diagnostic aids compared to surgical confirmation. Particular focus should be given to an assessment of clinical impact (e.g. improvements in diagnostic efficacy).

   b. A confidence score should be included and an ROC (receiver operating characteristic) analysis undertaken.

   c. Efficiency of reporting with and without image processing, based on reporting times.

   d. All of the above should provide the information necessary for analysis of any economic benefits.

4. If successful, several hurdles would need to be overcome to move the technique to clinical practice and be more widely adopted:

   a. Compliance with medical device legislation [109]

b. CE marking (or USA FDA approval)

c. Demonstration of significant clinical, economical or procedural benefit (hopefully demonstrated via steps 1-3 above)

If the above conditions were met it could be considered for NICE approval and be made available for clinical uptake by individual hospitals. In Sheffield, a route into clinical practice and delivery of the processing as a service could be facilitated via existing links with Devices 4 Dignity[12], Sheffield Teaching Hospitals (to advise on legislative barriers) and the 3D Imaging Laboratory[13], Sheffield Teaching Hospitals (for service delivery).

7.3.5 Other potential areas to explore

In addition to the above, other areas for investigation could include:

1. **Automated detection of adhesions using machine learning:** If the technique becomes robust and reliable enough it could be a candidate for machine learning to automatically identify drops in movement/shear that are likely to correlate with adhesions. This or a similar method could potentially alleviate some of the subjectivity introduced in sheargram interpretation (discussed in Chapter 5, Section 5.4.4).

2. **Ultrasound elastography:** Ultrasound elastography is an imaging technique which estimates the stiffness of objects based on deformation response to an applied force/acoustic waves. During the PhD, a short project investigated the potential of ultrasound elastography for early detection of EPS. A medical ultrasound scanner (capable of elastography) was used to scan phantoms/test objects designed to simulate tissues of different stiffness. The test objects were constructed using a cryogel (polyvinyl alcohol) which increased in stiffness with the number of freeze/thaw cycles. Layers of cryogel of different stiffness (having undergone different numbers of freeze-thaw cycles) were produced. Results indicated that elastography was capable of distinguishing the stiffness in different layers and that elastography could offer diagnostic information. Further investigation is warranted, but was considered beyond the scope of this PhD.

---

[12] Devices 4 Dignity is an NHS-based body headquartered in Sheffield. It has a wealth of experience in traversing legislative framework in the UK.

[13] The 3D Laboratory is a unique NHS-based facility in Sheffield that offers image processing support for radiology and the wider hospital.

7.3.6 Future work summary

There is merit in the 2D technique developed in this PhD and this deserves further work. The recommendation for immediate future work is for 2D and 3D development to run in parallel. The 2D work should focus on increasing the robustness of the sheargram technique, while the fledgling 3D work discussed in Section 6.8 should be completed and advanced for adhesion analysis throughout the abdomen. It is likely that information from both 2D and 3D analyses will complement each other to inform diagnosis. The success of the work presented in this thesis has fuelled further grant applications aimed at advancing technical developments in these areas.

7.4 Future gazing: The impact of virtual reality in medicine

The work into 3D visualisation with the Oculus Rift led to the conception of several other ideas for the technology's application to medicine. Two principal ideas were pursued to good effect:

- Virtual reality CT colonoscopy: Instead of diagnosing from a 2D representation of the colon, VR enables a different viewing perspective; placing the reporter within the 3D colon environment. For instance, the wearer of a VR headset can travel through a patient's colon segmented from CT colonography data. The development of a VR colon examination is a good example of how VR can be applied to data visualisation in medicine. Radiologists have commented that several features may offer advantages over conventional CT colonoscopy viewing on a 2D monitor:
    - Head tracking allows reporters to change their gaze direction with natural head movements (rather than clunky operations with a mouse and keyboard)
    - Stereoscopic vision permits easier identification of undulations in the mucosal surface of the colon
    - Immersion within the colonoscopy removes potential distractions
    - A feature to travel outside the lumen of the colon and examine the mucosal surface from the outside permits a wider view of the colon's surface and potentially increases examination efficiency.

    This work won the Mimics Innovation Award at the European Society of Biomechanics annual meeting and resulted in a journal publication (Appendix 7) and conference proceeding [110, 111].

- Oscillopsia Simulation: Growing confidence in VR encouraged application to other areas in medicine, in this case the simulation of an ocular disorder. Nystagmus is a

condition where the eyes move involuntarily and consequently some sufferers experience the world in constant motion – a symptom called oscillopsia. In this project, eye tracking data from nystagmus sufferers were imposed onto 'virtual eyes' in virtual reality. The wearer of a VR headset is presented with a realistic experience of the world from the sufferer's perspective. Immersion and stereoscopic viewing offered by VR are the key features which make this type of visualisation both possible and produce a powerful evocative experience. Although seemingly unconnected from the application of VR presented in this thesis, it does raise novel and interesting possibilities for data visualisation: via an experience rather than passive observation.

[This application has been released as a mobile phone app called "Nystagmus Oscillopsia Sim VR" on Android Play and iPhone App Store and has received over 800 downloads (02/08/2017)].

Our experience is that virtual reality has attributes that are complementary to medical data visualisation. The use of this technology in medicine is only likely to increase and it could be an important aspect for future data visualisation in this project if moving towards a 3D analysis.

7.5 PhD: Final message

Evidence supporting the visceral slide quantification technique's application has gradually been built throughout this thesis: a theoretical underpinning in Chapter 2 supported a change in approach; which was justified and matched to an analytical example in Chapter 3; successfully measured shear in synthetic examples and proved capable of detecting adhesions in Chapter 4; to successful clinical application in a pilot study in Chapter 5. The project has successfully produced, and provided evidence for, a technique capable of aiding non-invasive detection of abdominal adhesions to the abdominal wall. While shortcomings in the technique have been exposed, these initial successes license further work, with clinical adoption being a credible goal. Production of a 3D analysis technique has been suggested as the next major challenge.

Appendices

Appendix 1: Analytical registration of cos(x) to sin(x)

To demonstrate an analytical registration *cos(x)* will be registered to *sin(x)*:

$$f(x) = \sin(x)$$
$$m(x) = \cos(x)$$

A sum of square differences similarity metric (from Eq 2.1 in main text) gives the cumulative error over a convenient range *(-2π → 2π)* for an imposed translation of *u* on *m(x)*:

$$\varepsilon(u) = \int_{-2\pi}^{2\pi} (\sin(x) - \cos(x - u))^2 \, dx$$

Expanding the bracket gives:

$$\varepsilon(u) = \int_{-2\pi}^{2\pi} \sin^2(x) + \cos^2(x - u) - 2\sin(x)\cos(x - u) \, dx$$

The evaluation of this integral results in the following:

$$\varepsilon(u) = -4\sin(u)\,\pi + 4\,\pi$$

This equation describes the cumulative error function. A plot of this function is shown in Figure A1.1 and illustrates the presence of several minima. Other constraints would need to be imposed to force a particular solution.
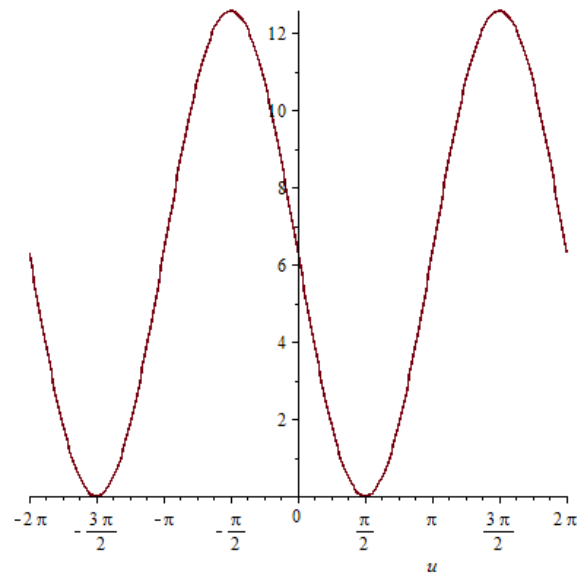
Figure A1.1: Cumulative error function for analytical registration of cos(x) to sin(x)

The minima and maxima in Figure A1.1 correspond to the phases of the trigonometric waves (maximum = π radians out of phase, minimum = in phase). To extract these values mathematically the first derivative is set to equal 0:

$$\frac{d\left(-4\sin(u)\,\pi + 4\,\pi\right)}{du} = 0$$

$$-4\cos(u)\,\pi = 0 \;=>\; \cos(u) = 0$$

$$u = -\frac{3}{2}\,\pi,\; -\frac{1}{2}\,\pi,\; \frac{1}{2}\,\pi,\; \frac{3}{2}\,\pi$$

It would then be possible to determine which were minima and maxima using the sign of the second derivative at these u values but for this example this is not necessary. It is clear from Figure A1.1 that the minima occur at *π/2, ±2π* radians.

Appendix 2: Formulation of a 1D elastic system and the process of balancing forces for incorporation into a 1D registration algorithm (in Chapter 2)

The force, F, in a spring is related to displacement, u, by Hooke's law:

$$F = ku$$

Consider Figure 2.4, pg30 in the main text as a model, where the nodes are interconnected by springs. Consider each node in turn: For node 1 the driving force, F_{D1}, must be cancelled by the forces acting on the nodes by the compression and extension of springs either side of the node. Mathematically, the force on node 1 from spring 1, F_{S11}, is given by:

$$F_{S11} = -k_{01}u_1$$

Where u_1 is the displacement of node 1 and k_{01} is the spring constant of the spring between the edge of the image and node 1. Similarly, the force on node 1 from spring 2 depends on the net compression/extension of the spring resulting from both node 1 and node 2's displacements:

$$F_{S21} = -k_{12}(u_1 - u_2)$$

Thus, for node 1 to be in equilibrium, the overall force on node 1 must be zero:

$$F_{D1} + F_{S11} + F_{S21} = 0$$

$$F_{D1} = k_{12}(u_1 - u_2) + k_{01}u_1$$

A similar process can be applied to any node, resulting in the following equations for nodes 2 and 3 (for the three node system in Figure 2.4, pg30):

$$F_{D2} = (k_{12} + k_{23})u_2 - k_{12}u_1 - k_{23}u_3$$

$$F_{D3} = (k_{23} + k_{34})u_3 - k_{23}u_2$$

The solution to this set of simultaneous equations will ensure all nodes are in equilibrium. This is effectively represented in a matrix form as below. The matrix of k-values/stiffness constants is referred to as the stiffness matrix.

$$
\begin{bmatrix} F_{D1} \\ F_{D2} \\ F_{D3} \\ F_{D4} \\ \vdots \end{bmatrix} = \begin{bmatrix} (k_{01} + k_{12}) & -k_{12} & 0 & 0 & \cdots \\ -k_{12} & (k_{12} + k_{23}) & -k_{23} & 0 & \cdots \\ 0 & -k_{23} & (k_{23} + k_{34}) & -k_{34} & \cdots \\ 0 & 0 & -k_{34} & (k_{34} + k_{45}) & \cdots \\ \vdots & \vdots & \vdots & \vdots & \ddots \end{bmatrix} \begin{bmatrix} u_1 \\ u_2 \\ u_3 \\ u_4 \\ \vdots \end{bmatrix}
$$

Appendix 3: Application of a 1D registration algorithm to a 1D representation of the abdomen

The blue and red curves in Figure A3.1 below represent the moving and fixed 'images', respectively. The 1D registration algorithm described in Chapter 2, Section 2.2.5 was applied to the curves/images and the snapshots below show the registration progression through 50 iterations. Figure A3.2 shows the actual displacements across the 1D image (blue line) compared to the final displacements computed by the 1D registration algorithm (green crosses). The curves shown in Figure A3.1 are designed to represent the relative intensities encountered in an abdominal MR image. A single line of pixels drawn inferiorly-superiorly down the abdomen was used to estimate intensities.
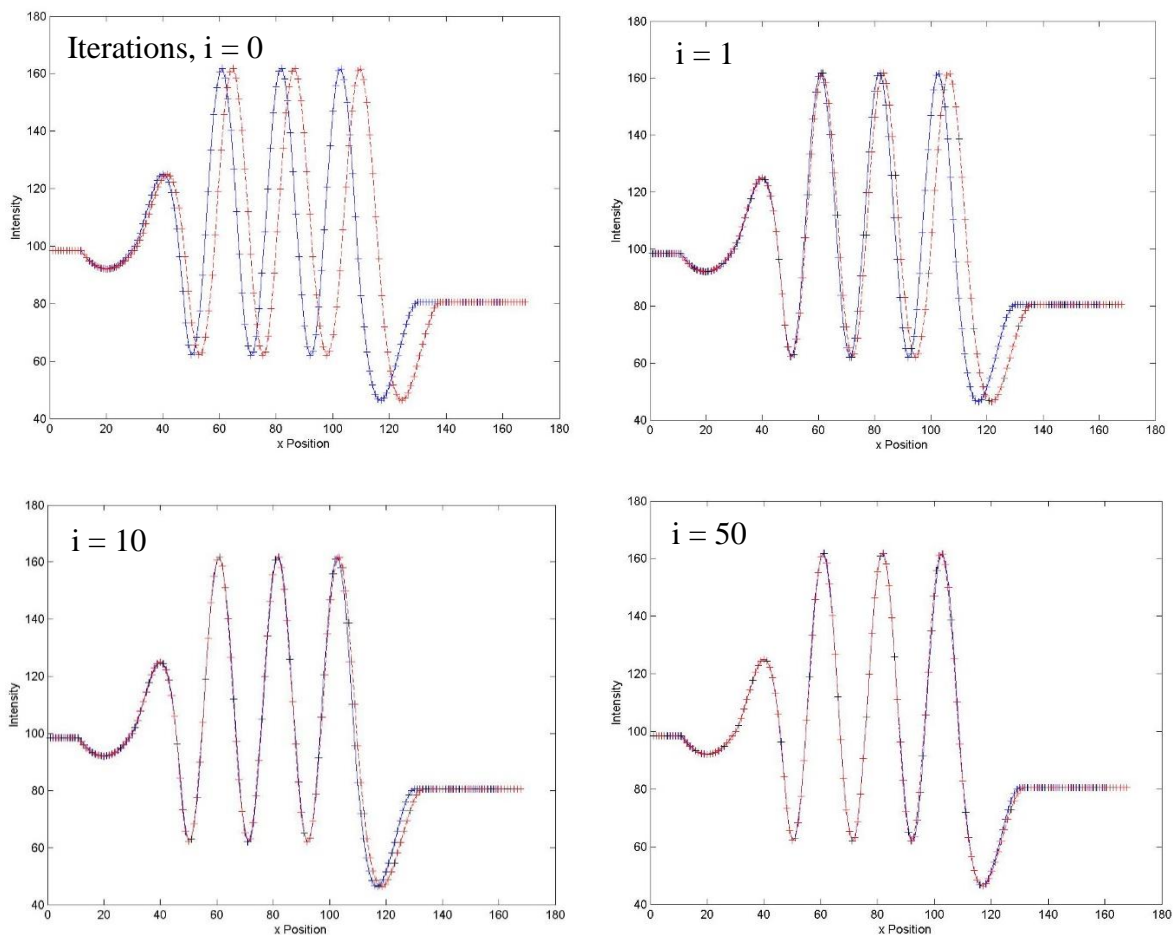
Figure A3.1: The 1D registration algorithm outlined in Section 2.2.5 was able to spatially match the two curves that loosely represent the changes in intensity on a single vertical line through the abdomen
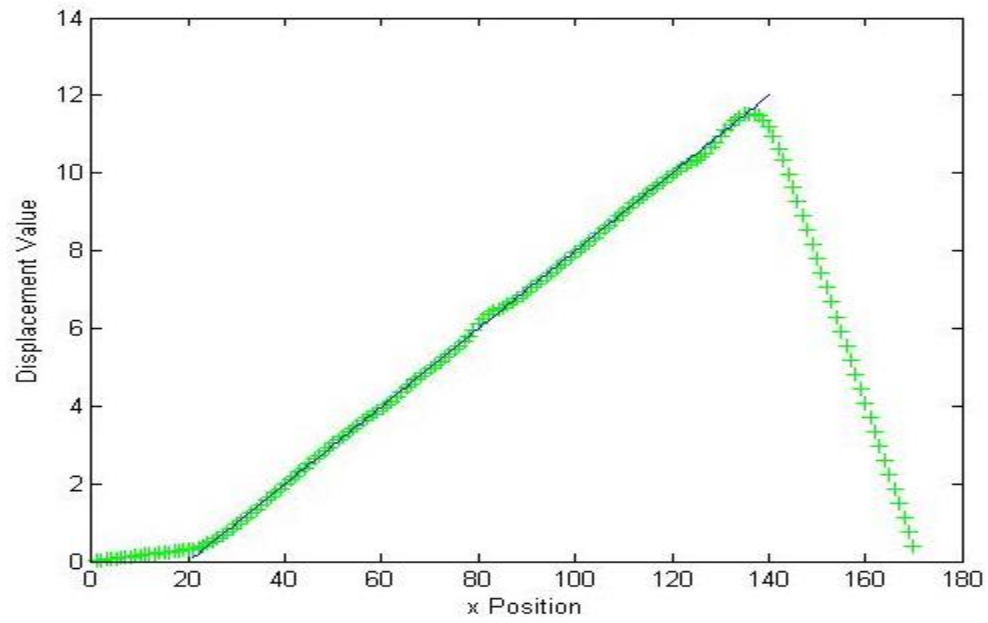
Figure A3.2: The displacements calculated by the 1D registration algorithm across the 1D curve in Figure A3.1 (green crosses) and the actual displacement imposed across the image (blue line).

Appendix 4: Analytical calculation of a displacement gradient tensor example

This appendix derives an analytical solution for the displacement gradient tensor for a particular vector field that can occur at any angle, θ. The vector field for an angle $\theta = 0°$ is defined by the vector in Eq A4.1 and depicted in Figure A4.1:

$$\underline{v} = 0\hat{\underline{\imath}} + x\hat{\underline{\jmath}}$$

<div align="right">*Eq A4.1*</div>
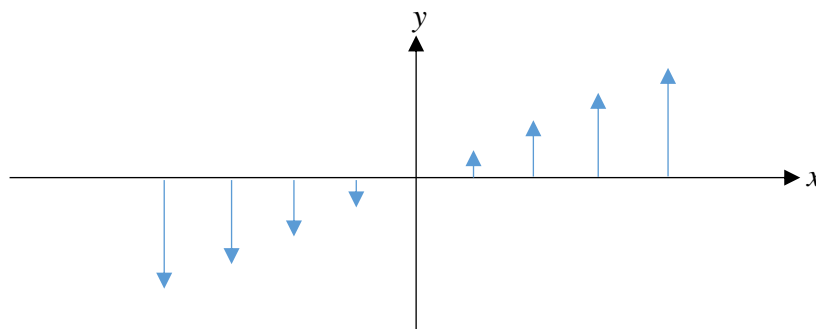
Figure A4.1: A simple vector field for which an analytical description of the displacement gradient tensor is derived

The vector field in Figure A4.1 increases in magnitude in the y-direction proportionally to x. This creates a constant shear strain of magnitude 1 along the x direction (and no tensile strain). The field can occur at any angle and a general description of the strain for varying rotations is sought. For the same field orientated at an angle θ to the x-axis, varying along x', produces Figure A4.2 (sign convention used denotes a positive angle results in a clockwise rotation).
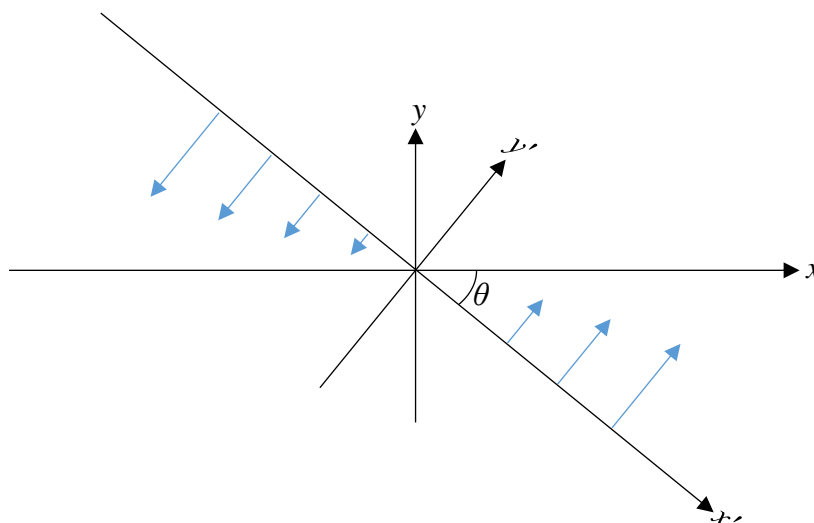
Figure A4.2: The vector field in Figure A4.1 rotated through an arbitrary angle θ which will also be described within the displacement gradient tensor.

The magnitude of the vector is proportional to the position of the rotated vector field on x', as shown by Eq A4.2:

$$\underline{v}' = 0\underline{\hat{\imath}}' + x'\underline{\hat{\jmath}}'$$

Figure A4.3 depicts the conversion between the rotated axis in Eq A4.2 and the original x, y coordinate system. This produces Eq A4.3 for the magnitude of the vector, v_{mag}.
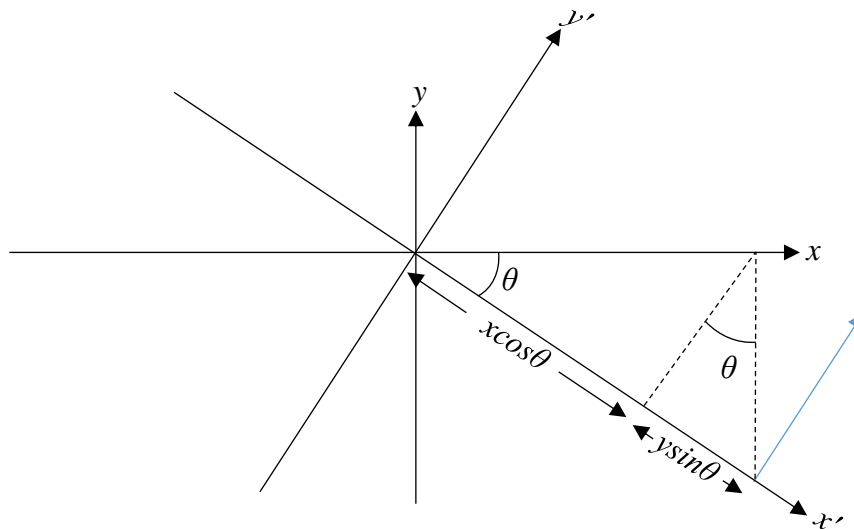
Figure A4.3: Length of a vector along a rotated axis x' in terms of the original coordinate system

$$v_{mag} = x\cos\theta - y\sin\theta$$

The *ysinθ* term in Eq A4.3 is negative due to the sign convention used for θ. The *x* and *y* ($\underline{\hat{\imath}}$ and $\underline{\hat{\jmath}}$) components of $\underline{v}$ are given by Eq A4.4 and depicted in Figure A4.4:
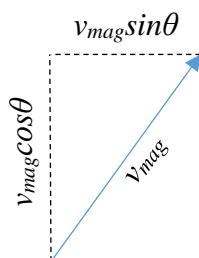
$$v_x = v_{mag}\sin\theta$$
$$v_y = v_{mag}\cos\theta$$

Figure A4.4: components of vector $\underline{v}_{mag}$

Substituting Eq A4.3 into Eq A4.4 provides a description of the vector field shown in Eq A4.5.

$$\underline{v} = v_x\hat{\underline{i}} + v_y\hat{\underline{j}}$$

$$\underline{v} = (xcos\theta sin\theta - ysin^2\theta)\hat{\underline{i}} + (xcos^2\theta + ysin\theta cos\theta)\hat{\underline{j}} \qquad Eq\ A4.5$$

The displacement gradient tensor, T, for this vector field (orientated at any angle) can therefore be calculated by differentiating the vector field for each of the tensor components, as shown below, to produce the tensor shown in Eq A4.6.

$$\frac{\partial v_x}{\partial x} = cos\theta sin\theta$$

$$\frac{\partial v_x}{\partial y} = -sin^2\theta$$

$$\frac{\partial v_y}{\partial x} = cos^2\theta$$

$$\frac{\partial v_y}{\partial y} = -sin\theta cos\theta$$

$$T = \begin{bmatrix} \dfrac{\partial v_x}{\partial x} & \dfrac{\partial v_x}{\partial y} \\ \dfrac{\partial v_y}{\partial x} & \dfrac{\partial v_y}{\partial y} \end{bmatrix} = \begin{bmatrix} cos\theta sin\theta & -sin^2\theta \\ cos^2\theta & -sin\theta cos\theta \end{bmatrix} \qquad Eq\ A4.6$$

Eq A4.6 can be used to calculate the tensor components for this vector field at any angle. This equation has been used in Chapter 3 to compare a known displacement gradient tensor in an image to that calculated by the visceral slide quantification technique.

Appendix 5: Paper: A Novel Diagnostic Aid for Detection of Intra-Abdominal Adhesions to the Anterior Abdominal Wall Using Dynamic Magnetic Resonance Imaging, Gastroenterology Research and Practice, 2015

Research Article

A Novel Diagnostic Aid for Detection of Intra-Abdominal Adhesions to the Anterior Abdominal Wall Using Dynamic Magnetic Resonance Imaging

David Randall,[1] John Fenner,[1] Richard Gillott,[2] Richard ten Broek,[3] Chema Strik,[3] Paul Spencer,[2] and Karna Dev Bardhan[2]

[1] *Medical Physics Group, Department of Cardiovascular Science, University of Sheffield, Beech Hill Road, Sheffield S10 2RX, UK*
[2] *The Rotherham NHS Foundation Trust, Rotherham Hospital, Moorgate Road, Rotherham S60 2UD, UK*
[3] *Radboud University Medical Centre, Department of Surgery, P.O. Box 9101, 6500 HB Nijmegen, Netherlands*

Correspondence should be addressed to David Randall; drandall1@sheffield.ac.uk

Introduction. Abdominal adhesions can cause serious morbidity and complicate subsequent operations. Their diagnosis is often one of exclusion due to a lack of a reliable, non-invasive diagnostic technique. Development and testing of a candidate technique are described below. *Method.* During respiration, smooth visceral sliding motion occurs between the abdominal contents and the walls of the abdominal cavity. We describe a technique involving image segmentation and registration to calculate shear as an analogue for visceral slide based on the tracking of structures throughout the respiratory cycle. The presence of an adhesion is attributed to a resistance to visceral slide resulting in a discernible reduction in shear. The abdominal movement due to respiration is captured in sagittal dynamic MR images. *Results.* Clinical images were selected for analysis, including a patient with a surgically confirmed adhesion. Discernible reduction in shear was observed at the location of the adhesion while a consistent, gradually changing shear was observed in the healthy volunteers. *Conclusion.* The technique and its validation show encouraging results for adhesion detection but a larger study is now required to confirm its potential.

1. Introduction

Abdominal adhesions are pathological formations of fibrous scar tissue that tether or adhere abdominal structures. As a complication of abdominal surgery they may be the cause of serious morbidity and may complicate subsequent operations. A combination of non-specific symptoms and an aversion to unnecessary surgery leads to a conservative patient management strategy that often fails to tackle the underlying condition. Surgical procedures (laparoscopy, laparotomy) are currently the only reliable way to determine if a patient has adhesions, but such intervention may induce further adhesions. A non-invasive diagnostic technique would therefore be invaluable for effective patient management and reducing surgical complications.

During the respiratory cycle the abdominal contents slide smoothly against the confines of the abdominal cavity (abdominal wall, etc.)—a process termed visceral slide. Although absence of, or disturbance to, visceral slide is considered an indicator of adhesions, the literature contains very few quantitative attempts at visceral slide measurement [1–3]. The use of dynamic MR for adhesion detection has had reported success but examination of the images in sufficient detail to detect abnormal slide has proven labour intensive and results are subject to high inter-operator variability [4–6]. We have previously presented a technique to mathematically analyse movement within the whole of the abdomen to help infer the presence of gross abnormalities (extensive adhesions) [6]. This current paper outlines a refinement of this technique using image segmentation and registration to exclusively interrogate more subtle abnormalities on the abdominal wall by examination of visceral slide.

Image registration is a mathematical process which aims to warp points in one image to match their corresponding

points in another. It has a proven value in tracking features or structures between incrementally varying images. However, sliding geometry (such as in the abdomen) is recognised to challenge registration algorithms [7–11]. To address this issue the literature has largely focused on development of highly sophisticated, bespoke registration algorithms to accurately account for sliding [7–11]. In this paper our focus is different: we intend to evaluate the sliding motion itself. We consider that there is benefit in using "off-the-shelf" registration technology combined with a protocol optimised for shear detection, and for this purpose we promote a segmentation-registration method. Such a pragmatic approach makes the technique more transparent and the technology more accessible, hopefully encouraging clinical adoption.

To the authors' knowledge nobody has accomplished quantitative characterisation/measurement of the sliding motion in the abdomen nor has a reliable technique been developed for non-invasive abdominal adhesion detection. With this in mind this paper is a "work in progress" that communicates an overview of the methodology developed and presents preliminary results.

2. Method

Our scanning protocol was developed independently which led to a protocol that echoed that of Lienemann et al. (2000) [4]. Dynamic MR images are acquired using a True FISP (true fast imaging with steady-state precession) MR imaging sequence. Images are obtained in the sagittal plane from the mid ascending colon to mid descending colon, which covers the full extent of the abdominal contents. Scanning parameters include a matrix size of 256×256, a slice thickness of 7 mm, and 10 mm gaps between slices. 30 frames are acquired at each sagittal slice location with an approximate time between frames of 0.4 seconds. Patients are scanned in the supine position and asked to bear down and breathe normally during the acquisition of each sagittal slice (for ~12 seconds) capturing approximately 3 respiratory cycles.

The focus of our method is a particular sliding motion system, characterised as one in which two adjacent structures in contact slide independently against each other. A schematic of the type of motion observed in the abdomen during respiration is shown in Figure 1.

These types of systems involve a discontinuity in the motion along the boundary separating the two moving objects. The method aims to determine the degree of sliding by quantifying shear as an analogue for the sliding motion taking place at the discontinuity. The amount of shear refers to the difference in the relative displacement of the two objects on either side of the motion discontinuity along the boundary.

The method relies on a segmentation step that requires that the boundary between the two regions of motion be defined, as shown in step 1 of Figure 2. This is done semi-automatically by manually defining the boundary on a single frame, after which the position of the boundary is tracked for all subsequent frames. The motion within the two regions can now be mathematically interrogated separately without
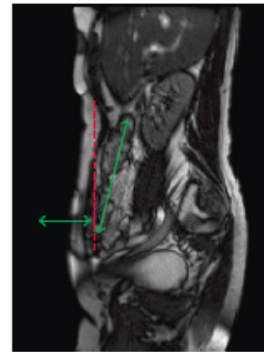
FIGURE 1: Schematic of the motion discontinuity in the abdomen during respiration. The horizontal green arrow indicates the predominant motion of the abdominal wall whilst the mostly vertical arrow represents the predominant motion of the abdominal contents. The dotted red line indicates the approximate location of the motion discontinuity.

interference from one another. Separate registrations quantify the motion in each region which are then recombined to reconstruct a full description of motion over the whole image. The motion is depicted as arrows (vectors) in step 2 of Figure 2. The relative motions along the boundary over the whole dynamic image sequence are then computed to determine the amount of shear. The result is a "sheargram": the coloured band in step 3 of Figure 2 depicting the total shear along the boundary over approximately 3 respiratory cycles.

3. Results

For the purposes of this exercise we obtained a selection of suitable MR images in which complementary surgical confirmation was available to clarify the degree of adhesive pathology. Of particular interest was a patient with a surgically confirmed adhesion to the anterior abdominal wall following a hernia repair. The result of the shear summed over approximately 3 respiratory cycles for this patient is compared to two healthy volunteers without adhesions in Figure 3.

An apparent reduction in shear is observed at the site of the surgically confirmed adhesion (highlighted by the arrow) which contrasts with the relatively uniform, gradually changing shear observed along the abdominal wall of the two healthy volunteers.

4. Validation

A critical assessment of our method demands evidence that the technique is robust and bereft of artefacts. In the absence of a clinical trial or a pilot study this section discusses two examples of validation tests, with interpretation of results and
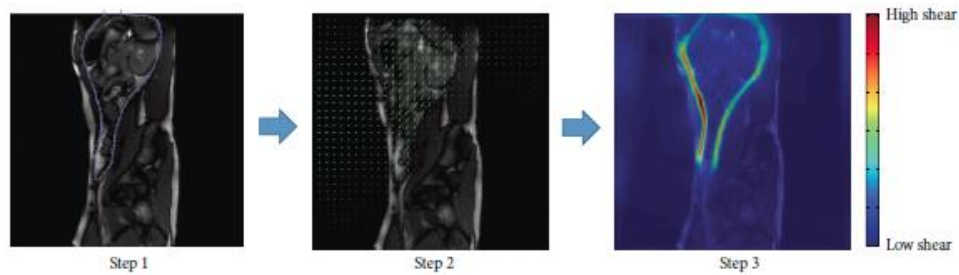
FIGURE 2: Flow chart describing the methodology. Step 1: typical region drawn to separate (segment) the two regions of different motion; step 2: depiction of the mathematically quantified movement; step 3: depiction of the shear taking place along the boundary in a "sheargram".
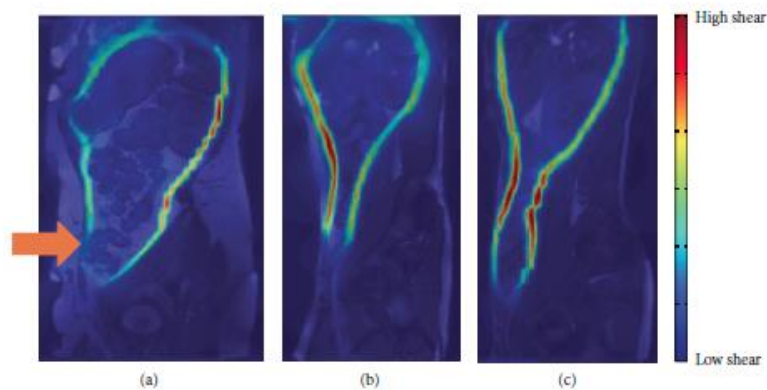
FIGURE 3: Comparison of the sheargrams from (a) a patient with an adhesion (arrow) and (b) and (c) two healthy volunteers.

implications for clinical use. Validation tests that have been performed to assess the robustness of the technique include:

(1) A highly idealised computer-generated stretching of a rectangular region of an MR image

(2) Imaging of a physical system involving the compression of a sponge in a syringe to generate a sliding against the syringe wall.

4.1. Test 1. A rectangular section of an abdominal MR image was artificially stretched relative to the surrounding MR image (shown in Figure 4(a)) to create a movie of discontinuous sliding with known, time-dependent shear at the boundary. The shear along the boundary was calculated with and without the segmentation step and compared to the known shear along the boundary in Figure 4(b).

The shear calculated when motion segmentation is included closely matched the known shear at the boundary of the stretched section. The largest discrepancy occurred at the top of the image (see Figure 4(b)) and is attributable to detail being stretched outside the image space. Even with the relatively small shears present in this example the measured

shear agreed within approximately 5% of the actual shear. The simple nature of the deformation (uniform stretch) does not challenge the registration algorithm but it does demonstrate the inherent accuracy of the procedure in the absence of "real-world" complexities.

4.2. Test 2. The second validation test was physical rather than computationally simulated and involved the compression of a textured sponge within a syringe (Figure 5). The plunger was used to gradually compress the sponge while images were taken with a standard DSLR camera (Cannon EOS 1100D). Two separate sets of acquisitions were made: in the first, the sponge was allowed to be freely compressed; for the second, an adhesive piece of double sided sticky tape was added to the inside of the syringe to create a localised resistance to the sponge's "motion" thereby disrupting slide (an analogue for an adhesion). The images in Figures 5(a) and 5(b) show the uncompressed and compressed sponge while the images in Figures 5(c) and 5(d) used our segmentation-registration protocol to depict the shear summed over the whole compression with and without the presence of the adhesive tape. This test offers a more realistic challenge for
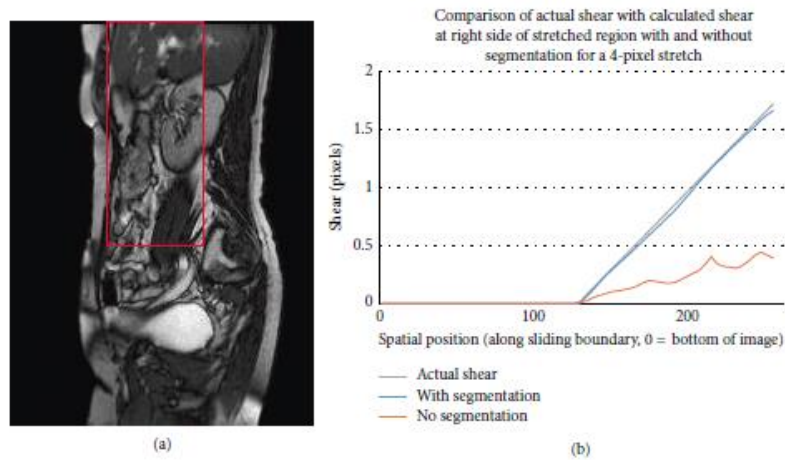
FIGURE 4: Validation experiment 1 with an idealised stretch of the portion of a MR image shown in (a) and shear results compared to actual shear in the system in (b).
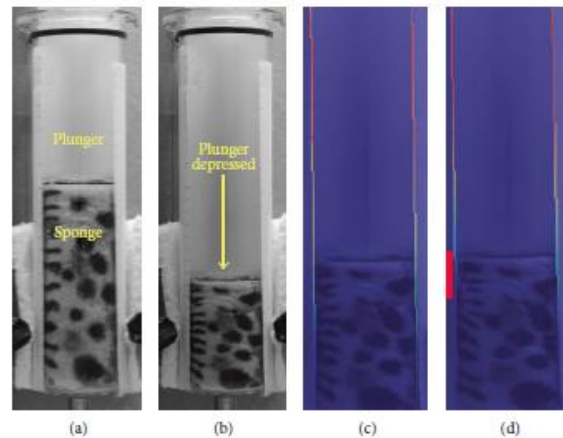
FIGURE 5: Syringe test object displaying (a) uncompressed sponge, (b) compressed sponge, (c) shear result without adhesive tape, and (d) shear result with adhesive tape (indicated by red block).

the algorithm as it includes non-uniform deformation and localised variations in sliding motion. It not only assesses the technique's ability to quantify shear but also its ability to detect an adhesive area along the boundary—proof of principle for adhesion detection.

When qualitatively observing the sponge's motion unaided by the sheargram, determining the location of the adhesion was extremely challenging. When combined with the images in Figures 5(c) and 5(d), a sufficient reduction in shear around the location of the adhesion was observed to accurately raise awareness of its presence.

5. Discussion

Intra-abdominal adhesions can form anywhere in the abdomen, vary in shape and size, and therefore cause a spectrum of symptoms: little or none at one end to severe, frequent pain at the other. A proportion of patients with adhesions are forced to repeatedly seek medical attention for their unexplained abdominal pain. In current clinical practice a patient with severe abdominal pain and suspected bowel obstruction will undergo non-invasive imaging [12–15]. Planar X-ray, fluoroscopy, CT or MRI may be used in an attempt

to detect a proximal region of distended bowel with an abrupt reduction in bowel calibre to a collapsed distal region [13]. Importantly, the radiological features determine the site of obstruction but not necessarily the cause: an adhesion may be likely but not proven. The only definitive method to prove the presence of adhesions is by surgery (laparotomy or laparoscopy) which itself is often the primary cause of adhesions [16]. As a result they place a significant burden on healthcare worldwide [16–18] and the lack of a reliable non-invasive diagnostic technique results in conservative patient management and prolonged patient discomfort [12].

It is recognised that improved diagnostic methods are required to reliably inform patient management strategies for adhesive bowel obstruction [12] but additionally we propose a requirement for diagnosis of adhesions in symptomatic patients *without* intestinal obstruction. A potential diagnostic technique is radiological examination of cine-MRI to observe the motion of the abdominal contents. This was first described by Lienemann et al. in 2000 [4] and has led to several further publications [5, 19, 20] from the same group. The cine-MRI acquisition acquires slices in the transverse and sagittal planes and requires a radiologist to identify regions of absence of movement which could correspond to adhesive pathology. The technique has shown promise and reported impressive accuracies, identifying up to 89% of surgically confirmed adhesions [19].

However, in our experience, radiological assessment of cine-MR images is limited by its difficulty, high inter-operator variability, and excessive reporting time. These factors led to our previous publication which described mathematical mapping and depiction of movement in the abdomen to aid the radiologist [6]. This current paper offers a refinement to our previous approach by presenting shear measurements as a diagnostic metric for the presence and location of more subtle adhesive pathologies around the perimeter of the abdominal cavity. The measurement of shear could be used to influence decisions on whether to operate, facilitate more efficient surgery due to improved adhesion localisation, and reduce the risk of serious surgical complications such as bowel perforation during incisions.

5.1. Non-Clinical Validation.
The validation tests were idealised and non-clinical but permitted the analysis method to be verified, offering a proof of principle for the detection of adhesive regions. The result of Test 1 (stretched MRI region) showed a close match between the output of the computer analysis and actual shear, indicating correct shear calculation. This was echoed equally well in the less idealised experiment of Test 2 (textured sponge). Although a small amount of shear was observed at the site of the adhesion (see Figure 5), this was visibly attributable to the weakness in bonding between tape and sponge as a small amount of slippage occurred. A more subtle observation is the reduction in shear on the opposite wall to the adhered region in Figure 5(d) when compared to the acquisition without an adhesion in Figure 5(c). Close examination of the images and registration deformation field confirm that this is not a failing in the shear analysis but rather the adhesion influenced the deformation at the right-hand boundary as well as the left. With the region below

the adhesion remaining largely uncompressed some sponge moved laterally into this space rather than sliding vertically downward against the syringe wall.

The results of both tests offer support for the technique showing that it accurately captured shear and that this could be used to detect an area disturbed by an adhesive influence.

5.2. Clinical Test.
Application to a handful of clinical examples has thus far continued to produce promising results. In the case reported here reduced shear was observed at the site of a surgically confirmed adhesion while in a sample of healthy abdominal scans ($n = 4$) a smoother more gradual change in shear was observed. The combined evidence of the clinical outcome and the validation tests provides reassurance that the technique has merit. Developing our system for clinical use requires two major steps: retrospective application to a larger patient cohort with surgical confirmation and a prospective programme.

The clinical results in Figure 3 also reveal areas of reduced shear which do not correspond to a confirmed adhesion (e.g., upper left Figure 3(a) and at the very base of the abdomen in all images). Inspection of movement in these areas reveals that this is not a failure of the technique to measure shear correctly but rather confirms that sliding is genuinely reduced in these areas. At this stage of development the aim of this technique is not to provide a standalone diagnostic outcome but to draw the eye of the radiologist toward specific suspect areas, which when combined with other diagnostic information can enable an informed decision to be made. This initial extra investment by the radiologist is potentially more than offset by increased accuracy of diagnosis and reduction in examination time. It is likely that there will be common sites of shear reduction which, with experience, should be easily identified and interpreted appropriately. A future ambition is the production of a shear "atlas" to provide a typical map of shear in health and disease to help clarify such issues.

5.3. Challenges and Future Work.
This paper has reported on a work in progress and there remain challenges which must be addressed before the proposed diagnostic protocol for anterior wall adhesions can be considered reliable. The principal concerns relate to (i) sensitivity of the results to position of boundary placement between the moving regions and (ii) possible artefacts introduced by structures moving through the 2D imaging plane. With reference to (i), our experience confirms that the placement of the boundary is relatively consistent due to high contrast anatomy; consequently reproducible results are achievable. With respect to (ii), through plane motion in 2D is most effectively addressed by 3D imaging. However, advantages gained from the 2D implementation are the high temporal resolution not available in 3D imaging and the simplicity and speed of implementation. Also, notably, movement within the abdomen is mostly superior-inferior; therefore objects largely remain in the sagittal imaging plane. It is for these reasons that complementary 2D and 3D analyses are being pursued.

As a final comment, the protocol is intentionally designed to support the use of different "off-the-shelf" registration algorithms. Currently the majority of work has been

performed using the Sheffield Image Registration Toolkit (ShIRT) but ANTs (Advanced Normalisation Toolkit, an open source registration algorithm) has also been successfully incorporated and used.

6. Conclusion

A technique to measure shear to infer the amount of visceral slide along the extremities of the abdominal cavity has been proposed, investigated, and validated. Despite the acknowledged limitations of the current implementation, the preliminary results have shown the adopted methodology to be successful in determining and detecting the locations of adhesions. Clinical application is currently limited by the small number of patients examined but an additional study is being pursued with a larger cohort of patients for further assessment.

Conflict of Interests

The authors declare that there is no conflict of interest regarding the publication of this paper.

References

[1] J. A. Caprini, J. A. Arcelus, J. Swanson et al., "The ultrasonic localization of abdominal wall adhesions," *Surgical Endoscopy*, vol. 9, no. 3, pp. 283–285, 1995.

[2] B. Sigel, R. M. Golub, L. A. Loiacono et al., "Technique of ultrasonic detection and mapping of abdominal wall adhesions," *Surgical Endoscopy*, vol. 5, no. 4, pp. 161–165, 1991.

[3] N. B. Zinther, A. Zeuten, E. Marinovskij, M. Haislund, and H. Friis-Andersen, "Detection of abdominal wall adhesions using visceral slide," *Surgical Endoscopy*, vol. 24, no. 12, pp. 3161–3166, 2010.

[4] A. Lienemann, D. Sprenger, H. O. Steitz, M. Korell, and M. Reiser, "Detection and mapping of intraabdominal adhesions by using functional cine MR imaging: preliminary results," *Radiology*, vol. 217, no. 2, pp. 421–425, 2000.

[5] R. A. Lang, S. Buhmann, A. Hopman et al., "Cine-MRI detection of intraabdominal adhesions: correlation with intraoperative findings in 89 consecutive cases," *Surgical Endoscopy and Other Interventional Techniques*, vol. 22, no. 11, pp. 2455–2461, 2008.

[6] J. Fenner, B. Wright, J. Emberey et al., "Towards radiological diagnosis of abdominal adhesions based on motion signatures derived from sequences of cine-MRI images," *Physica Medica*, vol. 30, no. 4, pp. 437–447, 2014.

[7] V. Vishnevskiy, T. Gass, G. Szekely, and O. Goksel, "Total variation regularization of displacements in parametric image

registration," in *Abdominal Imaging. Computational and Clinical Applications*, vol. 8676 of *Lecture Notes in Computer Science*, pp. 211–220, Springer, 2014.

[8] V. Delmon, S. Rit, R. Pinho, and D. Sarrut, "Registration of sliding objects using direction dependent B-splines decomposition," *Physics in Medicine and Biology*, vol. 58, no. 5, pp. 1303–1314, 2013.

[9] D. F. Pace, M. Niethammer, and S. R. Aylward, "Sliding geometries in deformable image registration," in *Abdominal Imaging. Computational and Clinical Applications*, vol. 7029 of *Lecture Notes in Computer Science*, pp. 141–148, Springer, Berlin, Germany, 2012.

[10] Y. Xie, M. Chao, and G. Xiong, "Deformable image registration of liver with consideration of lung sliding motion," *Medical Physics*, vol. 38, no. 10, pp. 5351–5361, 2011.

[11] B. W. Papiez, M. P. Heinrich, J. Fehrenbach, L. Risser, and J. A. Schnabel, "An implicit sliding-motion preserving regularisation via bilateral filtering for deformable image registration," *Medical Image Analysis*, vol. 18, no. 8, pp. 1299–1311, 2014.

[12] T. R. van Oudheusden, B. A. C. Aerts, I. H. J. T. de Hingh, and M. D. P. Luyer, "Challenges in diagnosing adhesive small bowel obstruction," *World Journal of Gastroenterology*, vol. 19, no. 43, pp. 7489–7493, 2013.

[13] E. Amzallag-Bellenger, A. Oudjit, A. Ruiz, G. Cadiot, P. A. Soyer, and C. C. Hoeffel, "Effectiveness of MR enterography for the assessment of small-bowel diseases beyond crohn disease," *Radiographics*, vol. 32, no. 5, pp. 1423–1444, 2012.

[14] D. P. Beall, B. J. Fortman, B. C. Lawler, and F. Regan, "Imaging bowel obstruction: a comparison between fast magnetic resonance imaging and helical computed tomography," *Clinical Radiology*, vol. 57, no. 8, pp. 719–724, 2002.

[15] A. S. Kumar, J. Coralic, R. Vegeler et al., "Magnetic resonance enterography: the test of choice in diagnosing intestinal 'Zebras'," *Case Reports in Gastrointestinal Medicine*, vol. 2015, Article ID 206469, 8 pages, 2015.

[16] R. P. G. ten Broek, Y. Issa, E. J. P. van Santbrink et al., "Burden of adhesions in abdominal and pelvic surgery: systematic review and met-analysis," *British Medical Journal*, vol. 347, no. 7929, Article ID f5588, 2013.

[17] B. Tingstedt, J. Isaksson, and R. Andersson, "Long-term follow-up and cost analysis following surgery for small bowel obstruction caused by intra-abdominal adhesions," *British Journal of Surgery*, vol. 94, no. 6, pp. 743–748, 2007.

[18] N. F. Ray, W. G. Denton, M. Thamer, S. C. Henderson, and S. Perry, "Abdominal adhesiolysis: inpatient care and expenditures in the United States in 1994," *Journal of the American College of Surgeons*, vol. 186, no. 1, pp. 1–9, 1998.

[19] S. Buhmann-Kirchhoff, R. Lang, C. Kirchhoff et al., "Functional cine MR imaging for the detection and mapping of intraabdominal adhesions: method and surgical correlation," *European Radiology*, vol. 18, no. 6, pp. 1215–1223, 2008.

[20] S. Kirchhoff, R. Ladurner, C. Kirchhoff, T. Mussack, M. F. Reiser, and A. Lienemann, "Detection of recurrent hernia and intraabdominal adhesions following incisional hernia repair: a Functional Cine MRI-Study," *Abdominal Imaging*, vol. 35, no. 2, pp. 224–231, 2010.

Appendix 6: Paper: A novel diagnostic aid for intra-abdominal adhesion detection in cine-MR imaging: Pilot study and initial diagnostic impressions, British Journal of Radiology, 2017

Title:
A novel diagnostic aid for intra-abdominal adhesion detection in cine-MR imaging: Pilot study and initial diagnostic impressions

David Randall[1], Frank Joosten[2], Richard ten Broek[3], Richard Gillott[4], Karna Dev Bardhan[4], Chema Strik[3], Wiesje Prins[2], Harry van Goor[3], John Fenner[1]

[1] Medical Physics, Infection, Immunity and Cardiovascular Disease, The University of Sheffield, Sheffield, UK
[2] Radiologie, Rijnstate Hospital, Arnhem, Netherlands
[3] Radboud University Medical Centre, Department of Surgery, Nijmegen, Netherlands
[4] The Rotherham NHS Foundation Trust, Rotherham, UK

Declaration: The authors have no conflicts of interest.

Abstract

Objectives: A non-invasive diagnostic technique for abdominal adhesions is not currently available. Capture of abdominal motion due to respiration in cine-MRI has shown promise, but is difficult to interpret. This article explores the value of a complimentary diagnostic aid to facilitate the non-invasive detection of abdominal adhesions using cine-MRI.

Method: An image processing technique was developed to quantify the amount of sliding that occurs between the organs of the abdomen and the abdominal wall in sagittal cine-MRI slices. The technique produces a 'sheargram' which depicts the amount of sliding which has occurred over 1-3 respiratory cycles. A retrospective cohort of 52 patients, scanned for suspected adhesions, made 281 cine-MRI sagittal slices available for processing. The resulting sheargrams were reported by two operators and compared to expert clinical judgement of the cine-MRI scans.

Results: The sheargram matched clinical judgement in 84% of all sagittal slices and 93–96% of positive adhesions were identified on the sheargram. The sheargram displayed a slight skew towards sensitivity over specificity, with a high positive adhesion detection rate but at the expense of false positives.

Conclusions: Good correlation between sheargram and absence/presence of inferred adhesions indicates quantification of sliding motion has potential to aid adhesion detection in cine-MRI.

Advances in Knowledge: This is the first attempt to clinically evaluate a novel image processing technique quantifying the sliding motion of the abdominal contents against the abdominal wall. The results of this pilot study reveal its potential as a diagnostic aid for detection of abdominal adhesions.

Introduction

Abdominal adhesions are formations of fibrous tissue that develop between abdominal structures in response to tissue damage. They are a major cause of morbidity and place a substantial burden on healthcare worldwide having been reported to cost $1.3bn annually in the USA (in 1994) and ~€60mil per year in Sweden.[1][2][3] Diagnosis of adhesions remains a challenge, with explorative laparoscopic surgery the primary diagnostic tool. Surgery itself is widely regarded to be the leading cause of adhesions and a non-invasive diagnostic technique could be of significant benefit.[4][5]

Cine-MRI is a dynamic imaging modality that can capture motion of the abdominal contents. Cine-MRI has shown potential for adhesion detection with two studies indicating sensitivities of at least 93% when compared to gold standard surgical confirmation.[6][7] Their detection relies on examination of movement of the abdominal contents with respiratory motion, also called 'visceral slide'. The radiologist qualitatively examines this motion for regions where displacement appears reduced or hindered – potentially linking them to the presence of adhesions. Movement examination remains a time consuming challenge and a diagnostic aid may be of benefit, particularly for less experienced radiologists in training.[8]

We have previously described an image processing technique to aid abdominal wall adhesion detection in cine-MRI.[9] The principal output of the technique is a 'sheargram', depicting the cumulative amount of sliding which occurs along the abdominal wall. The technique was trialled on synthetic data and a preliminary set of clinical images. Tests confirmed the ability of the sheargram to accurately measure shear and showed that a drop in shear could correspond to surgically confirmed adhesions.[9] This article further explores clinical application of the technique through a pilot study. Correlation of the sheargram with clinical judgement is used as a metric to clarify its potential as an indicator for adhesive pathology.

Method

The Sheargram

The movement of the diaphragm during respiration induces an inferior-superior displacement of the abdominal contents which is captured on cine-MRI. Simultaneously the abdominal wall exhibits a different, anterior-posterior mode of motion. The disconnect between the motion of the two structures creates a movement discontinuity along the interface between the abdominal contents and abdominal wall. In the healthy, the abdominal contents slide unimpeded at the discontinuity but where adhesive pathology exists, sliding is inhibited.

The sheargram technique quantifies the amount of sliding at the interface between the abdominal wall and abdominal contents. First, the images are segmented to create two new sets of images: frames containing only the abdominal contents and frames with the abdominal contents removed. Image registration is then used to track the movement of objects in each of the two regions independently. Using the quantified displacement information generated by the image registration, the shear at the sliding interface between the two regions can be calculated. Shear is used as a quantifiable analogue for sliding. The output of the technique is a 'sheargram' depicting the cumulative amount of sliding which has occurred over the entire dynamic

imaging sequence. A region of reduced shear on the sheargram is expected to correlate with a structure adhered to the abdominal wall: this principle is investigated in this paper via a pilot study.

Pilot Study

A cohort of 52 patients were randomly selected from a retrospective pool of 106 patients who had a dynamic MRI for undiagnosed abdominal pain with suspected adhesions. The MRI scans were undertaken on a 1.5 T Siemens Avanto scanner. The cine-MRI scanning protocol is similar to that previously described by Leinemann et al.: it is a true-FISP, with echo and relaxation times of 1.53 and 3.66 msec, flip angle of 60°, a matrix size of 192x256, slice thickness of 5 mm, 0.4 seconds per frame and 30 frames per imaged slice.[6 9] Patients were positioned supine and instructed to bear down and breathe deeply to induce suitable superior-inferior movement of the abdominal organs. No patient preparation or contrast was used. Typically, five sagittal slices were acquired at the midline, left/right paramedian and left/right lateral at the ascending/descending colon. The 52 patients contained 281 unique dynamic sagittal slices.

The quality of the dynamic images is dependent on the amount of respiratory motion generated by the patient. Small amounts of respiratory motion induce less movement of the abdominal contents, less shear at the abdominal wall and are therefore difficult to interpret. Each slice was graded as high and low quality data, based on the amount of respiratory motion. For example, a dynamic sagittal slice which contained less than one full respiratory cycle was deemed to be low quality. We excluded low quality slices from this pilot study because we sought proof of principle. This removed potential complications introduced by unsuitable data for a clearer assessment of the correlation of the reduced shear in the sheargram to adhesions identified on the cine-MRI. Approximately 50% (141/281) sagittal slices (from 37 patients) were judged to be of high quality and processed.

Two operators reported on all 141 sheargrams: one a technical expert in the image processing technique, the other a consultant radiologist with experience in cine-MRI reporting for adhesion diagnosis. Prior to commencing the pilot study, the radiologist was trained in sheargram interpretation using a training dataset of 10 sheargrams accompanied by their cine-MRI videos. Both reporters came to an independent judgement on whether the sheargram contained a reduction of shear which could correspond to an adhesion. The reporting procedure allowed the reporters three options in their judgement of the sheargram:

    i)   '**Yes**', there is a significant reduction in shear inferring an adhesion is present

    ii)   '**No**', the sheargram depicts a normal shear pattern inferring no adhesions

    iii)   '**Equivocal**', the sheargram shows a reduction in shear but it is not clear whether it is sufficient to infer the presence of an adhesion

The radiologist examined each of the cine-MR image sequences after reviewing the sheargram to confirm the presence of an adhesion in that slice. This reporting procedure emulated how sheargrams might be used clinically. The same scoring system was used ('yes', 'no' or 'equivocal') for the radiologist's examination of the cine-MRI. The original diagnostic reports of the cine-MRIs were also available for comparison.

Analysis primarily compared sheargram interpretation with the radiologist's clinical examination of the cine-MRI. The level of correlation was adjudicated based on percentage agreement between the two. The cohort size ensured statistical significance in correspondence between sheargram and radiologist examination if correlation exceeded 63% (to a p-value of <0.01). The study therefore permitted evaluation of whether the sheargram produced results that were representative of the actual shear occurring in the images and whether this corresponded to clinically indicated adhesive pathology.

Results

Figure 1 shows four example sheargrams: two with inferred adhesions and two healthy slices. The sheargrams display a coloured band overlaid on the MRI image, which depicts the amount of shear: red indicating high shear, blue – low shear. The sharp reductions in shear observed in Figure 1(a) and 1(b) correspond to areas with inferred adhesions, as marked by the white arrows. The lack of a sharp shear reduction in Figure 1(c) and 1(d) should indicate smooth sliding and an absence of adhesions.
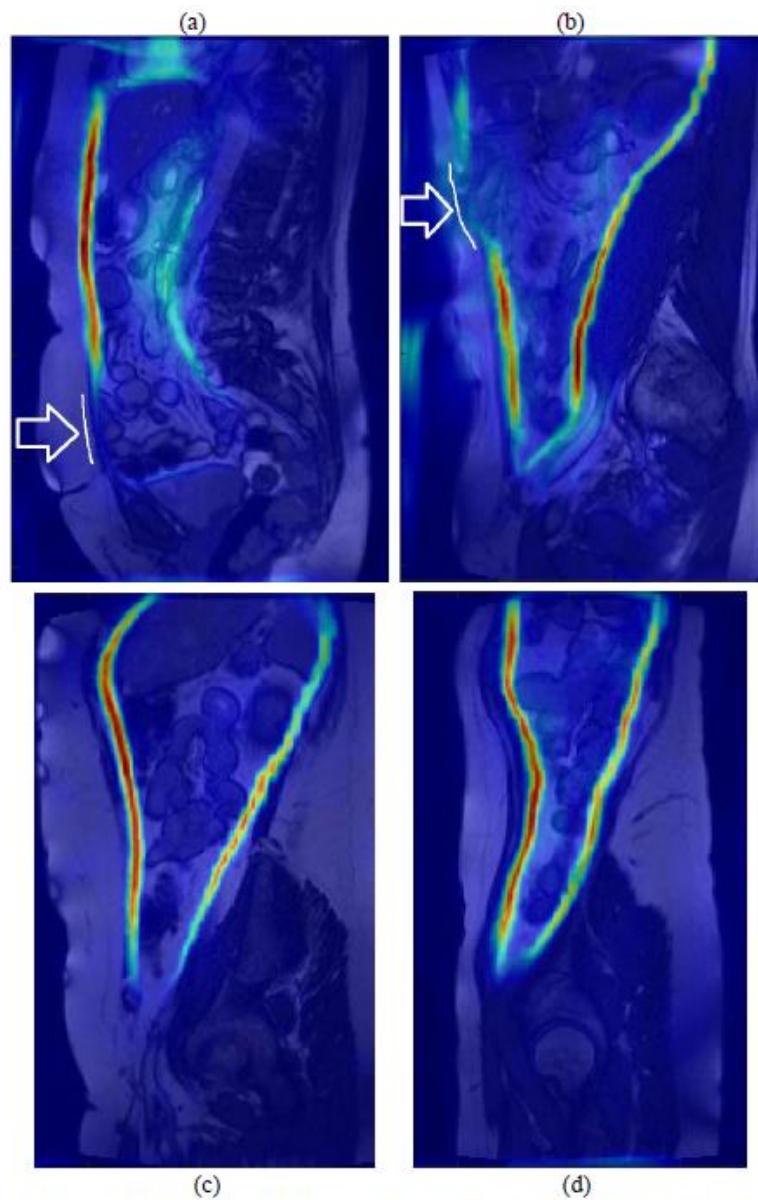
Figure 1: Two examples where the sheargram correctly correlated with positively inferred adhesions and two healthy sheargrams which correctly correlated with an absence of adhesions. White arrows and lines annotate location and extent of each adhesion.

The primary goal of the analysis was to correlate sheargram interpretation with expert clinical opinion of the cine-MRI. The scoring system ('yes', 'no', 'equivocal') creates nine possible combinations for comparison, summarised in Table 1.

Table 1: The 9 categories used to classify agreement between sheargram and clinical decision. Broader groupings of agreement, partial agreement and disagreement are also indicated.

Classification Number	Adhesion inferred on cine-MRI?	Adhesion identified on sheargram?	Broad Agreement Classification
1	Yes	Yes	Agreement (True positives/negatives)
2	No	No	Agreement (True positives/negatives)
3	Equivocal	Equivocal	Agreement (True positives/negatives)
4	Equivocal	Yes	Partial Agreement
5	Equivocal	No	Partial Agreement
6	Yes	Equivocal	Partial Agreement
7	No	Equivocal	Partial Agreement
8	No	Yes	Disagreement (False positives/negatives)
9	Yes	No	Disagreement (False positives/negatives)

The classification system described in Table 1 formed the basis for assessing correlation between sheargram and clinical decision of the cine-MRI. The greyed out categories in Table 1 were not used in subsequent results and analysis. These are cases where the radiologist made an equivocal clinical decision on the cine-MRI and therefore the presence of an adhesion is ambiguous and unknown. These cases do not present a definitive answer for the sheargram result to be compared against. There was only one sagittal slice where an equivocal cine-MRI judgement was made, leaving 140 sagittal slices remaining for comparison with the sheargram.

The nine different agreement classifications can be collated to form three broad classification categories, as shown in Table 1. Figure 2 plots the number of sagittal slices in each of the broad classification categories to provide a coarse overview of the correlation.
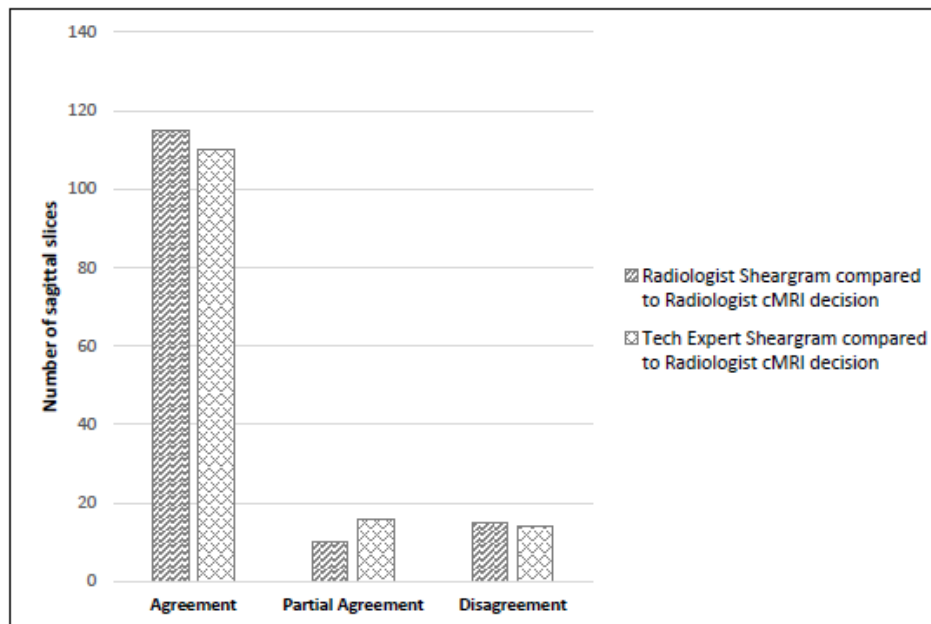
Figure 2: Number of sheargrams which agree/disagree with clinical decision on adhesions in the cine-MRI (broad classification)

Figure 2 shows a strong correlation between the interpretation of the sheargram and clinical opinion. 82% and 78% of sheargrams, judged by the radiologist and technical expert respectively, agreed with the clinical judgement on the presence of adhesions; 11% and 10% of cases disagreed.

A breakdown of the correlation for each of the possible combinations in Table 1 is presented in
Figure 3. For clarification, true positives, true negatives, false positives and false negatives in this study refer to the comparison of the sheargram interpretation with adhesions identified by the radiologist on the cine-MRI, i.e. a 'true positive' refers to a reduction in shear on the sheargram that correctly correlates to an inferred adhesion on the cine-MRI.
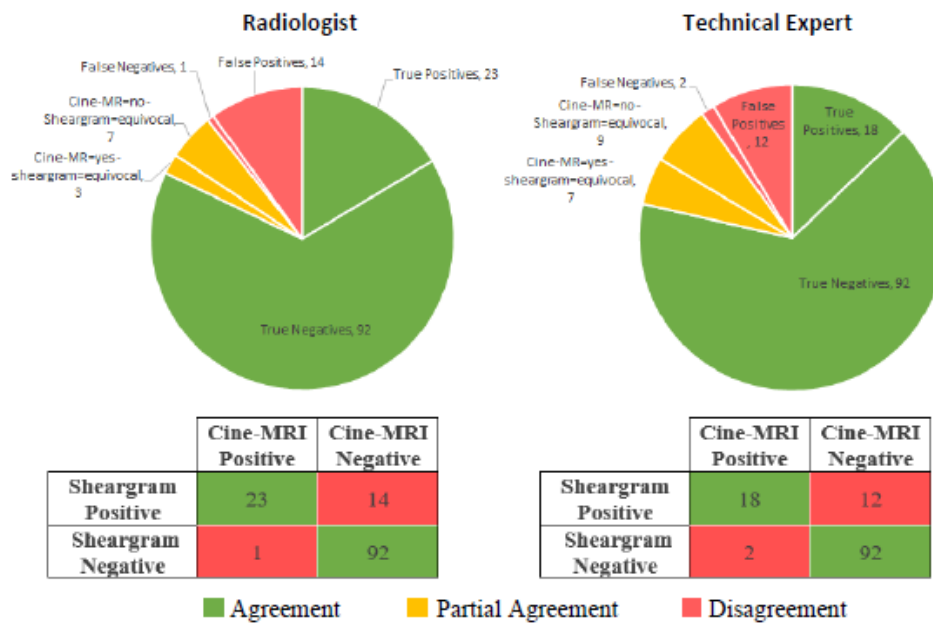
Figure 3: Correlation between the sheargram and clinically inferred adhesions on the cine-MRI for each of the two reporters represented as pie charts and 2x2 contingency tables. The numbers on the charts are the number of sagittal slices (total sagittal slices = 140).

In the pie charts, the green shaded segments highlight the true positives and true negatives, the red segments the false positives and false negatives and the yellow portions are partial agreements. The contingency tables in Figure 3 exclude all equivocal cases to permit an estimate of sensitivity and specificity. The sensitivity was 96% for the radiologist and 90% for the technical expert. The vast majority of slices without adhesions were also correctly identified on the sheargram, with the specificity approaching 90% (87% for the radiologist and 88% for the technical expert) when excluding all equivocal sheargram judgements..

The original diagnostic cine-MRI reports were also available for interrogation. The original report was produced by the same radiologist that participated in this pilot study. Comparison between the original report and the clinical decision made during this pilot study reveals twelve cases where the radiologist changed their opinion after reviewing the sheargram. The changes are summarised in Figure 4.
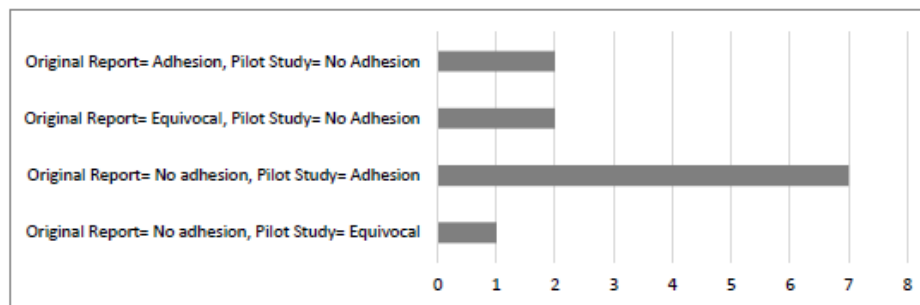
Figure 4: The 12 changes made between the original cine-MRI report and the radiologist's clinical decision in the pilot study

The majority of changes involved re-designation from negative to positive presence of adhesions. The identification of these additional adhesions were all paired with a positive or equivocal sheargram, potentially indicating its influence on clinical decisions.

Discussion

We have previously presented a technique to quantify the sliding motion of the abdominal contents against the abdominal wall and tested its ability to measure sliding.[9] With this pilot study, we aim to verify the potential clinical usefulness of the sheargram to aid detection of abdominal wall adhesions. The primary metric for assessment was how well the interpretation of the sheargram matched clinical interpretation of the cine-MRI.

Sheargram correlation with cine-MRI

Good agreement between sheargram and clinical judgement is indicated in Figure 2 and 3. The combination of complete and partial agreements accounted for 89% and 90% of cases for the radiologist and technical expert respectively. Calculation of a conclusive figure for the level of agreement depends on the interpretation of an 'equivocal' sheargram. Notably, an equivocal reduction in shear on a sheargram still draws the attention of the reporter to that specific location. Consequently, there is justification that an equivocal judgement is more aligned to a positive sheargram than a negative. Applying this justification and reclassifying 'equivocal' sheargrams as a positive 'yes', results in the following figures:

- **Overall agreement:** The sheargram correctly correlated with clinical opinion in 84% of cases for both reporters. This comfortably exceeded the 63% agreement required for statistical significance (i.e. p-value <0.01).
- **Detection of positive adhesions:** Sensitivities of 96% (26/27) and 93% (25/27) were recorded for the radiologist and technical expert respectively.
- **Identification of healthy cases:** The proportion of healthy sagittal slices that correctly correlated with negative sheargrams is given by a specificity of 81% for both reporters.

The high percentage of adhesions correctly identified on the sheargram and the lower percentage of agreement for negative cases highlights a skew towards sensitivity over specificity. There were 14 and 12 false positives compared to 1 and 2 false negatives for the radiologist and technical expert respectively (see

Figure 3). The intention of the sheargram is for it to become a diagnostic aid; designed to alert the radiologist to suspicious areas with possible adhesions. Therefore, a high sensitivity is favoured as it is preferable to draw the attention of the reporter to suspected adhesions subsequently deemed to be healthy, rather than miss adhesions.

The analysis has assumed each slice is independent; however, some slices belong to the same patient and potentially demonstrate correlation with one another. Considering multiple slices within each patient: 63% of patients had agreement between sheargram and cine-MRI in all slices; 34% had one disagreement and 3% had two disagreements. The spread of disagreement between sheargram and expert opinion was shared across the patient cohort rather than concentrated in particular patients and implies that two slices belonging to the same patient are no more likely to both lead to a disagreement than two slices from different patients. Consequently, it was appropriate to treat the sagittal slices as independent entities.

The evidence presented supports the premise that the sheargram produces a shear profile representative of the sliding that occurs along the abdominal wall and that a reduction in quantified shear correlates to adhesive pathology.

Where did it fail?
There was a single sheargram which produced a healthy shear profile (judged by both reporters) in which an adhesion was identified on the cine-MRI resulting in a false negative. This case is shown in Figure 5(a). The technical expert recorded a second false negative, shown in Figure 5(b).

(a)   (b)
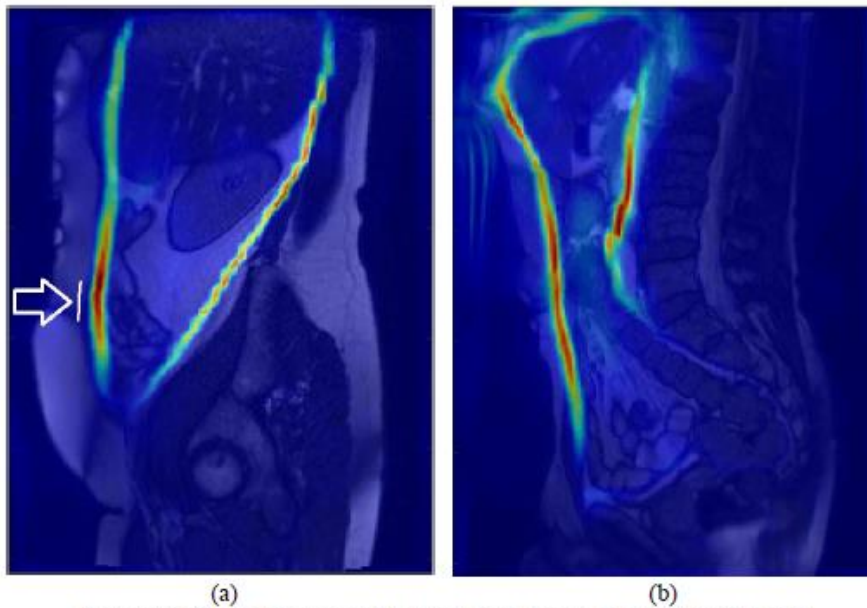
Figure 5: The two false negative sheargram examples from the pilot study

At the area of the adhesion in Figure 5(a) there was considerable lateral movement through the imaging plane. The adhered bowel loop was only visible in approximately half of the 30-frame dynamic image sequence. Substantial movement occurring through the imaging plane at the sliding interface is interpreted as displacement by the image registration algorithm and culminates in anomalous shear. The case in Figure 5(b) can be explained by a difference in sheargram interpretation. The technical expert noted that the reduction in shear in the lower abdomen, although significant, was in the absence of structure adjacent to the abdominal wall and was therefore discounted. The radiologist documented bowel close enough to the abdominal wall to contribute to shear and an adhesion to the pelvic floor and therefore reported a positive adhesion.

Changes in clinical opinion
The radiologist originally reported the cine-MRI scans at least 5 months prior to undertaking this pilot study. This ensured that the radiologist was not influenced by recent memory. Alterations between the original report and this pilot study have greater pertinence as inter-operator variability is negated.

The majority, 10/12, of the alterations shown in Figure 4 aligned with the judgement made on the sheargram. This insinuates the sheargram influenced the interpretation of the cine-MRI. The two remaining sagittal slices were from the same patient and the radiologist's sheargram interpretation matched the original report. The technical expert made an 'equivocal' judgement on these two sheargrams implying it was a challenging scan to interpret. There were seven alterations in opinion from 'no adhesion' (on the original report) to a positive adhesion, potentially resulting in identification of new adhesions previously missed. However, these potential additional adhesions cannot be confirmed without surgery. The evidence suggests the sheargram had the capability to inform adhesion identification to the abdominal wall. However, it should be stressed that the radiologist did not review the transaxial slices in this pilot study which were available when constructing the original report. This difference could also account for some of the changes in clinical opinion.

Limitations
This paper acknowledges that the gold standard diagnostic method for abdominal adhesion diagnosis is explorative surgery, not cine-MRI. However, in the absence of surgical confirmation, comparison of the sheargram to cine-MRI serves as a practical alternative and permitted a much larger patient cohort to be evaluated. Moreover, a recent in-house assessment confirmed a low false positive rate of cine-MRI when compared to surgical confirmation of identified adhesions: providing circumstantial evidence for the sheargram's correlation with surgery. However, confirming the interpretation of the sheargram and cine-MRI to surgical findings remains a necessity to determine the true diagnostic usefulness of the technique.

Despite the demonstrated link between a drop in shear and inferred presence of adhesions, the true clinical benefit of the technique has yet to be determined. There is a disconnect between detecting adhesions and determining their contribution to clinical presentation. However, non-invasive detection would provide the clinician with additional information with which to make a more informed decision on diagnosis and surgical intervention.

Exclusion criteria ensured that only images of high quality would be evaluated. We argue that this is appropriate for this proof of principle exercise, permitting analysis on real but suitable data. This should be taken into consideration when interpreting the results. Only 50% of the data was considered as 'high quality'. Patient compliance was the primary source of poorer quality data and this invites an opportunity to refine the scanning protocol. Over 90% of the poor quality data could be attributed to a lack of respiratory motion that induced insufficient displacement of the abdominal contents. Trials are underway to investigate the training of participants (via an instructional video) to improve breathing during image acquisition, complemented by simplified instructions. The reliability of the sheargram on lower quality data also needs to be ascertained.

Although the sheargram is produced from a quantitative parameter, interpretation of the sheargram itself introduces subjectivity. The two reporters in this pilot study were from differing backgrounds and therefore provide a good indication of the inter-operator variability in sheargram interpretation. 85% (120/141) of sheargram interpretations between the two reporters agreed, 13% (19/141) partially agreed and 1.4% (2/141) disagreed. The notable number of partial agreements can be ascribed to the technical expert reporting more equivocally due to a lack of experience in diagnostic decision-making. 76% of the partial agreements were related to an observed drop in shear in the lower abdomen. A gradual reduction in shear at the lower extremities of the abdomen is often observed in healthy individuals. This can lead to a sometimes ambiguous judgement on whether the reduction is significant and sharp enough to be abnormal or whether it is gradual and mild enough to be normal. The partial agreements are less concerning than the two cases where a complete disagreement was recorded. One of the two cases where a complete sheargram disagreement was recorded is shown in Figure 5(b), while the other can be accounted for by a difference in clinical experience. Greater objectivity would benefit the technique but a more automated process would require considerable effort to implement. Arguably, the variability between the two reporters can be considered acceptable.

The false negative case in Figure 5(a) resulting from out-of-plane motion highlights a fundamental problem with imaging a 3-dimensional object in a 2-dimensional plane. Progression to 3D pseudo-dynamic imaging to capture a complete view of movement within the entire abdomen is being considered. Successful implementation of 3D imaging would also permit movement analysis of structures deeper within the abdominal cavity rather than being limited to its perimeter, as in the current 2D implementation.

Conclusion

Our sheargram technique for measuring the sliding motion of the abdominal contents against the abdominal wall in cine-MRI has already been described. This pilot study confirms the sheargram is capable of matching areas of reduced shear to inferred adhesive pathology identified by expert clinical judgement on cine-MRI. A subset of approximately 50% of the most suitable data was selected from a total of 281 sagittal slices from a cohort of 52 patients. The sheargram matched the final clinical cine-MRI adjudication in 84% of cases and at least 93% of all located adhesions were identified on the sheargram. Arguably, the sheargram influenced decision-making since changes in the radiologist's opinion were observed between the original report and the pilot study after examination of the sheargram. Identification of

seven potentially new adhesions were made, with all seven matching interpretation of the sheargram. However, poor patient compliance indicates the need to simplify the breathing procedure and provide clearer instructions along with clarification of the minimum amount of respiratory motion required.

The evidence presented has indicated that visceral slide quantification presented in a sheargram can be a diagnostic aid for cine-MRI interpretation. This interim study has provided confidence that the technique deserves further development and a more thorough clinical trial is warranted.

References

[1] R. P. G. ten Broek, Y. Issa, E. J. P. van Santbrink, N. D. Bouvy, R. F. P. M. Kruitwagen, J. Jeekel et al., "Burden of adhesions in abdominal and pelvic surgery: systematic review and met-analysis," *British Medical Journal, 2013,* vol. 347, p. f5588.

[2] B. Tingstedt, J. Isaksson and R. Andersson, "Long-term follow-up and cost analysis following surgery for small bowel obstruction caused by intra-abdominal adhesions," *British journal of Surgery, 2007,* vol. 94, no. 6, pp. 743-8.

[3] N. F. Ray, W. G. Denton, M. Thamer, S. C. Henderson and S. Perry, "Abdominal Adhesiolysis: Inpatient Care and Expenditures in the United States in 1994," *Journal of the American College of Surgeons, 1998,* vol. 186, no. 1, pp. 1-9.

[4] D. Bruggmann, G. Tchartchian and A. Hackethal, "Intra-abdominal Adhesions: Definition, Origin, Significance in Surgical Practice, and Treatment Options," *Dtsch Arztebl Int., 2010,* vol. 107, no. 44, pp. 769-775.

[5] J. Dubuisson, R. Botchorishvili, S. Perrette, N. Bourdel, K. Jardon, B. Rabischong et al., "Incidence of intraabdominal adhesions in a continuous series of 1000 laparoscopic procedures," *American Journal of Obstetrics and Gynecology, 2010,* vol. 203, no. 2, pp. 111.e1-111.e3.

[6] A. Lienemann, D. Sprenger, H. O. Steitz, M. Korell and M. Reiser, "Detection and Mapping of Intraabdominal Adhesions by Using Functional Cine MR Imaging: Preliminary Results," *Radiology, 2000,* vol. 217, pp. 421-5.

[7] R. A. Lang, S. Buhmann, A. Hopman, H.-O. Steitz, A. Lienemann, M. F. Reiser et al., "Cine-MRI detection of intraabdominal adhesions: correlation with intraoperative findings in 89 consecutive cases," *Surg. Endosc., 2008,* vol. 22, pp. 2455-2461.

[8] J. Fenner, B. Wright, J. Emberey, P. Spencer, R. Gillot, A. Summers et al., "Towards radiological diagnosis of abdominal adhesions based on motion signatures derived from sequences of cine-MRI images," *European Journal of Medical Physics, 2013,* pp. 1-11.

[9] D. Randall, J. W. Fenner, R. Gillott, R. ten Broek, C. Strik, P. Spencer et al., "A Novel Diagnostic Aid for Detection of Intra-Abdominal Adhesions to the Anterior Abdominal Wall Using Dynamic Magnetic Resonance Imaging," *Gastroenterology Research and Practice, 2016,* vol. 2016, p. Article ID 2523768.

Appendix 7: Paper: The Oculus Rift virtual colonoscopy: introducing a new technology and initial impressions, Journal of Biomedical Graphics and Computing, 2016

ORIGINAL RESEARCH

The Oculus Rift virtual colonoscopy: introducing a new technology and initial impressions

David Randall*[1], Peter Metherall[2], Karna Dev Bardhan[3], Paul Spencer[3], Richard Gillott[3], Rebecca de Noronha[4], John W Fenner[5]

[1]Medical Physics Group, Department of Cardiovascular Science, The University of Sheffield, Sheffield, UK
[2]3D Imaging Laboratory, Sheffield Teaching Hospitals NHS Foundation Trust, Sheffield, UK
[3]The Rotherham NHS Foundation Trust, Rotherham, UK
[4]Medical Imaging and Medical Physics, Sheffield Teaching Hospitals NHS Foundation Trust, Sheffield, UK
[5]INSIGNEO Institute for in silico Medicine, The University of Sheffield, Sheffield, UK

ABSTRACT

Introduction: Virtual colonoscopy has proven to be a reliable, sensitive technique and is now widely adopted in routine clinical practice. We present a novel extension to virtual colonoscopy by incorporating the immersive Oculus Rift virtual reality technology. We describe our initial experience to explore its potential diagnostic benefit. To the best of our knowledge, this is the first Oculus Rift related publication in the radiology field.

Method: A procedure for generating an Oculus Rift virtual colonoscopy (ORVC) has been created. It is derived from a CT image of an air/CO_2 inflated colon with contrast labelled faecal matter. The mucosal surface is segmented from its surroundings and subsequently meshed and rendered to produce a 3D surface. The mucosal surface is then imported into the Unity game engine along with the calculated coordinates of its centreline. Within Unity, a virtual reality camera is assigned to travel both outside and inside the colon, aided by controls allocated to an Xbox controller. Two ORVCs were created from differing quality CT data and trialled by two experienced radiologists and a gastroenterologist.

Results: The ORVCs prompted an enthusiastic response from the clinicians. It was considered to offer potential for improved diagnostic power but further development is required if its full capability is to be realised.

Conclusions: A mechanism for examining virtual colonoscopies within the immersive environment of the Oculus Rift has been developed. The resulting ORVCs were trialled by three clinicians with largely positive feedback providing encouragement for pursuing this work further.

Key Words: Oculus Rift, Virtual reality, Virtual colonoscopy, CT colonoscopy, Radiology, Diagnostic imaging

1. INTRODUCTION

Bowel cancer is the second most common cause of cancer related deaths, with an estimated 16,000 deaths per year in the UK.[1] Optical colonoscopy is the preferred method of colonic examination and is considered the "gold standard".

During the procedure the full length of the colon can be examined in detail with an externally controlled camera inserted into the rectum while also allowing therapeutic procedures (polypectomies – removal of potentially pre-cancerous lesions). Its limitations however are that it has many contraindi-

*Correspondence: David Randall; Email: drandall1@sheffield.ac.uk; Address: Medical Physics, IICD, O-Floor, the Royal Hallamshire Hospital, Glossop Rd, Sheffield, South Yorkshire, UK.

cations and the process is invasive: involving a thorough bowel cleansing, which patients often find unpleasant.[2] Virtual colonoscopy therefore offers an attractive alternative because of its minimally-invasive nature and nominal bowel preparation. A wealth of evidence now offers significant support for the use of virtual colonoscopy as a diagnostic tool[3–6] and as such it has almost entirely replaced barium enemas in the developed world.

The virtual colonoscopy procedure involves an abdominal CT scan, inflation of the colon with air/carbon dioxide and the addition of a contrast medium to distinguish between bowel wall and faecal matter (*e.g.* gastrografin). The colon is separated (segmented) from the CT image and its inner surface rendered so it can be viewed from inside the lumen of the colon. Virtual colonoscopies are typically viewed and reported on a standard reporting workstation and the camera position/orientation controlled via mouse and keyboard. This paper explores the potential improvements offered to this traditional user interface by the introduction of virtual reality.

The Oculus Rift is a virtual reality headset capable of providing stereoscopic vision and head tracking capabilities [Oculus VR, Irvine, California, USA]. The commercialised version of the Oculus Rift has yet to be released and this paper has experimented with its precursor - the Development Kit 2 (DK2). It has primarily been developed for the gaming industry but has features which could prove useful

to the medical field. A handful of publications indicate the Oculus Rift has begun to find applications in medicine[7–12] but as yet none have been applied to diagnostic imaging. Virtual colonoscopy is one medical imaging example where the power of the examination is naturally augmented by the incorporation of stereoscopic vision and head tracking.

An immersive virtual colonoscopy experience has been previously attempted by Mirhosseini *et al.* in 2014[13] using a CAVE (cave automatic virtual environment) – placing the user in a room where the inner surface of the colon is projected onto the surrounding walls. They discuss several aspects of their technique and conclude that it offers potential for improved examination time and accuracy. However, a CAVE system is not practicable for the clinic nor is it financially viable. This paper describes an alternative immersive method for viewing virtual colonoscopies with the Oculus Rift DK2, followed by a discussion of our experiences: highlighting any benefits/downfalls regarding image interpretation.

2. METHOD

A total of two Oculus Rift virtual colonoscopies (ORVC) have been produced for viewing by a diagnostician. The following text describes the procedure employed to view a high resolution rendered colon within the immersive environment of the Oculus Rift DK2. An outline of the process used to produce an ORVC is shown in Figure 1.
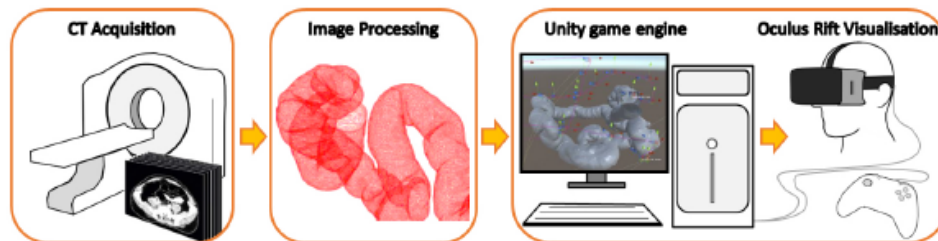
Figure 1. Schematic of the process used to produce an Oculus Rift virtual colonoscopy (ORVC)

2.1 CT acquisition and image processing

Demonstration virtual colonoscopy images, freely available for research purposes, were provided by TeraRecon Inc [Foster City, California, USA]. This comprised two studies with differing acquisition parameters in order to assess the technique with varying quality data. The acquisition parameters of the studies are tabulated in Table 1.

Only supine images were examined in this work although the

same technique is equally valid for prone positions. Images were processed using Mimics Medical 18.0 [Materialise NV, Leuven, Belgium]. The DICOM images were first segmented using threshold and region growing methods. A 3D surface mesh was next generated and optimised to ensure sufficient mesh quality using standard meshing tools available in the software. The ends of the meshed colon were cut to create an open ended vessel structure. The mesh was exported in

DXF format so that it could be imported directly into the Unity game engine, version 5.1 [Unity Technologies, San Francisco, California, USA].

A centreline analysis was performed on the surface mesh and edited to give a single path through the colon. In the second study obstructed segments of the colon were joined together using a straight line connection between the discrete segments to give a continuous path. The centreline path was exported in an xml format using the associated 3-matic Medical software 10.0 [Materialise NV, Leuven, Belgium].

Table 1. CT acquisition parameters for the two virtual colonoscopy studies

Study 1	Study 2
Siemens Sensation 16	GE Medical Systems LightSpeed Plus
280 mA	150 mA
120 kV	120 kV
Pixel size 0.74 mm	Pixel size 0.81 mm
Slice increment 0.5 mm	Slice increment 1.5 mm
Slice thickness 1 mm	Slice thickness 3 mm

2.2 Unity game engine and visualisation

The meshed colons and coordinates of the centreline were imported into the Unity game engine v5.1. Unity is an effective development environment for Oculus Rift applications and inherently supports virtual reality visualisation and interaction. Two rendered versions of the colon were imported – one with the normal vectors facing inward the other with them pointing outwards (allowing the colon to be visible from both inside and out). This allowed the user to gain an overall view of the colon from the outside by "flying" along an arbitrary path around its exterior before entering via the caecum. Once inside the colon the coordinates of the centreline were plotted using the iTween plugin for Unity [Pixel Placement, Baltimore, Maryland, USA] and the virtual reality camera assigned to travel along the centreline coordinates. A point light source was used to light the mucosal surface and was assigned to track the camera, maintaining a constant distance beneath it throughout the colonoscopy.

The camera was assigned to automatically travel at a set speed through the colon but its positon could be controlled using an Xbox gaming controller with the following assigned functionalities:

- The "A" button paused and resumed the automatic movement of the camera along the centreline at its predefined speed.
- The up/down keys on the directional pad (D-pad) moved the camera forwards and backwards along the centreline in the colon. Usage of these buttons auto-

matically overrides the automatic movement of the camera.
- The "B" button allowed the user to view their current position within the colon. It paused the movement of the camera inside the colon and switched to a stationary camera positioned above the colon. When viewing from the second, external camera the position of the user inside the colon was highlighted by a visible red dot. A second tap of the "B" button returned the view to the camera in the colon and resumed its motion.

The speed at which the camera travelled through the colon was carefully chosen to limit the chance of inducing nausea. During the development phase the transit speed was reduced incrementally and tested on an operator known to be sensitive to simulation sickness. The maximum speed at which the operator experienced a complete absence of nausea was selected. At the speed selected a complete, uninterrupted transit of study 1 takes 2 minutes and study 2, 4 minutes.

Camera orientation was controlled entirely by the movement of the user's head using the Oculus Rift head tracker. The Oculus Rift DK2 was connected to a middle to high-end desktop PC (Intel i7 4770k 3.5GHz, NVidia GeForce GTX 770, Windows 7) with no noticeable latency in the image. The observer was confronted with an external view of the colon when first wearing the Oculus Rift, providing an external flyby before briefly coming to a halt at the entrance to the caecum. The observer was then either automatically moved through the anatomy or, by utilising the Xbox controller, could proceed at their own speed whilst exploring the views via natural head movements.

3. RESULTS

Our developments have permitted stereoscopic 3D exploration of the interior surface of the colon both from the inside and out by utilisation of the Oculus Rift and Unity game engine. The experimental setup and example views from inside and outside the colon are shown in Figures 2-4.

Figure 2. Schematic of the process used to produce an Oculus Rift virtual colonoscopy (ORVC)
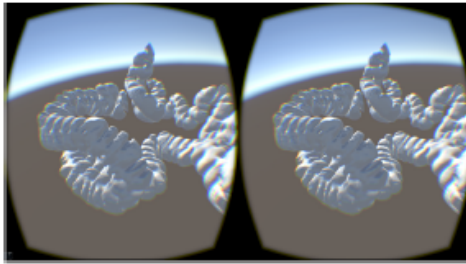
Figure 3. Oculus Rift DK2 stereoscopic view of the colon exterior of Study 2
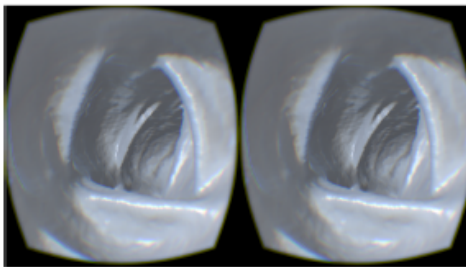

Figure 4. Oculus Rift DK2 stereoscopic view during the virtual colonoscopy of Study 1

Both the ORVCs studies were reviewed by three experienced clinicians all familiar with virtual colonoscopies: two radiologists and a gastroenterologist. All three were asked to provide a reflective statement on the experience and to draw comparisons to conventional virtual colonoscopy and optical colonoscopy. The comments are summarised in bullet point form below:

Radiologist 1

(1) Generally: Gained an immediate impression of the great potential of the technique. It offers a number of potential improvements on the conventional virtual colonoscopy fly-through technique but certain refinements are necessary for the ORVC technique to replace conventional virtual colonoscopy.

(2) The immersion and stereoscopic vision presents a strong possibility for increased sensitivity and specificity. A greater effect may be expected in less experienced radiologists who have yet to become overly familiar with the conventional virtual colonoscopy and have not developed a refined routine for their reporting. For radiologists exposed to the ORVC as standard training the rewards are likely to be even greater.

(3) Currently no more than four virtual colonoscopies would be reported in one morning/day due to fatigue in their labour intensive reporting. The ORVC felt comfortable and presents a possibility of reducing fatigue.

(4) An experienced virtual colonoscopy radiologist takes approximately 20 minutes per examination whereas an inexperienced radiologist may take in excess of 30 minutes. With appropriate training and experience with the ORVC, a reduction in examination time is a plausible prospect, particularly for less experienced radiologists.

(5) For the ORVC to be viable, an option for the camera to be orientated with the direction of travel is a necessity.

(6) When reporting on current systems a raft of supplementary information is available to the radiologist. This information would be useful if incorporated into the ORVC, in particular: indication of the direction of travel, information on current location in relation to the CT slices and the ability to mark suspicious areas on the fly-through and triangulate their positions on the CT image planes.

Radiologist 2

(1) Generally: The prospect of incorporating virtual reality imaging into diagnostics is an exciting potential development that would significantly impact on the way radiologists work. It removes the demanding process of assimilating a large data set.

(2) The Oculus Rift's intuitive head tracking ability provides the opportunity of looking around the haustral folds of the colon simply by turning one's head rather than complex movements with the mouse and screen.

(3) Immersion within the data removes the potential for error generated by distractions.

(4) The strong visual stimulus provided by the Oculus Rift means the generation of motion sickness is a real possibility.

(5) When reporting, the virtual colonoscopy cannot be utilised on its own, several pieces of information are considered in order to make diagnostic decisions. The CT slices contain information of structures outside the colon and this cannot be ignored. A primary tool used during reporting is the marking of features in the virtual colonoscopy and subsequently matching these to the CT slices and vice-versa. Such a feature would need to be incorporated into the ORVC technique for its clinical implementation. Routine reporting of the rest of the abdomen and pelvis would still be required.

(6) The psychophysiology of perception is complex and this new way of generating and looking at images

needs to be assessed. This work gives motivation for comparisons of sensitivities and specificities with a current "gold standard". This could be optical colonoscopy but a comparison with CT colonography would be equally valid.

Gastroenterologist

(1) In optical colonoscopy the colonoscopist drives forward from anal canal to caecum. The gradual withdrawal of the instrument from the caecum allows the reverse view, likened to that seen in the wing mirrors of a car. The colon is a haustral structure: hence a polyp within a recess may be missed when driving toward the caecum but detected in the "wing mirrors" while exiting. Virtual colonoscopy offers a similar view with the advantage of driving forwards in both directions.

(2) The wider field of view offered in the ORVC is far greater than that offered by optical colonoscopy. Self-evidently this is of potential benefit for detecting lesions, which in turn increases confidence that fewer lesions might have been missed.

(3) Oculus Rift assisted virtual colonoscopy, by its very nature, offers unique and major advantages. In standard virtual colonoscopy, driving is guided by a mouse/keyboard control which is often "jerky" and does not readily afford fine changes. In contrast ORVC offers a refined natural method of viewing by slight movements of the head and changes in body position.

(4) The ORVC technique implemented allows a birds-eye view of the inner wall of the colon, but crucially, viewed from the exterior. Consequently polyps located in haustral recesses are more readily identified, particularly at areas of natural angulation of the colon. The same view also allows identification of diverticulae. Colonic diverticulae are mucosal herniations through its confining wall, hence are more prominent when viewed from the outside.

(5) ORVC offers a different and unique advantage, that of total immersion within the environment, supplemented by looking at that same environment from the outside *i.e.* being both within the data and then viewing it from outwith. Put differently this can be likened to looking at the fish tank from the inside and outside.

The two radiologists independently shared several similar views while the gastroenterologist also had some overlapping points. All parties commented that full examination of the first colon (*i.e.* high resolution) had identified all lesions: polyp and diverticulum, and were confident that no other abnormality had been missed. An example of a diverticulum

viewed on the Oculus Rift (from both inside and outside) is shown in Figure 5.
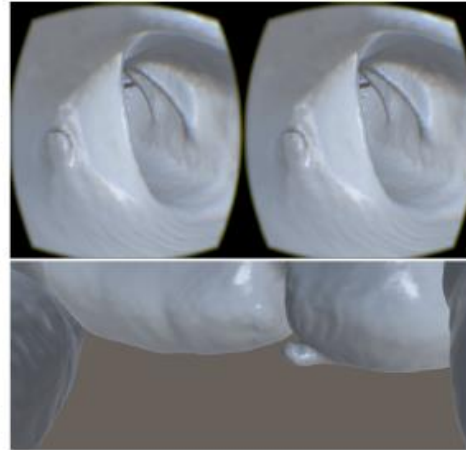
Figure 5. Both inside and outside views of a diverticulum spotted during examinations of Study 1

4. DISCUSSION

Optical colonoscopy is widely considered the most sensitive diagnostic procedure for the detection of colonic pathologies.[14, 15] There is however growing evidence that virtual colonoscopy is improving towards similar sensitivity values,[3, 16] this is reflected by several national guidelines endorsing its use.[2, 17] With wider uptake encouraged, the numbers undergoing virtual colonoscopy will steadily rise. It is therefore important to optimise the technique for both lesion detectability and examination time.

Current practice of reporting CT uses sequential, thin 2-dimensional slices, which are projected in 3 different planes (axial, sagittal and coronal). Alternating between the 3 different planes and moving backwards and forwards within them, the reporting radiologist will create a "3D" image in the mind. This is a complex process which is time consuming, requires experience, and involves the mental processing of large amounts of information whilst physically scrolling with the mouse on different screens. Although current software will allow 3D reconstructions for further interrogation, these too are displayed on the flat screen. The innovative addition of virtual reality potentially by-passes much of the mental processing and mechanical scrolling and presents the radiologist with a "simple" image for interpretation.

A wide range of immersive virtual reality headset technologies have entered the market. Figure 6 ranks the major virtual

reality headsets (both those available now and those soon to be released) according to their respective prices at time of writing (November 2015).

All headsets listed in Figure 6 offer stereoscopic vision and head tracking capabilities but each offers slight variations and unique selling points such as customisability, cost, comfort and compatibility/integration with software. The Google Cardboard was tested using a variety of smartphones and the lack of processing power led to framerate limitations that were judged to be too debilitating for the virtual colonoscopy application. This issue was expected to apply to other smartphone-based headsets (all those with blue columns in Figure 6) and therefore these were not considered. Of the dedicated virtual reality headsets FOVE VR is of particular interest. It has not yet been released but offers the intriguing addition of built in eye tracking that makes it a consideration for future applications. Other high profile headsets not included in Figure 6 are Playstation VR and the Avegant Glyph. Playstation VR has not yet been released or associated with a price and is likely to be heavily geared toward development for the PlayStation game console platform – it was therefore not considered. The Avegant Glyph is a different implementation, employing retinal projection technology rather than OLED (organic light-emitting diode) screens. The projectors are embedded into a portable visor/headphone device primarily designed to project media from connected devices (such as smartphones) directly to the eye for an enhanced display. At present the Oculus Rift DK2 headset offered the best prospect for our application due to its more advanced stage of development, extensive community support, competitive price and integration with the Unity game engine. The commercialised version of the Oculus Rift has yet to be released but applications developed for the DK2 are expected to be easily transferable to the commercial version.
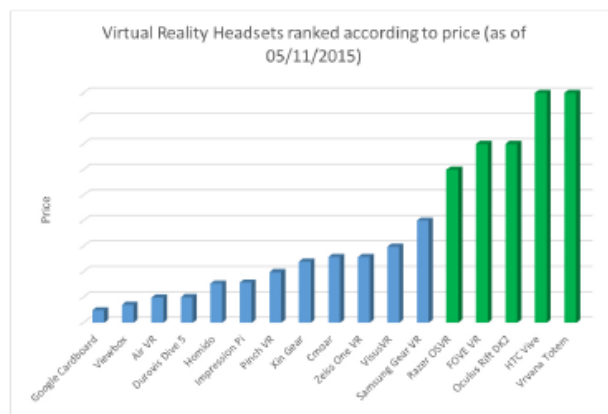
Figure 6. List of virtual reality devices ranked according to price. Columns in blue indicate devices which require a smartphone, columns in green indicate dedicated virtual reality headset devices. *Prices of some devices not yet released are speculative at time of writing (05/11/2015)*

The Oculus Rift DK2 performed very smoothly in the tests and the high specification PC and graphics card ensured lag free and artefact free viewing. The Unity game engine provided the flexibility for rapid development of the environment and accommodation of the Xbox game controller. Although application development within Unity involves a fairly steep learning curve for the uninitiated, the breadth of online resources helps considerably. At our current stage we are able to go from raw CT data to visualisation in the Oculus Rift within approximately 2 hours (without significant complications) and this is likely to reduce with increased experience. Furthermore, improvements in all areas can be expected as the technology progresses.

The conventional method of viewing colonoscopies (on a workstation monitor) presents some challenges. Firstly, the use of a mouse and keyboard, although familiar, is not an optimal user interface. Secondly, in colonoscopies the region of interest is the entire inner surface of the colon wall which is a large 3D surface area being represented by a series of 2D projections on a monitor. In order for a single projection to show the data effectively requires either a sufficiently wide angle view (*e.g.* fisheye-like lens) which distorts the image, or the user needs to be able to change the view quickly and efficiently while maintaining orientation – limited by the mouse/keyboard interface. Our pilot observations suggest the Oculus Rift offers a major improvement on these aspects:

- It presents the user with stereoscopic viewing ability and depth perception, potentially allowing for height-

ened localisation/characterisation of protrusions or lumps such as polyps.

- The head tracking gives a more natural means for camera reorientation, which the clinicians found particularly useful when examining areas behind haustral folds.

The design chosen also allowed the colonic mucosa to be viewed from both its luminal aspect and from the outside, the two together giving a more complete view. This novel feature of the ORVC proved useful to the radiologists and the gastroenterologist in detecting abnormalities. Additionally, the Oculus Rift provides a fully immersive experience by providing the user with a sense of "presence within the data", rather than as a passive distant observer as is the case when using a mouse/keyboard and a monitor screen. This is likely to reduce distraction and heighten awareness of their virtual surroundings. Finally, when viewing from within the colon it is not always possible for the user to be aware of their precise location. Despite this being made possible by the external camera which rapidly provided the triangulation necessary, the comments made by the radiologists suggest a need for advancing this feature in order to place specific features into context with the original CT slices.

The resolution of the DK2 display is 960×1080 to each eye. The DK2 OLED display has a visible grid-like appearance which may be attributed to a poor pixel fill factor (no. of pixels per unit area) effectively producing small gaps between pixels. Generally speaking this feature is more noticeable on still scenes with smaller objects. During the ORVC examination this issue is less noticeable probably due to the user's attention being drawn to larger objects spanning across a large number of pixels. Also the post-processing of the CT images used to create the virtual colonoscopy effectively smooths the data. For these reasons it is unlikely that this affects the interpretation of the virtual colonoscopy. However, when considering viewing high resolution, unprocessed CT slices this is expected to adversely affect interpretation. With subsequent releases of the technology the resolution and pixel fill factor will improve and its effect on CT slice reporting should be assessed.

The variety in data quality of the two ORVC studies gave an appreciation of a range of appearances to be expected when using this technique. From our own experience and the clinicians' comments, a summarised collation of advantages and disadvantages relative to the conventional virtual colonoscopy are noted below:

- Advantages
    (1) Immersive experience – more engaged with the data leading to improved awareness without distractions.
    (2) More intuitively interactive – instead of moving a mouse to change camera direction the natural movement of the head changes the view.
    (3) Stereoscopic vision to help detection of 3D undulations in the surface of the colon (*e.g.* polyps).
    (4) Improved examination around colonic folds.
    (5) No wide angle lens distortion as currently implemented in virtual colonoscopy software on 2D monitors.
    (6) Less mentally intensive experience leading to a potential for fatigue reduction.
    (7) View of the inside surface of the colon from the outside offers a potentially useful diagnostic angle.
- Drawbacks
    (1) User must rotate their body/head up to 180° adding an ergonomic complication and inconvenience.
    (2) Some users can find the experience mildly nauseating due to the mismatch between visual and vestibular inputs (*i.e.* visually moving while remaining physically stationary).
    (3) Lack of functionality to quickly and efficiently correlate findings between virtual colonoscopy and CT slices.
    (4) The current resolution displayed to each eye by the Oculus Rift DK2 (960×1080 pixels) and the poor pixel fill factor (no of pixels per unit area), combined with the proximity of the eye, creates a pixelated appearance that is not present on a standard monitor. While potentially distracting with the DK2 this is unlikely to be an issue as virtual reality headset technology matures.

Solutions to these drawbacks are beyond the scope of this paper, but improvements such as the option to orientate the camera along the direction of movement (such as in a roller-coaster) and incorporation of CT slice visualisation in the virtual world, have been considered and will form the basis of future work. The success of viewing the colon from the outside introduces another focus for further development. Currently the user is presented with a series of arbitrary, pre-set viewing positions but given the feedback, there is merit in offering a greater range of viewing angles and giving the user more positional control.

Implementation of the future developments above may also enhance the ability to stage cancer. Firstly, the ability to review the original CT data is important to help determine the

40

extent/spread of the lesion. Secondly, additional information could be presented to the radiologist via segmentation and external observation of the outer lining of the colon. Such a view could highlight prominent undulations in the external surface of the colon to help determine whether the cancer is of an early stage (T1, T2 – contained within the inner layers of the bowel wall) or later stage (T3, T4 – penetrated the outer layers of the bowel wall). However, segmentation of the outer wall of the colon is likely to pose significant challenges due to the reduced contrast between the colon and surrounding tissue compared to its gas-filled lumen. Nonetheless this remains a consideration for the future.

At this early stage it is difficult to comment on any improvement in examination time offered relative to the conventional virtual colonoscopy. However, with the ease of camera orientation offered by the head tracking capability of the Oculus Rift and as more experience is acquired, a decrease in examination time is conceivable. The transit speed through the lumen of the colon is ultimately limited by the operator's susceptibility to nausea from simulation sickness. For each of the two studies presented the transit speed was optimised for a single operator known to be sensitive to simulation sickness with the expectation that this speed was comfortable for most other operators. This proved to be the case as none of the clinical operators experienced nausea during the examinations. The nauseating effects are further reduced with the functionality of controlling the position using the D-pad on the Xbox controller. This feature may be optimised further by allowing the user to change the transit speed and sensitivity of the D-pad buttons.

This preliminary work has highlighted the benefits and challenges of virtual colonoscopy in an immersive environment and indicated further steps that are necessary to make the ORVC a more viable diagnostic technique. Upon completion of the development work the trajectory is toward a prospective pilot study to compare conventional and Oculus Rift virtual colonoscopies. Assessment of this new technique with the use of the Receiver Operative Curve (ROC) would help define its place in the rapidly developing world of diagnostic technology.

5. CONCLUSION

A mechanism for viewing virtual colonoscopies with an Oculus Rift has been successfully implemented and trialled on three clinicians. Initial testing has produced promising reactions from clinical colleagues and confirms the potential of this novel visualisation method. It has been acknowledged that several improvements are necessary before this technique is likely to be of significant clinical benefit but early potential has been demonstrated. Overall, the feedback is one of support, providing encouragement for pursuing this work further. After incorporation of the necessary developments, the next steps will involve a semi-quantitative pilot study which will aim to compare clinicians' experiences and reporting confidence with ORVC and traditional virtual colonoscopy.

ACKNOWLEDGEMENTS

CONFLICTS OF INTEREST DISCLOSURE

The authors declare that they have no competing interests.

REFERENCES

[1] Bowel Cancer Mortality Statistics [Internet]. London: Cancer Research UK; c2002-2015 [cited 2015 Sept 12]. Available from: http://www.cancerresearchuk.org/health-professional/cancer-statistics/statistics-by-cancer-type/bowel-cancer/mortality#heading-Two

[2] Levin B, Lieberman DA, McFarland B, et al. Screening and Surveillance for the Early Detection of Colorectal Cancer and Adenomatous Polyps, 2008: A Joint Guideline From the American Cancer Society, the US Multi-Society Task Force on Colorectal Cancer, and the American College of Radiology. Gastroenterology. 2008; 134: 1570-95. PMid: 18384785. http://dx.doi.org/10.1053/j.gastro.2008.02.002

[3] Pickhardt PJ, Hassan C, Halligan S, et al. Colorectal Cancer: CT Colonography and Colonoscopy for Detection – Systematic Review and Meta-Analysis. Radiology. 2011; 259: 393-405. http://dx.doi.org/10.1148/radiol.11101887

[4] Halligan S, Altman DG, Taylor SA, et al. CT Colonography in the Detection of Colorectal Polyps and Cancer: Systematic Review, Meta-Analysis, and Proposed Minimum Data Set for Study Level Reporting. Radiology. 2005; 237: 893-904. http://dx.doi.org/10.1148/radiol.2373050176

[5] d. Haan MC, v. Gelder RE, Graser A, et al. Diagnostic value of CT-colonography as compared to colonoscopy in an asymptomatic screening population: a meta-analysis. European Radiology. 2011; 21: 1747-63. http://dx.doi.org/10.1007/s00330-011-2104-8

[6] Barish MA, Soto JA, Ferrucci JT. Consensus on current clinical practice of virtual colonoscopy. Am J Roentgenol. 2005; 184: 786-792. PMid: 15728598. http://dx.doi.org/10.2214/ajr.184.3.01840786

[7] Ball S, Bluteau P, Clouder L, et al. myShoes: An Immersive Simulation of Dementia. Proceedings of the 10th International Conference on E-Learning (ICEL 2015); 2015 June 25-26; Nassau, Bahamas. Sonning Common, UK: Academic Conferences and Publishing International Limited; 2015.

[8] Chiarovano E, de Waele C, MacDougall HG, et al. Maintaining Balance when Looking at a Virtual Reality Three-Dimensional Display of a Field of Moving Dots or at a Virtual Reality Scene. Frontiers in Neurology. 2015; 6: 164. PMid: 26284023. http://dx.doi.org/10.3389/fneur.2015.00164

[9] Fulvio J, Wang M, Rokers B. Head tracking in virtual reality displays reduces the misperception of 3D motion. Journal of Vision. 2015; 15: 1180. PMid: 26326868. http://dx.doi.org/10.1167/15.12.1180

[10] Hoffman HG, Meyer WJ, Ramirez M, et al. Feasibility of Articulated Arm Mounted Oculus Rift Virtual Reality Goggles for Adjunctive Pain Control During Occupational Therapy in Pediatric Burn Patients. Cyberpsychology Behavior and Social Networking. 2014; 17: 397-401. PMid: 24892204. http://dx.doi.org/10.1089/cyber.2014.0058

[11] Kim J, Chung CYL, Nakamura S, et al. The Oculus Rift: a cost-effective tool for studying visual-vestibular interactions in self-motion perception. Frontiers in Psychology. 2015; 6: 248. PMid: 25821438. http://dx.doi.org/10.3389/fpsyg.2015.00248

[12] Xu X, Chen KB, Lin J, et al. The accuracy of the Oculus Rift virtual reality head-mounted display during cervical spine mobility measurement. Journal of Biomechanics. 2015; 48: 721-4. PMid: 25636855. http://dx.doi.org/10.1016/j.jbiomech.2015.01.005

[13] Mirhosseini K, Sun Q, Gurijala KC, et al. Benefits of 3D immersion for virtual colonoscopy. Proceedings of: 3DVis, 2014 IEEE VIS International Workshop; 2014 Nov 9; Paris, France. IEEE. 2014. 75-79 p. http://dx.doi.org/10.1109/3DVis.2014.7160105

[14] Asfaw A, Gustafsson-Wright E, Vander Gaag J. Willingness to pay for health insurance: An analysis of the potential market for new low-cost health insurance products in Namibia, Amsterdam Institute for International Development. 2008; 1-22. http://dx.doi.org/10.1016/j.amjmed.2006.05.061

[15] Lieberman D. Progress and Challenges in Colorectal Cancer Screening and Surveillance. Gastroenterology. 2010; 138: 2115-26. http://dx.doi.org/10.1053/j.gastro.2010.02.006

[16] Graser A, Stieber P, Nagel D, et al. Comparison of CT colonography, colonoscopy, sigmoidoscopy and faecal occult blood tests for the detection of advanced adenoma in an average risk population. Gut. 2009; 58: 241-8. http://dx.doi.org/10.1136/gut.2008.156448

[17] Chapman K, editor. Guidelines for the use of imaging in the NHS Bowel Cancer Screening Programme, second edition. NHS Cancer Screening Programmes; 2012 Nov.

240

References

[1] D. Randall, C. Strik, H. v. Goor, J. B. Joosten, R. Gillott, P. A. Spencer, J. W. Fenner and K. D. Bardhan, "Mo2016 Intra-Abdominal Adhesions: Identifying the "Sticking Point(s)" Using Novel Cine-Magnetic Resonance Image Analysis. Pilot Results," *Gastroenterology,* vol. 148, no. 4, pp. S-769, 2015.

[2] D. Randall, J. Fenner, R. Gillott, P. Spencer, C. Strik, H. Goor, F. Joosten and K. Bardhan, "PTH-243 Intra-abdominal adhesions: identifying the "sticking point(s)" using novel cine-magnetic resonance image analysis. pilot results," *Gut,* vol. 64, p. A517, 2015.

[3] D. Randall, J. Fenner, R. Gillott, R. t. Broek, C. Strik, P. Spencer and K. D. Bardhan, "A Novel Diagnostic Aid for Detection of Intra-Abdominal Adhesions to the Anterior Abdominal Wall Using Dynamic Magnetic Resonance Imaging," *Gastroenterology Research and Practice,* vol. 2016, p. Article ID 2523768, 2016.

[4] D. Randall, F. Joosten, R. ten Broek, R. Gillott, K. D. Bardhan, C. Strik, W. Prins, H. van Goor and J. Fenner, "A novel diagnostic aid for intra-abdominal adhesion detection in cine-MR imaging: Pilot study and initial diagnostic impressions," *British Journal of Radiology,* 2017.

[5] A. D. Jeays, P. V. Lawford, R. Gillott, P. Spencer, D. C. Barber, K. D. Bardhan and D. R. Hose, "Characterisation of the haemodynamics of the superior mesenteric artery," *J Biomech,* vol. 40, no. 9, pp. 1916-26, 2007.

[6] B. Wright, "The Use of Image Registration to Aid Identification of Abdominal Adhesions," University of Sheffield, Sheffield, 2010.

[7] M. A. Weibel and G. Majino, "Peritoneal adhesions and their relation to abdominal surgery: A postmortem study," *The American Journal of Surgery,* vol. 126, no. 3, pp. 345-353, 1973.

[8] K. Okabayashi, H. Ashrafian, E. Zacharakis, H. Hasegawa, Y. Kitagawa, T. Athanasiou and A. Drazi, "Adhesions after abdominal surgery: a systematic review of the incidence, distribution and severity," *Surg. Today,* 2013.

[9]   H. Ellis, B. Moran, J. N. Thompson, M. C. Parker, M. S. Wilson, D. Menzies, A. McGuire, A. M. Lower, R. J. Hawthorn, F. O'Brien, S. Buchan and A. M. Crowe, "Adhesion-related hospital readmissions after abdominal and pelvic surgery: a retrospective cohort study," *The Lancet,* vol. 353, no. 9163, pp. 1476-1480, 1999.

[10]   D. Bruggmann, G. Tchartchian and A. Hackethal, "Intra-abdominal Adhesions: Definition, Origin, Significance in Surgical Practice, and Treatment Options," *Dtsch Arztebl Int.,* vol. 107, no. 44, pp. 769-775, 2010.

[11]   X. Zong, S. Li, E. Chen, B. Garlick, K. Kim, D. Fang, J. Chiu, T. Zimmerman, C. Brathwaite, B. S. Hsiao and B. Chu, "Prevention of Postsurgery-Induced Abdominal Adhesions by Electrospun Bioabsorbable Nanofibrous Poly(lactide-co-glycolide)-Based Membranes," *Annals of Surgery,* vol. 240, no. 5, pp. 910-915, 2004.

[12]   G. S. diZerega and J. D. Campeau, "Peritoneal repair and post-surgical adhesion formation," *Hum Reprod Update.,* vol. 7, no. 6, pp. 547-555, 2001.

[13]   J. Dubuisson, R. Botchorishvili, S. Perrette, N. Bourdel, K. Jardon, B. Rabischong, M. Canis and G. Mage, "Incidence of intraabdominal adhesions in a continuous series of 1000 laparoscopic procedures," *American Journal of Obstetrics and Gynecology,* vol. 203, no. 2, pp. 111.e1-111.e3, 2010.

[14]   T. Liakakos, N. Thomakos, P. M. Fine, C. Dervenis and R. L. Young, "Peritoneal Adhesions: Etiology, Pathophysiology, and Clinical Significance," *Digestive Surgery,* vol. 18, pp. 260-273, 2001.

[15]   D. E. Beck, F. G. Opelka, H. R. Bailey, S. M. Rauh and C. L. Pashos, "Incidence of small-bowel obstruction and adhesiolysis after open colorectal and general surgery," *Dis Colon Rectum.,* vol. 42, no. 2, pp. 241-8, 1999.

[16]   N. F. Ray, W. G. Denton, M. Thamer, S. C. Henderson and S. Perry, "Abdominal Adhesiolysis: Inpatient Care and Expenditures in the United States in 1994," *Journal of the American College of Surgeons,* vol. 186, no. 1, pp. 1-9, 1998.

[17]   B. Tingstedt, J. Isaksson and R. Andersson, "Long-term follow-up and cost analysis following surgery for small bowel obstruction caused by intra-abdominal adhesions," *British journal of Surgery,* vol. 94, no. 6, pp. 743-8, 2007.

[18]   D. Stanciu and D. Menzies, "The magnitude of adhesion-related problems," *Colorectal Disease,* vol. 9, no. sup 2, 2007.

[19] F. Catena, S. D. Saverio, M. D. Kelly, W. L. Biffl, L. Ansaloni, V. Mandala, G. C. Velmahos, M. Sartelli, G. Tugnoli, M. Lupo, S. Mandala, A. D. Pinna, P. H. Sugarbaker, H. V. Goor, E. E. Moore and J. Jeekel, "Bologna Guidelines for Diagnosis and Management of Adhesive Small Bowel Obstruction (ASBO): 2010 Evidence-Based Guidelines of the World Society of Emergency Surgery," *World Journal of Emergency Surgery,* vol. 6, no. 5, 2011.

[20] A. Lienemann, D. Sprenger, H. O. Steitz, M. Korell and M. Reiser, "Detection and Mapping of Intraabdominal Adhesions by Using Functional Cine MR Imaging: Preliminary Results," *Radiology,* vol. 217, pp. 421-5, 2000.

[21] B. Sigel, R. M. Golub, L. A. Loiacono, R. E. Parsons, I. Kodama, J. Machi, J. Justin, A. K. Sachdeva and H. A. Zaren, "Technique of ultrasonic detection and mapping of abdominal wall adhesions," *Surg. Endosc.,* vol. 5, pp. 161-165, 1991.

[22] F. F. Tu, G. M. Lamvu, K. E. Hartmann and J. F. Steege, "Preoperative ultrasound to predict infraumbilical adhesions: A study of diagnostic accuracy," *American Journal of Obstetrics & Gynecology,* vol. 192, no. 1, pp. 74-79, 2005.

[23] J. Conze, S. Truong and V. Schumpelick, "Value of Ultrasonography in Diagnosis of Peritoneal Adhesions," in *Peritoneal Adhesions*, Berlin, Springer-Verlag Berlin Heidelberg, 1997, pp. 163-171.

[24] R. V. Kolecki, R. M. Golub, B. Sigel, J. Machi, H. Kitamura, T. Hosokawa, J. Justin, J. Schwartz and H. A. Zaren, "Accuracy of viscera slide detection of abdominal wall adhesions by ultrasound," *Surgical Endoscopy,* vol. 8, no. 8, pp. 871-4, 1994.

[25] R. Uberoi, H. D'Costa, C. Brown and P. Dubbins, "Visceral slide for intraperitoneal adhesions? A prospective study in 48 patients with surgical correlation," *Journal of Clinical Ultrasound,* vol. 23, no. 6, pp. 363-6, 1995.

[26] D. Piccolboni, F. Ciccone and A. Settembre, "High resolution ultrasound for pre-operative detection of intraperitoneal adhesions: An invaluable diagnostic tool for the general and laparoscopic surgeon," *Journal of Ultrasound,* vol. 12, no. 4, pp. 148-150, 2009.

[27] C. H. Nezhat, E. C. Dun, A. Katz and F. A. Wieser, "Office visceral slide test compared with two perioperative tests for predicting periumbilical adhesions," *Obstet Gynecol.,* vol. 123, no. 5, pp. 1049-56, 2014.

[28] N. Braun, M. D. Alscher, M. Kimmel, K. Amann and M. Buttner, "Encapsulating Peritoneal Sclerosis - An Overview," *Nephrologie & Therapeutique,* vol. 7, pp. 162-171, 2011.

[29] T. Augustine, P. W. Brown, S. D. Davies, A. M. Summers and M. E. Wilkie, "Encapsulating Peritoneal Sclerosis: Clinical Significance and Implications," *Nephron Clinical Practice,* vol. 111, pp. c149-c154, 2009.

[30] S. Buhmann-Kirchhoff, R. Lang, C. Kirchhoff, H. O. Steitz, K. W. Jauch, M. Reiser and A. Lienemann, "Functional cine MR imaging for the detection and mapping of intraabdominal adhesions: method and surgical correlation," *Gastrointestinal,* vol. 18, pp. 1215-1223, 2008.

[31] R. A. Lang, S. Buhmann, A. Hopman, H.-O. Steitz, A. Lienemann, M. F. Reiser, K.-W. Jauch and T. P. Huttl, "Cine-MRI detection of intraabdominal adhesions: correlation with intraoperative findings in 89 consecutive cases," *Surg. Endosc.,* vol. 22, pp. 2455-2461, 2008.

[32] N. B. Zinther, A. Zeuten, E. Marinovskij, M. Haislund and H. Friis-Andersen, "Detection of abdominal wall adhesions using visceral slide," *Surg Endosc,* vol. 24, pp. 3161-6, 2010.

[33] B. Wright, A. Summers, J. Fenner, R. Gillot, C. E. Hutchinson, P. A. Spencer, M. Wilkie, H. Hurst, S. Herrick, P. Brenchley, T. Augustine and K. D. Bardhan, "Initial Observations Using a Novel "Cine" Magnetic Resonance Imaging Technique to Detect Changes in Abdominal Motion Caused by Encapsulating Peritoneal Sclerosis," *Perit Dial Int.,* vol. 31, pp. 287-290, 2011.

[34] S. Stuart, "Can Dettection of Changes in the Motion of Abdominal Contents Using Cine MRI Help in the Management of Encapsulating Peritoneal Sclerosis," *Peritoneal Dialysis International,* vol. 31, pp. 267-8, 2011.

[35] B. C. Ward and A. Panitch, "Abdominal Adhesions: Current and Novel Therapies," *Journal of Surgical Research,* vol. 165, no. 1, pp. 91-111, 2011.

[36] D. E. Beck, "The role of Seprafilm bioresorbable membrane in adhesion prevention," *Eur J Surg Suppl.,* vol. 577, pp. 49-55, 1997.

[37] R. Mactier and M. Brown, "Encapsulating Peritoneal Sclerosis in Incident PD Patients in Scotland," in *Progress in Peritoneal Dialysis*, InTech, 2011, pp. 157-166.

[38] S. Guest, "Tamoxifen Therapy for Encapsulating Peritoneal Sclerosis: Mechanism of Action and Update on Clinical Experiences," *Perit Dial Int.,* vol. 29, no. 3, pp. 252-5, 2009.

[39] A. K. Jain, P. Blake, P. Cordy and A. X. Garg, "Global Trends in Rates of Peritoneal Dialysis," *J Am Soc Nephrol.,* pp. 533-544, 2012.

[40] H. Kawanishi, "Encapsulating Peritoneal Sclerosis in Japan: Prospective Multicentre Controlled Study," *Perit Dial Int,* vol. 21, no. sup 3, pp. S67-S71, 2001.

[41] H. Kawanishi, Y. Kawaguchi, H. Fukui, S. Hara, A. Imada, H. Kubo, M. Kin, M. Nakamoto, S. Ohira and T. Shoji, "Encapsulating peritoneal sclerosis in Japan: A prospective, controlled, multicenter study," *American Journal of Kidney Diseases,* pp. 729-737, 2004.

[42] A. M. Summers, M. J. Clancy, F. Syed, N. Harwood, P. E. C. Brenchley, T. Augustine, H. Riad, A. J. Hutchison, P. Taylor, R. Pearson and R. Gokal, "Single-center experience of encapsulating peritoneal sclerosis in patients on peritoneal dialysis for end-stage renal failure," *Kidney International,* pp. 2381-2388, 2005.

[43] M. C. Brown, K. Simpson, J. J. Kerssens and R. A. Mactier, "Encapsulating Peritoneal Sclerosis in the New Millennium: A National Cohort Study," *Clin J Am Soc Nephrol,* vol. 4, pp. 1222-9, 2009.

[44] C. Gayomali, U. Hussein, S. F. Cameron, Z. Protopapas and F. O. Finkelstein, "Incidence of Encapsulating Peritoneal Sclerosis: A Single-center Experience with Long-Term Peritoneal Dialysis in the United States," *Perit Dial Int,* vol. 31, no. 3, pp. 279-286, 2011.

[45] R. J. Rigby and C. M. Hawley, "Sclerosing Peritonitis: The Experience in Australia," *Nephrol Dial Transplant,* vol. 13, pp. 154-159, 1998.

[46] S. M. Habib, M. G. H. Betjes, M. W. J. A. Fieren, E. W. Boeschoten, A. C. Abrahams, W. H. Boer, D. G. Struijk, W. Ruger, C. Krikke, R. Westerhuis, R. G. L. de Sevaux, F. m. van der Sande, A. Gaasbeek and M. R. Korte, "Management of encapsulating peritoneal sclerosis: a guideline on optimal and uniform treatment," *The Netherlands Journal of Medicine,* vol. 69, no. 11, pp. 500-7, 2011.

[47] Y. Kawaguchi, H. Kawanishi, S. Mujais, N. Topley and D. G. Oreopoulos, "Encapsulating Peritoneal Sclerosis: Definition, Etiology, Diagnosis and Treatment," *Peritoneal Dialysis International,* vol. 20, no. Sup 4, 2000.

[48] R. M. Tarzi, A. Lim, S. Moser, S. Ahmad, A. George, G. Balasubramaniam, E. J. Clutterbuck, W. Gedroyc and E. A. Brown, "Assessing the Validity of an Abdominal CT Scoring System in the Diagnosis of Encapsulating Peritoneal Sclerosis," *Clin J Am Soc Nephrol.,* vol. 3, no. 6, pp. 1702-1710, 2008.

[49] A. Vlijm, J. Stoker, S. Bipat, A. M. Spijkerboer, S. S. K. S. Phoa, R. Maes, D. G. Struijk and R. T. Krediet, "Computed tomography findings haracteristic for encapsulating peritoneal sclerosis: A case control study," *Peritoneal Dialysis Interntional,* vol. 29, no. 5, pp. 517-522, 2009.

[50] C. Goodlad, R. Tarzi, W. Gedroyc, A. Lim, S. Moser and E. A. Brown, "Screening for encapsulating peritoneal sclerosis in patients on peritoneal dialysis: role of CT scanning," *Nephrology Dialysis Transplantation,* vol. 26, no. 4, pp. 1374-9, 2011.

[51] T. Sawada, Y. Ishii, I. Nakajima, S. Fuchinoue, K. Kubota and S. Teraoka, "An experimental model of encapsulating peritoneal sclerosis," *Peritoneal Dialysis International,* vol. 29, no. sup 2, 2008.

[52] H. Arai, A. Furusu, T. Nishino, Y. Obata, Y. Nakazawa, M. Nakazawa, M. Hirose, K. Abe, T. Koji and S. Kohno, "Thalidomide prevents the progression of peritoneal fibrosis in mice," *Acta Histochem Cytochem,* vol. 44, no. 2, pp. 51-60, 2011.

[53] M. L. Lambie, B. John, L. Mushahar, C. Huckvale and S. J. Davies, "The peritoneal osmotic conductance is low well before the diagnosis of encapsulating peritoneal sclerosis is made," *Kidney International,* vol. 78, pp. 611-618, 2010.

[54] W. B. Dunn, A. Summers, M. Brown, R. Goodacre, M. Lambie, T. Johnson, M. Wilkie, S. Davies, N. Topley and P. Brenchley, "Proof-of-principle study to detect metabolic changes in peritoneal dialysis effluent in patients who develop encapsulating peritoneal sclerosis," *Nephrol. Dial. Transplant,* vol. 27, no. 6, pp. 2502-2510, 2012.

[55] M. Moriishi and H. Kawanishi, "Fibrin degradation products are a useful marker for the risk of encapsulating peritoneal sclerosis," *Advances in Peritoneal Dialysis,* vol. 24, pp. 56-59, 2008.

[56] K. Yokoyama, H. Yoshida, N. Matsuo, Y. Maruyama, Y. Kawamura, R. Yamamoto, K. Hanaoka, M. Ikeda, H. Yamamoto, M. Nakayama, Y. Kawaguchi and T. Hosoya, "Serum beta2 microglobulin (beta2MG) level is a potential predictor for encapsulating peritoneal sclerosis (EPS) in peritoneal dialysis patients," *Clinical Nephrology,* vol. 69, no. 2, pp. 121-6, 2008.

[57] N. Braun, D. M. Alscher, P. Fritz, I. Edenhofer, M. Kimmel, A. Gaspert, F. Reimold, B. Bode-Lesniewska, U. Ziegler, D. Biegger, R. P. Wuthrich and S. Segerer, "Podoplanin-positive cells are a hallmark of encapsulating peritoneal sclerosis," *Nephrology Dialysis Transplantation,* vol. 26, no. 3, pp. 1033-1041, 2011.

[58] D. E. Sampimon, A. M. Coester, D. G. Struijk and R. T. Krediet, "The time course of peritoneal transport parameters in peritoneal dialysis patients who develop encapsulating peritoneal sclerosis," *Nephrology Dialysis Transplantation,* vol. 26, pp. 291-8, 2010.

[59] D. E. Sampimon, M. R. Korte, D. L. Barreto, A. Vlijm, R. de Waart, D. G. Struijk and R. T. Krediet, "Early Diagnosis Markers for Encapsulating Peritoneal Sclerosis: A Case-control Study," *Peritoneal Dialysis International,* vol. 30, no. 2, pp. 163-9, 2010.

[60] G. Woodrow, T. Augustine, E. A. Brown, M. Cowling, N. El-Sherbini, H. Hurst, P. F. Williams and R. Williams, "UK Encapsulating Peritoneal Sclerosis Clinical Practice Guidelines," UK EPS Clinical Guidelines Group, 2009.

[61] J. H. Hansson, S. F. Cameron, Z. Protopapas and R. Mehrotra, "Encapsulating Peritoneal Sclerosis (EPS)," April 2011. [Online]. Available: http://ispd.org/NAC/wp-content/uploads/2010/11/Encapsulating-Peritoneal-Sclerosis-Hansson-April-2011.pdf. [Accessed 25 June 2013].

[62] A. S. Hollman, M. A. McMillian, J. D. Briggs, B. J. R. Junor and P. Morley, "Ultrasound Changes in Sclerosing Peritonitis Following Continuous Ambulatory Peritoneal Dialysis," *Clinical Radiology,* vol. 43, pp. 176-9, 1991.

[63] J. Fenner, B. Wright, J. Emberey, P. Spencer, R. Gillot, A. Summers, C. Hutchinson, P. Lawford, P. Brenchley and K. D. Bardhan, "Towards radiological diagnosis of abdominal adhesions based on motion signatures derived from sequences of cine-MRI images," *European Journal of Medical Physics,* pp. 1-11, 2013.

[64] L. Sajn and M. Kukar, "Image processing and machine learning for fully automated probabilistic evaluation of medical images," *Computational Methods and Programs Biomedicine,* vol. 104, no. 3, pp. e75-e86, 2011.

[65] A. Lungu, J. M. Wild, D. Capener, D. G. Kiely, A. J. Swift and D. R. Hose, "MRI model-based non-invasive differential diagnosis in pulmonary hypertension," *Journal of Biomechanics,* vol. 47, no. 12, pp. 2941-2947, 2014.

[66] A. Norouzi, M. S. M. Rahim, A. Altameem, T. Saba, A. E. Rad, A. Rehman and M. Uddin, "Medical Image Segmentation Methods, Algorithms and Applications," *IETE Tecchnical Review,* vol. 31, no. 3, pp. 199-213, 2014.

[67] D. L. G. Hill, P. G. Batchelor, M. Holden and D. J. Hawkes, "Medical image registration," *Physics in Medicine and Biology,* vol. 46, pp. R1-R45, 2001.

[68] A. Sotiras, C. Davatazikos and N. Paragios, "Deformable Medical Image Registration: A Survey," Informatics Mathematics Inria, 2012.

[69] A. J. B. Maintz and M. A. Viergever, "A survey of medical image registration," *Medical Image Analysis,* vol. 2, no. 1, pp. 1-36, 1998.

[70] V. R. S. Mani and S. Arivazhagan, "Survey of Medical Image Registration," *Journal of Biomedical Engineering and Technology,* vol. 1, no. 2, pp. 8-25, 2013.

[71] D. C. Barber and D. R. Hose, "Automatic Segmentation of Medical Images Using Image Registration: Diagnostic and Simulation Applications," *Journal of Medical Engineering and Technology,* vol. 29, no. 2, pp. 53-63, 2005.

[72] M. Freiman, S. D. Voss and S. K. Warfield, "Abdominal Images Non-rigid Registration Using Local-Affine Diffeomorphic Demons," *Lecture Notes in Computer Science,* vol. 7029, pp. 116-124, 2012.

[73] A. Elnakib, G. Gimel'farb, J. Suri and A. El-Baz, "Medical Image Segmentation: A Brief Survey," in *Multi Modality State-of-the-Art Medical Image Segmentation and Registration Methodologies*, New York, Springer Science + Business Media, 2011, pp. 1-39.

[74] Z. Ma, J. M. R. S. Tavares, R. N. Jorge and T. Mascarenhas, "A review of algorithms for medical image segmentation and their applications to the female pelvic cavity," *Computer Methods in Biomechanics and Biomedical Engineering,* vol. 13, no. 2, pp. 235-246, 2010.

[75] A. Norouzi, M. S. M. Rahim, A. Altameen, T. Saba, A. E. Rad, A. Rehman and M. Uddin, "Medical Image Segmentation Methods, Algorithms, and Applications," *IETE Technical Review,* vol. 31, no. 3, pp. 199-213, 2014.

[76] D. J. Withey and Z. J. Koles, "A Review of Medical Image Segmentation: Methods and Available Software," *International Jounral of Bioelectromagnetism,* vol. 10, no. 3, pp. 125-148, 2008.

[77] N. Sharma and L. M. Aggarwal, "Automated medical image segmentation techniques," *Journal of Medical Physics,* vol. 35, no. 1, pp. 3-14, 2010.

[78] Z. Ma, J. M. R. S. Tavares and R. M. Natal Jorge, "A review on the current segmentation algorithms for medical images," *Computer Methods in Biomechanics and Biomedical Engineering,* vol. 13, no. 2, pp. 235-246, 2010.

[79] U. Clarenz, M. Droske, S. Henn, M. Rumpf and K. Witsch, "Computational methods for nonlinear image registration," in *Mathematical Models for Registration and Applications to Medical Imaging*, Berlin, Springer, 2006, pp. 81-101.

[80] B. Fischer and J. Modersitzki, "Ill-posed medicine - an introduction to image registration," *Inverse Problems,* vol. 24, 2008.

[81] R. Bajcsy and S. Kovacic, "Multiresolution Elastic Matching," *Computer Vision, Graphics and Image Processing,* vol. 46, no. 1, pp. 1-21, 1989.

[82] T. Schormann, S. Henn and K. Zilles, "A new approach to fast elastic alignment with applications to human brains," *Lecture Notes in Computer Science,* vol. 1131, pp. 337-342, 1996.

[83] B. Zitova and J. Flusser, "Image registration methods: a survey," *Image and Vision Computing,* vol. 21, pp. 977-1000, 2003.

[84] F. Odille, A. Menys, A. Ahmed, S. Punwani, S. A. Taylor and D. Atkinson, "Quantitative assessment of small bowel motility by nonrigid registration of dynamic MR images," *Magnetic Resonance in Medicine,* vol. 68, no. 3, pp. 783-793, 2012.

[85] A. R. Osorio, R. A. Isoardi and G. Mato, "Deformable CT registration using Fourier basis functions in 3D," in *23rd SIBGRAPI - Conference on Graphics, Patterns and Images*, 2010.

[86] D. F. Pace, M. Niethammer and S. R. Aylward, "Sliding Geometries in Deformable Image Registration," *Lecture Notes in Computer Science,* vol. 7029, pp. 141-8, 2011.

[87] J. V. Hajnal, D. L. G. Hill and D. J. Hawkes, Medical Image Registration, Boca Raton: CRC Press LLC, 2001.

[88] J. Modersitzki, Numerical Methods for Image Registration, New York: Oxford University Press, 2004.

[89] M. Bro-Neilsen and C. Gramkow, "Fast Fluid Registration of Medical Images," *Lecture Notes in Computer Science,* vol. 1131, pp. 265-276, 1996.

[90] G. E. Christensen, R. D. Rabbitt and M. I. Miller, "Deformable Templates Using Large Deformation Kinematics," *IEEE Transactions on Image Processing,* vol. 5, no. 10, pp. 1435-1447, 1996.

[91] S. Tang and T. Jiang, "Nonrigid Registration of Medical Image by Maxwell Model of Viscoelasticity," in *IEEE International Symposium on Biomedical Imaging: Nano to Macro*, 2004.

[92] D. C. Barber, E. Oubel, A. F. Frangi and D. R. Hose, "Efficient computational fluid dynamics mesh generation by image registration," *Med Image Anal.,* vol. 11, no. 6, pp. 648-662, 2007.

[93] D. C. Barber, "Automatic alignment of radionuclide images," *Physics in Medicine and Biology,* vol. 27, no. 3, pp. 387-396, 1982.

[94] F. C. Horn, M. H. Deppe, H. Marshall, J. Parra-Robles and J. M. Wild, "Quantification of regional fractional ventilation in human subjects by measurement of hyperpolarized 3He washout with 2D and 3D MRI," *Journal of Applied Physiology,* vol. 116, no. 2, pp. 129-139, 2014.

[95] P. Lamata, S. Niederer, D. Nordsletten, D. C. Barber, I. Roy, D. R. Hose and N. Smith, "An accurate, fast and robust method to generate patient-specific cubic Hermite meshes," *Medical Image Analysis,* vol. 15, no. 6, pp. 801-13, 2011.

[96] B. B. Avants, "Advanced Normalization Tools," stnava, [Online]. Available: http://stnava.github.io/ANTs/. [Accessed 31 03 2017].

[97] V. Delmon, S. Rit, R. Pinho and D. Sarrut, "Registration of sliding objects using direction dependent B-splines decomposition," *Physics in Medicine and Biology,* vol. 58, pp. 1303-1314, 2013.

[98] B. W. Papiez, M. P. Heinrich, J. Fehrenbach, L. Risser and J. A. Schnabel, "An implicit sliding-motion preserving regularisation via bilateral filtering for deformable image registration," *Medical Image Analysis,* vol. 18, pp. 1299-1311, 2014.

[99] Y. Xie, M. Chao and G. Xiong, "Deformable Image Registration of Liver With Consideration of Lung SLiding Motion," *Medical Physics,* vol. 38, no. 10, pp. 5351-61, 2011.

[100] V. Vishnevskiy, T. Gass, G. Szekely and O. Goksel, "Total Variation Regularization of Displacements in Parametric Image Registration," *Lecture Notes Computer Science,* vol. 8676, pp. 211-220, 2014.

[101] A. Lausch, M. Ebrahimi and A. Martel, "Image Registration for Abdominal Dynamic Contrast-enhanced Magnetic Resonance Images," in *Proceedings of the 8th IEEE International Symposium on Biomedical Imaging: From Nano to Macro, ISBI 2011*, Illinois, 2011.

[102] S. Kiriyanthan, K. Fundana, T. Majeed and P. C. Cattin, "Discontinuity Preserving Image Registration through Motion Segmentation: A Primal-Dual Approach," *Computational and Mathematical Methods in Medicine,* vol. 2016, p. 9504949, 2016.

[103] R. Amelon, K. Cao, J. M. Reinhardt, G. E. Christensen and M. Raghavan, "Estimation of lung lobar sliding using image registration," in *Medical Imaging 2012: Biomedical Applications in Molecular, Structural and Functional Imaging*, San Diego, 2012.

[104] K. Ding, Y. Yin, K. Cao, G. E. Christensen, C.-L. Lin, E. A. Hoffman and J. M. Reinhardt, "Evaluation of Lobar Biomechanics during Respiration using Image Registration," *Medical Image Computing and Computer-Assisted Intervention,* vol. 12, no. 1, pp. 739-746, 2009.

[105] S. Ukil and J. M. Reinhardt, "Anatomy-Guided Lung Lobe Segmentation in X-Ray CT Images," *IEEE Transactions on Medical Imaging,* vol. 28, no. 2, pp. 202-214, 2009.

[106] DICOM Standards Committee, NEMA, "DICOM PS3 2017a," NEMA, Rosslyn, Virginia, 2017.

[107] J. Canny, "A Computational Approach to Edge Detection," *IEEE Transactions on Pattern Analysis and Machine Intelligence,* Vols. PAMI-8, no. 6, pp. 679-698, 1986.

[108] A. M. C. Ltd, "Respiratory Gating System AZ-733VI (Overview) - Anzai Medical Co. Ltd," [Online]. Available: http://www.anzai-med.co.jp/en/product/item/az733vi/index.html. [Accessed 1st July 2017].

[109] "The Medical Devices Regulations 2002," The Stationery Office Limited, London, 2002.

[110] D. Randall, P. Metherall, K. D. Bardhan, P. Spencer, R. Gillott, R. de Noronha and J. W. Fenner, "The Oculus Rift virtual colonoscopy: introducing a new technology and initial impressions," *Journal of Biomedical Graphics and Computing,* vol. 6, no. 1, pp. 34-42, 2016.

[111] D. Randall, P. Metherall, J. Belkhu, K. D. Bardhan, P. Spencer, R. Gillott, R. de Noronha and J. W. Fenner, "The virtual reality virtual colonoscopy: introducing a new technology and a novel application to diagnostic research," in *23rd Congress of the European Society of Biomechanics 2017*, Sevilla, 2017.